Systematic development of coarse-grained polymer models

by

Patrick Theodore Underhill

B.S. Chemical Engineering, Washington University (2001),
B.S. Physics, Washington University (2001).

Submitted to the Department of Chemical Engineering
in partial fulfillment of the requirements for the degree of

Doctor of Philosophy in Chemical Engineering

at the

MASSACHUSETTS INSTITUTE OF TECHNOLOGY
[September 2006]
August 2006

Author_____
Department of Chemical Engineering
August 18, 2006

Certified by_____
Patrick S. Doyle
Doherty Associate Professor of Chemical Engineering
Thesis Supervisor

Accepted by_____
William M. Deen
Professor of Chemical Engineering
Chairman, Committee for Graduate Students

Systematic development of coarse-grained polymer models

by
Patrick Theodore Underhill

Submitted to the Department of Chemical Engineering
on August 18, 2006, in partial fulfillment of the
requirements for the degree of
Doctor of Philosophy in Chemical Engineering

Abstract

The coupling between polymer models and experiments has improved our understanding of polymer behavior both in terms of rheology and dynamics of single molecules. Developing these polymer models is challenging because of the wide range of time and length scales. Mechanical models of polymers have been used to understand average rheological properties as well as the deviation a single polymer molecule has from the average response. This leads to more physically significant constitutive relations, which can be coupled with fluid mechanic simulations to predict and understand the rheological response of polymer solutions and melts.

These models have also been used in conjunction with single molecule polymer experiments. While these have provided insight into the dynamics of polymers in rheological flows, they have also helped to design single molecule manipulation experiments. Promising research in this area includes DNA separation and stretching devices. A typical atomic bond has a length of 10^{-10}m and vibration time scale of 10^{-14}s. A typical experiment in a microfluidic device has lengths of order 10^{-5}m and times of order 10^{2}s. It is not possible to capture these larger length and time scales of interest while capturing exactly the behavior at the smaller length and time scales. This necessitates a process of coarse-graining which sacrifices the details at the small scale which are not necessary while retaining the important features that do affect the response at the larger scales.

This thesis focuses on the coarse-graining of polymers into a series of beads connected by springs. The function which gives the retractive force in the spring as a function of the extension is called the spring force law. In many new microfluidic applications the previously used spring force laws produce significant errors in the model. We have systematically analyzed the coarse-graining and development of the spring force law to understand why these force laws fail. In particular, we analyzed the force-extension behavior which quantifies how much the polymer extends under application of an external force. We identified the key dimensionless group that governs the response and found that it is important to understand the different constraints under which the polymer is placed. This understanding led to the development of new spring force laws which are accurate coarse-grained models by construction. We also examined the response in other situations such as weak and strong flows. This further illustrated the disadvantages of the previous force laws which were eliminated by using the new force laws.

This thesis will have practical impact because the new spring force laws can easily be implemented in current polymer models. This will improve the accuracy of the models and place the models on firmer theoretical footing. Because the spring force law has been developed independently of other coarse-grained interactions, this thesis will also help in determining the best parameters

for other interactions because they will not need to compensate for an error in the spring force law. These new spring force laws will help form the framework of coarse-grained models which can help understand a wide range of situations in which the behavior at a small scale affects the large time and length scale behavior.

Thesis Supervisor: Patrick S. Doyle
Title: Doherty Associate Professor of Chemical Engineering

Acknowledgments

A PhD thesis is both a challenging and rewarding endeavor. A large number of people have helped and supported me along the way, which I would like to acknowledge. I would first like to thank my advisor Professor Pat Doyle for all his help and advice. He has helped me with research problems I encountered, but also helped me to find a better way of presenting my research to others.

As members of my thesis committee, Professors Gareth McKinley and Bob Armstrong have provided many comments and questions as my research progressed. They have also provided valuable advice towards my goal of an academic position. I would also like to thank the other faculty and staff in the Chemical Engineering department that have helped me.

The members of the Doyle group have provided me a lot of academic support, particularly from Ramin Haghgooie and Thierry Savin who came to MIT and joined the Doyle group at the same time as I did. Ramin and I often compared approaches to Brownian dynamics simulations, and he answered countless questions of mine about every aspect of my research. Thierry also offered much advice about my research and particularly helped me with ways of presenting my results more clearly. Greg Randall and Anthony Balducci helped me with me brief foray into experiments, which did not become a part of this thesis. We also had countless discussions about polymer theory.

The Doyle group was also a great atmosphere to do a PhD apart from academics. I would like to thank all the current and past members of the group. Even without the couch we always wanted in the office, they provided numerous chances to have a good laugh before returning to work (or while trying to work). It will not be the same doing research without them. I would also like to thank

a number of people I met at MIT that I have spent countless hours with outside of school. They have helped to make these past 5 years unforgettable. I will miss them tremendously but know that I have gained many life-long friends. They include Ramin Haghgooie, Anna Pisania, Keith Tyo, Brad Cicciarelli, Luwi Oluwole, Daryl Powers, Mike Rappel, Wanda Lau, Chad Augustine, and Adi Augustine.

I would also like to thank my family for always being there for me. My brother, Greg Underhill, is also in engineering and has been someone for me to look up to for many years. I would also like thank my sister-in-law, Shoba Raj-Underhill. Finally, I would like to thank my mom and dad, Fred and Candy Underhill, who have always believed in me and supported me. They have always been interested in my research, even if they do not always understand it all, and encouraged me to be the best person I can be.

Funding for this research was provided by a National Science Foundation Graduate Research Fellowship Program and the National Science Foundation CAREER Grant No. CTS-0239012.

Table of Contents

List of Figures

List of Tables

CHAPTER 1

Introduction

1.1 Motivation

The coupling between polymer models and experiments has improved our understanding of polymer behavior both in terms of rheology and dynamics of single molecules. Developing these polymer models is challenging because of the wide range of time and length scales [1, 2]. Mechanical models of polymers have been used to understand average rheological properties as well as the deviation a single polymer molecule has from the average response. This leads to more physically significant constitutive relations, which can be coupled with continuum fluid mechanic simulations to predict and understand the rheological response of polymer solutions and melts [3].

These models have also been used in conjunction with single molecule polymer experiments [4, 5, 6]. While these have provided insight into the dynamics of polymers in rheological flows, they have also helped to design single molecule manipulation experiments. Promising research in this area includes DNA separation and stretching devices.

1.2 General Polymer Physics

A natural place to begin talking about the modeling of polymers is to consider explicitly each of the atoms. However the bonds between two atoms are quite stiff, with typical frequencies of oscillation of 10^{14}Hz and also small fluctuations away from the average bond length. On the scale of the entire molecule these small fluctuations will have a minimal impact on the static (configurational)

properties. To resolve this fast vibration physics in dynamical simulations, the time resolution must be very small, which would make these too computationally intensive for the long chains and long simulation times of interest here. However, a number of researchers are interested in properties at that length and time scales, for which models at this scale must be used [7, 8]. The conventional choice is to replace these bonds with rigid rods (or infinitely stiff springs). Using this idea, the simplest and first attempt at coarse-graining a polymer is to replace the atomic bonds with rods and assume that the rods are freely jointed [9, 10, 11].

Consider a model of N beads connected by $N-1$ rods, each of length a. We will take advantage of the equivalence between this problem and a random walk to calculate the properties of this model. Note that there is a difference in behavior, even static distributions, between a system where the rods are rigid constraints and where the rods are the limit of very stiff springs [12, 13]. The system of very stiff springs is considered more physically relevant, thus we consider that system here instead of the system with rigid constraints. The very stiff spring system behaves as a random walk. The average end-to-end distance squared of a random walk is

$$\langle r^2 \rangle = (N-1)a^2 \ . \tag{1.1}$$

While this model does neglect the fluctuations of the bond lengths (making them rods), the much more severe assumption is that neighboring bonds in a real polymer are not freely jointed. A better approximation is that the neighboring rods have a constant bond angle. This is called the freely rotating chain. The common sp3 hybridized orbitals of atoms such as carbon prefer to have tetrahedral symmetry and thus a bond angle of $\theta = 109°$ between subsequent bonds (i.e. rods). A similar analysis as for the freely jointed chain can be performed for the freely rotating chain to obtain [10]

$$\langle r^2 \rangle = (N-1)a^2 \frac{1+\cos(\gamma)}{1-\cos(\gamma)} \tag{1.2}$$

if the number of rods is large, and $\gamma = 180 - \theta$. We see that the result still scales with the number of rods but with an altered prefactor which depends on the details of the model. This is in essence analogous to the idea of the central limit theorem applied to random walks. If a large number of steps are taken and the system is at equilibrium (not stretched), it looks like a random walk with some effective (average) step size.

Even this freely rotating chain model does not accurately represent some features of real polymers. The first deviation is evident by looking at the behavior of butane. With each bond angle fixed, the configuration is specified using a dihedral or torsional angle. In the freely rotating chain, each of these dihedral angles is equally likely. However, in butane, these angles are not equally likely because of steric interactions between parts of the chain. The trans configuration reduces these interactions and so is most likely. The cis configuration maximizes these interactions and thus is most unlikely. There also exists a gauche configuration which is a local minimum in the interactions. This is still considered a "local" interaction along the chain because it only affects monomers that are a finite distance along the contour independent of the length of the polymer. Thus including this effect will not change the scaling exponent with N of the average end-to-end distance squared, but only will change the prefactor (like how the prefactor was different when comparing the freely rotating chain with the freely jointed chain).

A similar interaction occurs at the next level along the chain, and first appears for pentane, so is called the pentane effect. For a molecule of pentane, it is possible for a set of rotations to be

made which bring two terminal hydrogen atoms into very close contact. Steric repulsions prevent this from occurring. Including this effect also will only change the prefactor to the scaling with N, as long as N is large enough. These type of "local" interactions are accounted for by using the rotational isomeric state (RIS) model [14].

To this point in our analysis we have examined the configuration space of the polymer. The solvent has only acted as a temperature bath. No explicit interactions have been included between the polymer and solvent. Other than the local (along the contour) steric interactions, we have also not included interactions between segments of polymer. In a real system, segments of polymer can not occupy the same position in space. This has been neglected in our previous analysis, a so-called "phantom chain". The inclusion of these other effects can cause a change in the exponent of the scaling of the size with length (or number of steps). Under certain conditions, known as "theta conditions", these two additional interactions cancel in the sense that the scaling exponent is the same as if both effects were neglected. In this special circumstance, both effects can be neglected while obtaining an accurate prediction. This should be done with caution in nonequilibrium situations because there may be subtle variations that have not been explored yet in the literature in nonequilibrium situations [15]. This also neglects physics such as knots which can be present in theta conditions.

If the polymer has a size which is smaller than the theta size, the solvent is considered poor. If the size is larger than under theta conditions, it is considered a good solvent. It is important to note that the solvent quality is also a function of temperature. For a given polymer-solvent pair, there is only a single temperature which corresponds to theta conditions.

The simplest model to show an example of a good solvent is to consider a self avoiding random walk instead of the random walk already considered. For a self avoiding walk, the scaling behavior is approximately $N^{0.6}$ [9].

1.3 Progression of Coarse-grained Models

1.3.1 Necessity of coarse-graining

In the previous section we discussed the progression of polymer models, in which each new model correctly included more and more details about the polymer behavior. The result of this is a good understanding of the static properties of the polymer. However, we are also interested in dynamic properties of very long polymers over a wide range of time scales. For these purposes, the models such as RIS are still too intensive to deal with.

Flexible polymers near equilibrium

Consider a polymer under theta conditions. Suppose some detailed model, such as RIS, can calculate the average end-to-end distance squared. It can be written as

$$\langle r^2 \rangle = (N-1)a^2 C_N \ , \tag{1.3}$$

which serves as a definition of C_N. If N is large enough, C_N becomes close to the infinite value C_∞ [15]. For these large N

$$\langle r^2 \rangle \simeq (N-1)a^2 C_\infty \ , \tag{1.4}$$

where the parameter C_∞ depends on the details of the polymer. This looks very similar to the behavior of a chain which is freely jointed, equation (1.1). It is possible to define a coarse-grained freely jointed chain, made up of N_K steps, each of length a_K. The parameter a_K is called the Kuhn length. We can choose the values of N_K and a_K such that

$$L = (N-1)a\beta = N_K a_K \tag{1.5}$$

$$\langle r^2 \rangle = (N-1)a^2 C_\infty = N_K a_K^2 \ , \tag{1.6}$$

where L is the contour length (fully extended length) of the chain. The contour length is shorter by a factor β from the length of extending all of the bonds because the bond angles cannot be straightened. Solving these two equations for the Kuhn length and number of Kuhn lengths gives

$$a_K = \frac{aC_\infty}{\beta} \tag{1.7}$$

$$N_K = \frac{(N-1)\beta^2}{C_\infty} \ . \tag{1.8}$$

Provided the polymer is long enough that equation (1.4) holds ($C_N \simeq C_\infty$), this coarse-grained model represents the contour length and end-to-end distance squared correctly (by construction). The main question becomes, does this model represent other properties of the polymer and under what conditions does it? This freely jointed chain is rigid over the length of a rod and those rods are freely jointed. Although the polymer is very stiff over the length of an atomic bond, over the length of a Kuhn length it is not a rigid rod. Those segments of the polymer are also not freely jointed. However, for long enough polymers (such that $C_N \simeq C_\infty$) and if the concern is only near equilibrium, the freely jointed chain does describe other equilibrium properties correctly. For configurational properties, this is basically a statement of the central limit theorem. In other words, if the properties of the polymer only depend on the two matched properties, then the polymer and the coarse-grained model will have the same behavior.

Many polymers of interest contain a very large number of Kuhn lengths for which this holds and the freely jointed chain models well many properties near equilibrium. These are generally called flexible polymers. Some polymers, however, do not contain a large number of Kuhn lengths. This includes so called semiflexible ($N_K \sim 1$) and rigid ($N_K \ll 1$) polymers. Thus even in the equilibrium state the polymer must contain many Kuhn lengths to be modeled well by the freely jointed chain. This is in part because N needs to be a large number for $C_N \simeq C_\infty$, but also so that all properties only depend on L and $\langle r^2 \rangle$.

Flexible polymers out of equilibrium

The question of whether the freely jointed chain models the behavior of the polymer out of equilibrium is a separate question. Out of equilibrium, the central limit theorem does not hold. The details of the steps matter. This is clearly evident if you examine two models in which one has steps with a finite maximum extent versus one which can have infinite extent. If the behavior is examined at extensions comparable to the maximum possible extension, the response will certainly depend on whether there exists a maximum extension or not. It is conventional to analyze this

response in terms of the ratio of the Kuhn length to the bond length, $a_K/a = C_\infty/\beta$. If this ratio is only slightly greater than one, such as 5 to 15, it is generally believed that the freely jointed chain correctly represents the behavior out of equilibrium. This is the typical range for many synthetic polymers.

However, if the value of C_∞/β is very large, such as about 300 for double stranded DNA, the freely jointed chain does not represent the behavior of the polymer out of equilibrium. Note that this is true even if the chain is flexible in that the chain contains many Kuhn lengths, $N_K \gg 1$. The typical micromechanical model which is used to describe these polymers is the continuous worm-like chain instead of the freely jointed chain [16, 17, 18, 19, 20, 21, 22]. The continuous worm-like chain is a continuous space-curve like a string which has a bending rigidity. Essentially the backbone of the chain is so stiff that the Kuhn length is much larger than the bond length. Therefore, at the scales of interest, the bonds look essentially as a continuum.

The worm-like chain micromechanical model is defined by a space curve $\mathbf{r}(s)$ where s measures the position along the contour and runs from 1 to L. A unit tangent vector is defined by

$$\mathbf{t}(s) = \left(\frac{\partial \mathbf{r}}{\partial s}\right) \Big/ \left|\frac{\partial \mathbf{r}}{\partial s}\right| \ . \tag{1.9}$$

The energy of a configuration is

$$E = \frac{\kappa}{2}\int_0^L \left(\frac{\partial \mathbf{t}}{\partial s}\right)^2 \mathrm{d}s \tag{1.10}$$

where κ is the bending modulus. It is common to replace the bending modulus with a persistence length, which in three dimensional space is defined by $\kappa = k_B T A_p$. Because of the energetic cost to bending, within short distances along the contour the chain persists in the same direction. At long distances along the contour, the chain orientation becomes uncorrelated with previous orientations. The persistence length is the characteristic distance over which this decorrelation occurs. Mathematically this is written as

$$\langle \mathbf{t}(s) \cdot \mathbf{t}(p) \rangle = \exp(-|s-p|/A_p) \ . \tag{1.11}$$

Another important property of the worm-like chain is

$$\langle r^2 \rangle = 2LA_p + 2A_p^2(\exp(-L/A_p) - 1) \ . \tag{1.12}$$

In order to be in the limit where $\langle r^2 \rangle \propto L$, the contour length must be much larger than the persistence length. The response of the continuous worm-like chain in this limit is

$$\langle r^2 \rangle = 2LA_p \ . \tag{1.13}$$

Recall that in this limit, near equilibrium, any polymer can be describe by the freely jointed chain. By comparing this formula with the formula for a freely jointed chain, we see that for the freely jointed chain to model a very long continuous worm-like chain near equilibrium, the Kuhn length must be equal to twice the persistence length. Note however that this whole discussion of the worm-like chain was motivated by the fact the freely jointed chain does not model the response correctly away from equilibrium.

Even though this discussion was motivated by flexible polymers which are not modeled correctly

by the freely jointed chain out of equilibrium, the continuous worm-like chain model is often an accurate model for semiflexible and rigid polymers, such as F-actin and tobacco mosaic virus. In essence these polymers are not long enough such that $C_N \simeq C_\infty$, so the freely jointed chain does not represent well the equilibrium properties.

Linear bead-spring chains (near equilibrium)

At this point we see that most polymers are typically modeled by one of two micromechanical models, the freely jointed chain or the worm-like chain. Only for flexible polymers at equilibrium are these two models equivalent. These models are still too computationally intensive for many dynamical calculations for long polymers. Therefore, these micromechanical models are often coarse-grained even further to bead-spring chains. The simplest bead-spring chain model contains Hookean, or linear, springs [9, 12]. In this model, the restoring force in the spring is proportional to the length of the spring

$$F_{\text{spr}} = Hr \ . \tag{1.14}$$

This can be motivated from a number of different but equivalent methods. One method is to consider a random walk of linear springs. At equilibrium the spring will be sampling all possible lengths weighted according to the Boltzmann factor, since the system is at constant temperature, with a harmonic potential $Hr^2/2$. The average end-to-end distance squared is

$$\langle r^2 \rangle = 3N_{\text{spr}} \frac{k_B T}{H} \ . \tag{1.15}$$

For this to match the behavior of the freely jointed chain, the spring constant must be taken to be

$$H = \frac{3N_{\text{spr}} k_B T}{L A_K} \ , \tag{1.16}$$

where the number of springs remains arbitrary. In the same way that the freely jointed chain only models a polymer if that polymer has $N_K \gg 1$, this Hookean chain will only model the freely jointed chain if $N_K \gg 1$ and it is near equilibrium. A more detailed analysis could consider not just the average end-to-end distance squared, but the entire probability distribution of the end-to-end vector. The probability distribution for the freely jointed chain can be analyzed from the theory of random walks. In the limit of a large number of Kuhn steps the equilibrium distribution approaches a Gaussian distribution. The distribution for a chain of linear springs is exactly a Gaussian distribution. Matching these two Gaussian distribution gives the same value for H as above.

Another motivation for the chain of linear springs is the so called entropic restoring force. We just saw that a freely jointed chain with a large number of Kuhn steps has a Gaussian distribution for the end-to-end vector near equilibrium. The most likely value of the end-to-end vector is zero, the ends are not separated at all. Therefore, in order to separate the ends apart, an external force must be applied. This restoring force is not due to internal energy differences because the freely jointed chain does not have any internal energy. It is due to the fact that the number of configurations which give a small vector is larger than the number that gives a larger vector.

The bead-spring chain model with linear springs is often called a Gaussian chain because the chain has a Gaussian distribution between any two beads. The Gaussian chain is analogous to the

random walk in Brownian motion, but where the number of steps is like the time of the walk.

The Gaussian chain has the advantage that many calculations can be done analytically. Also the formulas can be examined in the limit of an infinite number of springs. This limit of $N_{\text{spr}} \to \infty$ can be done at constant H, which corresponds to chains of progressively larger LA_K, or at constant LA_K, which means H must be be made larger as N_{spr} increases. The first case represents the behavior of progressively larger chains while the second case represents a finer discretization of the same polymer. The fact that these two view points are equivalent is because of the scale invariant nature of the Gaussian distribution. For this reason, the limit of an infinite number of springs is typically taken and the methods of renormalization group theory are often applied to this and related models. We will see later in this thesis similar ideas but with nonlinear bead-spring chains. It is important to note that this scale invariance is due to the linearity of the springs. Recall that the freely jointed chain only matched the behavior of the polymer if the polymer contained a large number of Kuhn lengths and was near equilibrium. Similarly the Gaussian chain only matches the behavior of the freely jointed chain if the freely jointed chain contains a large number of Kuhn lengths. This is true for the Gaussian chain no matter how small $L/(N_{\text{spr}}A_K)$ is because of the structure of the Gaussian distribution.

Nonlinear bead-spring chains (out of equilibrium)

Recall the discussion of flexible polymers out of equilibrium. Although we found that all flexible polymers looked the same near equilibrium, equivalent to the freely jointed chain, the details of the chain mattered out of equilibrium. Similarly, the Gaussian chain can be used to model flexible polymers near equilibrium, but fails to describe the behavior out of equilibrium. The details of the micromechanical model will determine the type of bead-spring chain needed to describe the response out of equilibrium.

This is clearly evident from the fact that the Gaussian chain can be infinitely extended, while real polymers and micromechanical models such as the freely jointed chain and the worm-like chain can not be extended past the contour length. To represent this finite extensibility, the spring force law can be changed from a linear spring to one that becomes infinite at a finite distance. The diverging force prevents the chain from being extended past that point. Extensions near this finite extent are far from equilibrium and thus the central limit theorem does not hold; the behavior depends on the details of the individual steps, even for flexible chains which contain many Kuhn lengths.

The development of the nonlinear force laws to represent coarse-grained models can proceed in a similar manner as with the Gaussian chain. The spring force law can be chosen to give the correct probability distribution of the end-to-end vector or the correct force-extension behavior (how much the molecule extends under application of an external force). These methods are equivalent and are typically performed in the limit of an infinite number of Kuhn lengths in the chain. This has been done for the two common micromechanical models, the freely jointed chain and the worm-like chain. For the freely jointed chain, the result is that the spring force should be taken to be [23]

$$F_{\text{spr}} = \frac{k_B T}{A_K} \mathcal{L}^{-1}(r/L) \ , \tag{1.17}$$

where $\mathcal{L}^{-1}$ is the inverse Langevin function. The Langevin function is

$$\mathcal{L}(x) = \coth(x) - 1/x \ . \tag{1.18}$$

A simple formula does not exist for the equivalent response for the worm-like chain; it must be calculated numerically. However, a number of approximate formulas exist. Most of them come about from examining the large and small force limits, in which series expansions can be developed, and patching together those expansions. Many of the analytical techniques used to investigate the worm-like chain proceed through analogies to the path integral formulation of quantum mechanics. The simplest and most common approximation is due to Marko and Siggia [18]

$$F_{\text{spr}} = \frac{k_B T}{A_p}\left(\frac{r}{L} - \frac{1}{4} + \frac{1}{4(1-r/L)^2}\right) \ . \tag{1.19}$$

Note that just like the Gaussian chain, these force laws only represent the micromechanical model if the chain contains a very large number of Kuhn lengths or persistence lengths. However, these force laws have the advantage that they also model the behavior out of equilibrium, such as the force-extension behavior. A more subtle aspect concerns using these force laws in bead-spring chain rather than simply dumbbell models. The natural extension would be to assume that, even in a chain model, each spring represents a large number of Kuhn lengths, and thus the contour length in the spring force law is replaced by $\ell = L/N_{\text{spr}}$, which is the fully extended length of a single spring. This is similar to what was done for the Gaussian chain. For the Gaussian chain, we noted that the chain retained accuracy if the chain contained a large number of Kuhn lengths regardless of the number of springs, and therefore regardless of how much of the polymer is represented by a single spring. This is true only because of the special nature of the Gaussian distribution and so is not true for the nonlinear bead-spring chains. At equilibrium, even though the polymer is not represented correctly at a small scale by the Gaussian distribution, the Gaussian chain is able to correctly model the global behavior of the chain which, in total, contains many Kuhn lengths. In order for nonlinear chains to retain accuracy, each spring must represent a large number of Kuhn lengths. This difference is a major focus of this thesis. This thesis will be examining the coarse-graining of micromechanical models such as the freely jointed chain and worm-like chain into nonlinear bead-spring chains. We will be analyzing the error introduced by using these spring force laws to represent small segments of polymer, even if the whole polymer contains a large number of Kuhn lengths, and generating new nonlinear spring force laws which can be used to represent these situations accurately.

Coarse-graining other interactions

To this point we have discussed coarse-grained models in terms of the distribution function of the chain, which represents the size of the polymer coil and represents the response of the chain to external forces applied to the ends of the chain or forces applied to the positions of the beads in the coarse-grained model. However, there are a number of other interactions which should be included in the coarse-grained model.

The coarse-graining analysis, both from the polymer to the micromechanical model and further to bead-spring chains, has not treated the solvent other than as a temperature bath. In discussing the behavior of the real polymers we have already discussed the interactions of the polymer and

solvent and the existence of a theta state. The Gaussian chain model and the nonlinear chain models developed thus far only give the correct behavior in the theta state. To give the correct behavior outside of the theta state, additional interactions must be included between the beads. It is common to study good solvent conditions because those are prevalent for polymers that do not precipitate from solution. In these conditions, the chain acts as a self-avoiding walk which has an expanded coil size. For a coarse-grained model, a repulsive interaction must be included between the beads to obtain an expanded coil size. This repulsion measures the penalty for the two segments of polymer modeled by a bead (or spring) to overlap. It is common to use a repulsive Gaussian potential energy between the beads [24]. This is motivated by the repulsion between two Gaussian chains. Note that even when two beads are overlapping, the potential is still finite, therefore it is still possible for two beads to pass through each other. This is because, although the atoms of the polymer can not overlap, two beads which represent the average behavior of the polymer can still overlap. The excluded volume interactions could also be included through spring-spring repulsions [25] or Lennard-Jones type repulsions [26].

The solvent also has a viscosity which exerts hydrodynamic drag on the chain. It is typical to treat the beads in the bead-spring chain as spheres with radius a, for which the Stokes drag on the sphere corresponds to the drag due to the solvent on the segment of polymer modeled by the bead.

This Stokes drag on each bead represents the hydrodynamic drag on a segment of polymer due to the solvent, neglecting the presence of the other beads. The other beads will disturb the solvent flow field, which alters the drag from the simple Stokes formula. This additional drag is a result of hydrodynamic interaction. [27] Hydrodynamic interaction does not affect any static properties such as the probability distribution of the end-to-end vector or the force-extension behavior. Through an analysis of Stokes flow, it has been shown that the velocity disturbance in the far field due to a force on the fluid can be calculated using the Oseen-Burgers tensor [12]

$$\Delta \boldsymbol{v} = \boldsymbol{\Omega}_{OB} \cdot \boldsymbol{F} \tag{1.20}$$

$$\boldsymbol{\Omega}_{OB} = \frac{1}{8\pi\eta_s R}\left(\boldsymbol{\delta} + \frac{\mathbf{RR}}{R^2}\right) . \tag{1.21}$$

The Oseen-Burgers tensor can produce numerical issues if two beads interact with this tensor and are allowed to be closer than the diameter of a bead. To correct for this problem and to approximately account for the near field disturbance, an alternative form due to Rotne-Prager-Yamakawa [28, 29] is often used.

1.4 Problems with Current Models

The problems with the current models essentially stem from an issue already mentioned. The nonlinear spring force laws that are currently used were derived assuming each spring represents a very large number of Kuhn lengths. These spring force laws have been used, though, to represent smaller segments of polymer. Doyle et al. [30] performed simulations in which they held two ends of a freely jointed chain at a fixed distance r apart and calculated the average force necessary to keep them held fixed. A plot of $\langle f \rangle$ versus r was compared with the inverse Langevin function. It was found that if the freely jointed chain contained more than about 10 Kuhn lengths, the response was close to the inverse Langevin function.

Somasi et al. [31] argued based on these simulations that a spring should not be used to model a freely jointed chain if each spring represents less than 10 Kuhn lengths, and should not model a worm-like chain if each spring represents less that 20 persistence lengths. They performed simulations of bead-spring chain models in which they changed the number of beads in the chain used to represent the same polymer. They found for λ-phage DNA that the response changed up to the limit, that is 20 persistence lengths per spring. Thus they proposed to operate at this limit for λ-phage DNA. This is an example of the balance which must be made between using too few springs such that the drag is not exerted continuously along the contour and using too many springs for which each spring represents a small number of Kuhn lengths.

Larson and coworkers [32, 33, 34] have also examined the behavior of the bead-spring chains. They examined the force-extension behavior of bead-spring chain models of λ-phage DNA which contains about 400 persistence lengths. Force-extension experiments have shown that it is well modeled by the worm-like chain. Larson and coworkers examined a series of bead-spring chain models with a constant L but with increasing N_{spr} and noticed that the force-extension behavior of the bead-spring chain model deviated from the behavior of the worm-like chain. They argued that the introduction of more beads in the chain has introduced more locations that are free hinges and thus increased the flexibility of the chain. They found that if they artificially increased the persistence length used in the spring force law, they could reduce the error.

The use of this effective persistence length has not been quantified, and the residual error even after changing the persistence length has not been analyzed and understood. The argument about free hinges does not explain why the same effect is seen when using bead-spring chain models of the freely jointed chain. When using this effective persistence length, are there still limits on how few persistence lengths can be represented by a single spring? Why does the same issue not present itself when using a Gaussian chain to model a chain with a large number of Kuhn lengths, even when each spring represents a very small number of Kuhn lengths?

1.5 Importance of New Models

It is important to understand the coarse-graining of polymers into bead-spring chains so that the error in current models can be quantified. The limits on the current models are critical, not only to better understand any effect on previous work, but also to enable new simulations which are not possible with the current models. This will help us understand the response better even if it is not necessary to use small springs to obtain accurate simulations of the physics of interest.

Some problems exist in which the behavior at the scale of small springs is critical to understanding the physics of the problem. Consider for example the problem of the dynamics of double stranded DNA in microfluidic or nanofluidic devices [35, 36, 37, 38, 39, 40, 41, 42, 43, 44]. To predict the behavior correctly in these devices the response of the polymer must be captured at the scale of the features in the device, typically a few microns or less. Double stranded DNA has a persistence length of about 50 nm, so these features correspond to smaller than about 20 persistence lengths. To correctly understand the response in these devices it is necessary to have a feasible model which can capture the DNA behavior at a scale smaller than this scale.

In this thesis, I will analyze the role that the spring force law plays in producing these new accurate models. By understanding the failure of the current force laws, I will be able to develop new force laws which do not have the same errors. These new force laws provide more accurate predictions of the response of the micromechanical models in a variety of different situations.

CHAPTER 2

Methodology

In this chapter, I will review the two methods used to calculate the behavior of bead-spring chain polymer models. The first method is equilibrium statistical mechanics. When this method is applicable, it has the advantage that it is an analytical method so that the governing parameters can be explicitly derived. It is also useful in developing exact asymptotic expansions. However, the properties of some systems can not be written in terms of equilibrium statistical mechanics and certainly non-equilibrium transient behavior can not. To address these situations we use Brownian dynamics simulations. While this method naturally addresses non-equilibrium situations, the intrinsic stochastic noise makes it more difficult to make exact statements of equality, especially at equilibrium where the noise is larger. In this way the two methods are complementary even though both can be used in equilibrium situations.

2.1 Statistical Mechanics

Within the context of equilibrium statistical mechanics the probability density of a configuration is proportional to [45]

$$\exp\left[\frac{-\mathcal{H}_{\text{eff}}}{k_{\text{B}}T}\right] \tag{2.1}$$

if the configuration is consistent with the macroscopic constraints. The quantity $\mathcal{H}_{\text{eff}}$ is the effective Hamiltonian, k_{B} is Boltzmann's constant, and T is the absolute temperature. The specific form of

the effective Hamiltonian depends on the macroscopic constraints, i.e. the ensemble. For the often used canonical ensemble the effective Hamiltonian is equal to the energy.

Given the above definition, the probability density at the configuration i, p_i, is given by

$$p_i = \frac{1}{\mathcal{Z}} \exp\left[\frac{-\mathcal{H}_{\text{eff},i}}{k_{\text{B}}T}\right] , \tag{2.2}$$

where $\mathcal{Z}$ is the partition function and is equal to

$$\mathcal{Z} = \int \cdots \int_{\{\text{configurations}\}} \exp\left[\frac{-\mathcal{H}_{\text{eff}}}{k_{\text{B}}T}\right] \mathrm{d}\mathbb{V} \tag{2.3}$$

to ensure that the probability density is properly normalized. It should be noted that for the bead-spring chains considered in this paper we do not need to worry about the kinetic energy contribution to the effective Hamiltonian and the momentum configuration space [12]. This is because our system has no rigid constraints that freeze-out degrees of freedom, and also we will not compute the average of any quantity that depends on momentum.

Average quantities are computed by integrating that quantity times the probability density over all the configuration space. Thus, for a property signified by $\mathcal{F}$, the average is

$$\langle \mathcal{F} \rangle = \int \cdots \int_{\{\text{configurations}\}} \mathcal{F} \frac{1}{\mathcal{Z}} \exp\left[\frac{-\mathcal{H}_{\text{eff}}}{k_{\text{B}}T}\right] \mathrm{d}\mathbb{V} . \tag{2.4}$$

2.2 Brownian Dynamics

The technique of Brownian dynamics (BD) [46, 47] has been widely used to study the non-equilibrium and equilibrium properties of polymer models in flow, in particular bead-rod and bead-spring models [48, 49, 50, 51, 30, 52, 53, 54, 24]. Most previous investigations of the dynamical behavior of bead-spring chains have used BD. BD allows researchers to study the time-evolution of the system which is not possible using equilibrium statistical mechanics.

It is a mesoscopic method which integrates forward in time the equation of motion similar to molecular dynamics (MD), although in BD explicit solvent is not included. The solvent is replaced by two forces, a drag force resulting from movement through a continuous, viscous solvent and a stochastic force resulting from the random collisions the solvent molecules make with the particles of interest. This stochastic force causes the particles to undergo Brownian motion and makes the equation of motion a stochastic differential equation.

Having developed the governing stochastic differential equation, one performs a BD simulation by integrating this equation forward in time. The stochastic nature means that one must produce many independent trajectories that are averaged together, producing the time-evolution of an ensemble-averaged property. The repetition of many independent trajectories is a time-consuming but necessary part to follow the time-evolution of a property. However, to calculate a steady-state property, one uses the ergodic hypothesis to time-average a single trajectory.

2.2.1 *Stochastic differential equation*

The equation of motion is given by

$$m_i \ddot{\mathbf{r}}_i = \mathbf{F}_i^{\text{net}} = \mathbf{F}_i^{\text{B}} + \mathbf{F}_i^{\text{d}} + \mathbf{F}_i^{\text{s}} \simeq \mathbf{0} \ , \tag{2.5}$$

where the subscript i denotes bead i, m is the mass of each bead, $\ddot{\mathbf{r}}$ is the acceleration, $\mathbf{F}^{\text{net}}$ is the net force, $\mathbf{F}^{\text{B}}$ is the Brownian force due to collisions of the solvent molecules with the beads, $\mathbf{F}^{\text{d}}$ is the drag force due to the movement of each bead through the viscous solvent, and $\mathbf{F}^{\text{s}}$ is the systematic force on each bead due to the springs and any external forces. We neglect the inertia (mass) of the beads, and so the net force is approximately zero. In some situations this is a singular limit and should be done with care.

The drag on each bead is taken to be the Stokesian drag on a sphere, and we will neglect any hydrodynamic interaction between beads. Thus,

$$\mathbf{F}_i^{\text{d}} \simeq -\zeta\big(\dot{\mathbf{r}}_i - \mathbf{u}^{\infty}(\mathbf{r}_i)\big) \ , \tag{2.6}$$

where ζ is the drag coefficient, and $\mathbf{u}^{\infty}(\mathbf{r}_i)$ is the undisturbed solvent velocity evaluated at the center of bead i. The governing stochastic differential equation (SDE) then becomes

$$\dot{\mathbf{r}}_i(t) \simeq \mathbf{u}^{\infty}\big(\mathbf{r}_i(t)\big) + \frac{1}{\zeta}\Big[\mathbf{F}_i^{\text{s}}\big(\{\mathbf{r}_j(t)\}\big) + \mathbf{F}_i^{\text{B}}(t)\Big] \ . \tag{2.7}$$

Note that the systematic force depends on the set of all particle positions $\{\mathbf{r}_j(t)\}$. This is a stochastic differential equation because the Brownian force is taken from a random distribution. In order for the dynamics to satisfy the fluctuation-dissipation theorem, the expectation values of the Brownian force are

$$\langle\, \mathbf{F}_i^{\text{B}}(t) \,\rangle = \mathbf{0} \ , \tag{2.8}$$

$$\langle\, \mathbf{F}_i^{\text{B}}(t)\mathbf{F}_j^{\text{B}}(t') \,\rangle = 2k_{\text{B}}T\zeta\delta_{ij}\delta(t-t')\boldsymbol{\delta} \ . \tag{2.9}$$

The symbol δ_{ij} is the Kronecker delta, $\boldsymbol{\delta}$ is the unit second-order tensor, and $\delta(t-t')$ is the Dirac delta function.

2.2.2 *Integration methods*

Explicit method

The most basic integration scheme, which we use for most of the simulations in this thesis, is a simple explicit first-order time-stepping algorithm:

$$\mathbf{r}_i(t+\delta t) \simeq \mathbf{r}_i(t) + \dot{\mathbf{r}}_i(t)\,\delta t \ . \tag{2.10}$$

In this type of discrete time-stepping, the Brownian force at any discrete time represents the collective effect (or average) of the Brownian force over the time step. Thus, the correlation between these Brownian forces becomes

$$\langle\, \mathbf{F}_i^{\text{B}}(t)\mathbf{F}_j^{\text{B}}(t') \,\rangle = 2k_{\text{B}}T\zeta\delta_{ij}\frac{\delta_{tt'}}{\delta t}\boldsymbol{\delta} \ , \tag{2.11}$$

where now the times t and t' are discrete times.

The main disadvantage of this scheme for this thesis is that, when simulating bead-spring chains with finitely extensible springs, there can be a small probability that the length of a spring at the end of a step will be greater than the finite length. Unless specifically noted, all simulations in this thesis using the explicit scheme used a time step small enough that no examples of overstretching were observed over the course of the simulation time.

It should also be noted that, within the restrictions on the two expectation values of the Brownian force, the exact random distribution used to obtain the random forces is arbitrary. This is essentially an example of the central limit theorem. If a large enough of these random steps are taken, the result will look like a Gaussian distribution which is determined by the mean and variance of the steps. However, care should be taken because this only holds when the number of steps is large enough (the time step is small enough) and the observation is not made in the tail of the distribution. Obviously the result after a single time step will depend on the distribution used for the Brownian force in that step. Because of the prevalence of random number generators which produce a uniform distribution, we often sample the Brownian force from a uniform distribution (appropriately scaled and shifted to obtain the correct mean and variance). The standard generator which is used in most simulations in this thesis is given by Öttinger [46], denoted by routines *RANILS* and *RANULS*. For some situations it is convenient to use random numbers taken from a Gaussian distribution. For this task we use the subroutine *RANGLS* from ref. [46] to convert uniform random numbers into Gaussian distributed ones. We also use the uniform random number generator *ran3* from the Numerical Recipes in FORTRAN. Although this generator has not withstood as many rigorous tests, it performs in only about half the time.

Semi-implicit method

In some situations, the time step required to have no occurrences of overstretching is so small that the computation is no longer feasible. To make these simulations feasible we use a semi-implicit method [31].

This algorithm is essentially an implicit algorithm for the spring force law in which the equations are solved iteratively until it converges to an implicit solution. The iteration proceeds in terms of the spring connector vectors instead of the explicit positions of the beads. This is possible when the strain rate is homogeneous in space. The strain rate tensor is defined as

$$\boldsymbol{\kappa} = (\nabla \mathbf{u}^{\infty})^{\dagger} \ . \tag{2.12}$$

Because this strain rate tensor is a constant (does not depend on position), the velocity can be written as

$$\mathbf{u}^{\infty} = \boldsymbol{\kappa} \cdot \mathbf{r} + \mathbf{u}_0 \ , \tag{2.13}$$

where $\mathbf{u}_0$ is a constant. The connector vectors are defined as $\mathbf{Q}_i = \mathbf{r}_{i+1} - \mathbf{r}_i$, defined for i from 1 to $N-1$. By taking the difference between equation (2.7) for neighboring beads, we can write the stochastic differential equation for the connector vectors

$$\dot{\mathbf{Q}}_i(t) \simeq \boldsymbol{\kappa} \cdot \mathbf{Q}_i(t) + \frac{1}{\zeta}\Big[\mathbf{F}^{\mathrm{s}}_{i+1}\big(\{\mathbf{r}_j(t)\}\big) - \mathbf{F}^{\mathrm{s}}_{i}\big(\{\mathbf{r}_j(t)\}\big) + \mathbf{F}^{\mathrm{B}}_{i+1}(t) - \mathbf{F}^{\mathrm{B}}_{i}(t)\Big] \ . \tag{2.14}$$

Before it becomes obvious that this set of equations only depends on the connector vectors, we

must replace the systematic forces, $\mathbf{F}^{\mathrm{s}}$, with the spring forces, $\mathbf{F}^{\mathrm{spr}}$. The systematic forces on a bead are the sum of the spring forces pulling on that bead. We define $\mathbf{F}_i^{\mathrm{spr}}$ to be the spring force on bead i due to the spring connecting it to bead $i+1$, and therefore it only depends on the connector vector $\mathbf{Q}_i$. The systematic force on bead i is the difference between two spring forces

$$\mathbf{F}_i^{\mathrm{s}} = \mathbf{F}_i^{\mathrm{spr}} - \mathbf{F}_{i-1}^{\mathrm{spr}} \ . \tag{2.15}$$

In order for this formula to be valid even for the terminal beads (beads $i = 1$ and $i = N$), we define $\mathbf{F}_0^{\mathrm{spr}} = 0$ and $\mathbf{F}_N^{\mathrm{spr}} = 0$. In terms of the spring forces, the SDE becomes

$$\dot{\mathbf{Q}}_i(t) \simeq \boldsymbol{\kappa} \cdot \mathbf{Q}_i(t) + \frac{1}{\zeta}\Big[\mathbf{F}_{i+1}^{\mathrm{spr}}\big(\mathbf{Q}_{i+1}(t)\big) - 2\mathbf{F}_i^{\mathrm{spr}}\big(\mathbf{Q}_i(t)\big) + \mathbf{F}_{i-1}^{\mathrm{spr}}\big(\mathbf{Q}_{i-1}(t)\big) + \mathbf{B}_i(t)\Big] \ , \tag{2.16}$$

where we have used a short-hand notation

$$\mathbf{B}_i(t) = \mathbf{F}_{i+1}^{\mathrm{B}}(t) - \mathbf{F}_i^{\mathrm{B}}(t) \ . \tag{2.17}$$

The algorithm proceeds as a series of iterations, calculating from the current set of vectors $\mathbf{Q}_i(t)$ a new set $\mathbf{Q}_{i,j}(t+\delta t)$, where j signifies the j-th iteration. The algorithm starts with $j = 1$ and proceeds from $i = 1 \rightarrow N-1$. Then the cycle repeats with $j = 2$ from $i = 1 \rightarrow N-1$. This procedure continues until the iterations converge. This converged set of vectors then becomes the new set of vectors $\mathbf{Q}_i(t+\delta t)$. From this point on, we will drop the subscript notation with the spring force because it is redundant with the subscript to the connector vector in its argument.

The first iteration is an explicit first order step similar to the method discussed earlier

$$\mathbf{Q}_{i,1}(t+\delta t) = \mathbf{Q}_i(t) + \boldsymbol{\kappa}\cdot\mathbf{Q}_i(t)\delta t + \frac{\delta t}{\zeta}\Big[\mathbf{F}^{\mathrm{spr}}\big(\mathbf{Q}_{i+1}(t)\big) - 2\mathbf{F}^{\mathrm{spr}}\big(\mathbf{Q}_i(t)\big) + \mathbf{F}^{\mathrm{spr}}\big(\mathbf{Q}_{i-1}(t)\big) + \mathbf{B}_i(t)\Big] \ . \tag{2.18}$$

The second iteration uses a semi-implicit method in which the connector vectors from previous calculations in the second iteration are used, while for connector vectors that have not been calculated yet in the second iteration, the values from a previous iteration are used

$$\begin{aligned} \mathbf{Q}_{i,2}(t+\delta t) + \frac{2\delta t}{\zeta}\mathbf{F}^{\mathrm{spr}}\big(\mathbf{Q}_{i,2}(t+\delta t)\big) &= \mathbf{Q}_i(t) + \frac{1}{2}\boldsymbol{\kappa}\cdot\big(\mathbf{Q}_i(t) + \mathbf{Q}_{i,1}(t+\delta t)\big)\delta t \\ &+ \frac{\delta t}{\zeta}\Big[\mathbf{F}^{\mathrm{spr}}\big(\mathbf{Q}_{i+1}(t)\big) + \mathbf{F}^{\mathrm{spr}}\big(\mathbf{Q}_{i-1,2}(t+\delta t)\big) + \mathbf{B}_i(t)\Big] \ . \end{aligned} \tag{2.19}$$

Note that one of the spring forces has been moved to the left hand side and is being treated implicitly. We must solve this nonlinear equation for $\mathbf{Q}_{i,2}(t+\delta t)$. Note however that the right hand side is simply a sum over known quantities, and can be written for the purposes of solving the nonlinear equation as a vector $\mathbf{R}$. We will be solving this same nonlinear equation many times, but with different values of $\mathbf{R}$. For this reason, it is beneficial to generate a lookup table for the solutions to this nonlinear equation. We will return to the use of a lookup table.

Iterations $j \geq 3$ proceed like iteration 2 except for one slight change

$$\begin{aligned}\mathbf{Q}_{i,j}(t+\delta t) + \frac{2\delta t}{\zeta}\mathbf{F}^{\text{spr}}\big(\mathbf{Q}_{i,j}(t+\delta t)\big) &= \mathbf{Q}_i(t) + \frac{1}{2}\boldsymbol{\kappa}\cdot\big(\mathbf{Q}_i(t) + \mathbf{Q}_{i,j-1}(t+\delta t)\big)\delta t \\ &+ \frac{\delta t}{\zeta}\Big[\mathbf{F}^{\text{spr}}\big(\mathbf{Q}_{i+1,j-1}(t+\delta t)\big) + \mathbf{F}^{\text{spr}}\big(\mathbf{Q}_{i-1,j}(t+\delta t)\big) + \mathbf{B}_i(t)\Big] .\end{aligned} \tag{2.20}$$

After iterations $j \geq 3$ a residual error between iterations is calculated as

$$\epsilon = \sqrt{\sum_{i=1}^{N-1}\big(\mathbf{Q}_{i,j}(t+\delta t) - \mathbf{Q}_{i,j-1}(t+\delta t)\big)^2} . \tag{2.21}$$

The iterations are stopped when this ϵ is below a specified tolerance. We have chosen a tolerance of 10^{-6} times the fully-extended length of a single spring. Note that it should be verified that the tolerance is small enough such that the results are independent of the size of the tolerance.

Let us pause here to review the result of the semi-implicit method. The Brownian force contribution is treated in a explicit manner. Note that the Brownian force is evaluated once, during the first iteration, and the same value is used for all subsequent iterations. The flow force is treated in a type of midpoint algorithm. The flow force used is the average between the explicit force and the force at the next to last iteration. However, because the iterations have converged, the next to last iteration value and the final value are essentially the same. Therefore, the flow force is essentially an average between the initial force and final force. The spring force for the current connector vector i and the previous vector $i-1$ in the current iteration are treated implicitly. The spring force in the next connector vector $i+1$ (not yet calculated in the current iteration) is used from the previous iteration. Since the iterations have converged, this is essentially like calculating all spring forces implicitly. Therefore, by construction, each spring will not be beyond the fully-extended length of a spring.

The final issue to discuss in terms of the semi-implicit method is solving the nonlinear equation and the use of a look up table. Recall the equation to be solved is

$$\mathbf{Q} + \frac{2\delta t}{\zeta}\mathbf{F}^{\text{spr}}(\mathbf{Q}) = \mathbf{R} . \tag{2.22}$$

Because $\mathbf{F}^{\text{spr}}(\mathbf{Q})$ is parallel to $\mathbf{Q}$, we can deduce that $\mathbf{R}$ is also parallel and reduce the equation to a scalar equation by taking the dot product with a unit vector in the direction of $\mathbf{Q}$. We now can consider the scalar equation

$$Q + \frac{2\delta t}{\zeta}F^{\text{spr}}(Q) = R , \tag{2.23}$$

where Q is the magnitude of the vector $\mathbf{Q}$, R is the magnitude of the vector $\mathbf{R}$, and F^{spr} is the scalar spring force function defined by

$$F^{\text{spr}}(Q) = \mathbf{Q}\cdot\mathbf{F}^{\text{spr}}(\mathbf{Q})/Q . \tag{2.24}$$

Figure 2.1 shows a sketch of the solution to equation (2.23). The function is generally a smooth function which would lend itself to using a look up table with linear interpolation between points in the look up table. However, some issues must be noted and addressed. First, as the time step

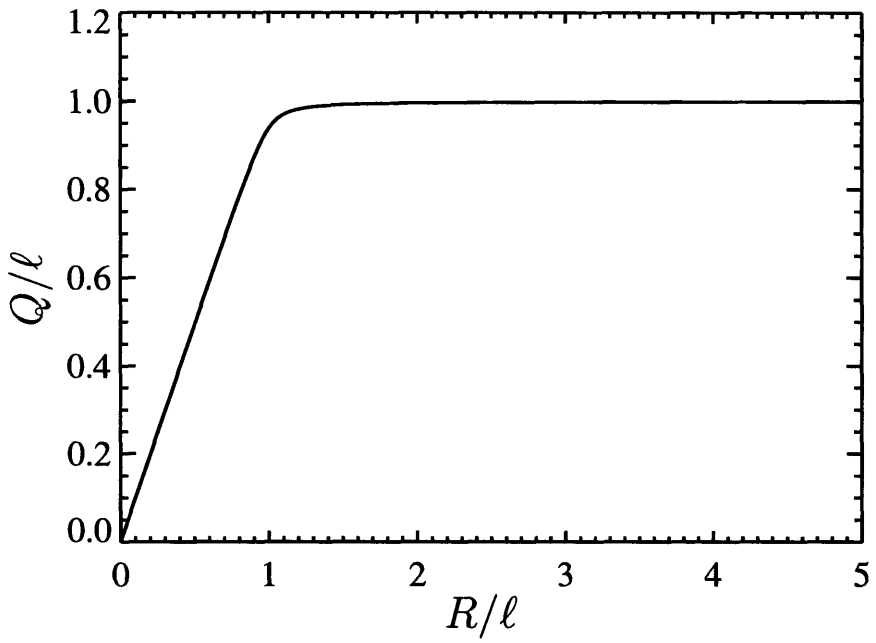

Fig. 2.1: *Sketch of the solution to the nonlinear equation for Q as a function of R used in the semi-implicit integration method, where ℓ is the fully-extended length of a spring.*

gets progressively smaller, the function has a sharp turn over from a slope of nearly 1 to a slope of nearly zero. This sharp turn over does not lend itself well to linear interpolation, and linearly interpolating in that region results in serious errors. Moreover, that is precisely the region of most importance because it is near full extension of the springs. The only times where the semi-implicit method is necessary is when the springs are near full extension. This can result in the strange result that as the time step is reduced, the error in the simulation actually increases because of the large error from the linear interpolation.

Another word of caution with respect to a look up table concerns the maximum value of R within the table. Because the range of R extends to infinity but the look up table is necessarily finite, a method must be devised to choose the maximum R value in the look up table and to deal with situations in which the R value needed in the simulation is larger than the maximum value in the look up table. We can deal with these issues by expanding Q for large R. This is done by expanding the left hand side of equation (2.23) as Q approaches the fully-extended length. This series can then be inverted to obtain the series expansion of Q for large R. If the value of R in the simulation is larger than in the look up table, a truncated series expansion is used. The maximum value of R in the look up table and the number of terms used in the truncated expansion must be determined such that the error in Q because of the use of the truncated series is small enough.

The last word of caution is concerning the accuracy required for Q, both in terms of the tolerance needed when generating the look up table, in terms of the linear interpolation and the

use of a truncated series at large R, and even when stopping the iterations with ϵ. When solving the nonlinear equation for Q, it is not only sufficient to specify a tolerance on the accuracy of Q. In addition to knowing Q accurately, it is also necessary to know the spring force accurately. Because the spring force law diverges, it is sensitive to small changes in the spring length. We can calculate the change in the spring force due to a change in the spring length using the derivative

$$\Delta F^{spr} \simeq \frac{\partial F^{spr}}{\partial Q} \Delta Q \ . \tag{2.25}$$

This can be written as

$$\frac{\Delta F^{spr}}{F^{spr}} \simeq \frac{Q}{F^{spr}} \frac{\partial F^{spr}}{\partial Q} \frac{\Delta Q}{Q} \ , \tag{2.26}$$

which means that

$$\text{(relative error in F)} \simeq \frac{Q}{F^{spr}} \frac{\partial F^{spr}}{\partial Q} \text{(relative error in Q)} \ . \tag{2.27}$$

Typically force laws are proportional to extension for small extensions, $F \propto Q$, which results in

$$\text{(relative error in F)} \simeq \text{(relative error in Q)} \ . \tag{2.28}$$

However, force laws will diverge near full extension, $F \propto (\ell - Q)^{-n}$, which results in

$$\text{(relative error in F)} \simeq \frac{nQ}{\ell - Q} \text{(relative error in Q)} \ . \tag{2.29}$$

The key point here is that when Q is very close to the maximum extension, the relative error in the spring force becomes very large. In order to have a small relative error in the force, which we require, the relative error in the extension must be very small. When solving equation (2.23) for Q, it is important to keep in mind the accuracy to which Q must be known in order to have an accurate solution.

CHAPTER 3

Force-extension Behavior

As was mentioned in the introduction, one of the most important and widely known properties of polymers is elasticity, and in particular the presence of an "entropic restoring force." Furthermore, with the advent of optical and magnetic tweezer technologies, much more attention is being paid to the relation between force and extension [55]. In particular, these experiments have been used to test polymer models which are then used in other contexts. *Making quantitative calculations of the force-extension behavior of bead-spring chains for comparison with the polymers they represent is the goal of this chapter.* This chapter was reproduced in part with permission from Underhill, P.T. and Doyle, P.S., *J. Non-Newtonian Fluid Mech.*, **122**, 3 (2004), copyright 2004 Elsevier B.V.

3.1 System Definition

The typical set-up used to calculate the restoring force using statistical mechanics is shown in Figure 3.1. One end of the polymer is tethered at the origin, and a constant external force, f, is applied to the other end of the polymer. The direction of this constant force defines the z-direction of the coordinate system. The x and y coordinates are therefore in the plane perpendicular to the applied force. The expectation value of the polymer's z displacement, $\langle z \rangle$, can be calculated as a function of the applied force. This function, $\langle z \rangle$ vs. f, defines the polymer's force-extension (F-E) behavior. Note that this is different from the behavior found by performing the analysis shown in Figure 3.2, in which the ends of the polymer are held fixed at points that are z (or equivalently r)

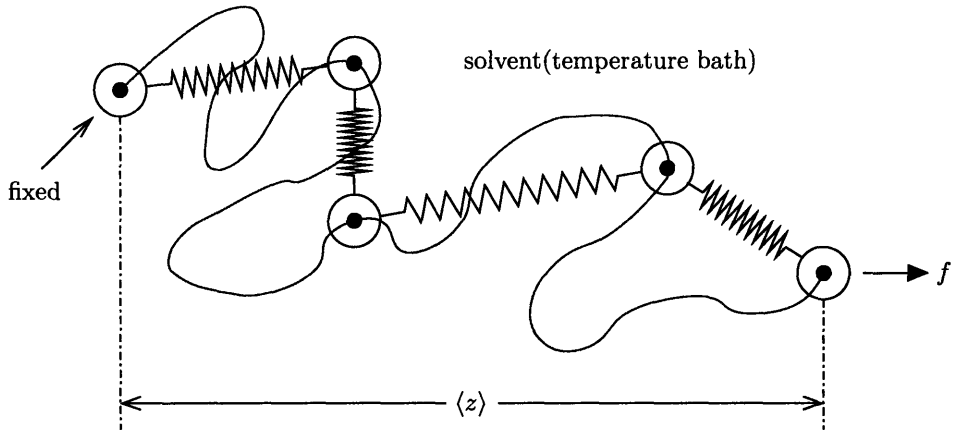

Fig. 3.1: *Illustration of a polymer and bead-spring model in the constant force ensemble. One end is held fixed, while a constant force is applied to the free end. The direction of the force defines the z-direction. The z-displacement of the chain is averaged.*

distance apart and the average force, $\langle f \rangle$, to hold them at those positions is calculated. Because the former approach is more computationally tractable than the latter, it has been the preferred approach by previous investigators using bead-spring chains, and it will be the approach initially used here. See Chapter 4 for a more detailed comparison of the two approaches.

When developing a bead-spring model for the polymer, it is crucial to verify that the model accurately describes the polymer. Because the concept of replacing the polymer by a bead-spring chain is largely motivated by the F-E behavior, it seems natural to verify the accuracy of the coarse-graining by requiring that the F-E behavior of the bead-spring chain is the same as the polymer it represents. However, it is also critical that the bead-spring chain is compared to the polymer using the exact same "experiment." Since the polymer behavior is calculated by applying a constant force, as shown in Figure 3.1, the bead-spring behavior will be calculated in the same way.

3.2 Decoupled Springs

Because the bead-spring model is in the $(N_p)fT$ ensemble (the number of polymers N_p is trivially held constant at one), the effective Hamiltonian is obtained by performing a Legendre Transform from z to f [45]. Thus the effective Hamiltonian is

$$\mathcal{H}_{\text{eff}} = U - f z_{\text{tot}} \ , \tag{3.1}$$

where U is the potential energy of the bead-spring system (recall that all kinetic energy has been dropped), and z_{tot} is the z coordinate of the end of the chain. For all the systems considered here, the potential energy will have no bending potentials, and the energy for each spring will only

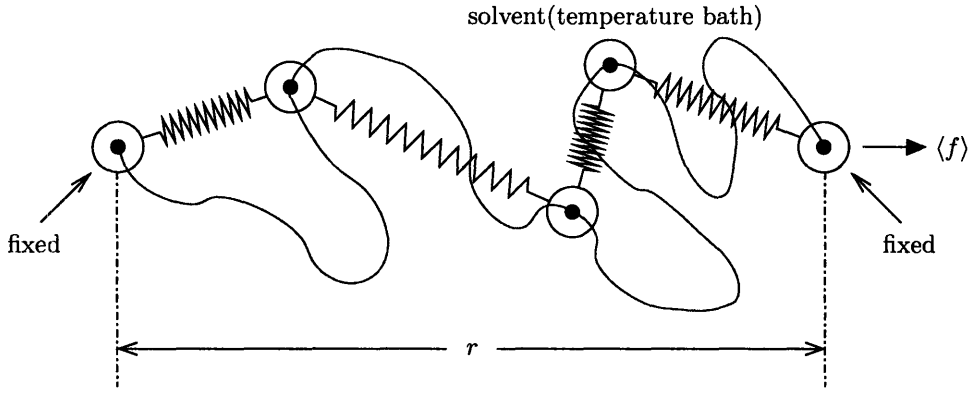

Fig. 3.2: *Illustration of a polymer and bead-spring model in the constant extension ensemble. Both ends are held fixed at a distance r apart. The external force required to hold one of the ends fixed is averaged.*

depend on the magnitude of extension. It should then be clear that the effective Hamiltonian can be separated into a sum over each spring

$$\mathcal{H}_{\text{eff}} = \sum_j \left[U_{\text{s}}(r_j) - f z_j\right] \ , \tag{3.2}$$

where j denotes each spring, $U_{\text{s}}(r_j)$ is the potential energy of each spring as a function of the radial extension of the spring, and z_j is the z displacement of spring j. Because the effective Hamiltonian can be decomposed into a sum over each spring, the partition function for the whole chain, $\mathcal{Z}_{\text{w}}$, splits into a product of the partition functions for single springs, $\mathcal{Z}_{\text{s}}$,

$$\mathcal{Z}_{\text{w}} = (\mathcal{Z}_{\text{s}})^{N_{\text{s}}} \ , \tag{3.3}$$

where N_{s} is the number of springs in the chain, and $\mathcal{Z}_{\text{s}}$ is given by

$$\mathcal{Z}_{\text{s}} = \int \exp\left[\frac{-U_{\text{s}}(r) + fz}{k_{\text{B}}T}\right] \mathrm{d}^3 r \ . \tag{3.4}$$

This separation of the partition function has two important consequences. First, the computational effort needed to calculate the F-E behavior is greatly reduced because the properties of any size chain can be determined by knowing the properties of a *single spring* (a single integral). Second, it illustrates that for this set of conditions the springs are decoupled. In particular, it will be shown later that the F-E behavior of these bead-spring chain models does not depend explicitly on the number of beads, which act as free hinges, but only depends on the level of coarse-graining for each spring. This is counter to other investigators who have argued the importance of the number of springs in the bead-spring chain model [33].

Table 3.1: *Summary of dimensionless parameters*

parameter	definition	physical interpretation
$\hat{z}_{\text{tot}}$	$\frac{z_{\text{tot}}}{L}$	total z-displacement as fraction of contour length
$\hat{r}$	$\frac{r}{\ell}$	radial single spring displacement as fraction of fully-extended length
$\hat{f}$	$\frac{fA_{\text{true}}}{k_{\text{B}}T}$	externally applied force in units of $k_{\text{B}}T$ divided by true persistence length
α	$\frac{L}{A_{\text{true}}}$	number of true persistence lengths in polymer's contour length
λ	$\frac{A_{\text{eff}}}{A_{\text{true}}}$	effective persistence length in units of the true persistence length
ν	$\frac{\ell}{A_{\text{true}}}$	number of true persistence lengths represented by each spring
$\widehat{U}_{\text{eff}}(\hat{r})$	$\frac{U_{\text{eff}}(r)}{k_{\text{B}}T}\frac{\lambda}{\nu}$	potential energy of a spring in units of $k_{\text{B}}T$ times the number of effective persistence lengths represented by each spring

3.3 Dimensionless Parameters

In describing the the behavior of bead-spring chains it is useful to define a set of dimensionless variables. Many of these variable transformations are motivated by the worm-like chain (WLC) force law, which is the force law that correctly describes the behavior of dsDNA. Specifically the transformations are motivated by the interpolation formula approximation to the WLC by Marko and Siggia [18]. However, it must be noted that the formula remain general, as will be shown later in Section 3.9. A summary of these parameters and their physical interpretations is given in Table 3.1. These dimensionless variables are

$$\begin{aligned} \hat{z}_{\text{tot}} \equiv \frac{z_{\text{tot}}}{L}\ ,\ \hat{r} \equiv \frac{r}{\ell}\ ,\ \hat{f} \equiv \frac{fA_{\text{true}}}{k_{\text{B}}T} \\ \alpha \equiv \frac{L}{A_{\text{true}}}\ ,\ \lambda \equiv \frac{A_{\text{eff}}}{A_{\text{true}}}\ ,\ \nu \equiv \frac{\alpha}{N_{\text{s}}} = \frac{\ell}{A_{\text{true}}}\ , \end{aligned} \tag{3.5}$$

where L is the contour length of the chain, $\ell \equiv L/N_{\text{s}}$ is the fully extended length of a spring, A_{true} is the true persistence length of the polymer, α is the number of true persistence lengths in the polymer's contour, A_{eff} is the effective persistence length, λ is the ratio of the effective persistence length to the true persistence length, and ν is the number of true persistence lengths represented by each spring. It is also useful to define two energy functions. First, we will denote as $U_{\text{eff}}(r)$ the spring potential, $U_{\text{s}}(r)$, with all additive constants dropped. This is done as a convenience and changes no results. Second, a dimensionless energy is defined as

$$\widehat{U}_{\text{eff}}\left(\hat{r}\right) = \frac{U_{\text{eff}}(r)}{k_{\text{B}}T}\frac{\lambda}{\nu}\ . \tag{3.6}$$

It will become clear later that this scaling is the one appropriate for the spring potential, in which it is scaled by $k_{\text{B}}T$ times the number of effective persistence lengths represented by each spring.

3.4 Force-extension Results

The F-E behavior is now calculated using a general result based on equations (2.3), (2.4), and (3.1):

$$\langle z_{\text{tot}} \rangle = k_{\text{B}}T \frac{\partial}{\partial f} \ln \mathcal{Z} \ . \tag{3.7}$$

For bead-spring chains in particular, for which $\mathcal{Z} \rightarrow \mathcal{Z}_{\text{w}}$, using equation (3.3) and non-dimensionalizing with equation (3.5) shows that

$$\langle \hat{z}_{\text{tot}} \rangle_{\text{m}} = \frac{1}{\nu} \frac{\partial}{\partial \hat{f}} \ln \mathcal{Z}_{\text{s}} \ , \tag{3.8}$$

where the m-subscript on the mean fractional extension is used to signify that it is for the bead-spring model. The angular integration for the single spring partition function can be performed, resulting in the following formula for the mean fractional extension

$$\langle \hat{z}_{\text{tot}} \rangle_{\text{m}} = \frac{1}{\nu} \left\{ \frac{-1}{\hat{f}} + \frac{\partial}{\partial \hat{f}} \ln \left(\int_0^1 \mathrm{d}\hat{r} \ \hat{r} \ \sinh\left[\nu \hat{f} \hat{r}\right] \exp\left[\frac{-\nu}{\lambda} \widehat{U}_{\text{eff}}(\hat{r}) \right] \right) \right\} \ . \tag{3.9}$$

This shows explicitly that the F-E behavior of the model depends parametrically only on ν and λ, but not explicitly on the number of springs, N_{s}. This means that a polymer with $\alpha = 400$ represented by 40 springs has an *identical* F-E behavior as a polymer with $\alpha = 10$ represented by 1 spring because both have $\nu = 10$.

At this point it is useful to apply these definitions to the Marko and Siggia interpolation formula. It should be noted that within the context of this Chapter the differences between the interpolation formula and the exact numerical solution for the WLC are unimportant. Thus the polymer modeled by our so-called WLC model is not quantitatively the "true" WLC, but is a hypothetical polymer for which the Marko and Siggia formula is exact. For this polymer, the F-E behavior is given by [18]

$$\hat{f} = \langle \hat{z}_{\text{tot}} \rangle_{\text{p}} - \frac{1}{4} + \frac{1}{4\left(1 - \langle \hat{z}_{\text{tot}} \rangle_{\text{p}}\right)^2} \ , \tag{3.10}$$

where the p-subscript on the mean fractional extension signifies that it is the exact value for the polymer (to separate it from the behavior of the bead-spring model). It has been conventional for this behavior to directly motivate the following choice for the spring force law

$$f_{\text{spring}}(r) = \left(\frac{k_{\text{B}}T}{A_{\text{eff}}} \right) \left\{ \left(\frac{r}{\ell} \right) - \frac{1}{4} + \frac{1}{4(1 - \frac{r}{\ell})^2} \right\} \ . \tag{3.11}$$

It should be emphasized that this *assumption* has replaced the mean fractional z projection of the polymer with the fractional radial extension of the spring. The true persistence length appearing in the polymer behavior has also been replaced by the effective persistence length in the spring force law to use as a "correction-factor." Integrating the spring force law gives the effective spring potential

$$U_{\text{eff}}(r) = k_{\text{B}}T \left(\frac{\ell}{A_{\text{eff}}} \right) \left\{ \frac{1}{2} \left(\frac{r}{\ell} \right)^2 - \frac{1}{4} \left(\frac{r}{\ell} \right) + \frac{1}{4(1 - \frac{r}{\ell})} \right\} \ , \tag{3.12}$$

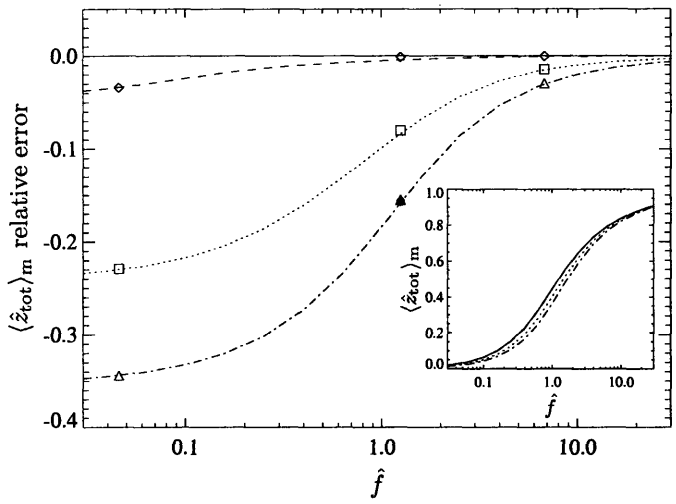

Fig. 3.3: *Calculation of the relative error of the mean fractional extension,* $(\langle \hat{z}_{tot} \rangle_m - \langle \hat{z}_{tot} \rangle_p)/\langle \hat{z}_{tot} \rangle_p$, *for a bead-spring model as the level of coarse-graining changes. The Marko and Siggia potential was used with* $\lambda = 1$. *The curves correspond to* $\nu = 400$ *(*dashed*),* $\nu = 20$ *(*dotted*), and* $\nu = 10$ *(*dash-dot*). The symbols represent Brownian dynamics simulations. The single spring simulations correspond to* $\nu = 400$ *(*◇*),* $\nu = 20$ *(*□*), and* $\nu = 10$ *(*△*). The twenty spring simulation corresponds to* $\nu = 10$ *(*•*).* Inset*: The mean fractional extension of the models compared with the "true polymer" (*solid line*, equation* (3.10)*).*

which results in a dimensionless energy of

$$\widehat{U}_{\text{eff}}(\hat{r}) = \frac{\hat{r}^2}{2} - \frac{\hat{r}}{4} + \frac{1}{4(1-\hat{r})} \,. \tag{3.13}$$

Specific examples of F-E behavior, calculated using both equation (3.9) and BD simulations, can be seen in Figure 3.3 as the level of coarse-graining, ν, is changed. The spring potential used is the Marko and Siggia interpolation formula (equation (3.13)), and for all examples in the figure the effective persistence length equals the true persistence length ($\lambda = 1$). Most of the Brownian dynamics simulations were performed using a single spring for simplicity. However, we calculate one of the points also using twenty springs to explicitly show dependence only on the level of coarse-graining, ν.

The fact that the F-E curve for a bead-spring model changes as more springs are added for a fixed contour length has been seen before [33]. However, the conventional explanation for this discrepancy is that the introduction of more springs directly introduces extra flexibility, which pulls in the end of chain, resulting in a shorter extension for the same force. From equation (3.9) we see that this can not be fully correct because the absolute number of springs never appears, only the

level of discretization of each spring. *Thus the force-extension curve of a bead-spring chain under any conditions can be understood by only considering the behavior of a single spring, and how its force-extension behavior changes as the number of persistence lengths it represents changes.*

3.5 Phase Space Visualization

To get a better physical understanding of why the F-E behavior deviates from the polymer, let us examine the probability density function over the configuration space. In general for a bead-spring chain the phase space has too many dimensions to visualize easily. However as we just saw the F-E behavior can be understood by looking at a single spring, which has a phase space of only three dimensions.

Recall that the probability density is proportional to

$$\exp\left[\frac{-\mathcal{H}_{\text{eff}}}{k_{\text{B}}T}\right] , \tag{3.14}$$

so that only configurations near the minimum of the effective Hamiltonian contribute significantly to the average. The configurations that contribute must have a $\mathcal{H}_{\text{eff}}$ less than $k_{\text{B}}T$ above the minimum

$$\mathcal{H}_{\text{eff}} = (\mathcal{H}_{\text{eff}})_{\text{min}} + O(k_{\text{B}}T) . \tag{3.15}$$

For the case of a single spring as considered here the effective Hamiltonian is

$$\mathcal{H}_{\text{eff}} = U_{\text{eff}}(r) - fz = k_{\text{B}}T\nu\left(\frac{\widehat{U}_{\text{eff}}(\hat{r})}{\lambda} - \hat{f}\hat{z}\right) , \tag{3.16}$$

and therefore the important configurations are determined by

$$\widehat{\mathcal{H}}_{\text{eff}} \equiv \left(\frac{\widehat{U}_{\text{eff}}(\hat{r})}{\lambda} - \hat{f}\hat{z}\right) = \left(\frac{\widehat{U}_{\text{eff}}(\hat{r})}{\lambda} - \hat{f}\hat{z}\right)_{\text{min}} + O\left(\frac{1}{\nu}\right) , \tag{3.17}$$

where we have defined a dimensionless effective Hamiltonian, $\widehat{\mathcal{H}}_{\text{eff}}$. From equation (3.17) we see that $\frac{1}{\nu}$ plays a similar role in the F-E behavior as temperature usually does in statistical mechanics, determining the magnitude of fluctuations in phase space about the minimum. A detailed and quantitative description of fluctuations will be performed later in Section 3.7. Here we will discuss how the portion of phase space the system samples (fluctuates into) with significant probability determines the mean extension. In the limit $\nu \to \infty$, the system is "frozen-out" into the state of minimum $\widehat{\mathcal{H}}_{\text{eff}}$. Note that as $\nu \to \infty$, the polymer becomes infinitely long. By calculating the *fractional* extension, we are scaling all lengths by the contour length. Thus even though the fluctuations may not be getting small if a different length scale were used (such as the radius of gyration), the fluctuations of the end-to-end distance do go to zero compared to the contour length. Alternatively in the limit $\nu \to 0$, the system is equally likely to be in any state, and thus the mean fractional extension of the bead-spring chain, $\langle \hat{z}_{\text{tot}} \rangle_{\text{m}}$, approaches zero.

In order to understand the behavior at intermediate ν, Figure 3.4 shows a contour plot of $\widehat{\mathcal{H}}_{\text{eff}}$ for the four cases $\hat{f} = 0.444$, $\hat{f} = 5$, $\lambda = 1$, and $\lambda = 1.5$, and the Marko and Siggia spring potential (equation (3.13)). The contour lines correspond to lines of constant $\widehat{\mathcal{H}}_{\text{eff}}$ within the $\hat{x}$-$\hat{z}$ plane. Note

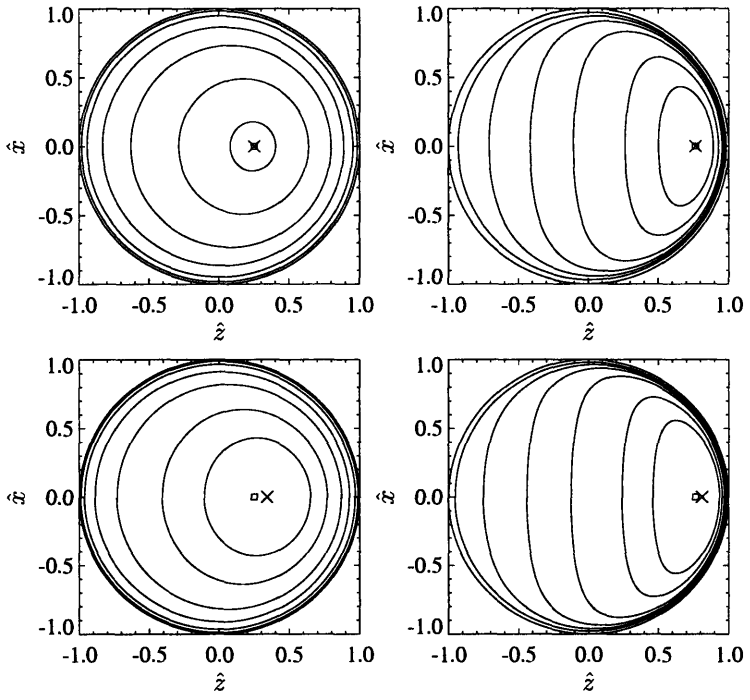

Fig. 3.4: *Visualization of phase space using contours of constant* $\widehat{\mathcal{H}}_{\text{eff}}$ *for a single spring with the Marko and Siggia potential. The square (□) represents the position of the "true polymer" mean fractional extension,* $\langle \hat{z}_{\text{tot}} \rangle_{\text{p}}$*. The cross (×) represents the position of minimum* $\widehat{\mathcal{H}}_{\text{eff}}$*.* Upper left*:* $\hat{f} = 0.444$, $\lambda = 1$ Lower left*:* $\hat{f} = 0.444$, $\lambda = 1.5$ Upper right*:* $\hat{f} = 5$, $\lambda = 1$ Lower right*:* $\hat{f} = 5$, $\lambda = 1.5$

that because all directions perpendicular to $\hat{z}$ are equivalent, rotating the contour lines about the $\hat{z}$ axis produces surfaces in the three-dimensional phase space with constant $\widehat{\mathcal{H}}_{\text{eff}}$. While $\widehat{\mathcal{H}}_{\text{eff}}$, and therefore the contour plots, are independent of ν, they can be used to understand the behavior at different values of ν because of equation (3.17). The value of ν governs the size of the fluctuations around the minimum, and thus the number of contour lines above the minimum the system samples with significant probability. We also see that each of the $\widehat{\mathcal{H}}_{\text{eff}}$ contours is not symmetric about the minimum of $\widehat{\mathcal{H}}_{\text{eff}}$, causing the mean extension of the bead-spring chain, $\langle \hat{z}_{\text{tot}} \rangle_{\text{m}}$, to deviate from the point of minimum $\widehat{\mathcal{H}}_{\text{eff}}$. For $\lambda = 1$ the minimum of $\widehat{\mathcal{H}}_{\text{eff}}$ corresponds to the mean extension of the true polymer, $\langle \hat{z}_{\text{tot}} \rangle_{\text{p}}$. This is because of the way of choosing the spring potential from the true polymer behavior as illustrated with equations (3.10) through (3.13). As λ is increased, the position of the minimum moves to larger $\hat{z}$ while the depth of the minimum increases. The minimum also moves to larger $\hat{z}$ and deepens when the force is increased. These plots explain why as $\nu \to \infty$ the bead-spring chain behavior only approaches the true polymer behavior if $\lambda = 1$, why as $\nu \to 0$ the mean fractional extension approaches zero, and why for intermediate ν there may exist a value of

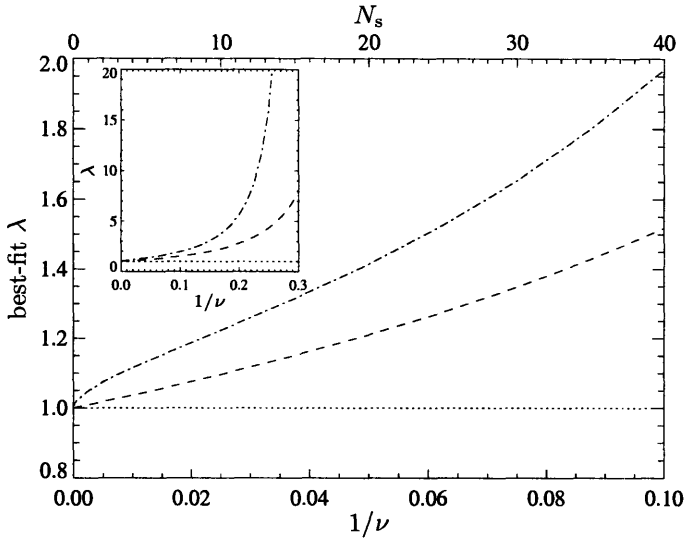

Fig. 3.5: *Calculation of λ for the three different criteria at different levels of coarse-graining for the Marko and Siggia potential. The criteria shown are low-force (*dash-dot*), half-extension (*dashed*), and high-force (*dotted*).* Upper axis*: The level of coarse-graining in terms of the number of springs, N_s, for a polymer with $\alpha = 400$ (approximately λ-phage DNA stained with YOYO at 4 bp:1 dye molecule).* Inset*: Expanded view showing the divergence of the criteria.*

λ for which the mean fractional extension matches the true polymer.

3.6 Effective Persistence Length

Now that we understand better the reasons why the F-E curve deviates from the true polymer F-E curve, we would like to change the model to get closer agreement. A very simple method that has been used by previous investigators [33] is to use a different persistence length in the spring force law (A_{eff}) from the true persistence length of the polymer (A_{true}), i.e. $\lambda \neq 1$. In particular, if λ is increased, the extension of the chain also increases, back to the extension of the true polymer. The conventional explanation for this is that the free hinges in the bead-spring chain have introduced extra flexibility. To counter-act the flexibility introduced by the hinges, the stiffness of the springs must be increased by increasing the effective persistence length. Let us now analyze the effect of increasing λ within the framework presented above. Looking at equation (3.9) shows that increasing λ acts to decrease the spring potential energy. Because the spring gets weaker (less stiff), it is not surprising that the extension gets larger. It should be noted that for infinitely long polymers increasing the persistence length causes a decrease in the restoring force.

Though it is true that by increasing λ from one the extension increases towards the true extension of the polymer, it does so non-uniformly. This means that there exists no value of λ such that the F-E curve exactly matches the true curve. It is unclear what value of λ to choose to give the

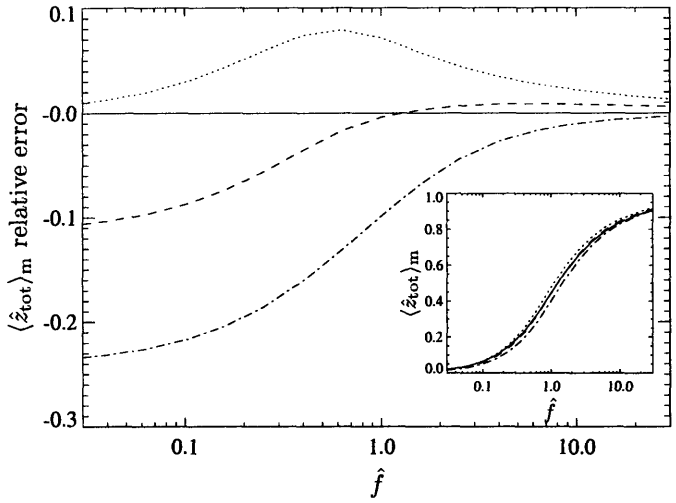

Fig. 3.6: *Calculation of the relative error of the mean fractional extension,* $(\langle \hat{z}_{tot} \rangle_m - \langle \hat{z}_{tot} \rangle_p)/\langle \hat{z}_{tot} \rangle_p$, *for a bead-spring model for different best fit criteria. The Marko and Siggia potential was used with* $\nu = 20$. *The curves correspond to* $\lambda = 1.41$ *(low-force,* dotted*),* $\lambda = 1.21$ *(half-extension,* dashed*), and* $\lambda = 1$ *(high-force,* dash-dot*).* Inset*: The mean fractional extension of the models compared with the "true polymer" (*solid line*, equation* (3.10)*).*

"best fit" between the model curve and the true curve. We will present here an analysis of possible choices and place bounds on the range of choices. The first criterion that might come to mind is some type of integrated sum of squared error. However, that quantity becomes very cumbersome to manipulate analytically and it is unclear that it is any better of a criterion than another. The criteria that we will consider looks at matching exactly one section of the F-E curve. The three sections are at zero applied force, at infinite applied force, and at the applied force for which the true polymer has a mean fractional extension of 0.5. Before calculations can be made of the "best-fit" λ in each region, the exact meaning of matching the true polymer behavior must be specified. The half-extension criterion is straight-forward: we will require that the model and polymer curves are equal at the point where the polymer is at half extension. The other two criteria are more subtle because the model and polymer become equal at zero and infinite force for all values of λ. For the low-force criterion we will require that the slopes of the F-E curves be equal at zero force. It should be noted that this is equivalent to requiring that the relative error of the model goes to zero at zero force. Again, a similar criterion can not be used at infinite force because the slope (or relative error) will always be zero at infinite force independent of λ. Thus our infinite force criteria will be that the relative error of the slope of the F-E curve at infinite force will equal zero. Physically, this means that the fractional extension versus force curves approach one at infinite force in the same manner. Figure 3.5 shows a plot of the "best-fit" λ versus $\frac{1}{\nu}$ for each of the three criteria for the WLC force law.

It is important to mention that both the low-force and half-extension curves diverge for a finite

Table 3.2: *Table of properties for models of unstained λ-phage DNA. Models with 10, 20, and 40 springs are compared using three best-fit λ criteria. Unstained λ-phage DNA has the following properties:* $L = 16.3\,\mu\text{m}$, $A_{\text{true}} = 0.053\,\mu\text{m}$, *and* $\alpha = 307.5$.

N_s	ν	region	λ	$A_{\text{eff}}(\mu\text{m})$	$R_g(\mu\text{m})$	$\frac{\eta_{0,p}}{n_p(N\zeta)}(\mu\text{m}^2)$	$\frac{b_2}{n_p(N\zeta)^2/k_BT}(\mu\text{m}^4)$	$\frac{\tau_0}{(N\zeta)/k_BT}(\mu\text{m}^2)$
10	30.8	low	1.28	0.068	0.56	0.052	-0.0011	0.021
		mid	1.13	0.060	0.53	0.047	-0.00091	0.019
		high	1.0	0.053	0.50	0.042	-0.00074	0.017
20	15.4	low	1.55	0.082	0.55	0.050	-0.0010	0.020
		mid	1.29	0.068	0.51	0.044	-0.00077	0.018
		high	1.0	0.053	0.47	0.036	-0.00052	0.014
40	7.7	low	2.52	0.133	0.54	0.049	-0.00096	0.019
		mid	1.78	0.094	0.50	0.041	-0.00068	0.016
		high	1.0	0.053	0.42	0.029	-0.00034	0.012

$\frac{1}{\nu}$. This means that there exists a ν small enough such that the low-force or half-extension region can not be matched simply by adjusting λ. The position of these divergences can be calculated *exactly* in a simple manner as will be shown in Section 3.8. For the WLC the low-force curve diverges at $\nu^* = 10/3$ while the half-extension curve diverges at $\nu^* = 2.4827$. However the high-force curve is always $\lambda = 1$ for finite $\frac{1}{\nu}$.

To illustrate the difference between the three choices of λ, let us look at a specific example. Figure 3.6 shows the relative error in the mean fractional extension versus force for the WLC force law, three different values of λ, and $\nu = 20$. The three values of λ correspond to the three criteria shown in Figure 3.5. By comparing the relative error curves, we can see the entire range of effects λ has on the F-E behavior. The criteria at low and high force form a bound on the choices for a "best-fit" λ as seen in Figure 3.6, even if none of the criteria presented here is believed best.

As a further example we show the parameters that would be chosen to model λ-phage DNA at different levels of coarse-graining, as well as some properties of the models. These parameters could be used in a Brownian dynamics simulation to capture the non-equilibrium properties of λ-phage DNA. Tables 3.2, 3.3, and 3.4 show what effective persistence length to choose for the model for the different "best-fit" criteria and for different staining ratios of dye. The parameters were calculated by repeated application of Figure 3.5. The resulting properties of the model were calculated from formulae in Chapter 5. The contour length and persistence length for unstained λ-phage DNA were taken from Bustamante et al. [17]. We used that the contour length is increased by 4Å per bis-intercalated YOYO dye molecule [56], and we assumed that the persistence length of the stained molecule is the same as the unstained value.

In these tables we see examples of the expected general trends. As the polymer is more finely discretized, the number of persistence lengths represented by each spring, ν, decreases. This causes a larger spread in the possible choices for the effective persistence length, and thus a larger spread in properties. We see the general trend that the magnitude of the properties decreases as ν decreases. Note that for the low-force criterion, R_g and $\eta_{0,p}$ are exactly the "Rouse result." The "Rouse

Table 3.3: *Table of properties for models of λ-phage DNA stained with YOYO at 8 bp:1 dye molecule. Models with 10, 20, and 40 springs are compared using three best-fit λ criteria. 8 bp:1 dye λ-phage DNA has the following properties:* $L = 18.7\,\mu\text{m}$, $A_{\text{true}} = 0.053\,\mu\text{m}$, *and* $\alpha = 352.8$.

N_s	ν	region	λ	$A_{\text{eff}}(\mu\text{m})$	$R_g(\mu\text{m})$	$\frac{\eta_{0,p}}{n_p(N\zeta)}(\mu\text{m}^2)$	$\frac{b_2}{n_p(N\zeta)^2/k_BT}(\mu\text{m}^4)$	$\frac{\tau_0}{(N\zeta)/k_BT}(\mu\text{m}^2)$
10	35.3	low	1.25	0.066	0.60	0.060	-0.0015	0.025
		mid	1.11	0.059	0.57	0.054	-0.0012	0.022
		high	1.0	0.053	0.55	0.050	-0.0010	0.020
20	17.6	low	1.47	0.078	0.59	0.058	-0.0013	0.023
		mid	1.24	0.066	0.55	0.051	-0.0010	0.020
		high	1.0	0.053	0.51	0.043	-0.00073	0.017
40	8.8	low	2.18	0.116	0.58	0.056	-0.0013	0.022
		mid	1.62	0.086	0.54	0.048	-0.00091	0.019
		high	1.0	0.053	0.46	0.035	-0.00049	0.014

Table 3.4: *Table of properties for models of λ-phage DNA stained with YOYO at 4 bp:1 dye molecule. Models with 10, 20, and 40 springs are compared using three best-fit λ criteria. 4 bp:1 dye λ-phage DNA has the following properties:* $L = 21.1\,\mu\text{m}$, $A_{\text{true}} = 0.053\,\mu\text{m}$, *and* $\alpha = 398.1$.

N_s	ν	region	λ	$A_{\text{eff}}(\mu\text{m})$	$R_g(\mu\text{m})$	$\frac{\eta_{0,p}}{n_p(N\zeta)}(\mu\text{m}^2)$	$\frac{b_2}{n_p(N\zeta)^2/k_BT}(\mu\text{m}^4)$	$\frac{\tau_0}{(N\zeta)/k_BT}(\mu\text{m}^2)$
10	39.8	low	1.22	0.065	0.64	0.068	-0.0019	0.028
		mid	1.10	0.058	0.61	0.062	-0.0016	0.025
		high	1.0	0.053	0.58	0.057	-0.0013	0.023
20	19.9	low	1.42	0.075	0.62	0.065	-0.0017	0.026
		mid	1.21	0.064	0.59	0.058	-0.00013	0.023
		high	1.0	0.053	0.54	0.049	-0.00097	0.020
40	9.95	low	1.98	0.105	0.62	0.064	-0.0016	0.025
		mid	1.52	0.081	0.57	0.054	-0.0012	0.022
		high	1.0	0.053	0.50	0.041	-0.00067	0.016

Result" is the value of the Rouse model if the spring constant is taken to be the zero-extension slope of the *spring* force law. The "Rouse result" will be discussed in more detail in Chapter 5. The only difference from the "true polymer" is that the mass and drag are localized at the beads instead of along a continuous contour. This is true until ν reaches the point of divergence of the low-force criterion. However, b_2 and τ_0 are only approximately the "Rouse result" as discussed in Chapter 5. The properties for the other best-fit criteria have even smaller magnitude than the low-force criterion. This decrease is due to an error in the zero-force slope of the force-extension curve, and thus a smaller coil size.

3.7 Fluctuations

In addition to discussing the F-E behavior of the model, it is important to discuss the fluctuations around the mean extension. We have already seen the use of fluctuations thus far. In Section 3.5 we saw how examining fluctuations can help us better understand the *mean* extension. The fluctuations in the F-E behavior are also important in trying to extend our understanding from the F-E behavior of the bead-spring chains to the behavior in a flow field. For a bead-spring chain in a flow field, the fluctuations of the chain determine how much of the flow field the chain can sample. In turn this determines the total force applied to the chain by the flow. This is particularly important in shear flow, in which the fluctuation of the chain in the shear gradient direction plays a central role [57, 58].

It is shown in Appendix A.1 that the fluctuations can be calculated as

$$(\delta\hat{z})^2 = \left\langle \left(\hat{z}_{\text{tot}} - \langle \hat{z}_{\text{tot}} \rangle_{\text{m}}\right)^2 \right\rangle_{\text{m}} = \frac{1}{N_{\text{s}}\,\nu} \frac{\partial}{\partial \hat{f}} \langle \hat{z}_{\text{tot}} \rangle_{\text{m}} = \frac{1}{\alpha} \frac{\partial}{\partial \hat{f}} \langle \hat{z}_{\text{tot}} \rangle_{\text{m}} \ , \tag{3.18}$$

$$(\delta\hat{x})^2 = \left\langle \left(\hat{x}_{\text{tot}}\right)^2 \right\rangle_{\text{m}} = \left\langle \left(\hat{y}_{\text{tot}}\right)^2 \right\rangle_{\text{m}} = \frac{1}{N_{\text{s}}\,\nu\,\hat{f}} \langle \hat{z}_{\text{tot}} \rangle_{\text{m}} = \frac{1}{\alpha\,\hat{f}} \langle \hat{z}_{\text{tot}} \rangle_{\text{m}} \ , \tag{3.19}$$

where we have defined the root-mean-squared fluctuations as $\delta\hat{z}$ and $\delta\hat{x}$. One important thing to notice about the fluctuations is that once the F-E behavior is known ($\langle \hat{z}_{\text{tot}} \rangle_{\text{m}}$ versus $\hat{f}$), the fluctuations can be calculated directly without performing any further integrations. In fact, both types of fluctuations can be calculated by finding the slope of a line on the F-E curve, as seen in Figure 3.7. From the figure we see that the longitudinal fluctuations are proportional to the slope of the curve, while the lateral fluctuations are proportional to the slope of the line connecting the point of the F-E curve to the origin. Because the F-E curve is concave, *the lateral fluctuations are always greater than or equal to the longitudinal fluctuations.*

Another important aspect of equations (3.18) and (3.19) is that the fluctuations depend explicitly on the number of springs in the chain, unlike the F-E curve which just depends on the level of coarse-graining for each spring. In fact we see the expected scaling of the root-mean-squared fluctuations as $\alpha^{-1/2}$. Since the persistence length is the length-scale over which the polymer backbone loses correlation, the fluctuation of the polymer length should scale like a sum of "independent" random variables. The number of these "independent" random variables is precisely the number of persistence lengths in the polymer contour, α. We show in Figures 3.8 and 3.9 plots of the root-mean-squared fluctuations for the same cases for which we showed the F-E behavior in Figure 3.3. We have scaled the fluctuations by $\alpha^{1/2}$ to collapse the fluctuations of different length chains onto the same curve. The fluctuations after this scaling only depend on the number of

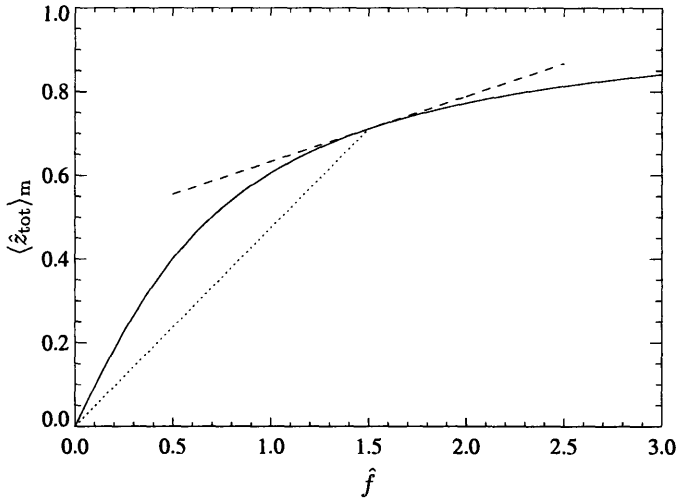

Fig. 3.7: *Graphical illustration of longitudinal and transverse fluctuations. For a given force $\hat{f}$, the longitudinal fluctuations are proportional to the slope of the tangent curve (*dashed*). The transverse fluctuations are proportional to the slope of the chord (*dotted*) connecting the origin to the point on the force-extension curve.*

persistence lengths represented by each spring, ν, and the ratio of the effective persistence length to the true persistence length, λ.

Note that it is easy to calculate exactly the high-force scalings for the fluctuations using equations (3.18) and (3.19) and our knowledge of the high-force scaling for $\langle \hat{z}_{tot} \rangle_m$. It is easy to show that for bead-spring chains using the Marko and Siggia potential (equation (3.13)) the high-force scaling is

$$\langle \hat{z}_{tot} \rangle_m \overset{\hat{f}\to\infty}{\sim} 1 - \frac{1}{2\lambda^{1/2}\hat{f}^{1/2}} + O\left(\frac{1}{\hat{f}}\right) . \tag{3.20}$$

Using this result, we can show that

$$\alpha^{1/2}\,\delta\hat{z} \overset{\hat{f}\to\infty}{\sim} \frac{1}{2\lambda^{1/4}\hat{f}^{3/4}} + O\left(\frac{1}{\hat{f}^{5/4}}\right) , \tag{3.21}$$

$$\alpha^{1/2}\,\delta\hat{x} \overset{\hat{f}\to\infty}{\sim} \frac{1}{\hat{f}^{1/2}} + O\left(\frac{1}{\hat{f}}\right) . \tag{3.22}$$

Of particular interest are the fluctuations at "equilibrium" (zero applied force) because it relates to the size of the polymer coil. In the context of the F-E behavior, these fluctuations at equilibrium are equivalent to calculating the slope of the F-E curve at zero force, as can be seen by taking the limit $\hat{f} \to 0$ in equation (3.18) or (3.19). By taking that limit, and rewriting the average as the

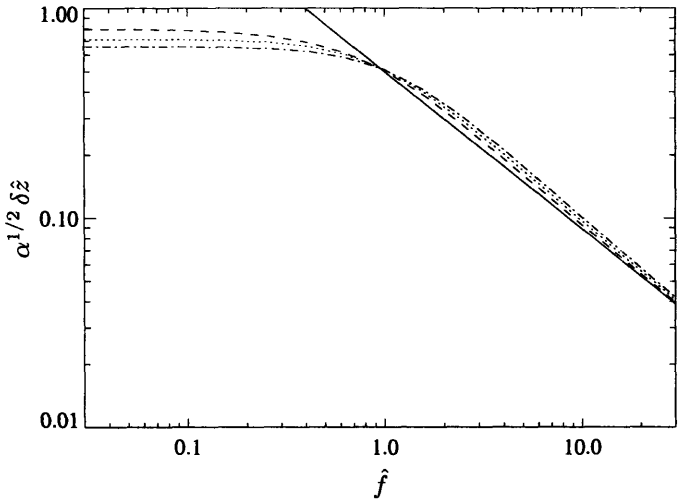

Fig. 3.8: *Calculation of the longitudinal root-mean-squared fluctuations at different levels of coarse-graining. The Marko and Siggia potential was used with* $\lambda = 1$. *The curves correspond to* $\nu = 400$ *(*dashed*),* $\nu = 20$ *(*dotted*), and* $\nu = 10$ *(*dash-dot*). The solid line corresponds to the high-force asymptotic behavior,* $1/(2\hat{f}^{3/4})$.

average of the radial coordinate of a single spring, it can be shown that

$$\lim_{\hat{f}\to 0}\left(\frac{\partial}{\partial \hat{f}}\langle \hat{z}_{\text{tot}}\rangle_{\text{m}}\right) = \frac{\nu}{3}\frac{\int_0^1 \mathrm{d}\hat{r}\;\hat{r}^4\;\exp\left[\frac{-\nu}{\lambda}\,\widehat{U}_{\text{eff}}(\hat{r})\right]}{\int_0^1 \mathrm{d}\hat{r}\;\hat{r}^2\;\exp\left[\frac{-\nu}{\lambda}\,\widehat{U}_{\text{eff}}(\hat{r})\right]}\,. \tag{3.23}$$

This expression was used previously in Section 3.6 to calculate the "best-fit" λ at zero force as seen in Figure 3.5, and it will be used extensively to understand rheological properties in Chapter 5.

We also note here that Ladoux and Doyle [58] derived an expression similar to equation (3.19) based on scaling arguments and a single spring. Based on the scaling argument, they developed a model which compared favorably to experimental data and lends support to the results presented here.

3.8 Limiting Behavior

We have seen thus far that the F-E behavior of bead-spring chains can be written analytically as integral formulae for arbitrary spring force law. This has allowed for the determination of the important dimensionless groups that determine the behavior, as well as provide for rapid and accurate calculation through numerical integration. However, another important advantage to having analytical formulae is that expansions can be performed. Those expansions can be used to illustrate limiting and universal behavior as well as obtain approximate algebraic formulae that

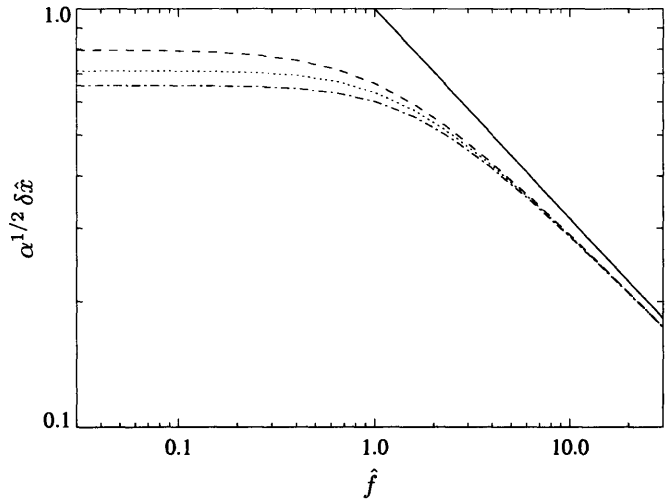

Fig. 3.9: *Calculation of the transverse root-mean-squared fluctuations at different levels of coarse-graining. The Marko and Siggia potential was used with* $\lambda = 1$. *The curves correspond to* $\nu = 400$ *(*dashed*),* $\nu = 20$ *(*dotted*), and* $\nu = 10$ *(*dash-dot*). The solid line corresponds to the high-force asymptotic behavior,* $1/(\hat{f}^{1/2})$.

illustrate what aspects of the force law are needed to estimate the exact behavior without performing numerical integration.

We have already seen numerically in Figure 3.3 that the F-E behavior of the model only matches the "true" polymer behavior if each spring represents a large number of persistence lengths. Thus it seems natural to find asymptotic expansions of the integrals in the limit $\nu \to +\infty$. We start by expanding directly the force-extension curve (equation (3.9)). The asymptotic expansion is a straightforward application of Laplace's Method [59]. The calculation is made significantly easier by noting that the hyperbolic sine can be replaced by only the growing exponential, because it only results in subdominant corrections. Up to first order, the expansion is given by

$$\langle \hat{z}_{\mathrm{tot}} \rangle_{\mathrm{m}} \overset{\nu \to \infty}{\sim} c + \frac{1}{\nu}\left[\frac{-1}{\hat{f}} + \frac{1}{c}\left(\frac{\partial c}{\partial \hat{f}}\right) + \frac{\left(\frac{\partial^2 c}{\partial \hat{f}^2}\right)}{2\left(\frac{\partial c}{\partial \hat{f}}\right)}\right] + O\left(\frac{1}{\nu^2}\right) , \tag{3.24}$$

where

$$c \equiv \langle \hat{z}_{\mathrm{tot}} \rangle_{\mathrm{p}}(\lambda \hat{f}) . \tag{3.25}$$

We thus see again that as $\nu \to \infty$ with $\lambda = 1$ the F-E behavior of the bead-spring model approaches the true polymer. However, we also have the correction terms written as a function of the *true polymer* F-E curve. *No assumption* has been made about the spring force law other than it is determined from the "true polymer" F-E behavior as was done for the WLC model in Section 3.4. Provided the value of ν is "large enough," equation (3.24) can be used to estimate the F-E behavior

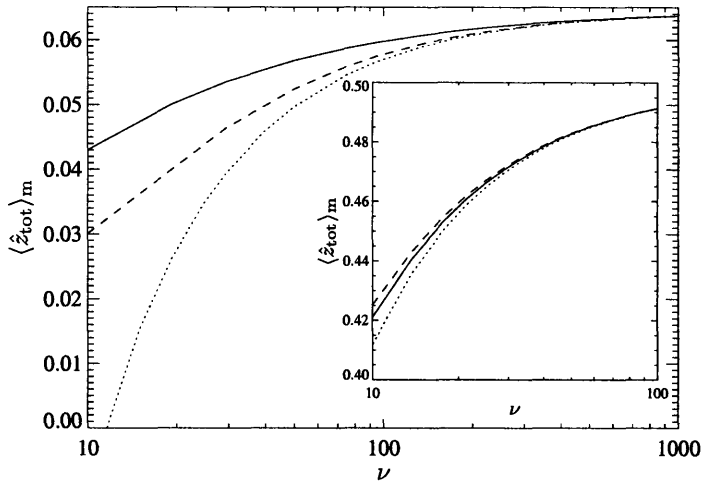

Fig. 3.10: *Comparison of the fractional extension with its high ν asymptotic expansion for the Marko and Siggia potential with $\lambda = 1$ and $\hat{f} = 0.1$. The curves correspond to the exact result (*solid line*), the expansion including $O(1/\nu)$ (*dotted*), and the zero-one Padé $P_1^0(1/\nu)$ (*dashed*).* Inset*: The analogous comparison for $\hat{f} = 1.25$.*

of a bead-spring model without performing any numerical integrations for any value of $\hat{f}$ or λ within

$$0 < \hat{f} < \infty \quad , \quad 0 < \lambda < \infty \; . \tag{3.26}$$

To give a sense of the applicability of the expansion in equation (3.24) to smaller ν, we show in Figure 3.10 a comparison of the exact force-extension result for the Marko and Siggia potential with $\lambda = 1$ and the asymptotic expansion for forces $\hat{f} = 0.1$ and $\hat{f} = 1.25$. We see that the expansion is applicable to smaller ν when $\hat{f}$ is larger. The zero-one Padé approximant $P_1^0(1/\nu)$ is seen to improve the small ν behavior.

Care must be taken if equation (3.24) is subsequently expanded for large or small $\hat{f}$ because of the order in which limits are taken. If the F-E curve is expanded to $O(\nu^{-a})$, then the asymptotic expansion $\hat{f} \to \infty$ can only be obtained to $O(\hat{f}^{-a})$. At low force, the quantity of greatest interest is the slope of the F-E curve at zero force, given by equation (3.23). In general, expanding equation (3.23) directly for $\nu \to \infty$ gives a different result from expanding equation (3.24) for small $\hat{f}$. The expansions are the same if and only if the spring force law is an odd function of its argument (the potential is an even function).

Even for the case of an odd spring force law, it is more computationally convenient to obtain the expansion of the slope of the F-E curve at zero force directly by expanding equation (3.23). Application of Laplace's Method requires the expansion of the spring force law, of the following form

$$\widehat{U}_{\text{eff}}(\hat{r}) = \phi_0 + \phi_2 \hat{r}^2 + \hat{r}^3 \sum_{i=0}^{\infty} h_i \hat{r}^i \; . \tag{3.27}$$

Note that there is no linear term because we require this potential to look Hookean near $\hat{r} = 0$ and that the value of the constant term, ϕ_0, does not affect the final answer. Also note that $\phi_2 > 0$.

Proceeding with Laplace's Method, the complete asymptotic series can be calculated to be

$$\lim_{\hat{f}\to 0}\left(\frac{\partial}{\partial \hat{f}}\langle \hat{z}_{\text{tot}}\rangle_{\text{m}}\right) \overset{\nu\to+\infty}{\sim} \left(\frac{\lambda}{2\phi_2}\right) \times \sum_{i=0}^{\infty} d_i \left(\frac{\lambda}{\nu\,\phi_2}\right)^{\frac{i}{2}} . \tag{3.28}$$

The coefficients of the series can be calculated from a collection of recursion relations that include the coefficients of the Taylor series of the spring potential. The recursion relations are given here for completeness

$$\begin{gathered} d_0 = F_0^{(4)}/F_0^{(2)} = 1 \\ d_i = \frac{1}{F_0^{(2)}}\left(F_i^{(4)} - \sum_{m=0}^{i-1} d_m F_{i-m}^{(2)}\right) = F_i^{(4)} - \sum_{m=0}^{i-1} d_m F_{i-m}^{(2)} \quad , \quad i \geq 1 \end{gathered} \tag{3.29}$$

$$F_i^{(n)} = \left[\sum_{j=0}^{i} {}_{(j)}G_{(i-j)} \left(\frac{-1}{\phi_2}\right)^j \left(\frac{\Gamma\left(j+\frac{i}{2}+\frac{n+1}{2}\right)}{j!\,\Gamma\left(\frac{n+1}{2}\right)}\right)\right] \tag{3.30}$$

$$\begin{gathered} {}_{(m)}G_{(n)} = \sum_{i=0}^{n} {}_{(m-1)}G_{(i)} h_{(n-i)} \quad \begin{cases} n = 0,1,2,\ldots \\ m = 1,2,3,\ldots \end{cases} \\ {}_{(0)}G_{(0)} = 1 \quad {}_{(0)}G_{(1,2,\ldots)} = 0 \end{gathered} \tag{3.31}$$

We have also examined the ability to use this expansion at smaller ν, as shown in Figure 3.11 for the Marko and Siggia potential with $\lambda = 1$. It should be noted that the zero-one Padé $P_1^0(1/\nu^{1/2})$ performs worse than the first two terms of the expansion in equation (3.28). However, the two-point zero-two Padé $P_2^0(1/\nu^{1/2})$ that includes the behavior at small ν does perform better. This low ν behavior will now be discussed.

In addition to examining the bead-spring chains in the limit $\nu \to \infty$, it is interesting to examine the F-E behavior in the limit $\nu \to 0$. In this limit the F-E behavior can approach a curve *independent* of the functional form of $\widehat{U}_{\text{eff}}(\hat{r})$. Physically one can think of this limit as taking a polymer with fixed contour length, and infinitely discretizing the model. Therefore each spring is becoming very small. However, it should also be noted that each spring is getting weaker, as seen in equation (3.16). It has been postulated previously that as the chain is infinitely discretized, the F-E behavior would approach that of the freely jointed chain [33]. Using the formalism presented thus far, we can examine explicitly this limit and test the postulated behavior. To understand the F-E behavior in this limit, we simply need to expand equation (3.9) for $\nu \to 0$.

It should first be noted that expanding the prescribed integral is an example of an integral that can only be expanded rigorously using asymptotic matching, but the leading-order behavior is relatively easy to obtain [59]. In fact, the leading order behavior is obtained by setting

$$\exp\left[\frac{-\nu}{\lambda}\,\widehat{U}_{\text{eff}}(\hat{r})\right] \simeq 1 \, . \tag{3.32}$$

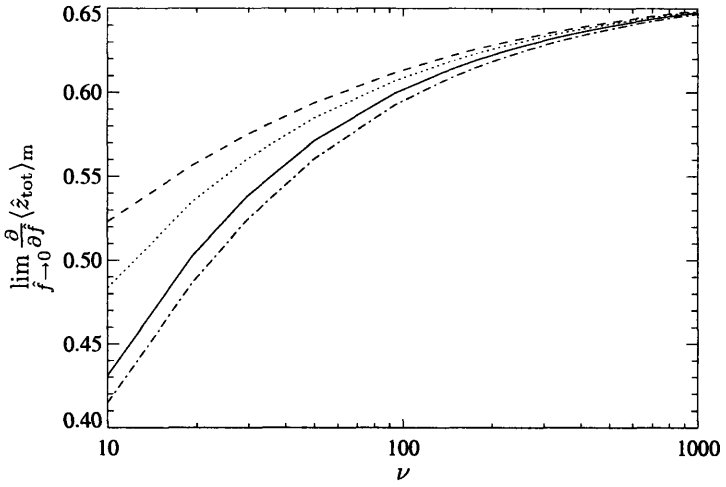

Fig. 3.11: *Comparison of the zero-force slope with its high ν asymptotic expansion for the Marko and Siggia potential with $\lambda = 1$. The curves correspond to the exact result (*solid line*), the expansion including $O(1/\nu^{1/2})$ (*dotted*), the zero-one Padé $P_1^0(1/\nu^{1/2})$ (*dashed*), and the two-point zero-two Padé $P_2^0(1/\nu^{1/2})$ (*dash-dot*).*

By further expanding the hyperbolic sine, it can be easily shown that

$$\langle \hat{z}_{\rm tot} \rangle_{\rm m} \overset{\nu \to 0}{\sim} \frac{\nu \hat{f}}{5} \quad , \quad \hat{f} \text{ fixed} . \tag{3.33}$$

Note that this is consistent with Section 3.5 in which we saw that, for $\hat{f}$ fixed, the mean fractional extension approaches zero as $\nu \to 0$. We also see explicitly that the F-E behavior *does not* approach the FJC, which is given by

$$\langle \hat{z}_{\rm tot} \rangle_{\rm m} = \mathcal{L}(\hat{f}) , \tag{3.34}$$

where

$$\mathcal{L}(x) = \coth(x) - \frac{1}{x} \tag{3.35}$$

is the Langevin function. We can also contrast the behavior in equation (3.33) with a different "experiment" in which free hinges are introduced into a true *continuous* worm-like chain while the force is held constant. If one considers ν to be the ratio of the contour length of the continuous curve between free hinges to the persistence length, then it is clear that the average extension of this discretized worm-like chain, $\langle \hat{z}_{\rm tot} \rangle_{\rm dwlc}$, approaches the limit

$$\langle \hat{z}_{\rm tot} \rangle_{\rm dwlc} \overset{\nu \to 0}{\sim} \mathcal{L}(\nu \hat{f}) \overset{\nu \to 0}{\sim} \frac{\nu \hat{f}}{3} \quad , \quad \hat{f} \text{ fixed} \tag{3.36}$$

It should be noted that holding $\hat{f}$ fixed corresponds to the physical process of holding the force

constant as the model is infinitely discretized. This is the appropriate limit to examine processes in which the force applied to the end of the system is independent of how the system is discretized. However, another universal result can be obtained by instead of holding $\hat{f}$ fixed, holding $\nu\hat{f}$ fixed. This corresponds to pulling harder and harder on the model as it is more finely discretized. One might expect that the length of a spring should play the role of the "Kuhn length", and thus the scale for the force. This corresponds to a dimensionless force of $\nu\hat{f}$. The expansion of the bead-spring chain model behavior with $\nu\hat{f}$ fixed is calculated by simply integrating the hyperbolic sine in equation (3.9) to obtain

$$\langle \hat{z}_{\text{tot}} \rangle_{\text{m}} \underset{\sim}{^{\nu \to 0}} \frac{-3}{\nu\hat{f}} + \frac{1}{\mathcal{L}(\nu\hat{f})} \quad , \quad (\nu\hat{f}) \text{ fixed} . \tag{3.37}$$

We see that even in this limit the system *does not* approach a modified "freely jointed chain" result of

$$\langle \hat{z}_{\text{tot}} \rangle_{\text{m}} = \mathcal{L}(\nu\hat{f}) . \tag{3.38}$$

To understand the true limiting shape (equation (3.37)) it can be shown that

$$\frac{-3}{x} + \frac{1}{\mathcal{L}(x)} \approx \mathcal{L}(x/2) \quad x \text{ large} , \tag{3.39}$$

$$\frac{-3}{x} + \frac{1}{\mathcal{L}(x)} \approx \mathcal{L}(3x/5) \quad x \text{ small} . \tag{3.40}$$

In addition to being used to understand the limit of infinite discretization, equation (3.37) can be used to understand the divergence of the "best-fit" λ curves in Figure 3.5 and discussed in Section 3.6. Recall that previously we considered the limit in equation (3.37) to be as $\nu \to 0$ as $(\nu\hat{f})$ was held fixed, and λ was implicitly being held constant. By examining equation (3.9), we see that if $(\nu\hat{f})$ is held constant, the only remaining parameter is ν/λ. Thus the expression in equation (3.37) can be rewritten as the limit $(\nu/\lambda) \to 0$:

$$\langle \hat{z}_{\text{tot}} \rangle_{\text{m}} \underset{\sim}{^{\lambda \to \infty}} \frac{-3}{\nu\hat{f}} + \frac{1}{\mathcal{L}(\nu\hat{f})} \quad , \quad \textit{both } \nu, \hat{f} \text{ fixed} . \tag{3.41}$$

Now suppose that one is choosing λ such that the model matches the true polymer at an extension of $\langle \hat{z}_{\text{tot}} \rangle_{\text{p}}$, which occurs at a force denoted $\hat{f}\big(\langle \hat{z}_{\text{tot}} \rangle_{\text{p}}\big)$. The value of ν for which that "best-fit" curve diverges (denoted ν^*) will be the value for which only as $\lambda \to \infty$ will the extension of the model equal that of the polymer. This condition is written as

$$\langle \hat{z}_{\text{tot}} \rangle_{\text{p}} = \frac{-3}{\nu^* \hat{f}\big(\langle \hat{z}_{\text{tot}} \rangle_{\text{p}}\big)} + \frac{1}{\mathcal{L}\big(\nu^* \hat{f}\big(\langle \hat{z}_{\text{tot}} \rangle_{\text{p}}\big)\big)} . \tag{3.42}$$

This can also be used to find the divergence of the low force criteria by examining the limit as $\hat{f} \to 0$. Because of the way of choosing the force law from the true polymer behavior, it can be shown easily that

$$\langle \hat{z}_{\text{tot}} \rangle_{\text{p}} \underset{\sim}{^{\hat{f} \to 0}} \frac{\hat{f}}{2\phi_2} . \tag{3.43}$$

It can also be shown that

$$\frac{-3}{\nu^* \hat{f}\left(\langle \hat{z}_{\text{tot}} \rangle_{\text{p}}\right)} + \frac{1}{\mathcal{L}\left(\nu^* \hat{f}\left(\langle \hat{z}_{\text{tot}} \rangle_{\text{p}}\right)\right)} \underset{\sim}{\hat{f} \to 0} \frac{\nu^* \hat{f}}{5} . \tag{3.44}$$

Therefore the point of divergence for the low force criteria is

$$\nu^* = \frac{5}{2\phi_2} . \tag{3.45}$$

By applying equation (3.45) to the Marko and Siggia force law we see that the low force criteria diverges at $\nu^* = 10/3$ as stated in Section 3.6. To calculate the divergence for the half-extension criteria, we set $\langle \hat{z}_{\text{tot}} \rangle_{\text{p}} = 1/2$ in equation (3.42) and substitute for $\hat{f}(1/2)$ from equation (3.10). The divergence is then given by the solution to

$$\frac{1}{2} = \frac{-3}{5\nu^*/4} + \frac{1}{\mathcal{L}(5\nu^*/4)} , \tag{3.46}$$

which is $\nu^* = 2.4827$ as stated in Section 3.6.

It must be noted that while equation (3.42) is valid for any $0 < \langle \hat{z}_{\text{tot}} \rangle_{\text{p}} < 1$, and can be used for the low force criteria, in general it *can not* be used for the high force criteria. This stems from the break-down of the assumption in equation (3.32) if $\hat{f} \to \infty$, in particular because the spring potential for the WLC model diverges at full extension fast enough. In fact, we know that equation (3.42) can not be valid for the WLC model for the high-force criterion because we know that the high force criteria does not diverge. It is shown in Section 3.9 that the high force criteria for the FENE model does diverge, and equation (3.42) *can* be used to calculate the position of divergence.

3.9 FENE and Fraenkel Force Laws

Thus far whenever a particular spring force law has been needed the Marko and Siggia interpolation formula has been used. It has been noted that the general formula will work for other force laws. Here we will explicitly show how the formulae can be made specific for two important force laws commonly used in modeling polymer rheology.

The first force law we will consider is the FENE force law [60], which is a widely used approximation to the behavior of a freely jointed chain (FJC). The FENE force law can be written in general as

$$f = \frac{H\ell \langle \hat{z}_{\text{tot}} \rangle_{\text{p}}}{1 - \langle \hat{z}_{\text{tot}} \rangle_{\text{p}}^2} . \tag{3.47}$$

In the sense that the FENE force law is an approximation to the true force law for a FJC, the spring constant H is given in terms of the length of a rod in the FJC, or Kuhn length a_{K}, as [12]

$$H = \frac{3k_{\text{B}}T}{\ell a_{\text{K}}} . \tag{3.48}$$

Combining equations (3.47) and (3.48), the appropriate scale for the force is $k_{\text{B}}T/a_{\text{K}}$, or for the general case $H\ell$. The general formalism presented earlier scaled the force by $k_{\text{B}}T/A_{\text{true}}$ where A_{true}

was called the true persistence length. Now it is clear that it would be more appropriate to call A_{true} a generalized flexibility length, and only for the WLC is it equal to the "persistence length." For the FJC the generalized flexibility length is proportional to the Kuhn length.

To apply the framework presented in Section 3.4 to the FENE force law in equation (3.47), we will let $A_{\text{true}} = k_{\text{B}}T/(H_{\text{true}}\,\ell) = a_{\text{K,true}}/3$ so that the "exact" polymer F-E behavior is

$$\hat{f} = \frac{\langle \hat{z}_{\text{tot}} \rangle_{\text{p}}}{1 - \langle \hat{z}_{\text{tot}} \rangle_{\text{p}}^2} \,. \tag{3.49}$$

This directly motivates the choice for the spring force law

$$f_{\text{spring}}(r) = \left(\frac{k_{\text{B}}T}{A_{\text{eff}}}\right) \frac{r/\ell}{1 - (r/\ell)^2} \,, \tag{3.50}$$

where A_{eff} is defined in the expected way as

$$A_{\text{eff}} = \frac{k_{\text{B}}T}{H_{\text{eff}}\,\ell} = \frac{a_{\text{K,eff}}}{3} \,. \tag{3.51}$$

It is then clear that the dimensionless energy for the FENE spring becomes

$$\widehat{U}_{\text{eff}}(\hat{r}) = \frac{-1}{2} \ln(1 - \hat{r}^2) \,, \tag{3.52}$$

and all formulae from Section 3.4 follow directly. However, while interpreting the previous discussion it must be kept in mind that the parameters dependent on A_{eff} and A_{true} can have slightly different physical interpretations depending on the exact force law used. What does not change is the concept that those parameters consist of generalized flexibility lengths. Thus, for example, ν still must be large in order for the bead-spring model to behave like the true polymer.

For the FENE force law many of the calculations (integrals) can be performed analytically. In particular, the F-E behavior is

$$\begin{aligned} \langle \hat{z}_{\text{tot}} \rangle_{\text{m}} &= \frac{I_{k+1}(\hat{f}\nu)}{I_k(\hat{f}\nu)} \\ k &= \frac{3 + \frac{\nu}{\lambda}}{2} \end{aligned} \tag{3.53}$$

where $I_k(x)$ is the modified Bessel function of the first kind, order k. The moments can also be calculated analytically in terms of the Beta function, or equivalently Gamma functions

$$\langle \hat{r}^n \rangle_{\text{eq}} = \frac{\Gamma\left(\frac{n+3}{2}\right)}{\Gamma\left(\frac{3}{2}\right)} \frac{\Gamma\left(\frac{3}{2} + \frac{\nu}{2\lambda} + 1\right)}{\Gamma\left(\frac{n+3}{2} + \frac{\nu}{2\lambda} + 1\right)} \,. \tag{3.54}$$

For even values of $n \geq 2$, they take an even simpler form:

$$\langle \hat{r}^n \rangle_{\text{eq}} = \frac{(n+1)\,(n-1)\cdots(3)}{\left(n+3+\frac{\nu}{\lambda}\right)\left(n+1+\frac{\nu}{\lambda}\right)\cdots\left(5+\frac{\nu}{\lambda}\right)} \,. \tag{3.55}$$

In order to more easily compare these results with the large body of literature on FENE springs,

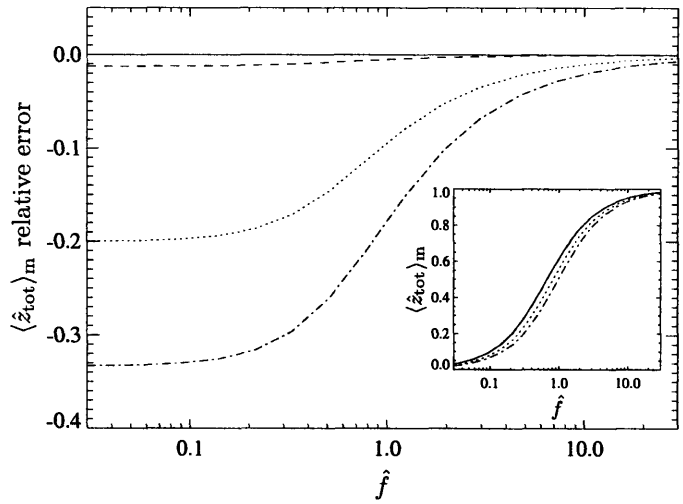

Fig. 3.12: *Calculation of the relative error of the mean fractional extension,* $(\langle \hat{z}_{tot} \rangle_m - \langle \hat{z}_{tot} \rangle_p)/\langle \hat{z}_{tot} \rangle_p$, *for a bead-spring model as the level of coarse-graining changes. The FENE potential was used with* $\lambda = 1$. *The curves correspond to* $\nu = 400$ *(*dashed*),* $\nu = 20$ *(*dotted*), and* $\nu = 10$ *(*dash-dot*).* Inset*: The mean fractional extension of the models compared with the "true polymer" (*solid line, *equation* (3.49)*).*

we will relate the common FENE notation to the notation used here. Typically the FENE force law is written as [12]

$$f_{lit}(Q) = \frac{H_{lit} Q}{1 - (Q/Q_o)^2} \cdot \tag{3.56}$$

Comparing equations (3.50) and (3.56) we see the following equalities in notation:

$$Q \rightarrow r \tag{3.57}$$

$$Q_o \rightarrow \ell \tag{3.58}$$

$$H_{lit} \rightarrow H_{eff} \cdot \tag{3.59}$$

The other very important parameter in the FENE notation is b defined by

$$b = \frac{H_{lit} Q_o^2}{k_B T} , \tag{3.60}$$

which can be related to our notation as

$$b \rightarrow \frac{\nu}{\lambda} \cdot \tag{3.61}$$

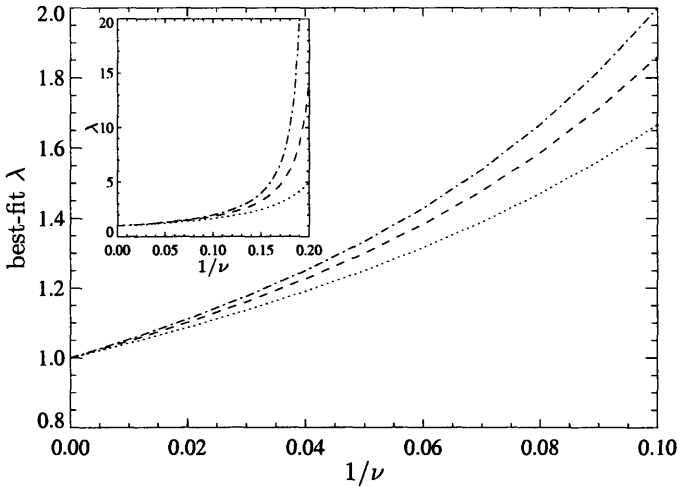

Fig. 3.13: *Calculation of λ for the three different criteria at different levels of coarse-graining for the FENE potential. The criteria shown are low-force (*dash-dot*), half-extension (*dashed*), and high-force (*dotted*).* Inset*: Expanded view showing the divergence of the criteria.*

For comparison with the WLC results presented thus far, we here present the corresponding results for the FENE model. In Figure 3.12 we show the F-E behavior of FENE bead-spring chains as the level of coarse-graining, ν, is changed. We see that the FENE result is qualitatively similar to the WLC result in Figure 3.3.

For the FENE force law λ can also be taken greater than 1 to obtain a better behavior from the model. Figure 3.13 shows the "best-fit" λ versus $\frac{1}{\nu}$ for each of the three criteria introduced in Section 3.6. The most obvious difference from the WLC result in Figure 3.5 is that for the FENE chain the high-force criterion curve deviates from $\lambda = 1$. In fact, the high-force criterion curve diverges similar to the other criteria. We will see that this high-force divergence is because of the weaker divergence of the FENE force law approaching full extension compared to the WLC force law. This divergence of the high-force criteria also causes the best fit λ curves to form a relatively narrow strip bounding the choices for λ. In Figure 3.14 we compare the force-extension behavior of the three criteria for $\nu = 20$. While we see a qualitative match for the relative error with the Marko and Siggia result (Figure 3.6), the error is greatly reduced. Thus for the FENE force law simply adjusting the effective flexibility length does a much better job at reproducing the true polymer behavior over the entire force range. This is due to the form of the high-extension divergence of the force law. The trade-off for this improved performance is that the range in ν that this correction-factor can be used is reduced.

The high-force and low-force best-fit λ curves can be calculated exactly. Recall that the low-force criterion is that the slope at zero force matches the true polymer slope. Using equation (3.23) for the slope, and using equation (3.55) for the second moment, we find that the low-force criteria

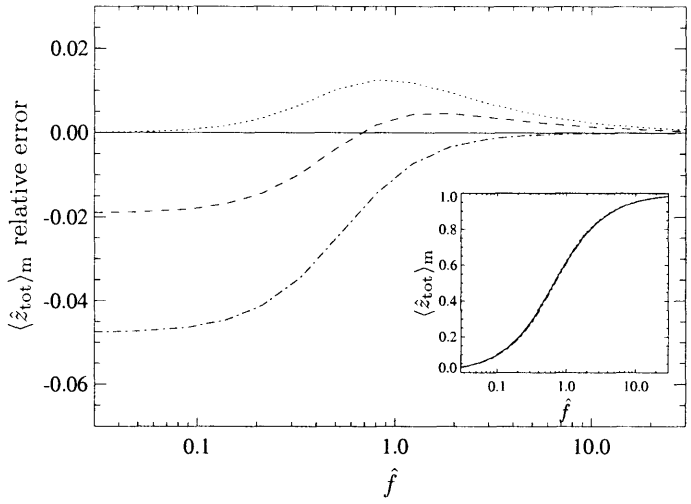

Fig. 3.14: *Calculation of the relative error of the mean fractional extension,* $(\langle \hat{z}_{\rm tot} \rangle_{\rm m} - \langle \hat{z}_{\rm tot} \rangle_{\rm p})/\langle \hat{z}_{\rm tot} \rangle_{\rm p}$*, for a bead-spring model for different best fit criteria. The FENE potential was used with* $\nu = 20$*. The curves correspond to* $\lambda = 1.33$ *(low-force,* dotted*),* $\lambda = 1.30$ *(half-extension,* dashed*), and* $\lambda = 1.25$ *(high-force,* dash-dot*).* Inset*: The mean fractional extension of the models compared with the "true polymer" (*solid line*, equation* (3.49)*).*

curve is given by

$$\lambda = \frac{1}{1 - \frac{5}{\nu}} \ , \tag{3.62}$$

from which it is easy to see the curve diverges at $\nu^* = 5$. This could also have been seen from the general low-force divergence formula in equation (3.45) since $\phi_2 = 1/2$ for the FENE force law. The high-force curve is calculated from the high-force expansion of the fractional extension

$$\langle \hat{z}_{\rm tot} \rangle_{\rm m} \overset{\hat{f}\to\infty}{\sim} 1 - \frac{\nu/\lambda + 4}{2\nu\hat{f}} + O\left(\frac{1}{\hat{f}^2}\right) \ . \tag{3.63}$$

Since the true polymer has a high-force expansion of

$$\langle \hat{z}_{\rm tot} \rangle_{\rm p} \overset{\hat{f}\to\infty}{\sim} 1 - \frac{1}{2\hat{f}} + O\left(\frac{1}{\hat{f}^2}\right) \ , \tag{3.64}$$

the high-force criteria curve is given by

$$\lambda = \frac{1}{1 - \frac{4}{\nu}} \ , \tag{3.65}$$

with a divergence at $\nu^* = 4$. This can also be derived from the general divergence criteria in

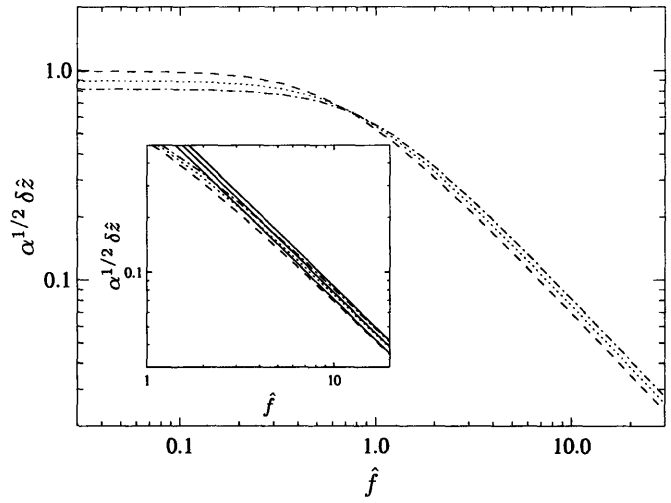

Fig. 3.15: *Calculation of the longitudinal root-mean-squared fluctuations at different levels of coarse-graining. The FENE potential was used with* $\lambda = 1$. *The curves correspond to* $\nu = 400$ *(*dashed*),* $\nu = 20$ *(*dotted*), and* $\nu = 10$ *(*dash-dot*).* Inset*: Detailed look at the high-force limit with solid lines corresponding to the asymptotic behavior,* $((\nu/\lambda + 4)/(2\nu))^{1/2}(1/\hat{f})$.

equation (3.42). By comparing the expansion

$$\frac{-3}{\nu^*\hat{f}\left(\langle\hat{z}_{\rm tot}\rangle_{\rm p}\right)} + \frac{1}{\mathcal{L}\left(\nu^*\hat{f}\left(\langle\hat{z}_{\rm tot}\rangle_{\rm p}\right)\right)} \overset{\hat{f}\to\infty}{\sim} 1 - \frac{2}{\nu^*\hat{f}} \tag{3.66}$$

with the expansion of the true polymer, we can verify that the high-force criteria diverges at $\nu^* = 4$. The half-extension divergence is found by solving the equation

$$\frac{1}{2} = \frac{-3}{2\nu^*/3} + \frac{1}{\mathcal{L}(2\nu^*/3)}\,, \tag{3.67}$$

which has a solution $\nu^* = 4.6551$.

In addition to the F-E behavior of the FENE chains, we should look at the fluctuations, as done for the WLC in Section 3.7. In Figures 3.15 and 3.16 we show the plots of the scaled root-mean-squared fluctuations for different levels of coarse-graining, ν. From the high-force expansion of the FENE force-extension behavior in equation (3.63) we can calculate the high-force scaling of the fluctuations:

$$\alpha^{1/2}\,\delta\hat{z} \overset{\hat{f}\to\infty}{\sim} \left(\frac{\nu/\lambda + 4}{2\nu}\right)^{1/2}\frac{1}{\hat{f}} + O\left(\frac{1}{\hat{f}^2}\right) \tag{3.68}$$

$$\alpha^{1/2}\,\delta\hat{x} \overset{\hat{f}\to\infty}{\sim} \frac{1}{\hat{f}^{1/2}} + O\left(\frac{1}{\hat{f}^{3/2}}\right)\,. \tag{3.69}$$

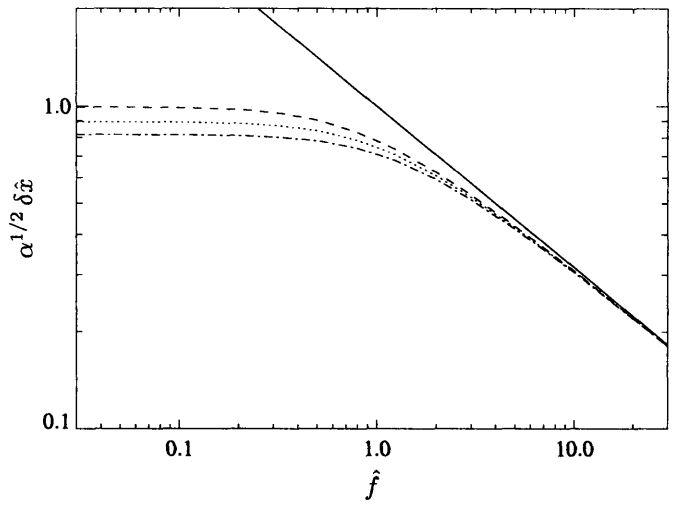

Fig. 3.16: *Calculation of the transverse root-mean-squared fluctuations at different levels of coarse-graining. The FENE potential was used with* $\lambda = 1$. *The curves correspond to* $\nu = 400$ *(*dashed*),* $\nu = 20$ *(*dotted*), and* $\nu = 10$ *(*dash-dot*). The solid line corresponds to the high-force asymptotic behavior,* $1/(\hat{f}^{1/2})$.

We can also analyze the limiting behavior from Section 3.8 in terms of the FENE force law. Because the FENE force law is an odd function of its argument, the general expansion of the F-E behavior in the large ν limit can additionally be used at zero force. We can examine in detail the expansion of the zero-force slope (equation (3.23)) because the zero-force slope can be calculated exactly. Using the expression for the second moment of the FENE force law

$$\lim_{\hat{f}\to 0}\left(\frac{\partial}{\partial \hat{f}}\langle \hat{z}_{\mathrm{tot}}\rangle_{\mathrm{m}}\right) = \frac{\nu}{5+\nu/\lambda}\ . \tag{3.70}$$

We see that the expansion of this slope for large ν should just be the Taylor expansion. Calculating the coefficients, d_i, using the FENE force law shows this explicitly. The parameters of the FENE force law are

$$\phi_2 = \frac{1}{2} \tag{3.71}$$

$$h_i = \begin{cases} 0 & , i \text{ even} \\ \frac{1}{i+3} & , i \text{ odd} \end{cases} \tag{3.72}$$

which gives coefficients

$$d_i = \begin{cases} 0 & , i \text{ odd} \\ (-5/2)^{i/2} & , i \text{ even} \end{cases} \tag{3.73}$$

Since this is the geometric series, the convergence is well-known. Note also that the zero-one Padé

$P_1^0(1/\nu)$ gives the exact result.

The other force law we consider explicitly is the infinitely-stiff Fraenkel force law, which is equivalent to the FJC. This force law differs from the others considered because the spring potential *is not* obtained by examining the force-extension behavior of a true polymer. In fact, this force law *is* a model of a "true polymer" (the FJC or random walk model). Thus the previous discussions of the comparison between the bead-spring model and the true polymer do not apply for this force law. However, we can still use the formulae developed to calculate the F-E and rheological behavior of this true polymer.

The Fraenkel force law is a Hookean force law, but with a minimum energy at a non-zero extension

$$f_{\text{spring}}(r) = H_{\text{F}}(r - a_{\text{K}}) \ . \tag{3.74}$$

H_{F} is the spring constant of the Fraenkel spring, and a_{K} is the position of minimum energy. We use the symbol a_{K} because for the infinitely-stiff Fraenkel spring this minimum corresponds to the Kuhn length in the FJC. After integrating, the spring potential becomes

$$U_{\text{eff}}(r) = \frac{H_{\text{F}}}{2}(r - a_{\text{K}})^2 \ . \tag{3.75}$$

For the infinitely-stiff model, $H_{\text{F}} \to \infty$, the Boltzmann factor becomes a Dirac delta function

$$\exp\left[\frac{-U_{\text{eff}}(r)}{k_{\text{B}}T}\right] \to \delta(r - a_{\text{K}}) \ . \tag{3.76}$$

Furthermore, in this limit the contour length of the model, L, becomes $N_{\text{s}}a_{\text{K}}$, so the length of a spring, ℓ, becomes a_{K}. Since the choice of A_{true} is arbitrary, we will take it to be the Kuhn length, a_{K}. Thus in dimensionless form

$$\exp\left[\frac{-\nu}{\lambda}\widehat{U}_{\text{eff}}(\hat{r})\right] \to \delta(\hat{r} - 1) \tag{3.77}$$

$$\nu = 1 \tag{3.78}$$

Using these expressions in equation (3.9) for the F-E behavior, we see that

$$\langle \hat{z}_{\text{tot}} \rangle_{\text{m}} = \left\{ \frac{-1}{\hat{f}} + \frac{\partial}{\partial \hat{f}} \ln\left(\int_0^1 \mathrm{d}\hat{r}\ \hat{r}\ \sinh\left[\hat{f}\hat{r}\right] \delta(\hat{r} - 1) \right) \right\} = \mathcal{L}(\hat{f}) \ , \tag{3.79}$$

which we already know is the F-E behavior of the FJC. Note that this is the F-E behavior for *any* integer number of springs (Kuhn lengths). Even a *single* rod of a FJC has the Langevin function for its F-E behavior. Also note that for the Fraenkel spring force law, the upper limit of integration should be ∞ instead of 1. However, for the infinitely-stiff case, replacing the ∞ by 1 causes no change to the F-E behavior.

3.10 Summary

In this chapter we have used statistical mechanics to systematically analyze the coarse-graining of polymers into bead-spring chains by examining the force-extension behavior. In this way we

could avoid the intrinsic stochastic noise of Brownian dynamics, identify the relevant dimensionless groups, and examine limiting and universal behavior.

The analysis of the force-extension behavior revealed that, because the springs are decoupled, the response depended only on the number of flexibility lengths represented by each spring, ν. This necessarily means that any deviation between the behavior of the spring model and the true polymer can not be due to the number of free hinges introduced. Instead we showed through direct visualization of the phase space that ν acts analogously to an inverse temperature, controlling the magnitude of fluctuations in phase space.

We also examined quantitatively the use of an effective flexibility length to partially correct the force-extension behavior. The corrected curve is not uniformly valid over the entire force range leading to multiple possible choices for the effective flexibility length. However, we were able to place bounds on the choices and examine these choices. Variability in behavior within these bounds depends on the form of the spring force law; the Marko and Siggia potential has larger variability than the FENE potential. This is mainly due to the difference in the divergence of the potentials at high extension.

In addition to the direct relevance of these results to understand the force-extension response of a polymer and the bead-spring chain model, this analysis forms the basis of subsequent chapters. We will show later that the response of a bead-spring chain in both weak and strong flows is related to its force-extension behavior. Much of the later discussion will reference back to the analysis in this chapter.

Also the ideas developed in this chapter naturally extend to the next chapter, in which new spring force laws are developed. Our detailed understanding of the force-extension behavior, in particular that the error results from fluctuations in phase space, will allow us to develop new and improved spring force laws which exactly represent the force-extension behavior of the polymer of interest.

CHAPTER 4

New Spring Force Laws

Recall that previously the spring force law was chosen by examining the force-extension behavior of the true polymer in the constant force ensemble, as shown in Sections 3.4 and 3.9. The mean fractional z-projection of the polymer was replaced by the fractional radial coordinate of the spring. In this chapter we examine a new method for determining the spring force law, which we term the Polymer Ensemble Transformation (PET) method. This method uses the constant extension behavior of the true polymer to determine the spring force law. The bead-spring model is then able to reproduce the behavior of the true polymer in both the constant extension and constant force ensembles. We will see later that reproducing the behavior in the constant force ensemble is important because many properties such as the the retarded-motion coefficients can be written in terms of the force-extension behavior in the constant force ensemble. This difference in paths to determine the spring force law from the micromechanical model is illustrated in Figure 4.1.
This chapter was reproduced in part with permission from Underhill, P.T. and Doyle, P.S., *J. Non-Newtonian Fluid Mech.*, **122**, 3 (2004), copyright 2004 Elsevier B.V. This chapter was also reproduced in part with permission from Underhill, P.T. and Doyle, P.S., *J. Rheol.*, **49**, 963 (2005), copyright 2005 by The Society of Rheology. This chapter was additionally reproduced in part with permission from Underhill, P.T. and Doyle, P.S., *J. Rheol.*, **50**, 513 (2006), copyright 2006 by The Society of Rheology.

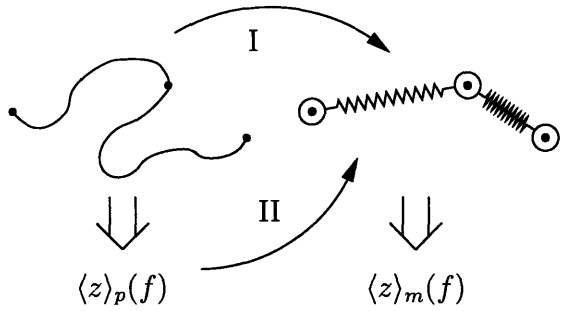

Fig. 4.1: *There are multiple paths to build a bead-spring model. The goal of coarse-graining is to produce a model such that its behavior, $\langle z \rangle_m(f)$, matches the polymer's behavior, $\langle z \rangle_p(f)$. The paths (arrows) represent different methods of taking a property of the polymer to be the spring force-law. The PET method introduced here, path I, uses the constant extension polymer behavior as the spring force-law. The conventional method, path II, uses the constant force behavior as the spring force-law.*

4.1 Justification

The method of using the constant extension ensemble behavior to obtain a spring force law is illustrated in Figure 4.2. In the figure, a polymer is shown in the constant force ensemble. The goal is to determine a spring force law that can model the polymer behavior at a given set of reference points (depicted by black circles in the figure), while coarse-graining out the details of the polymer between the reference points. To accomplish this, the segment of polymer to be modeled is placed in the constant extension ensemble, and the average external force required to keep the polymer at a fixed extension is calculated. The spring force in the model is taken to be equal to this average force:

$$f_{\text{spring}}(r) = \langle f \rangle(r) \tag{4.1}$$

If the reference points on the true polymer correspond to free hinges (as in the FJC with the reference points taken at the joints), then the spring model defined in this way reproduces exactly the force-extension behavior of the true polymer. However, for other polymers such as the WLC, there is coupling across the reference points. Therefore this preliminary bead-spring model can not reproduce the true polymer behavior for this class of polymers. We will discuss later the necessary steps to generalize the method to apply to the WLC.

We will first justify this method physically. Note that the behavior of the polymer is an average over all possible configurations. Consider performing that average by choosing a series of reference points on the polymer where the beads in the bead-spring model will be (shown by black circles in Figure 4.3) and separate all the polymer configurations into categories for which each category has fixed reference points. First the average is performed within each category, for which the reference points *are* fixed, thus the constant extension ensemble is needed. In this way we replace each category (which contains many configurations) by a single configuration of the bead-spring chain.

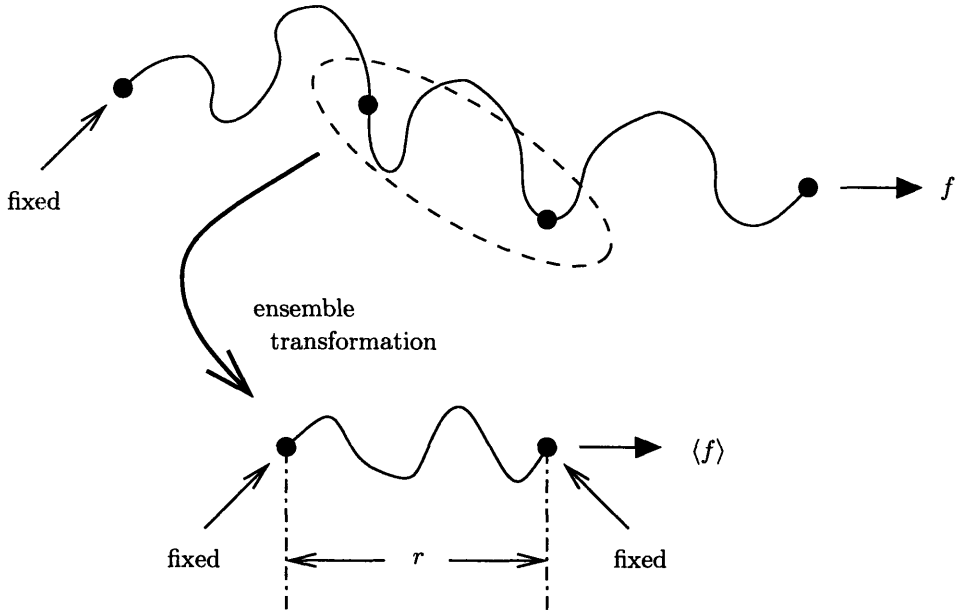

Fig. 4.2: *Physical interpretation of Polymer Ensemble Transformation (PET) method.* Above*: The true polymer in the constant force ensemble. The behavior is to be modelled between reference points (black circles).* Below*: The portion of true polymer between reference points is transformed to the constant extension ensemble to calculate the appropriate spring force law.*

To derive mathematically that the spring force law *must* be taken from the constant extension ensemble in order to reproduce the force-extension behavior in the constant force ensemble, we start by writing down the partition function in the constant force ensemble

$$\mathcal{Z}(\boldsymbol{f}) = \int \cdots \int_{\{\text{configurations}\}} \exp\left[\frac{-U + \boldsymbol{f} \cdot \mathbf{R}_{\text{tot}}}{k_{\text{B}}T}\right] \mathrm{d}\mathbb{V} \,, \tag{4.2}$$

where the force has not necessarily been taken to lie in the z-direction. We can introduce a new variable, $\boldsymbol{r}$, through the use of a Dirac delta function

$$\mathcal{Z}(\boldsymbol{f}) = \int \cdots \int_{\{\text{configurations}\}} \exp\left[\frac{-U + \boldsymbol{f} \cdot \mathbf{R}_{\text{tot}}}{k_{\text{B}}T}\right] \int \delta(\boldsymbol{r} - \mathbf{R}_{\text{tot}}) \mathrm{d}\boldsymbol{r} \; \mathrm{d}\mathbb{V} \,. \tag{4.3}$$

By interchanging the order of integration, we obtain

$$\mathcal{Z}(\boldsymbol{f}) = \int \int \cdots \int_{\{\text{configurations}\}} \exp\left[\frac{-U + \boldsymbol{f} \cdot \mathbf{R}_{\text{tot}}}{k_{\text{B}}T}\right] \delta(\boldsymbol{r} - \mathbf{R}_{\text{tot}}) \mathrm{d}\mathbb{V} \mathrm{d}\boldsymbol{r} \,. \tag{4.4}$$

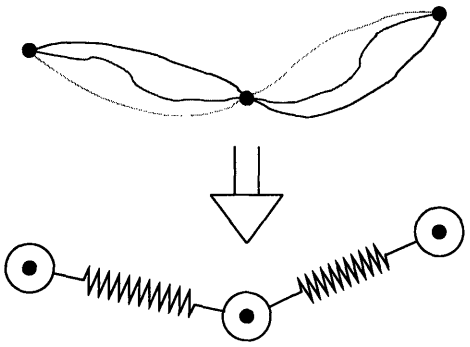

Fig. 4.3: *The physical justification for the PET method is based on sorting all configurations of the polymer into categories. Within each category the reference points (black circles) are held fixed. The lines signify different polymer configurations within the category. When performing the average over the configurations in a category, the segment between reference points is effectively in the constant extension ensemble. This segment is replaced by a spring in the bead-spring model.*

The force term can be taken out of the configuration integral because of the delta function so that

$$\mathcal{Z}(\boldsymbol{f}) = \int \Omega(\boldsymbol{r}) \exp\left[\frac{\boldsymbol{f}\cdot\boldsymbol{r}}{k_{\mathrm{B}}T}\right] \mathrm{d}\boldsymbol{r} \ , \tag{4.5}$$

where

$$\Omega(\boldsymbol{r}) = \int \cdots \int_{\{\text{configurations}\}} \exp\left[\frac{-U}{k_{\mathrm{B}}T}\right] \delta(\boldsymbol{r} - \mathbf{R}_{\mathrm{tot}}) \mathrm{d}\mathbb{V} \tag{4.6}$$

is the constant extension ensemble partition function. However, we see that this looks similar to the partition function of a single dumbbell model

$$\mathcal{Z}(\boldsymbol{f}) = \int \exp\left[\frac{-U_{\mathrm{s}}(\boldsymbol{r})}{k_{\mathrm{B}}T}\right] \exp\left[\frac{\boldsymbol{f}\cdot\boldsymbol{r}}{k_{\mathrm{B}}T}\right] \mathrm{d}\boldsymbol{r} \ . \tag{4.7}$$

Thus a single dumbbell model will have the exact same partition function as the true polymer (and thus the exact same equilibrium behavior) if the spring potential energy is taken from the constant extension partition function as

$$U_{\mathrm{s}}(\boldsymbol{r}) = -k_{\mathrm{B}}T \ln \Omega(\boldsymbol{r}) \ . \tag{4.8}$$

Here we illustrated how the spring potential can be derived for a single dumbbell. However, a similar procedure can be used to derive bead-spring chains. All of the spring coordinates can be introduced into the partition function by using Dirac delta functions (as in equation (4.3)). For

example, if three springs were desired the transformation would give

$$\mathcal{Z}(\boldsymbol{f}) = \int \Omega(\boldsymbol{r}_1, \boldsymbol{r}_2, \boldsymbol{r}_3) \exp\left[\frac{\boldsymbol{f} \cdot (\boldsymbol{r}_1 + \boldsymbol{r}_2 + \boldsymbol{r}_3)}{k_{\mathrm{B}}T}\right] \mathrm{d}\boldsymbol{r}_1 \mathrm{d}\boldsymbol{r}_2 \mathrm{d}\boldsymbol{r}_3 \ , \tag{4.9}$$

where $\boldsymbol{r}_i$ is the spring connector vector of spring i. The potential energy of the spring system would then be

$$U_{\mathrm{s}}(\boldsymbol{r}_1, \boldsymbol{r}_2, \boldsymbol{r}_3) = -k_{\mathrm{B}}T \ln \Omega(\boldsymbol{r}_1, \boldsymbol{r}_2, \boldsymbol{r}_3) \ . \tag{4.10}$$

Note that the total potential energy of the spring system is, in general, not separable into contributions from each spring, and thus includes coupling between springs.

We saw in equation (4.5) how the constant force and constant extension partition function are related. This is exactly analogous to the relationship between the microcanonical and canonical ensembles, as well as between other ensembles [45, 61]. If we look at the analytic continuation of the constant force partition function onto the imaginary force axis, we find that it is the Fourier transform of the constant extension partition function

$$\mathcal{Z}(ik_{\mathrm{B}}T\boldsymbol{k}) = \int \Omega(\boldsymbol{r}) \exp[i\boldsymbol{k} \cdot \boldsymbol{r}] \, \mathrm{d}\boldsymbol{r} \ . \tag{4.11}$$

Thus, the constant extension ensemble partition function can be calculated from the constant force ensemble partition function as

$$\Omega(\boldsymbol{r}) = \left(\frac{1}{2\pi}\right)^d \int \mathcal{Z}(ik_{\mathrm{B}}T\boldsymbol{k}) \exp[-i\boldsymbol{k} \cdot \boldsymbol{r}] \, \mathrm{d}\boldsymbol{k} \ , \tag{4.12}$$

where d is the dimensionality of the vectors. This means that there is a one-to-one correspondence between the two partition functions. If we produce a bead-spring chain with the same constant force ensemble partition function as the true polymer, then necessarily it has the same constant extension ensemble partition function as the true polymer. Though this is obvious for a single dumbbell model, it is not obvious for a multiple spring chain.

There has been recent interest in the constant extension and force ensembles, including what constitutes a "large system" so the ensembles are equivalent and what concepts from thermodynamics do not apply for the single molecule analysis [61]. While our work here also discusses the two ensembles, it is different from previous discussions. Most previous researchers studying these ensembles are discussing them in the context of comparison with stretching experiments of single molecules. Depending on the constraints imposed in the experiment, a different ensemble can be appropriate for the analysis. We have shown that when *coarse-graining*, the spring force-law should be taken from the constant extension ensemble so that the coarse-grained model has the same response as the polymer under all constraints.

4.2 Application to Freely Jointed Chain

4.2.1 Equal rod lengths

As an example of this new method, we apply it to the freely jointed chain model. The result, which we call the Random Walk Spring (RWS) model, is a set of spring forces that allow for the modeling of a FJC with a bead-spring chain at *any* level of discretization while still reproducing the entire

force-extension behavior.

We have seen in the previous section that in order to model the FJC with a bead-spring chain, we must choose the spring potential from the constant extension ensemble partition function. This can be calculated from equation (4.6) directly for the FJC by taking the Fourier transform of both sides, and then inverting the transform. Alternatively, the partition function can be calculated from equation (4.12) since the constant force ensemble partition function is known. The methods obviously give the same result, which is that the constant extension ensemble partition function is proportional to the probability density of a three dimensional random walk, given by the well-known Rayleigh's formula [12]. If the generalized flexibility length is taken to be the Kuhn length, $A_{\text{true}} = a_{\text{K}}$, then ν corresponds to the number of Kuhn lengths represented by each spring. In our notation the constant force ensemble partition function using Rayleigh's formula [62] is

$$\Omega(r) = \frac{1}{r}\int_0^\infty u\sin(ur)\left[\frac{\sin(uA_{\text{true}})}{uA_{\text{true}}}\right]^\nu \mathrm{d}u \ , \tag{4.13}$$

where the integral represents an inverse Fourier transform. Alternatively, the partition function can be written as Treloar's summation formula [63] as

$$\Omega(\mathbf{r}) \propto \frac{1}{r}\sum_{t=0}^{\tau}\frac{(-1)^t}{t!(\nu-t)!}\left[\frac{\nu-(r/A)-2t}{2}\right]^{\nu-2} \ , \tag{4.14}$$

where the upper limit τ is taken from the condition

$$(\nu - r/A)/2 - 1 \leq \ \tau \ < (\nu - r/A)/2 \ . \tag{4.15}$$

We can write the spring potential energy in the Random Walk Spring model, valid for integer ν, as

$$U_{\text{s}}(r) = -k_{\text{B}}T\ln\left\{\frac{1}{r}\int_0^\infty u\sin(ur)\left[\frac{\sin(uA_{\text{true}})}{uA_{\text{true}}}\right]^\nu \mathrm{d}u\right\} \ . \tag{4.16}$$

The spring force is calculated as the derivative of the spring potential

$$f_{\text{spring}}(r) = -k_{\text{B}}T\frac{\partial}{\partial r}\ln\left\{\frac{1}{r}\int_0^\infty u\sin(ur)\left[\frac{\sin(uA_{\text{true}})}{uA_{\text{true}}}\right]^\nu \mathrm{d}u\right\} \ . \tag{4.17}$$

By construction this model reproduces *exactly* the force-extension behavior of the FJC for integer ν. In Figure 4.4 we compare this spring force law with the inverse Langevin function for different values of ν. For $\nu = 2$ we see the RWS force law increasing with decreasing extension, and even diverging at zero extension, but also with a discontinuous divergence at full extension to prevent over-extension. By performing the integration for $\nu = 2$ it is easy to show

$$f_{\text{spring}} = \frac{k_{\text{B}}T}{r} \quad , r < \ell \ . \tag{4.18}$$

We also show in Appendix A.3 how one can verify that this force law gives the required F-E behavior of the FJC. For $\nu = 3$ the RWS model produces another interesting force law. Up to one-third extension, the force is zero. At one-third extension, the force discontinuously jumps to a finite value. The force law decreases to a minimum then increases up to a divergence at full extension.

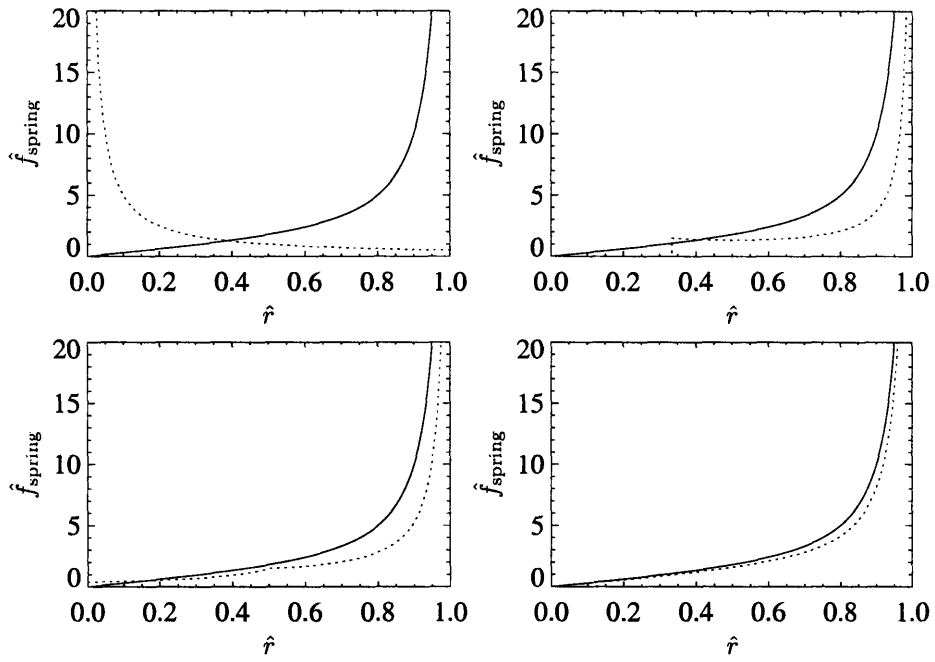

Fig. 4.4: *Comparison of the spring force law chosen from the Random Walk Spring (RWS) model (*dotted*) and chosen from the constant force ensemble force-extension behavior of the true polymer (the inverse Langevin function,* solid line*). The spring force is plotted as* $\hat{f}_{\text{spring}} = f_{\text{spring}} A_{\text{true}}/k_{\text{B}}T$*. The different plots correspond to* $\nu = 2$ *(*Upper left*),* $\nu = 3$ *(*Upper right*),* $\nu = 4$ *(*Lower left*), and* $\nu = 10$ *(*Lower right*).*

The functional form for the case of $\nu = 3$ is

$$f_{\text{spring}} = \frac{3k_{\text{B}}TA_{\text{true}}}{(3A_{\text{true}} - r)r} \quad , \ell/3 < r < \ell \, . \tag{4.19}$$

For $\nu > 3$ the RWS model spring force laws are continuous. However, $\nu = 4$ still shows notable characteristics. At half extension this force law has a discontinuous first derivative, and the force has a non-zero limit at zero extension. This force law is given by

$$f_{\text{spring}} = \begin{cases} \dfrac{3k_{\text{B}}T}{8A_{\text{true}} - 3r} & , 0 < r < \ell/2 \\ \dfrac{k_{\text{B}}T(4A_{\text{true}} + r)}{(4A_{\text{true}} - r)r} & , \ell/2 < r < \ell \end{cases} \tag{4.20}$$

Recall that the inverse Langevin function is the constant force ensemble force-extension behavior of the true polymer. Therefore, the inverse Langevin function would be the spring force law used in the "conventional" method of using the constant force ensemble to obtain the spring force law.

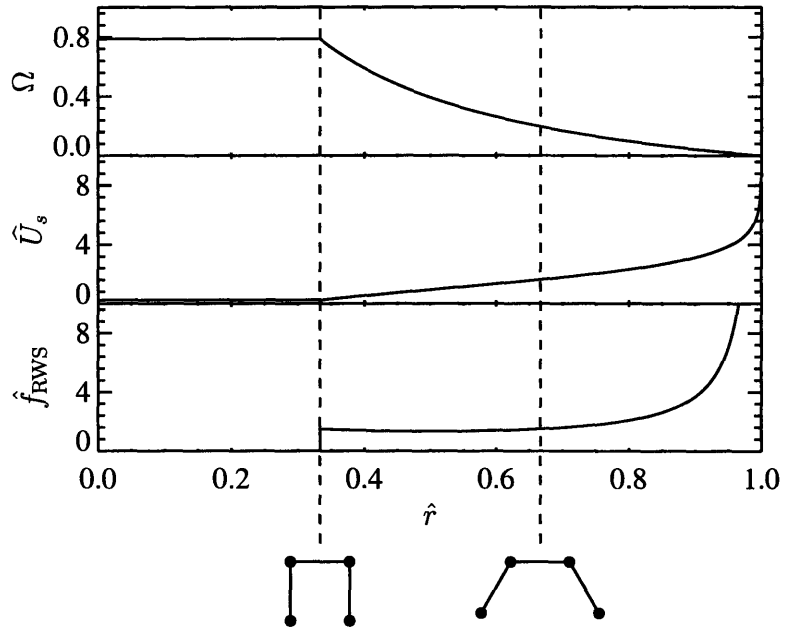

Fig. 4.5: *Progression from the constant extension partition function to the spring force in the Random Walk Spring model for* $\nu = 3$. *The dimensionless axes are* $\widehat{U}_s = U_s/(k_BT)$, $\hat{f}_{\mathrm{RWS}} = f_{\mathrm{RWS}}A/(k_BT)$ *and* $\hat{r} = r/\ell$. *Sample configurations are shown for the three rod system at fractional extensions of* $\hat{r} = 1/3$ *and* $\hat{r} = 2/3$.

The differences between the RWS model and the inverse Langevin function illustrate why the "conventional" method can not be used to model short segments of the FJC (small ν). Only for $\nu \to \infty$ are the constant force and constant extension ensembles equivalent, in which case the inverse Langevin function becomes the correct spring force law.

The dramatic changes in the form of the force-law come about when the true polymer takes configurations of a certain form. They also correspond to changes in the upper limit τ in Treloar's formula, equation (4.15). To better illustrate this, in Figure 4.5 we show Ω, U_s, f_{RWS}, and sample configurations for $\nu = 3$. We see that the step discontinuity occurs when the ends are separated by a distance equal to one rod. For end-to-end distances less than one rod, the partition function (number of configurations) is constant, resulting in a vanishing force. Beyond this special point the partition function decreases but with a discontinuous slope. This change in slope causes a jump discontinuity in the force. The change is discontinuous because the rods are stiff. If one were to coarse-grain three Fraenkel springs into a single spring, it would be continuous, with the discontinuity appearing when the Fraenkel springs become infinitely stiff.

4.2.2 Unequal rod lengths

The freely jointed chain discussed thus far consists of rods of equal length. We can examine how sensitive the spring potentials are to a distribution of rod lengths, which would correspond roughly to a polymer with regions of differing flexibility. If the scale over which the flexibility changes is larger than the Kuhn length, a freely jointed chain with changing rod lengths should be a reasonable model. This situation could appear in block copolymers, atactic polymers, and DNA having blocks with the same repeated base pair. We first must discuss the behavior of the system that is to be modeled. For the equal rod case, the constant force response is the Langevin function for any number of rods. However, the behavior of a general chain is a sum over the response of each rod

$$\langle z \rangle = \sum_{i=1}^{N_r} \langle z_i \rangle = \sum_{i=1}^{N_r} A_i \mathcal{L}\left(\frac{f A_i}{k_B T}\right) , \tag{4.21}$$

where i denotes the different rods in the chain which is to be modeled by a spring, N_r is the number of rods, A_i is the length of rod i, and $\mathcal{L}$ is the Langevin function. In general, this summation does not simplify. To understand how this response differs from the response with equal lengths, we examine the small and large force limits and try to identify an effective Kuhn length for which this appears like a single Langevin function.

If we examine the limit when f is large compared to $k_B T/A_i$ even for the smallest A_i, the average fractional extension of the chain becomes

$$\frac{\langle z \rangle}{\ell} \simeq 1 - \frac{k_B T N_r}{f \ell} , \tag{4.22}$$

where ℓ is the fully-extended length of spring and is equal to the sum of the rod lengths

$$\ell = \sum_{i=1}^{N_r} A_i . \tag{4.23}$$

Comparing this behavior with a system with equal rod lengths gives a high-force effective Kuhn length

$$A_{\text{eff,h}} = \frac{\ell}{N_r} = \frac{1}{N_r} \sum_{i=1}^{N_r} A_i = \overline{A} . \tag{4.24}$$

We have introduced the over-bar notation for the average over the rods in the chain. If we expand the fractional extension for small force, the behavior becomes

$$\frac{\langle z \rangle}{\ell} \simeq \frac{f}{3 k_B T} \sum_{i=1}^{N_r} A_i^2/\ell . \tag{4.25}$$

Therefore the low-force effective Kuhn length is

$$A_{\text{eff,l}} = \sum_{i=1}^{N_r} A_i^2/\ell = \sum_{i=1}^{N_r} A_i^2 / \sum_{i=1}^{N_r} A_i = \overline{A^2}/\overline{A} . \tag{4.26}$$

The high-force value is simply the average rod length, while the low-force value in equation (4.26) is larger. The larger the spread in rod lengths, the larger the difference between the two.

After understanding the constant force response of the bead-rod chain, we can examine the spring force needed in a bead-spring model that gives the same constant force response (which itself differs from a single Langevin function). As shown previously, this spring force comes from the constant extension response of the bead-rod chain. This can be written again using Rayleigh's formula but for a random walk with non-identical steps. For example, to use a spring to model a three rod system with rod lengths A_1, A_2, and A_3 one should use a spring potential energy of

$$U_s(\mathbf{r}) = -k_B T \ln \left\{ \frac{1}{r} \int_0^\infty u \sin(ur) \frac{\sin(uA_1)}{uA_1} \frac{\sin(uA_2)}{uA_2} \frac{\sin(uA_3)}{uA_3} \mathrm{d}u \right\} . \tag{4.27}$$

The spring force is the derivative of this potential.

Let us examine a specific system to illustrate the behavior of these unequal rod chains. Figure 4.6 shows the spring force needed for a series of chains each with m rods of length A and m rods of length $5A$ for m ranging from 1 to 6. Similar to the equal rod case, for short chains (small m) the spring force laws needed have discontinuities. For example, when $m = 1$ it is impossible for the fractional extension to be less than 2/3. Because a positive force is a retractive force, the force diverges to $-\infty$ to prevent the fractional extension from being less than 2/3. Only in the large m limit does the spring force law approach the constant force behavior. Note that even in this limit the spring force needed differs from a single Langevin function based on the average rod length.

Figure 4.6 allowed us to examine how the chains approach the infinitely long limit if the rods have a significant difference in lengths. To further examine how different rod lengths affect the spring force law needed to model the chain, we will compare chains will the same contour length but with different ratios of rod lengths. The system contains m rods of length A and m rods of length pA. The constraint of constant contour length means that $m(1 + p)$ is held constant. Figure 4.7 shows an example of the rod system with $m(1 + p) = 12$ and m ranging from 1 to 6. Note that the $m = 2$ case was already seen in Figure 4.6, and the $m = 6$ case has 12 equal length rods. For this example, two effects help make the response closer to the inverse Langevin function as m increases; not only does the number of rods increase with m but also the variance in rod lengths decreases.

In Figure 4.7 we scaled the force using the average rod length, which changes with m. We saw that for the constant force response this scaling made curves for all distributions of rod lengths and number of rods have the same high force limiting behavior. Let us examine closer the constant extension response near full extension. Consider a chain of ν rods with lengths A_1, A_2, to A_ν. We denote the smallest rod length by A_s. It has been observed that in the region $\ell - 2A_\mathrm{s} < r < \ell$ the partition function is

$$\Omega(\mathbf{r}) \propto \frac{(\ell - r)^{\nu-2}}{r} . \tag{4.28}$$

This has been explicitly verified for a number of examples for small ν, while a general proof for arbitrary ν appears excessively tedious like a related proof given in Appendix F of [10]. The spring force needed in this region of extension is

$$f_s(r) = k_\mathrm{B} T \left(\frac{1}{r} + \frac{\nu - 2}{\ell - r} \right) . \tag{4.29}$$

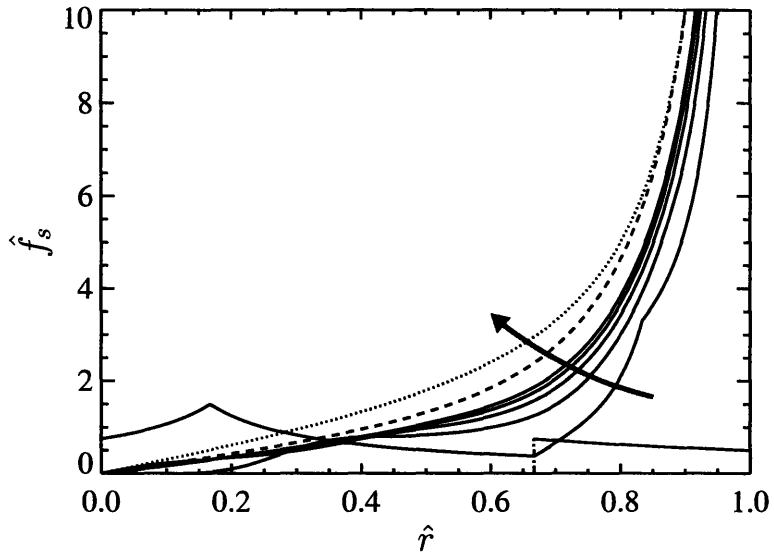

Fig. 4.6: *Series of spring forces necessary to model chains with m rods of length A and m rods of length 5A for* $m = 1, 2, 3, 4, 5, 6$, *with the arrow denoting increasing m. The dimensionless axes are* $\hat{f}_s = f_s 3A/k_B T$ *and* $\hat{r} = r/\ell$. *The dashed line corresponds to* $m = \infty$. *The dotted line is the inverse Langevin function. Note that the* $m = 1$ *force law diverges at* $\hat{r} = 2/3$ *and* $\hat{r} = 1$.

If we non-dimensionalize the force using the average Kuhn length, $\overline{A}$, the force as a function of fractional extension, $\hat{r}$, is

$$\frac{f_s \overline{A}}{k_B T} = \frac{1 + (\nu - 3)\hat{r}}{\nu \hat{r}(1 - \hat{r})} \,. \tag{4.30}$$

Because this force only depends on ν and not the exact distribution of rod lengths, the force is the same in this region as an equal rod system having ν rods each of length $\overline{A}$. Note that this relation is *exact* over a *finite* range which is determined by the smallest rod length. This can be compared with the constant force response, for which it only matches the response of ν rods each of length $\overline{A}$ in the *limit* $r \to \ell$.

By examining the FJC with unequal rod lengths, we have examined a crude model for chains with variable flexibility. Both the constant force response and the constant extension response differ from the equal rod case (a single Langevin function). In other words, even in the infinite chain limit, the unequal rod system *can* be distinguished from an equal rod model. Also, throughout the analysis, the order of the rods within a spring did not matter. This can be seen directly from equation (4.27) for the three rod system. The formula is the same independent of the ordering of the rods.

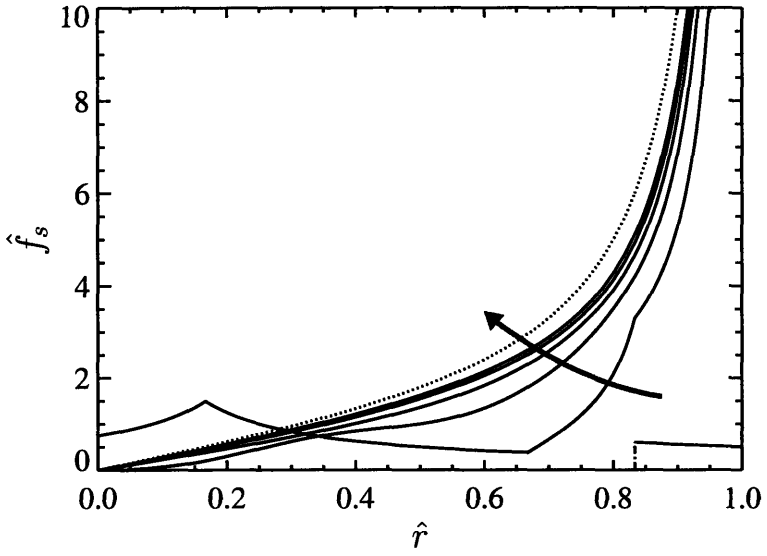

Fig. 4.7: *Series of spring forces necessary to model chains with m rods of length A and m rods of length pA for* $m = 1, 2, 3, 4, 5, 6$, *with the arrow denoting increasing m. The value of p is determined from the condition of constant contour length,* $m(1+p) = 12$. *The dimensionless axes are* $\hat{f}_s = f_s(6/m)A/k_BT$ *and* $\hat{r} = r/\ell$. *The dotted line is the inverse Langevin function. Note that the* $m = 1$ *force law diverges at* $\hat{r} = 5/6$ *and* $\hat{r} = 1$.

4.2.3 Approximate spring force law

While the models developed using the constant extension ensemble are advantageous in that they give the correct equilibrium behavior and provide a systematic method for changing levels of coarse-graining, some practical issues remain for using them in computations such as Brownian dynamics simulations. For small numbers of rods per spring, the spring force laws can have discontinuities. How do discontinuous force laws perform in BD simulations? We address this question by simulating directly using BD the two-rod and three-rod spring force laws at equilibrium.

The two-rod spring force law is proportional to r^{-1} for allowable extensions. At full extension, the retractive force must jump to $+\infty$ to prevent the spring from extending past that point. The two features not common to spring force laws are the divergence at small extension and the discontinuity at full extension. To test the ability to use this force law in a Brownian dynamics simulation, we use a simple explicit Euler integration scheme [46]. With this scheme it is possible for the length of the spring at the end of a time step to be larger than the fully-extended length of the spring. This is analogous to two hard spheres which are not allowed to have a separation distance smaller than their diameter. For this spring force law, we implement the same type of algorithm used for hard spheres [64, 65]. If the spring is past full extension at the end of a time step, we rescale the length of the spring to be at full extension. This algorithm is known to converge to the correct answer as the time step is reduced. For larger time steps, it is known that this algorithm produces a

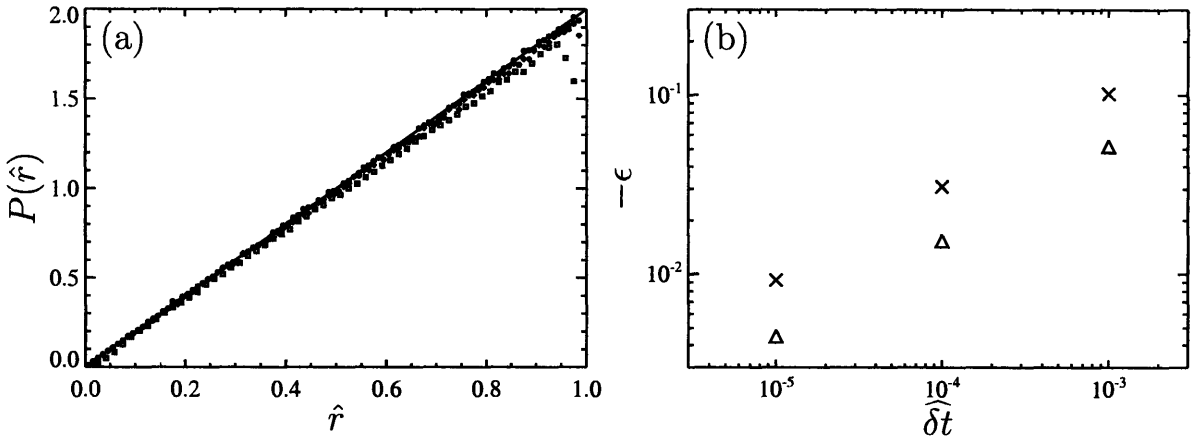

Fig. 4.8: *This shows the convergence of a BD simulation for a spring force law that models two rods of a freely jointed chain. (a) Histogram of the probability density of the spring length from a BD simulation compared with the exact distribution. The time steps used were* $\widehat{\delta t} = 10^{-3}$ *(□),* $\widehat{\delta t} = 10^{-4}$ *(◇), and* $\widehat{\delta t} = 10^{-5}$ *(○). (b) The relative error in the second moment* $\langle \hat{r}^2 \rangle_{\text{eq}}$ *(△) and the fourth moment* $\langle \hat{r}^4 \rangle_{\text{eq}}$ *(×) from the BD simulations.*

delta-function in the probability density at full extension with a corresponding depletion at smaller extensions.

We tested the algorithm by choosing a random starting configuration and stepping forward in time to equilibrate in a stagnant solvent. We then continued simulating at equilibrium and sampling the magnitude of the extension of the spring. From this we build a histogram of the probability distribution of the spring length. The spring length was sampled 10^6 times to reduce the statistical error from finite sampling so most of the error is due to the non-zero time step. We show in Figure 4.8(a) the histograms for different time steps compared to the true distribution. The time step is nondimensionalized as

$$\widehat{\delta t} \equiv \delta t \left(\frac{k_{\text{B}} T}{\zeta \ell^2} \right) \tag{4.31}$$

where ζ is the drag coefficient on a bead and ℓ is the fully-extended length of the spring. We also show in Figure 4.8(b) the convergence of the second and fourth moments of the spring length, $\langle \hat{r}^2 \rangle_{\text{eq}}$ and $\langle \hat{r}^4 \rangle_{\text{eq}}$, to the true values. To avoid ambiguity in the sign, we define the relative error as

$$\epsilon \equiv \frac{\text{true value - calculated value}}{\text{true value}} . \tag{4.32}$$

The three-rod spring force law also has a feature not common to force laws. It has a finite jump in the force at 1/3 extension. This jump is equivalent to a discontinuous slope in the probability density. We again test the ability of a simple explicit Euler scheme to capture this feature. Even

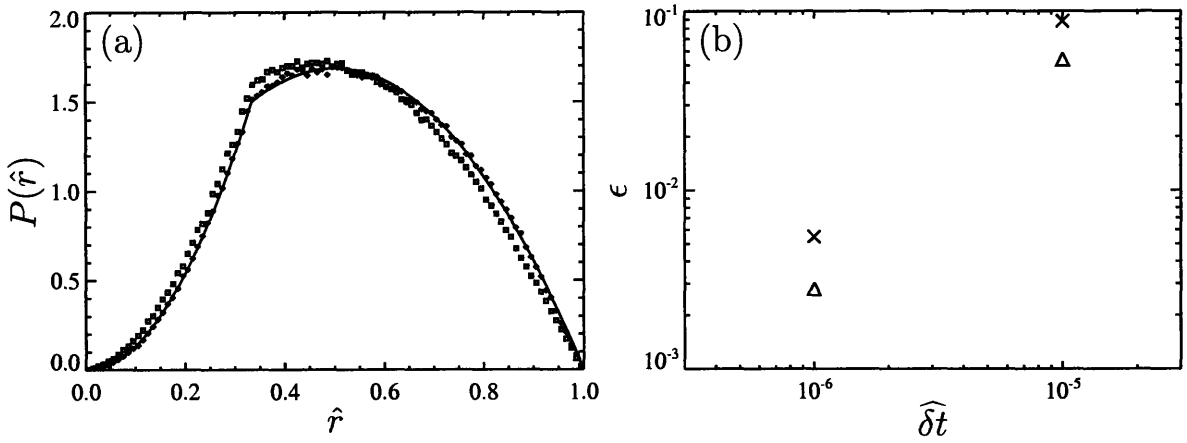

Fig. 4.9: *This shows the convergence of a BD simulation for a spring force law that models three rods of a freely jointed chain. (a) Histogram of the probability density of the spring length from a BD simulation compared with the exact distribution. The time steps used were* $\widehat{\delta t} = 10^{-5}$ *(□) and* $\widehat{\delta t} = 10^{-6}$ *(◇). (b) The relative error in the second moment* $\langle \hat{r}^2 \rangle_{\text{eq}}$ *(△) and the fourth moment* $\langle \hat{r}^4 \rangle_{\text{eq}}$ *(×) from the BD simulations.*

though the spring force law does continuously diverge at full extension, with this scheme it is possible to end a time step past full extension. While there exist more sophisticated schemes for handling this, we opt for the simple algorithm of rescaling the spring to be at 0.99999 of full extension.

We formed the probability density histogram in the same way as for the two-rod spring. In Figure 4.9(a) the histograms for different time steps are compared to the true distribution. We also show in Figure 4.9(b) the convergence of the second and fourth moments of the spring length to the true values.

These two examples show that it is possible to simulate the new spring force laws using simple BD algorithms. More elaborate schemes may be able to increase the size of time steps although at the increased computation cost of a more sophisticated algorithm.

The other main practical issue concerns the spring laws when each spring represents a larger number of springs. Although we have shown that the spring force from the RWS model (calculated from equation (4.17)) exactly represents the freely jointed chain, and similarly for the unequal rod case, the analytical expressions for the spring force laws become increasing complicated as each spring represents more rods. We have seen that the spring force law has different forms in different regions of fractional extension. For the equal rod length case the number of different regions is 1/2 of the number of rods per spring (rounding up to the nearest integer). Thus as the number of rods per spring increases, the number of different regions increases dramatically. Within each of these regions, the force law is a rational function where the degree of the polynomials typically increases rapidly as the number of rods per spring increases. The large number of regions and the complexity within each region decreases the practicality of these force laws for large number of rods per spring.

However in this limit the spring force laws are becoming smooth, making it likely that approximate force laws can be developed in the same spirit as approximating the inverse-Langevin function by a simple rational function.

Our task for the remainder of this section is to develop a spring force law which approximates the RWS model, because it is that spring force law that exactly models the freely jointed chain. We start by considering the equal rod case. We have shown that the RWS model can be used directly when each spring represents two or three rods. When each rod represents four rods, the RWS model only has two regions of extension, with a simple form in each region, and so could also be easily implemented in BD simulations.

For the cases where each spring represents five or six rods the spring force laws have three regions in extension. The force law in the third region (near full extension) is given by equation (4.30). We can develop a single functional form that can approximate the first two regions. In this way we can approximate the RWS model which has three regions in extension by a spring force law which only has two regions and so is easier to implement in simulations. An approximate force law for the five-rod case is

$$\frac{f_s A}{k_B T} \approx \frac{539\hat{r}/225}{1 - 3\hat{r}^2/5} \ , \ 0 < \hat{r} < 3/5 \ , \tag{4.33}$$

$$\frac{f_s A}{k_B T} = \frac{1 + 2\hat{r}}{5\hat{r}(1 - \hat{r})} \ , \ 3/5 < \hat{r} < 1 \ . \tag{4.34}$$

The parameters for the force law in the first region were chosen by first assuming a functional form in $\hat{r}$ with two adjustable constants. The parameters were constrained so that the force law is continuous at $\hat{r} = 3/5$ because the RWS model for five rods is continuous. The other free parameter was chosen to give a small error in the second and fourth moment of the spring length at equilibrium. The error in $\langle \hat{r}^2 \rangle_{eq}$ by using this approximate force law to model five rods is 0.02%. The error in $\langle \hat{r}^4 \rangle_{eq}$ is 0.0006%.

A similar method can be used to approximate the six-rod case. The approximate force law is

$$\frac{f_s A}{k_B T} \approx \frac{63\hat{r}/25 - 49\hat{r}^3/125}{1 - 9263\hat{r}^2/13500} \ , \ 0 < \hat{r} < 2/3 \ , \tag{4.35}$$

$$\frac{f_s A}{k_B T} = \frac{1 + 3\hat{r}}{6\hat{r}(1 - \hat{r})} \ , \ 2/3 < \hat{r} < 1 \ . \tag{4.36}$$

This approximate force law for the six-rod system has an error of 0.01% in $\langle \hat{r}^2 \rangle_{eq}$ and an error of 0.02% in $\langle \hat{r}^4 \rangle_{eq}$.

The advantage of still using two regions for the five and six-rod cases is that we can utilize exactly the RWS model in the final region of extension. This allows us to build an approximation that accurately represents many properties such as the second and fourth moments of the spring length and also the response under large stretching.

For even larger number of rods per spring the final region near full extension which has a simple force law is only valid over a smaller and smaller region of extension. In this case the advantage to using two spring force laws spliced together does not seem great and so we have chosen to develop a single approximate force law over the entire extension range. While many possible forms are

possible to approximate the true spring force laws, we choose the form

$$\frac{f_s A}{k_B T} = \frac{C\hat{r} + D\hat{r}^3}{1 - \hat{r}^2} \tag{4.37}$$

where A is the rod length and C and D do not depend on the fractional extension, $\hat{r}$, but will depend on the number of rods represented by the spring, ν. The dependence on $\hat{r}$ takes the same form as the Cohen force law [66]. We will see that with an appropriate choice of C and D, this can give an accurate representation of the freely jointed chain. Because we have chosen the same form in $\hat{r}$ as the Cohen force law, calculations such as BD simulations can be easily and quickly modified to use the new force law with no loss of computation speed but a uniformly more accurate result.

Although we are not using the RWS force law near full extension, we will still require that the limiting behavior of our approximate form match the limiting behavior of the RWS force law. The result of this choice will be that the approximate spring will behave like the freely jointed chain in the limit of strong stretching. As the fractional extension approaches 1, the RWS force law diverges as

$$\frac{f_s A}{k_B T} \to \frac{1 - 2/\nu}{1 - \hat{r}} \ . \tag{4.38}$$

For our approximate force law to diverge in the same manner, we obtain the constraint on C and D of

$$C + D = 2 - 4/\nu \ . \tag{4.39}$$

We must now develop a method for determining the remaining free parameter. One natural method would be to examine the RWS force law at small extension, find the coefficient to $\hat{r}$ in that expansion which will be a function of ν, and match this coefficient with C. Because the constraint on $C + D$ is to capture the strong stretching limit, the rationale behind this choice would likely be so that the spring correctly captures the equilibrium limit. However, with this choice the second moment of the spring length at equilibrium, $\langle \hat{r}^2 \rangle_{\text{eq}}$, is *not* correct. This is because, even at equilibrium, the spring samples the non-linear regions of the force law, and the shape of the approximate force law does not exactly capture the shape of the RWS model.

Alternatively, one could calculate numerically the function $C(\nu)$ such that the second moment of the spring length for the approximate force law matches exactly the freely jointed chain (which is also the same as the RWS model). Recall that the second moment of the spring length is a key property that is important to capture [67]. Not only is it related to the size of the coil at equilibrium, but also it is related to the zero-shear viscosity. In the constant-force ensemble, the slope of the average extension versus force curve at small force is also proportional to the second moment of the spring length.

Instead of having to deal with a numerical function $C(\nu)$, it would be better to have a simple approximate formula for $C(\nu)$ that still gives a very small error in the second moment of the spring length. Another reason an approximate form for $C(\nu)$ is sufficient is that even if we could make the error in the second moment vanish, the shape of the spring force law will limit the ability to capture other properties like the fourth moment exactly.

Using the asymptotic expansion developed in ref. [67], the second moment of the spring length

for the force law (equation (4.37)) with the constraint in equation (4.39) is

$$\langle \hat{r}^2 \rangle_{\text{eq}} \sim \frac{3}{\nu C} - \frac{30}{\nu^2 C^3} + \frac{30(24 - 7C + 2C^2)}{\nu^3 C^5} + \mathcal{O}\left(\frac{1}{\nu^4}\right) . \tag{4.40}$$

We want to choose $C(\nu)$ such that this second moment is the same as the freely jointed chain. The freely jointed chain has $\langle \hat{r}^2 \rangle_{\text{eq}} = 1/\nu$. By choosing

$$C = 3 - \frac{10}{3\nu} + \frac{10}{27\nu^2} , \tag{4.41}$$

the second moment of the spring length for the approximate spring force law (equation (4.37)) is

$$\langle \hat{r}^2 \rangle_{\text{eq}} \sim \frac{1}{\nu} + \mathcal{O}\left(\frac{1}{\nu^4}\right) . \tag{4.42}$$

The resulting approximate spring force law is

$$\frac{f_s A}{k_{\text{B}} T} = \frac{\left(3 - \frac{10}{3\nu} + \frac{10}{27\nu^2}\right)\hat{r} - \left(1 + \frac{2}{3\nu} + \frac{10}{27\nu^2}\right)\hat{r}^3}{1 - \hat{r}^2} . \tag{4.43}$$

To quantify the accuracy of this approximate spring force law, we need to compare it's properties with those of the underlying freely jointed chain. The average $\langle \hat{r}^2 \rangle_{\text{eq}}$ of this spring force law is compared in Figure 4.10(a) to the freely jointed chain it is meant to represent as a function of the number of rods per spring. From the asymptotic expansion of the second moment, equation (4.42), we see that the relative error should go like ν^{-3} which we see explicitly from Figure 4.10(a). The approximate spring force law has an error of 0.01% at $\nu = 6$ and smaller error for larger ν. For reference we show the error if the Cohen force law were used. An asymptotic expansion of the second moment of the spring length using the Cohen force law shows the relative error decays like ν^{-1} as seen in the figure. The slight changes made to the Cohen form have had a significant impact. The error has been reduced by over a factor of 1000. The new force law can even be used down to four rods per spring with only a small error.

The fourth moment of the spring length is also important to capture correctly because of it's impact on zero-shear rheology. Similar to the second moment, we show in Figure 4.10(b) the error in the fourth moment of the spring length for the approximate force law with the error of the Cohen form for comparison. The fourth moment of the spring length for the freely jointed chain is $\langle \hat{r}^4 \rangle_{\text{eq}} = (5\nu - 2)/(3\nu^3)$. Again we see that the error of the approximate force law (equation (4.43)) is very small, only about 1% at $\nu = 6$ and smaller at larger ν. The error has been reduced by about a factor of 40 below that of the Cohen force law.

The final property we analyze here is the force-extension behavior in the constant force ensemble. Recall that the response of the freely jointed chain in this ensemble is the Langevin function, $\langle \hat{z} \rangle = \mathcal{L}(\hat{f})$. We compare the error of the approximate force law and the Cohen force law in Figure 4.11 for $\nu = 4, 6, 20, \infty$. Note that the error does not exactly vanish in the limit $\nu \to \infty$ because the Cohen force law is not exactly the inverse Langevin function, although the error in fractional extension is less than 2% in that limit.

We have now developed and analyzed the error from using an approximate spring force law

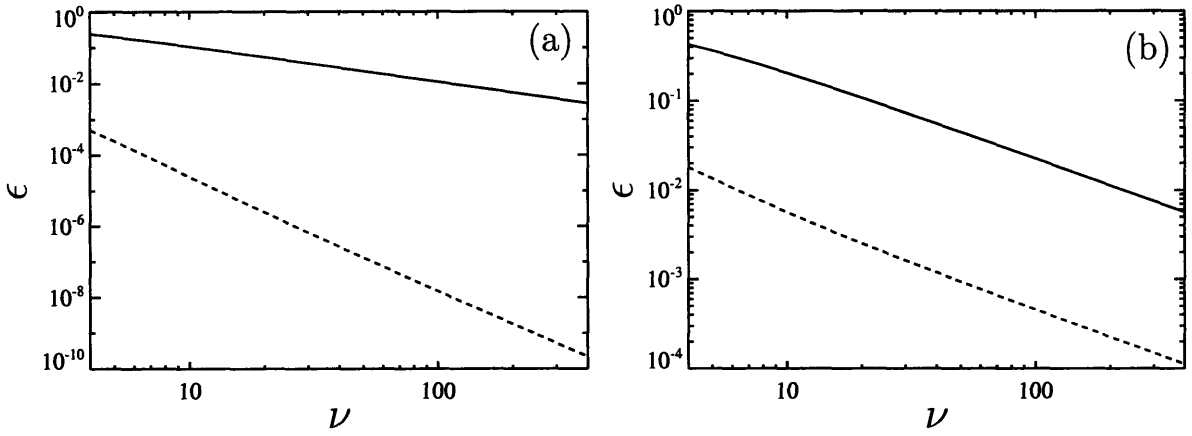

Fig. 4.10: *Relative error in the equilibrium moments of the spring length between an approximate spring force law compared with an equal rod freely jointed chain. The solid lines are for the Cohen force law, and the dashed lines are for the new force law (equation (4.43)). (a) Relative error in the second moment,* $\langle \hat{r}^2 \rangle_{\text{eq}}$. *(b) Relative error in the fourth moment,* $\langle \hat{r}^4 \rangle_{\text{eq}}$.

(equation (4.43)) to represent freely jointed chains. The error from using this approximate force law instead of the RWS model is small enough that the dominant error in a Brownian dynamics simulations will likely be from a nonzero integration time step and statistical error from a finite number of samples. *The error is small even when each spring represents only four rods.* It is important to emphasize that the new force law (equation (4.43)) outperforms the Cohen force law at all levels of discretization and so should be used instead of the Cohen force law by future simulators.

We can develop a similar approximate force law that models freely jointed chains with unequal rod lengths by proceeding in the exact same manner. As with the equal rod case, we will assume a form like the Cohen force law:

$$\frac{f_s \overline{A}}{k_{\text{B}} T} = \frac{B\hat{r} + G\hat{r}^3}{1 - \hat{r}^2} \ . \tag{4.44}$$

The values of B and G will depend on the number of rods and also the distribution of rod lengths. For the spring to have the correct limiting behavior at full extension we need

$$B + G = 2 - 4/\nu \tag{4.45}$$

where here ν is defined using the average rod length, $\nu = \ell/\overline{A}$, which is equal to the total number of rods that the spring represents. For the equal rod case, we used the expansion of the second moment of the spring length for the approximate spring to get the remaining parameter B. Because the spring force takes the same form as the equal rod case, the expansion of the second moment of

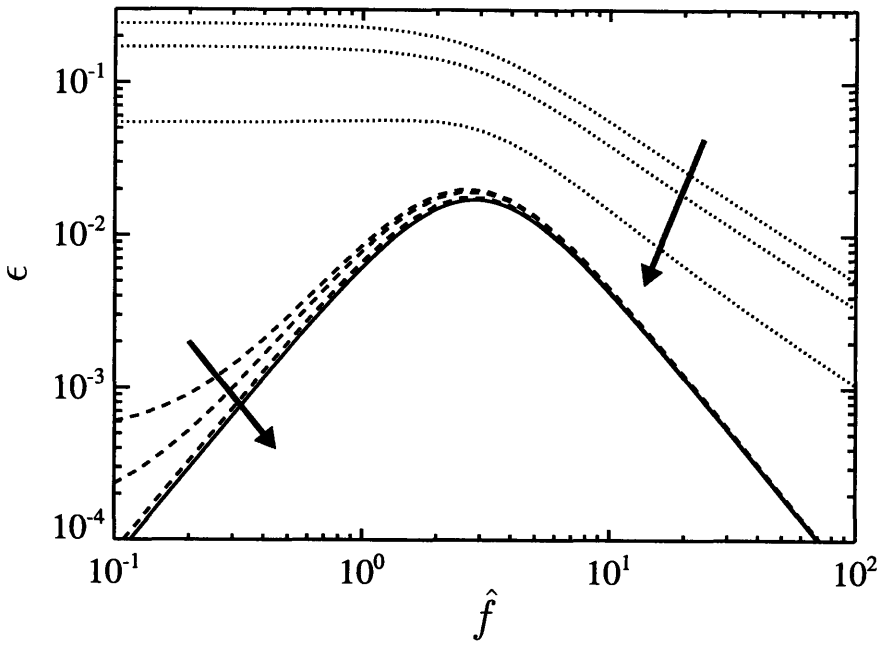

Fig. 4.11: *Relative error in the average fractional extension between an approximate spring force law compared with an equal rod freely jointed chain, where the number of rods each spring represents is* $\nu = 4, 6, 20, \infty$ *and the arrows denote increasing* ν. *The dotted lines are for the Cohen force law, the dashed lines are for the new approximate force law (equation* (4.43)*), and the solid line is the* $\nu = \infty$ *limit of both force laws. The force is nondimesionalized using the rod length,* $\hat{f} = fA/k_{\mathrm{B}}T$.

the spring length is the same:

$$\langle \hat{r}^2 \rangle_{\mathrm{eq}} \sim \frac{3}{\nu B} - \frac{30}{\nu^2 B^3} + \frac{30(24 - 7B + 2B^2)}{\nu^3 B^5} + \mathcal{O}\left(\frac{1}{\nu^4}\right) . \tag{4.46}$$

We choose B in order to match this second moment with the second moment of the freely jointed chain. The second moment of the freely jointed chain is $\langle \hat{r}^2 \rangle_{\mathrm{eq}} = A_2/\nu$, where A_2 is a function of the distribution of rod lengths and is defined as $A_2 \equiv \overline{A^2}/\overline{A}^2$. Similarly we will define $A_4 \equiv \overline{A^4}/\overline{A}^4$, which we will use later in discussing the fourth moment. By choosing

$$B = \frac{3}{A_2} - \frac{10A_2}{3\nu} + \frac{10A_2(4A_2^2 - 21A_2 + 18)}{27\nu^2} , \tag{4.47}$$

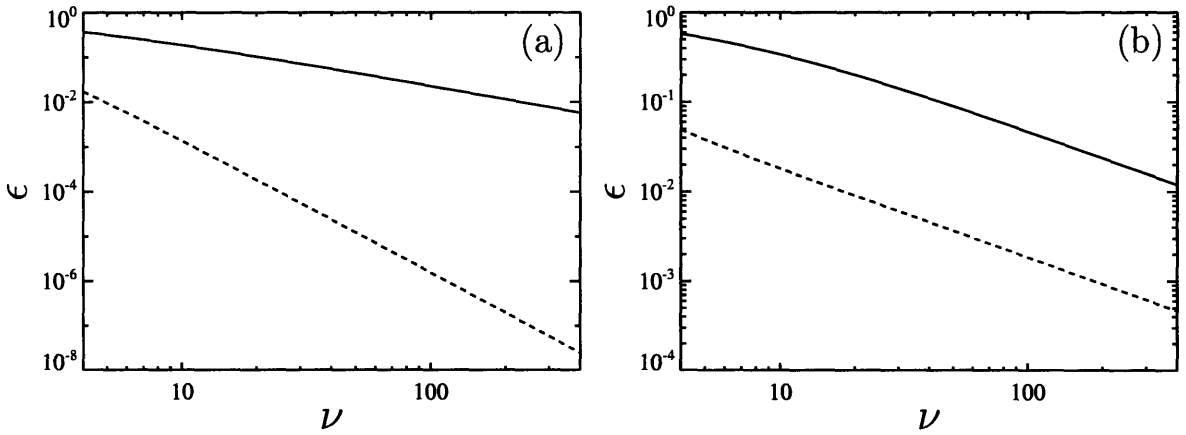

Fig. 4.12: *Relative error in the equilibrium moments of the spring length between an approximate spring force law compared with a unequal rod freely jointed chain. The solid lines are for the equation* (4.50) *force law, and the dashed lines are for the new force law (equation* (4.49)*). (a) Relative error in the second moment,* $\langle \hat{r}^2 \rangle_{\text{eq}}$. *(b) Relative error in the fourth moment,* $\langle \hat{r}^4 \rangle_{\text{eq}}$.

the second moment of the spring length for the approximate spring force law (equation (4.44)) is

$$\langle \hat{r}^2 \rangle_{\text{eq}} \sim \frac{A_2}{\nu} + \mathcal{O}\left(\frac{1}{\nu^4}\right) . \tag{4.48}$$

The resulting approximate spring force law is

$$\frac{f_s \overline{A}}{k_B T} = \left(\frac{3}{A_2} - \frac{10A_2}{3\nu} + \frac{10A_2(4A_2^2 - 21A_2 + 18)}{27\nu^2} \right) \hat{r} + \frac{(2 - 4/\nu)\hat{r}^3}{1 - \hat{r}^2} . \tag{4.49}$$

In the limit $\nu \to \infty$ this becomes

$$\frac{f_s \overline{A}}{k_B T} = \frac{3}{A_2}\hat{r} + \frac{2\hat{r}^3}{1 - \hat{r}^2} . \tag{4.50}$$

We can quantify the accuracy of the approximate force law by comparing the second and fourth moments of the spring length with the second and fourth moments for the underlying freely jointed chain. The fourth moment of the freely jointed chain is $\langle \hat{r}^4 \rangle_{\text{eq}} = (5A_2^2\nu - 2A_4)/(3\nu^3)$. Even when expressing a unequal rod system in terms of a few averages over the rods, the parameter space is large. We will quantify the error of the approximate spring force law for the same system shown in Figure 4.6. This system consists of equal numbers of rods of length A and rods of length $5A$, resulting in $A_2 = 1.444$ and $A_4 = 3.862$. With these parameters fixed, we change the number of rods, and examine the error in the moments of the spring length in Figure 4.12.

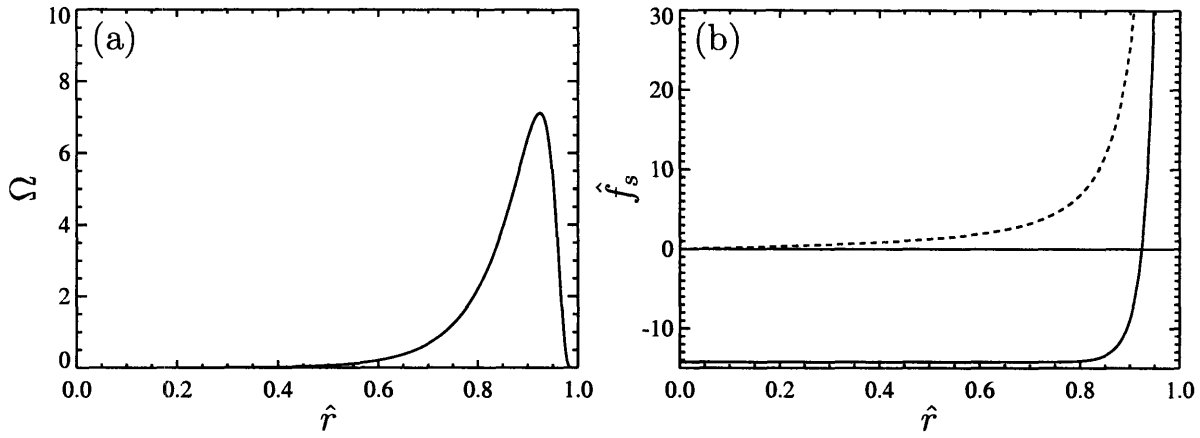

Fig. 4.13: *(a) Constant extension partition function of a single F-actin filament. (b) Comparison of the spring force law determined by the PET method (solid line) for a dumbbell model of an F-actin filament with the Marko-Siggia interpolation formula (dashed line). The force is made dimensionless using the persistence length,* $\hat{f}_s = f_s A_p / k_B T$.

4.3 Application to Worm-like Chain

4.3.1 Application to dumbbell model

The next polymer model we examine is the worm-like chain (WLC), but initially only for dumbbell models. The next section discusses the extension to multi-spring chains. The application for a dumbbell follows the general prescription given in equation (4.8). If the worm-like chain contains a large number of persistence lengths, then the spring force law reduces to the long chain limit approximated by the Marko-Siggia interpolation formula. However, many biopolymers of interest, such as F-actin and microtubules, do not contain many persistence lengths. In contrast to the FJC, for which exact analytical results can be obtained for short chains, the analytical calculation of the exact distribution function for short WLC's can not be done at this time. However, a number of numerical and approximate analytical techniques have been developed recently [68, 69, 70].

As an example, we calculate the spring force needed to model a single actin filament using a dumbbell. Because the end-to-end distance distribution for an actin filament has been measured experimentally [71], this example illustrates how the use of the distribution function to produce a bead-spring model is not restricted to analytical models. The distribution function can come directly from experiments.

Ref. [71] show that the distribution for actin matches well to the worm-like chain, and ref. [68] develops a good approximation to that behavior. In Figure 4.13(a) we show the distribution function of a 3-D WLC calculated from the approximate formula given by ref. [68] for the actin parameters found by ref. [71]: $L = 13.40\mu$m , $A_p = 16.1\mu$m. In Figure 4.13(b) we compare the resulting spring force necessary to reproduce the actin distribution with the Marko and Siggia interpolation

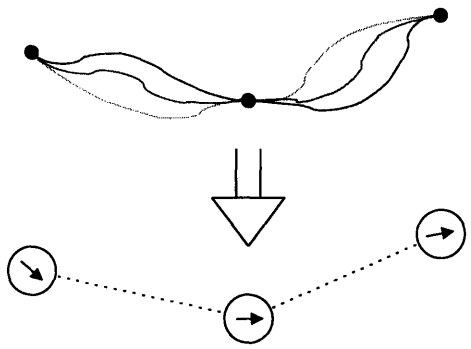

Fig. 4.14: *Restricting the configurations within a category eliminates the coupling in a multi-spring worm-like chain model. Within each category the reference points (black circles) are held fixed as well as the polymer's tangent vector at the reference point. The lines signify different polymer configurations within the category. The coarse-grained model consists of beads which have a vector direction which is the direction of the polymer's tangent vector. The interaction of neighboring beads depends both on the bead positions and the bead directions.*

formula. The dramatic difference between the force laws illustrates the importance of choosing the correct one, because the incorrect use of the Marko and Siggia form would result in significant errors.

4.3.2 Exact generalized model

In order to develop a multi-spring model of the worm-like chain, one must calculate the multidimensional partition function $\Omega(\mathbf{r}_1, \mathbf{r}_2, \ldots)$. This illustrates a hurdle with implementing the PET method. For models such as the worm-like chain with coupling across the reference points (black circles in Figure 4.3), the multidimensional partition function is not separable, and therefore the spring potential energy is not separable into a sum over each spring.

However, we can use the same thought process used in Figure 4.3 to overcome the difficulty in a systematic way. We can eliminate the coupling between the segments by further restricting the category of configurations. The new type of model is illustrated in Figure 4.14. In addition to holding points along the polymer with fixed positions, the tangent vector of the polymer is held fixed at each of these points. Because the tangent vector is held fixed, there is no coupling across the points. We can replace the category of configurations by a single configuration of a coarse-grained model. This new coarse-grained model is not a typical type of bead-spring chain, but a series of beads that have a direction associated with them (the direction of the polymer's tangent vector). The interaction of two neighboring beads depends both on the vector connecting the bead centers, $\mathbf{r}$, and the tangent vectors associated with the beads, $\mathbf{t}_1$ and $\mathbf{t}_2$. The "potential energy" of this interaction is

$$U(\mathbf{r}, \mathbf{t}_1, \mathbf{t}_2) = -k_B T \ln \Omega(\mathbf{r}, \mathbf{t}_1, \mathbf{t}_2) \tag{4.51}$$

where $\Omega(\mathbf{r}, \mathbf{t}_1, \mathbf{t}_2)$ is the partition function in the ensemble where both the separation of the ends and tangent vectors at the ends are held fixed.

While this new type of coarse-grained model will give the correct equilibrium distribution function as the worm-like chain at any level of discretization, it may not be computationally desirable to perform simulations such as Brownian dynamics (BD) with such a model.

We propose that this system can be approximated by a conventional bead-spring chain with bending potentials. The spring force in this approximation would be taken as the force in a dumbbell model of the short segment of polymer. This separation is a reasonable first approximation because it correctly models the behavior at the two extremes of discretization.

In the limit of a large number of persistence lengths between reference points, the coupling vanishes and thus the bending energy should vanish. In the limit of zero persistence lengths between reference points, the polymer acts like a rigid rod. The polymer model of rigid rods with bending potentials is the Kratky-Porod model if we choose the bending potential to be

$$U_{\text{bend}}(\theta) = \frac{k_B T A_p}{2\ell}\theta^2 \ , \tag{4.52}$$

where θ is the angle between the directions of successive rods, ℓ is the length of the rod, and A_p is the persistence length. In the limit of ℓ much smaller than A_p this approaches the continuous WLC model. This bending energy could also be used when the spring length, ℓ, is much larger than the persistence length, A_p, because it correctly vanishes in that limit. We leave a detailed analysis of the decomposition approximation using bending energy and an analysis of how the bending energy varies with $\nu = \ell/A$ for future work.

4.3.3 Use of bending potentials

Although the use of bending potentials to approximate the exact generalized model may provide the best approximation, there are still hurdles to overcome to implement that model and guarantee that it is in fact a good approximation. At large discretization these models with bending potentials would look similar to a Kratky-Porod model [16, 72, 73, 74]. However, in some situations it may be sufficient to develop a model without bending potentials, but simply with an altered spring force law. Before developing this new spring force law, we must discuss some implications of using a model without bending potentials between the springs as a coarse-grained version of the worm-like chain.

Consider the continuous worm-like chain in Figure 4.15. The vectors $\mathbf{r}_1$ and $\mathbf{r}_2$ correspond to segments of polymer which will be modeled by springs. The polymer has a persistence length A_p, and each segment has a contour length of ℓ, so represents $\nu = \ell/A_p$ number of persistence lengths. The segments are separated by an amount of polymer with contour length ℓc. One way of examining the assumptions in the coarse-grained model is to compare $\langle \mathbf{r}_1^2 \rangle$ and $\langle \mathbf{r}_1 \cdot \mathbf{r}_2 \rangle$ between the continuous worm-like chain and the bead-spring model. We can calculate these properties of the continuous WLC by using the average correlation of the tangent vector

$$\langle \mathbf{t}(s) \cdot \mathbf{t}(p) \rangle = \exp(-|s-p|/A_p) \ , \tag{4.53}$$

where s and p denote the positions along the contour of the WLC and $\mathbf{t}(s)$ is the unit tangent vector at position s. We will also use that the vector connecting two points on the chain is the sum

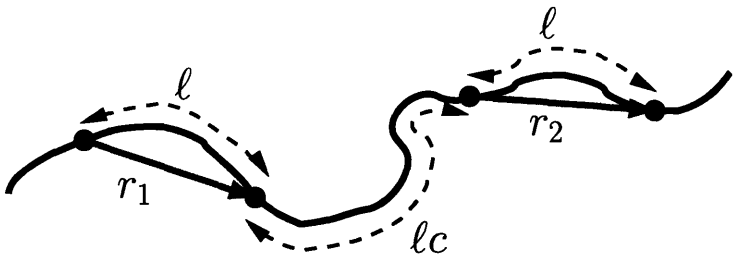

Fig. 4.15: *Illustration of a worm-like chain with vectors connecting positions on the chain. The coarse-grained model would ideally reproduce the average correlation of the vectors. The polymer has persistence length A_p. The contour length represented by the vectors is ℓ. The contour length between the two vectors is ℓc.*

over all the tangent vectors connecting those points, for example

$$\mathbf{r}_1 = \int_a^{a+\ell} \mathrm{d}s\ \mathbf{t}(s)\ , \tag{4.54}$$

where a is an arbitrary constant related to the convention of where s and p are defined to be zero. Using these two equations we can show that

$$\langle \mathbf{r}_1 \cdot \mathbf{r}_2 \rangle = A_p^2 (1 - e^{-\nu})^2 e^{-c\nu} \tag{4.55}$$

$$\langle \mathbf{r}_1^2 \rangle = 2\ell A_p + 2A_p^2 (e^{-\nu} - 1)\ . \tag{4.56}$$

We would like the coarse-grained version of the WLC (the bead-spring chain) to reproduce these two properties. Consider first the behavior of $\langle \mathbf{r}_1 \cdot \mathbf{r}_2 \rangle$. Without bending potentials in the bead-spring chain model, the mean dot product between two spring connector vectors is zero. Note that even if each spring represents a large segment of polymer (i.e. $\nu \to \infty$), neighboring sections ($c = 0$) would need to have a nonzero mean dot product to exactly model the continuous WLC. Next-nearest neighbors ($c = 1$) in the continuous WLC have an exponentially decaying mean dot product for large ν. As we will see later, it is not possible to use a bead-spring chain without bending potentials to accurately model a WLC with $\nu < 2$ (less than one Kuhn length). For the case $\nu \geq 2$ which we consider here, the correlation between next-nearest neighbors in the continuous WLC is small, so can be approximately modeled without bending potentials.

Another issue that must be addressed is the matching of the force-extension behavior between the bead-spring chain and the continuous worm-like chain. This turns out to be related to $\langle \mathbf{r}_1^2 \rangle$ because the slope of the force-extension behavior at small force is proportional to the second moment of the spring length [67].

Figure 4.16 shows a sketch of the force-extension behavior of a series of continuous worm-like chains of different contour lengths relative to the persistence length, $\alpha = L/A_p$. This represents the

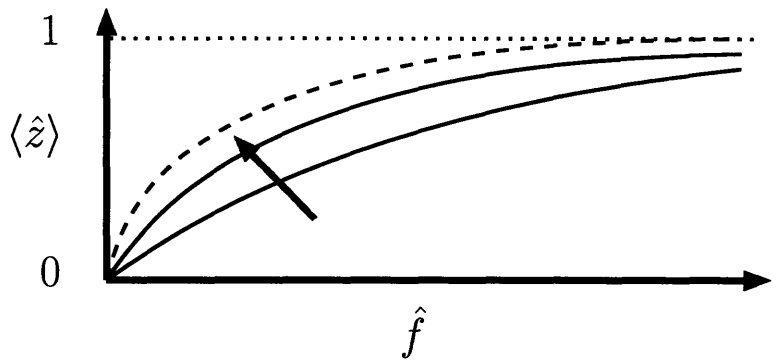

Fig. 4.16: *Sketch of the average fractional extension as a function of the applied force for a continuous worm-like chain model. The arrow denotes increasing* $\alpha = L/A_p$, *where* L *is the contour length and* A_p *is the persistence length. The dashed curve represents* $\alpha = \infty$. *The z-extension is made dimensionless using the contour length,* $\hat{z} = z/L$. *The externally applied force is made dimensionless using the persistence length,* $\hat{f} = (fA_p)/(k_B T)$.

behavior of the exact WLC which we want the bead-spring chain to reproduce. Using the second moment of the squared end-to-end distance for the exact WLC (similar to equation (4.56) but for the entire polymer) and its relation to the zero force slope, one can show that in this sketch, the slope at zero force is

$$\lim_{\hat{f}\to 0} \frac{\partial}{\partial \hat{f}} \langle \hat{z} \rangle = \frac{2}{3} + \frac{2}{3\alpha}(e^{-\alpha} - 1) \ . \tag{4.57}$$

As α increases, the slope increases until it saturates at 2/3. The behavior at large force has not been rigorously calculated for finite α. However, approximate calculations for worm-like chains with $\alpha \approx 1$ [68] suggest that the behavior at large enough force may behave as

$$\langle \hat{z} \rangle \sim 1 - \frac{1}{2\hat{f}^{1/2}} + \mathcal{O}\left(\frac{1}{\alpha \hat{f}}\right) \tag{4.58}$$

for all values of $\alpha > 0$.

Now consider two different bead-spring chain models, one with $N_s = 1$ number of springs and $\nu = 4$ number of persistence lengths represented by each spring and the other model with $N_s = 100$ number of springs and $\nu = 4$ number of persistence lengths represented by each spring. Because there are no bending potentials between the springs and the value of ν is the same, the average fractional extension versus force curves of these bead-spring chains are identical [67]. The total number of persistence lengths in the whole chain is $\alpha = N_s \nu$, so the continuous worm-like chains that are to be modeled contain $\alpha = 4$ and $\alpha = 400$ respectively. Figure 4.16 shows that these continuous worm-like chains have different force-extension behaviors. This would appear to be an inconsistency in our method of determining the spring force law by matching the force-extension behavior of the bead-spring model with the continuous worm-like chain. This inconsistency results

from the absence of bending potentials in the bead-spring chain model.

To proceed with a bead-spring model without bending potentials that is also consistent, we will only attempt to model continuous worm-like chains which are "long" in the sense that $\alpha \gg 1$. However, keep in mind that the systems of interest here, and any real system, will have a finite α no matter how large it is. For example, consider now two bead-spring models, one with $N_s = 25$ number of springs and $\nu = 10$ number of persistence lengths represented by each spring and the other model with $N_s = 100$ number of springs and $\nu = 4$ number of persistence lengths represented by each spring. The continuous worm-like chains to be modeled contain $\alpha = 250$ and $\alpha = 400$ respectively. While these continuous worm-like chains do not have identical force-extension behaviors, because $\alpha \gg 1$, they are very close to each other and also very close to the $\alpha = \infty$ force-extension behavior of the continuous WLC shown in Figure 4.16. From equations (4.57) and (4.58) we see that the maximum relative error between a curve with finite α and the $\alpha = \infty$ curve is $1/\alpha$ for large α. In this article the spring force law will be constructed so that the force-extension behavior of these bead-spring models with $\nu = 10$ and $\nu = 4$ will be identical (to within the error discussed later), and that force-extension behavior will be the $\alpha = \infty$ limit in Figure 4.16. In other words, the spring force law developed here will be valid even if each spring represents a relatively small amount of polymer (e.g. $\nu = 4$) as long as the entire chain contains many persistence lengths ($\alpha = N_s\nu \gg 1$). In practice this is not much of a restriction because many worm-like chains of interest contain many persistence lengths, such as the commonly modeled stained λ-phage DNA which contains about $\alpha \approx 400$ persistence lengths.

The more subtle point is that we are essentially sacrificing some accuracy at the scale of a single spring (as $\langle \mathbf{r}_1^2 \rangle$) or neighboring springs (as $\langle \mathbf{r}_1 \cdot \mathbf{r}_2 \rangle$ for $c = 0$) to obtain the correct behavior at the scale of the entire chain. We can see this sacrifice by comparing $\langle \mathbf{r}_1^2 \rangle$ for the bead-spring chain and the WLC. In order for the bead-spring chain to have the $\alpha = \infty$ force-extension behavior at small force without bending potentials, the bead-spring chain will be required to have $\langle \mathbf{r}_1^2 \rangle = 2\ell A_p$ because of the relation between this moment and the zero-force slope of the force-extension behavior. Comparing this with equation (4.56) we see that the relative error in this second moment decays as $1/\nu$ for large ν and is 76% when a spring represents two persistence lengths.

This is the same type of compromise at equilibrium that is made when the bead-rod chain is used to model $\alpha \gg 1$ worm-like chains. In fact, the bead-spring chain models developed here would become the bead-rod chain if each spring represents two persistence lengths. A worm-like chain of two persistence lengths is not a rigid rod and neighboring segments are not freely jointed. The bead-rod chain sacrifices this accuracy to describe the entire $\alpha \gg 1$ worm-like chain at equilibrium. The approximation made in this paper is less severe because each spring represents *at least* two persistence lengths and the bead-spring chains developed here also capture the response correctly when external forces are applied.

4.3.4 Real continuous WLC

As discussed in the previous section, the spring force law in the new bead-spring chain model will be chosen so that the force-extension behavior of the model matches that of the $\alpha = \infty$ continuous WLC in the limits of large and small force. Recall that the α of any system considered here is finite, but we are only considering systems with $\alpha \gg 1$ such that the force-extension behavior is very close to the $\alpha = \infty$ force-extension behavior. To gauge the accuracy of this bead-spring chain we will calculate the error in the force-extension behavior relative to the $\alpha = \infty$ behavior over the

entire force range. The force-extension behavior for an $\alpha = \infty$ worm-like chain cannot be written exactly as a simple analytic function, but the response can be calculated numerically. In this article we use the *numerical* calculation by [75] as the "true" worm-like chain.

The asymptotic expansions for both large and small forces are

$$\langle \hat{z} \rangle \sim 1 - \frac{1}{2\hat{f}^{1/2}} - \frac{1}{128\hat{f}^{3/2}} + \mathcal{O}\left(\frac{1}{\hat{f}^2}\right) \tag{4.59}$$

$$\langle \hat{z} \rangle \sim \frac{2}{3}\hat{f} - \frac{44}{135}\hat{f}^3 + \mathcal{O}\left(\hat{f}^5\right) , \tag{4.60}$$

where $\langle \hat{z} \rangle$ is the average fractional extension and $\hat{f}$ is the externally applied force made dimensionless using $k_{\mathrm{B}}T$ divided by the persistence length, A_p. The numerical data from Bouchiat et al. has these asymptotic behaviors. Bouchiat et al. also developed a simple formula to approximate the numerical evaluation. While this formula only introduces a small error, because of the functional form chosen, it does not have exactly the expansions above. Thus in the main body of this article we only use the numerical data from Bouchiat et al. See Appendix A.4 for a discussion of the simple functions to approximate the behavior.

4.3.5 Accuracy of Marko-Siggia spring

Before discussing the new spring force law, we will address the accuracy of using the Marko and Siggia interpolation formula as the spring force law at different levels of discretization. This analysis is related to that done previously in Chapter 3 and in ref. [67] though it differs in one very important aspect. Previously, we were concerned with understanding how the different ensembles and corresponding fluctuations affect the response. Therefore when analyzing the behavior of bead-spring chains using the Marko-Siggia force law, we compared the force-extension behavior of the bead-spring chain with a hypothetical polymer which has the Marko-Siggia formula as its "true" behavior. This is because we did not want the fact that the Marko-Siggia form is not the same as the real WLC to complicate our understanding of the different ensembles and fluctuations.

However, our concern here is to analyze how well a bead-spring chain models the real continuous WLC, so we compare the behavior of Marko-Siggia chain to the real WLC (using the numerical data from [75]). Note that because the hypothetical Marko-Siggia polymer is the same as the real WLC at small and large force, the error will be the same as the previous analysis in those two limits. It is at intermediate forces where there is a difference.

Recall that the Marko and Siggia spring force law takes the form

$$f_{\mathrm{spring}}(r) = \left(\frac{k_{\mathrm{B}}T}{A_{\mathrm{eff}}}\right)\left\{\left(\frac{r}{\ell}\right) - \frac{1}{4} + \frac{1}{4(1-r/\ell)^2}\right\} , \tag{4.61}$$

where A_{eff} is an effective persistence length which can be different from the true persistence length of the WLC being modeled A_{true} (previously denoted A_p). The effective persistence length is a fudge factor used to improve the behavior of the bead-spring chain. An extensive analysis of different choices for this effective persistence length was performed previously [67] in terms of the ratio $\lambda = A_{\mathrm{eff}}/A_{\mathrm{true}}$. The result is that a single choice of λ is not capable of correcting the force-extension behavior at both small and large forces. In this section we will see further evidence of this fact. The value of λ is a function of the number of persistence lengths represented by each

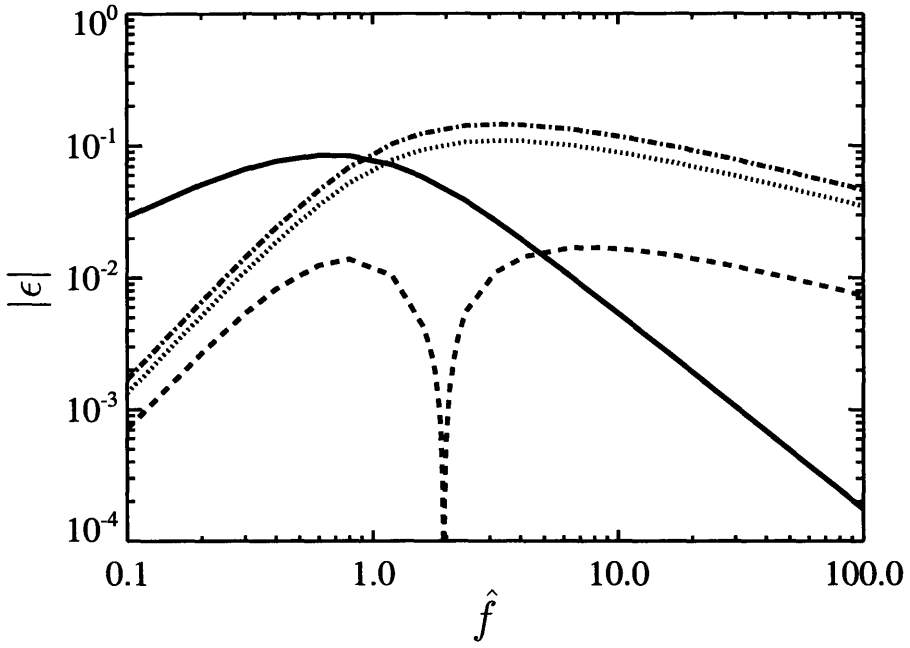

Fig. 4.17: *Relative error in the fractional extension versus force for the Marko-Siggia spring using the low-force criterion for the effective persistence length. The gray lines signify that $\epsilon < 0$, while the black lines signify that $\epsilon > 0$. The curves correspond to $\nu = 4$ (dotted), $\nu = 20$ (dashed), and $\nu = \infty$ (solid). As $\nu \to 10/3$ the curves approach the bead-string chain (dash-dot).*

spring ν. Here we will use the low-force criterion for λ, which chooses the function $\lambda(\nu)$ such that the force-extension behavior of the bead-spring chain matches the force-extension behavior of the $\alpha = \infty$ continuous WLC at zero force.

Figure 4.17 shows the relative error in the fractional extension versus force between using the Marko-Siggia spring force law and the $\alpha = \infty$ continuous WLC. The curves correspond to $\nu = 4, 20, \infty$, and the low-force criterion was used for λ. To avoid ambiguity in the sign of the relative error, we define it as

$$\epsilon \equiv \frac{\text{true value - calculated value}}{\text{true value}} . \tag{4.62}$$

The key point is that the error appears to not be the smallest at $\nu = \infty$. At intermediate ν (like $\nu = 20$) the maximum error can be smaller than when $\nu = \infty$. This is because the error discussed previously [67] counteracts the error because the Marko-Siggia formula does not match the real WLC.

The general response can be understood by examining the limiting behaviors of the bead-spring chain and the real WLC. At large force the average fractional extension using the Marko-Siggia

force law is

$$\langle \hat{z} \rangle \sim 1 - \frac{1}{2\lambda^{1/2}\hat{f}^{1/2}} + \mathcal{O}\left(\frac{1}{\hat{f}}\right) , \tag{4.63}$$

where the external force $\hat{f}$ is made dimensionless using the true persistence length, denoted A_{true}. Recall that in Figure 4.17, $\lambda(\nu)$ was determined using the low-force criterion. This means that for any $10/3 < \nu < \infty$, the relative error eventually decays as $\hat{f}^{-1/2}$ with a coefficient that is negative, and the error gets worse as λ grows (i.e. ν decreases for the low-force criterion).

The form of the Marko-Siggia formula makes the behavior at small force slightly more subtle. For any $10/3 < \nu < \infty$, the relative error at small enough force decays as $\hat{f}^2$. This is because $\langle \hat{z} \rangle$ is an odd analytic function of $\hat{f}$ around small force, and the low-force criterion for the effective persistence length makes the order $\hat{f}$ term match the real WLC. The coefficient to this decay in relative error is determined from the order $\hat{f}^3$ contribution to $\langle \hat{z} \rangle$, which is related to the second and fourth moments of the spring length, $\langle \hat{r}^2 \rangle$ and $\langle \hat{r}^4 \rangle$ [67]. The subtlety arises because as $\nu \to \infty$, the coefficient to $\hat{f}^2$ in the relative error diverges as $\nu^{1/2}$. Higher order terms in force also have diverging coefficients. This large number of terms each with diverging coefficients combine and cancel perfectly to give a relative error that decays as $\hat{f}$. The actual curve in the $\nu \to \infty$ limit is found by comparing the inverse of the Marko-Siggia force law with the behavior of the real WLC. The inverse of the Marko-Siggia force law is not an odd function, so has all terms in the expansion for small force.

It may appear that the Marko-Siggia spring force law with an effective persistence length has sufficiently small error at intermediate levels of discretization such as $\nu = 20$. However, in many cases it is not sufficient to simply have the relative error approach zero at large force. Any bead-spring model with a finite fully-extended length will have a fractional extension that approaches one as the force approaches infinity, thus the relative error in the fractional extension will approach zero as the force approaches infinity. It is also important for an accurate model to have the correct approach to full extension. As shown in equation (4.63), the approach to full extension is affected by the effective persistence length. The approach to full extension has been used to analyze the behavior in strong flows and the relaxation after cessation of elongational flow [58, 76] and is therefore important to capture with the coarse-grained model.

It is useful to pause at this point and recall how far the low-force criterion can be pushed. It was shown previously [67] that the low-force criterion for the Marko-Siggia force law can not be pushed past $\nu = 10/3$. At that point, the effective persistence length becomes infinite. What that means is the spring force is zero for all extensions less than the fully-extended length. This type of model is also called the bead-string chain [12]. The fractional extension as a function of the force for the bead-string chain is

$$\langle \hat{z} \rangle = \frac{-3k_{\text{B}}T}{f\ell} + \frac{1}{\mathcal{L}(f\ell/(k_{\text{B}}T))} , \tag{4.64}$$

where $\mathcal{L}$ is the Langevin function [67]. We show this curve in Figure 4.17, which is the limiting behavior of the Marko-Siggia system with low-force criterion when $\nu \to 10/3$. Note that the $\hat{f}^{-1/2}$ approach to full extension has totally vanished. In fact the response is not all that different from using the freely jointed chain to model the worm-like chain (with each rod representing two persistence lengths).

4.3.6 New approximate force law without bending potential

The main goal of this section is to systematically build a new spring force law which can be used in bead-spring chain models and performs better than the Marko-Siggia formula. We now develop that new spring force law. We proceed as for the freely jointed chain previously [77]. We start by assuming a form of the spring force law

$$\hat{f}_{\mathrm{s}} = \frac{C\hat{r}}{(1-\hat{r}^2)^2} + \frac{G\hat{r}}{\nu(1-\hat{r}^2)} + D\hat{r} + B\hat{r}(1-\hat{r}^2) \ . \tag{4.65}$$

We choose the values (functions of ν) for C, G, D, B such that the force-extension behavior of the bead-spring chain is the same (in the limits of small and large force) as the $\alpha = \infty$ continuous WLC.

For the similar analysis for the freely jointed chain we knew the way the spring force must approach full extension to have the desired force-extension behavior from the random walk spring (RWS) model. For the worm-like chain we must instead directly calculate the force-extension behavior of a bead-spring chain using the postulated form as the spring force law. For large force the fractional extension is

$$\langle \hat{z} \rangle \sim 1 - \frac{C^{1/2}}{2\hat{f}^{1/2}} - \frac{G+7}{4\nu\hat{f}} + \frac{1}{\hat{f}^{3/2}}\left(\frac{C^{1/2}(C-16D)}{64} + \frac{C^{1/2}(G+4)}{16\nu} - \frac{(G+1)(G+3)}{16\nu^2 C^{1/2}} \right) + \mathcal{O}\left(\frac{1}{\hat{f}^2}\right) \ . \tag{4.66}$$

To match with the behavior of the $\alpha = \infty$ WLC (equation (4.59)) we choose $C = 1$, $G = -7$, and

$$D = \frac{3}{32} - \frac{3}{4\nu} - \frac{6}{\nu^2} \ . \tag{4.67}$$

With these choices the average fractional extension expansion is

$$\langle \hat{z} \rangle \sim 1 - \frac{1}{2\hat{f}^{1/2}} - \frac{1}{128\hat{f}^{3/2}} + \mathcal{O}\left(\frac{1}{\hat{f}^2}\right) \ . \tag{4.68}$$

The remaining parameter, B, is chosen to match the behavior at small force (at equilibrium). We will first proceed in the same way as for the freely jointed chain, using the large ν expansion of the second moment of the spring length, $\langle \hat{r}^2 \rangle$. Because this second moment is proportional to the slope of the force-extension behavior at small force, matching the second moment between the spring and the WLC means that the force-extension behavior is correct at small force.

Provided $\hat{r} = 0$ is the global minimum of the spring potential energy, the behavior of the second moment for large ν is obtained by expanding the energy for small $\hat{r}$ [67, 77]. Recall that for our bead-spring chain to match the equilibrium behavior of the $\alpha = \infty$ WLC, each spring must have by construction $\langle \mathbf{r}_1^2 \rangle = 2\ell A_p$. In dimensionless form, this is equivalent to $\langle \hat{r}^2 \rangle = 2/\nu$. If we choose

$$B_{h\nu} = \frac{13}{32} + \frac{39}{16\nu} - \frac{323}{192\nu^2} \ , \tag{4.69}$$

then the expansion of the second moment for the spring with our new force law is

$$\langle \hat{r}^2 \rangle \sim \frac{2}{\nu} + \mathcal{O}\left(\frac{1}{\nu^4}\right) \ . \tag{4.70}$$

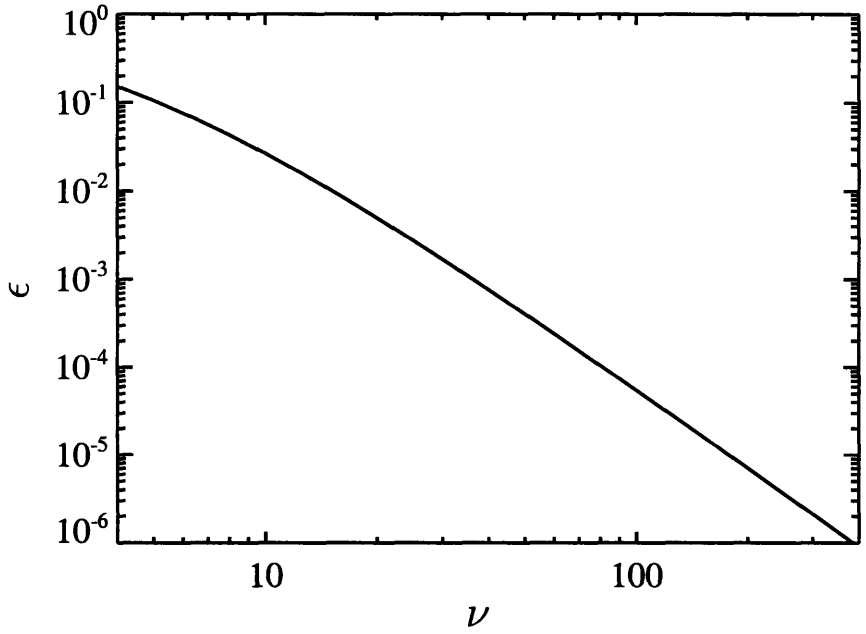

Fig. 4.18: *Relative error in the second moment of the spring length, $\langle \hat{r}^2 \rangle$, using the new spring force law and the function $B_{h\nu}$.*

We have denoted this $B_{h\nu}$ because the value comes from examining the expansion at high ν. For the freely jointed chain we found that using the high ν expansion allowed us to get a very small error even at smaller ν. Figure 4.18 shows the relative error in the second moment of the spring length as a function of ν. While the error does decay as ν^{-3} as we expect, the pre-factor is large enough that the relative error at $\nu = 4$ is about 15%. This is larger than we want. While one way to reduce the error is to continue the expansion to higher order in $1/\nu$, making the error decay as ν^{-4} or even higher, this will have most of its impact at large ν where the error is already small enough and will barely change the error at small ν.

An alternative is to determine numerically the function $B(\nu)$ such that the error is exactly zero. This is similar to how the effective persistence length is determined numerically as a function of ν when using the Marko-Siggia force law and low-force criterion. In fact, the low-force criterion function for the Marko-Siggia force law $\lambda(\nu)$ is the function such that $\langle \hat{r}^2 \rangle = 2/\nu$. It would be more useful to have an approximate formula for $B(\nu)$ that still has a small error. One such formula is

$$B = \frac{\frac{13}{32} + \frac{0.8172}{\nu} - \frac{14.79}{\nu^2}}{1 - \frac{4.225}{\nu} + \frac{4.87}{\nu^2}} \,. \tag{4.71}$$

Using this formula, the error in the second moment of the spring length vanishes at $\nu = 4, 5, 9, 30, \infty$ by construction and has a maximum relative error of 0.07% for $\nu \geq 4$.

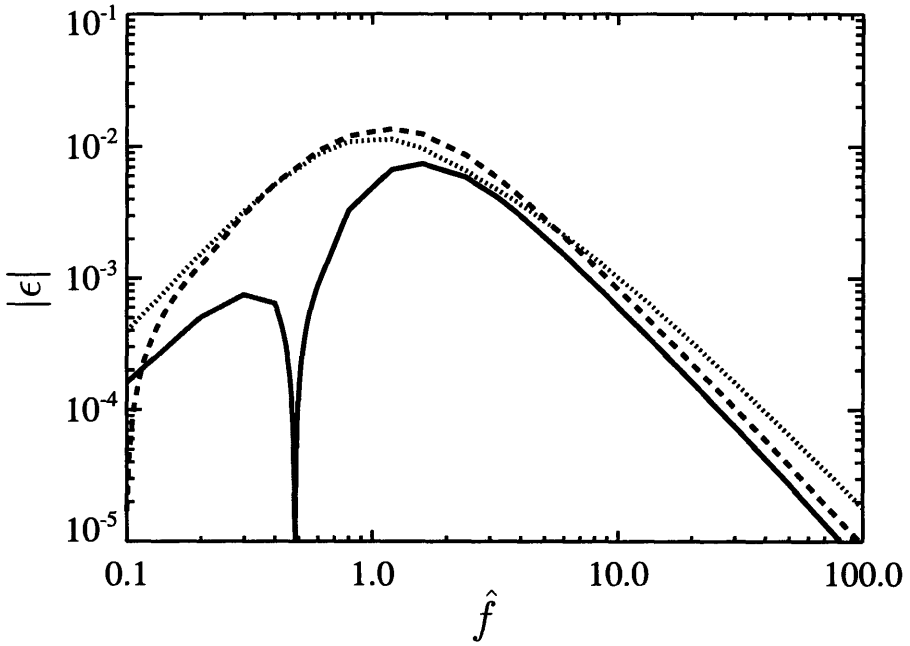

Fig. 4.19: *Relative error in the average fractional extension* $\langle \hat{z} \rangle$ *using the new spring force law (equation* (4.72)*). The gray lines signify that* $\epsilon < 0$*, while the black lines signify that* $\epsilon > 0$*. The curves correspond to* $\nu = 4$ *(dotted),* $\nu = 20$ *(dashed), and* $\nu = \infty$ *(solid).*

Using this function for the parameter B we obtain our new spring force law

$$\hat{f}_s = \frac{\hat{r}}{(1-\hat{r}^2)^2} - \frac{7\hat{r}}{\nu(1-\hat{r}^2)} + \left(\frac{3}{32} - \frac{3}{4\nu} - \frac{6}{\nu^2}\right)\hat{r} + \left(\frac{\frac{13}{32} + \frac{0.8172}{\nu} - \frac{14.79}{\nu^2}}{1 - \frac{4.225}{\nu} + \frac{4.87}{\nu^2}}\right)\hat{r}(1-\hat{r}^2) \ . \quad (4.72)$$

Figure 4.19 shows the relative error in the fractional extension versus force using this new spring force law. We see that the maximum error is approximately 1% even for $\nu = 4$. The response also has the correct approach to full extension, which can be seen from the steeper power law near large force than was seen for the Marko-Siggia force law.

We can use the expansions of the fractional extensions to examine the limiting behavior of the relative error. At large force our new spring force law captures correctly up to order $\hat{f}^{-3/2}$ so the relative error decays as $\hat{f}^{-2}$. For $\nu = 4, 5, 9, 30, \infty$ the parameter B makes the error vanish at small force, so the relative error decays as $\hat{f}^2$. For other values of ν, there is a small but nonzero relative error at zero force, so the relative error behaves as a small constant plus a term of order $\hat{f}^2$.

We will again pause to discuss how far this force law can be pushed. Recall that the force law uses the B parameter to make $\langle \hat{r}^2 \rangle = 2/\nu$. This is only possible if $\nu \geq 2$ because the spring can not be larger than the fully-extended length. If each spring represents two persistence lengths, then the

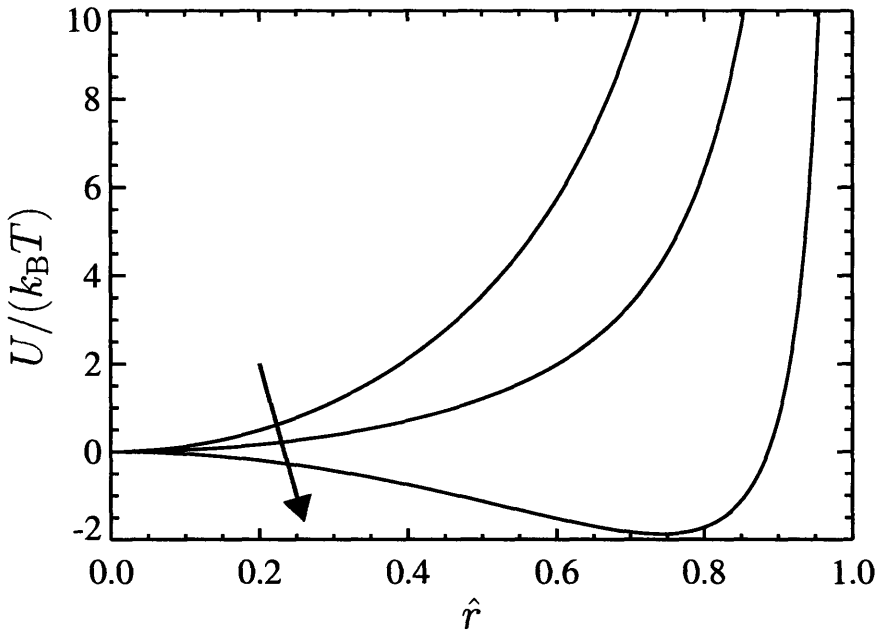

Fig. 4.20: *Spring potential energy versus fractional extension for the new spring force law (equation (4.72)). The curves correspond to $\nu = 20, 10, 4$, with the arrow denoting decreasing ν. The arbitrary additive constant has been chosen so the potential energy vanishes at zero extension.*

B value would need to make $\langle \hat{r}^2 \rangle = 1$. In other words, the spring will have to look more and more like a rigid rod because the average equilibrium length and fully-extended length become equal. To make this true it would be necessary to have $B = -\infty$. In this limit, the bead-spring chain becomes a freely jointed chain. This is best illustrated by examining the spring potential energy directly.

Figure 4.20 shows the spring potential energy calculated from our new spring force law (equation (4.72)) for a few values of ν. Initially as ν gets smaller, the potential energy weakens, allowing for fluctuations to larger extensions. As ν gets even smaller, the minimum in the potential appears at nonzero extension. This allows the spring to correctly model both the low and high force behaviors. The minimum is at nonzero extension because the spring is becoming more like a rigid rod. As ν decreases, this minimum moves towards full extension and gets deeper. For $B = -\infty$ (which is necessary to get the correct $\langle \hat{r}^2 \rangle = 1$ for $\nu = 2$), the potential is infinitely deep at $\hat{r} = 1$. In other words, one way of simulating a freely jointed chain using stiff springs would be to set $\nu = 2$ and $B \to -\infty$ in our spring force law.

The subtle point has to do with the behavior at large force. From the high force behavior in equation (4.66) and our choice of C, G, and D, one might think the behavior at high force is retained even in the limit $\nu = 2$ and $B \to -\infty$. This is not true because one of the neglected terms in equation (4.66) goes as $B/\hat{f}^2$. This means that for any finite B, there exists a force large

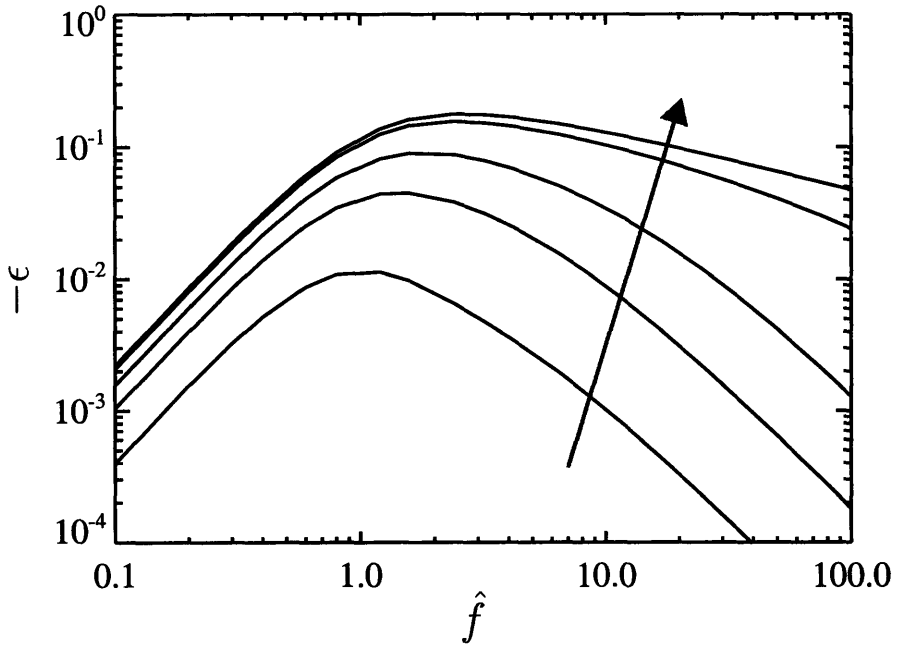

Fig. 4.21: *Relative error in the average fractional extension* $\langle \hat{z} \rangle$ *using the new type of spring force law as* $\nu \to 2$. *The value of* B *was determined numerically to make the error vanish at zero force. The curves correspond to* $\nu = 4, 3, 2.5, 2.1, 2$ *with the arrow denoting decreasing* ν. *The* $\nu = 2$ *curve is the response of the freely jointed chain.*

enough that the term is negligible. However at any finite force, as $B \to -\infty$ these higher order terms become important, so the response approaches that of the freely jointed chain.

We illustrate this approach by showing in Figure 4.21 the error in the fractional extension for $\nu \to 2$, where in this plot B is determined numerically such that $\langle \hat{r}^2 \rangle = 2/\nu$. The curves shown are for $\nu = 4, 3, 2.5, 2.1, 2$ with corresponding $B = -1.265, -9.836, -70.68, -8185.9, -\infty$. For the $\nu = 2, B = -\infty$ curve, we have plotted the behavior of the freely jointed chain. Note that each curve eventually decays like $\hat{f}^{-2}$ for large force, but the transition to that behavior is delayed as $\nu \to 2$. When $\nu = 2$, the transition never occurs. For each force, as $\nu \to 2$, the response approaches the freely jointed chain response.

4.4 Summary and Outlook

In this chapter we have examined a new method to generate coarse-grained models of polymers as bead-spring chains using the constant extension ensemble behavior of the polymer. We applied it to a number of toy problems to illustrate the mechanics of the method and important aspects of coarse-graining. Applying this method to the FJC polymer showed why current bead-spring chains are incapable of modeling polymers at high discretization. The analysis was applied to

freely jointed chains in which the rods can have different lengths showing that as the spread in rod lengths increases, the response of the chain can change dramatically. This change can not be accounted for solely by using an effective Kuhn length. We applied the method to construct a dumbbell model of actin filaments. This illustrated that the method in dumbbell form is applicable to the WLC as well as showing it can be used directly from experimentally data.

At the length and time scales that polymer kinetic theory aims to capture, the two common approaches are to use more detailed models such as the freely jointed chain or to use bead-spring chains where each bead represents a large segment of polymer. Because the current bead-spring models, such as the Cohen force law or Marko-Siggia force law, produce errors if they are pushed to high discretization, there exists a gap where there is no accurate coarse-grained version of the more detailed model. One method to reduce the size of this gap is to use an effective Kuhn length or persistence length as discussed previously. This method has significant limitations including that there is not a unique, "correct" choice of the effective Kuhn or persistence length valid for all situations.

The advance of the PET method is that it bridges this gap in a systematic manner, showing how to calculate the force law at any level of coarse-graining. However, in practice the force laws calculated from the PET method may be difficult to implement. In these situations it may be sufficient to use an approximate force law. The approximate force law can have a simple functional form that is easy to use in calculations and captures the underlying model to high accuracy. We have shown examples of developing approximate force laws, including equation (4.43) which is capable of modeling a freely jointed chain to high discretization (springs representing as few as four Kuhn steps). Simulations that have used the Cohen force law can be easily modified to use this new force law, equation (4.43), including the semi-implicit predictor-corrector method developed by ref. [31]. Because the new force law is always better than the Cohen force law, equation (4.43) should always be used instead of the Cohen force law for modeling of freely jointed chains.

While we have shown that there exists a generalized bead-spring chain model which is capable of exactly modeling the worm-like chain, it is currently not an appropriate option for simulations. Not only does the inclusion of orientation to the beads increase the complexity of the simulation algorithm, but currently a simple form does not exist for the interaction of this new type of beads. We have postulated that this model could be approximated by a bead-spring chain with bending potentials between the springs. However, the technical aspects of choosing the bending potential correctly have not been examined to obtain a simple but also accurate model.

If the entire worm-like chain to be modeled contains many persistence lengths, it seems possible to use a bead-spring chain without bending potentials. We developed a simple spring force law which is capable of accurately modeling a worm-like chain even if each spring represents as few as 4 persistence lengths, so long as the whole chain contains a large number of persistence lengths. This corresponds to the situation in most current situations modeling the worm-like chains with bead-spring chains. However, future situations may require even more detailed models. Thus, future possible work in this area would most likely focus on implementing the generalized bead-spring chain model or using bending potentials between the springs.

Up to this point, we have focused on the force-extension behavior of bead-spring chains. In the previous chapter we analyzed the behavior of current spring force laws. In this chapter we have developed new force laws which eliminate the error in the force-extension behavior which was present when using the previous force laws. The remainder of this thesis will look at the behavior of bead-spring chains beyond force-extension behavior. Along the way we will illustrate that the

other responses are related to force-extension behavior. This will allow us to understand why the new force laws developed in this chapter perform better than the previous force laws in situations other than simple force-extension.

CHAPTER 5

Low Weissenberg Number Response

Thus far we have only considered the force-extension behavior of the bead-spring chains. In addition to F-E behavior we are interested in the rheology of the bead-spring chains, and how it changes as the level of coarse-graining changes. In general, this is a much harder problem computationally than the work done thus far. In order to continue in the spirit of calculating properties near equilibrium and using equilibrium statistical mechanics, we will investigate the rheology of the bead-spring chains by looking at potential flow in the limit of small deformation rate. Potential flow has the desirable property that the chain behavior can be calculated using equilibrium statistical mechanics with an effective energy due to the flow. From this analysis the retarded-motion expansion coefficients can be calculated. These coefficients give insight into the rheological properties of the bead-spring chains in slow and slowly-varying flows. This chapter was reproduced in part with permission from Underhill, P.T. and Doyle, P.S., *J. Non-Newtonian Fluid Mech.*, **122**, 3 (2004),

5.1 Retarded-motion Expansion Coefficients

The goal of this section is to examine the retarded-motion expansion coefficients for bead-spring chains. This has been done previously for Finitely Extensible Non-linear Elastic (FENE) [78] springs and for Hookean springs. Bird et al. [12] also present a general framework for the retarded-motion coefficients for any bead-spring-rod chain. However, because of the generality, that analysis can

not simplify the integrals over phase space to a convenient and intuitive form. Here we present the results of a specific application of that framework to only bead-spring chains but for arbitrary spring force law. As assumed previously, we will assume that there are no bending potentials between springs and that the spring force only depends on the magnitude of extension. Furthermore we will neglect any hydrodynamic interaction and excluded volume between the beads and assume that the polymer solution is dilute. With these assumptions, the retarded-motion coefficients can be written as a function of simple moments of the force law probability distribution. These moments are given by

$$\langle r^n \rangle_{\text{eq}} = \frac{\int_0^\ell \mathrm{d}r\, r^{n+2} \exp\left[\frac{-U_{\text{eff}}(r)}{k_{\text{B}}T}\right]}{\int_0^\ell \mathrm{d}r\, r^2 \exp\left[\frac{-U_{\text{eff}}(r)}{k_{\text{B}}T}\right]} \,. \tag{5.1}$$

Written in terms of the moments, the first two retarded-motion expansion coefficients equal

$$b_1 - \eta_{\text{s}} = \eta_{0,\text{p}} = \frac{n_{\text{p}}\zeta(N^2-1)}{36}\langle r^2 \rangle_{\text{eq}} \tag{5.2}$$

$$\begin{aligned} b_2 = \frac{-\Psi_{1,0}}{2} = \left(\frac{-n_{\text{p}}\zeta^2}{120 k_{\text{B}}T}\right) \Bigg[&\left(\frac{\langle r^4 \rangle_{\text{eq}}}{15} - \frac{\langle r^2 \rangle_{\text{eq}}^2}{9}\right)\left(\frac{N^4-1}{N}\right) \\ &+ \left(\frac{\langle r^2 \rangle_{\text{eq}}^2}{9}\right)\left(\frac{(N^2-1)(2N^2+7)}{6}\right)\Bigg] \end{aligned} \tag{5.3}$$

where η_{s} is the viscosity of the Newtonian solvent, $\eta_{0,\text{p}}$ is the polymer contribution to the zero-shear viscosity, $\Psi_{1,0}$ is the zero-shear first normal stress coefficient, n_{p} is the number density of polymers, ζ is the drag coefficient of each bead, and N is the number of beads in the chain. Because we have neglected hydrodynamic interaction, we also know from Bird et al. [12] that b_{11} is zero. See Appendix A.2 for the derivation of these coefficients. It should be emphasized that for equations (5.2) and (5.3) *no assumption* has been made about the form of the spring force law $U_{\text{eff}}(r)$.

A more common approach to calculating the polymer contribution to the zero-shear viscosity is through the Giesekus form of the stress tensor, from which it can be shown that

$$\eta_{0,\text{p}} = \frac{n_{\text{p}}\zeta N}{6}\text{R}_{\text{g}}^2 \,, \tag{5.4}$$

where R_{g} is the root mean square radius of gyration at equilibrium. For bead-spring chains R_{g} is related to the single spring moments as

$$\text{R}_{\text{g}}^2 = \frac{N^2-1}{6N}\langle r^2 \rangle_{\text{eq}} \,. \tag{5.5}$$

From these equations we can verify equation (5.2). Equations (5.2), (5.3), and (5.5) were additionally used to calculate the model properties given in Tables 3.2, 3.3, and 3.4 as discussed in Section 3.6. A relaxation time for the bead-spring chain can also be calculated from the retarded-

motion expansion coefficients

$$\tau_0 = \frac{-b_2}{b_1 - \eta_s} \,. \tag{5.6}$$

Recalling from the definitions of the moments (equation (5.1)) that they are defined for a *single spring*, it seems natural to scale them by the fully-extended length of a spring, ℓ, if it is finite. For that case let us define dimensionless moments as

$$\langle \hat{r}^n \rangle_{\text{eq}} = \frac{\langle r^n \rangle_{\text{eq}}}{\ell^n} = \frac{\int_0^1 \mathrm{d}\hat{r}\ \hat{r}^{n+2}\ \exp\left[\frac{-\nu}{\lambda}\widehat{U}_{\text{eff}}(\hat{r})\right]}{\int_0^1 \mathrm{d}\hat{r}\ \hat{r}^2\ \exp\left[\frac{-\nu}{\lambda}\widehat{U}_{\text{eff}}(\hat{r})\right]} \,. \tag{5.7}$$

After a number of parameter substitutions the retarded-motion expansion coefficients can be rewritten as

$$b_1 - \eta_s = \eta_{0,\text{p}} = \left(\frac{n_{\text{p}}(N\zeta)LA_{\text{true}}}{12}\right)\left(\frac{N+1}{N}\right)\left(\frac{\nu\langle\hat{r}^2\rangle_{\text{eq}}}{3}\right) \tag{5.8}$$

$$\begin{aligned} b_2 = \frac{-\Psi_{1,0}}{2} = \left(\frac{-n_{\text{p}}(N\zeta)^2L^2A_{\text{true}}^2}{120k_{\text{B}}T}\right)\Bigg[&\left(\frac{\nu^2\langle\hat{r}^4\rangle_{\text{eq}}}{15} - \frac{\nu^2\langle\hat{r}^2\rangle_{\text{eq}}^2}{9}\right)\left(\frac{(N^2+1)(N+1)}{N^3(N-1)}\right) \\ &+ \left(\frac{\nu\langle\hat{r}^2\rangle_{\text{eq}}}{3}\right)^2\left(\frac{(N+1)(2N^2+7)}{6N^2(N-1)}\right)\Bigg] \end{aligned} \tag{5.9}$$

The advantage of working with the dimensionless moments is that they only depend on the parameters ν and λ but not on the absolute number of beads (or springs). Thus all dependence on the absolute number of beads is shown explicitly. In this way we have separated out in the formulae the contribution from the specific form of the spring force law and the contribution from the chain having multiple beads. Contrary to the force-extension behavior, we do see a dependence on the absolute number of beads. The coefficients are made dimensionless as

$$\hat{\eta}_{0,\text{p}} = \frac{\eta_{0,\text{p}}}{\left(\frac{n_{\text{p}}(N\zeta)LA_{\text{true}}}{12}\right)} \tag{5.10}$$

$$\hat{b}_2 = \frac{b_2}{\left(\frac{-n_{\text{p}}(N\zeta)^2L^2A_{\text{true}}^2}{120k_{\text{B}}T}\right)} \tag{5.11}$$

These were chosen as the scales because they depend only on properties intrinsic to the true polymer or the system of study. The polymer solution being modeled has a number density of polymers, n_{p}, and a temperature T. The true polymer being modeled has a value of the persistence length A_{true}, a contour length L, and a total drag. Because we are using a freely-draining model, the total drag on the chain is $N\zeta$. By comparing dimensionless quantities with $N\zeta$ as the scale of drag, we are looking at how the property changes if for bead-spring models with different number of beads, we recalculate the drag on a single bead, ζ, such that the whole chain has a constant drag.

To better understand the behavior of the retarded-motion coefficients, let us first examine how much the coefficients depend explicitly on the number of beads (in addition to the level of coarse-

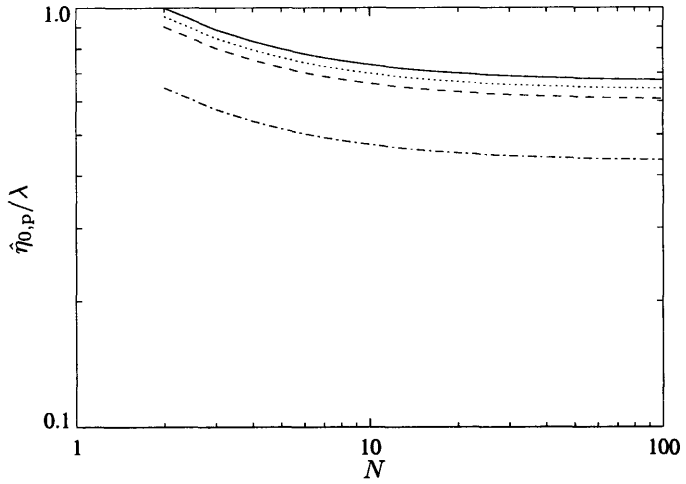

Fig. 5.1: *Polymer contribution to the zero-shear viscosity of Marko and Siggia bead-spring chains as the number of effective persistence lengths represented by each spring, ν/λ, is held constant. The curves correspond to $\nu/\lambda = \infty$ (*solid line*), $\nu/\lambda = 400$ (*dotted*), $\nu/\lambda = 100$ (*dashed*), and $\nu/\lambda = 10$ (*dash-dot*).*

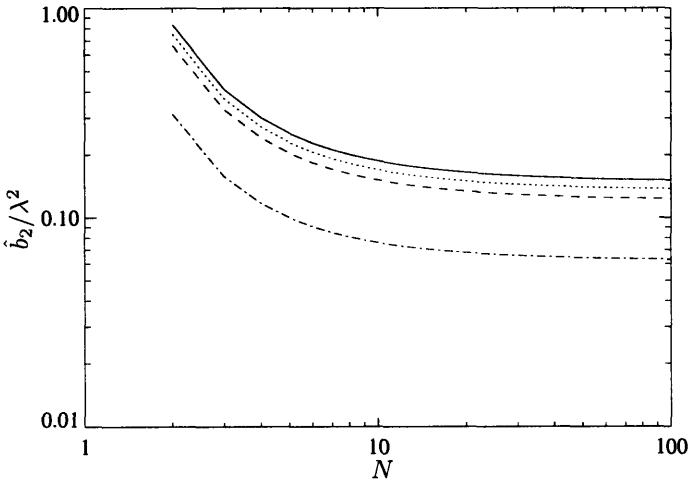

Fig. 5.2: *Zero-shear first normal stress coefficient of Marko and Siggia bead-spring chains as the number of effective persistence lengths represented by each spring, ν/λ, is held constant. The curves correspond to $\nu/\lambda = \infty$ (*solid line*), $\nu/\lambda = 400$ (*dotted*), $\nu/\lambda = 100$ (*dashed*), and $\nu/\lambda = 10$ (*dash-dot*).*

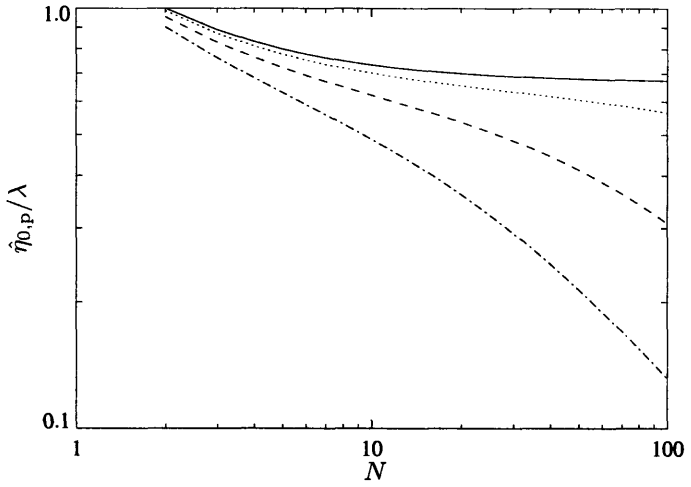

Fig. 5.3: *Polymer contribution to the zero-shear viscosity of Marko and Siggia bead-spring chains as the number of effective persistence lengths in the total polymer contour, α/λ, is held constant. The curves correspond to $\alpha/\lambda = \infty$ (*solid line*), $\alpha/\lambda = 4000$ (*dotted*), $\alpha/\lambda = 400$ (*dashed*), and $\alpha/\lambda = 100$ (*dash-dot*).*

graining, ν). In Figures 5.1 and 5.2 we show respectively $\hat{\eta}_{0,p}$ and $\hat{b}_2$ as a function of the number of beads, N, while the level of coarse-graining, ν, is held constant and using the Marko-Siggia force law. We will see later a similar application for other force laws. The $\hat{\eta}_{0,p}$ curves for different values of ν are exactly self-similar as could be seen from equation (5.8), while the $\hat{b}_2$ curves are approximately self-similar except when both ν and N are small. We attribute the change of the coefficients with N while ν is held fixed to the fact that for finite N the drag is not distributed along a continuous contour. Thus for the bead-spring model to be an accurate coarse-grained model of the true polymer, the number of beads must be large enough to operate in the large N region. The deviation for $\nu < \infty$ is due to the errors in the spring force law as discussed in Chapter 3 with regards to the F-E behavior. The $\nu = \infty$ curve corresponds to the "Rouse model" result. What we mean by the "Rouse model" result will be discussed later.

In order to model a given polymer with different numbers of beads, the value of ν is not constant. Instead the value of α (the number of true persistence lengths in the polymer's contour) is constant. In Figures 5.3 and 5.4 we show respectively $\hat{\eta}_{0,p}$ and $\hat{b}_2$ as a function of the number of beads, N, while α is held constant. Again we initially use the Marko-Siggia force law as an illustrative example. This type of progression corresponds to discretizing a polymer finer and finer. We can see the interplay between drag error and discretizing error as discussed in the introduction. When the number of beads is small, error is present because the drag on the polymer due to the solvent is lumped at the beads, not exerted along a continuous contour. When the number of beads is large, error is present because the polymer has been discretized so finely that each spring represents a small number of persistence lengths. As discussed previously this fine discretization

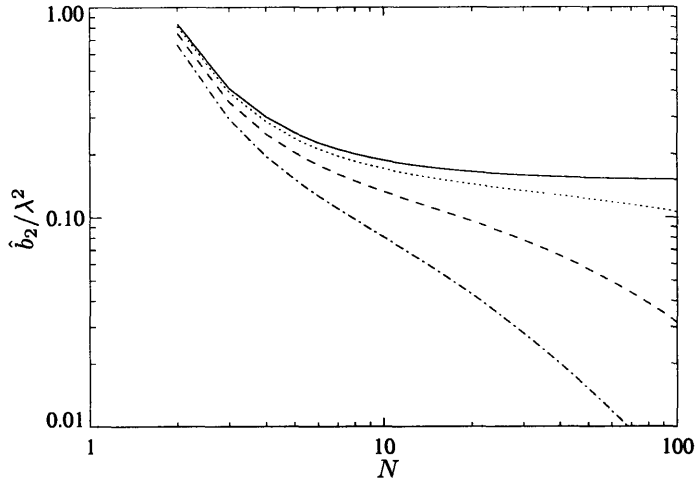

Fig. 5.4: *Zero-shear first normal stress coefficient of Marko and Siggia bead-spring chains as the number of effective persistence lengths in the total polymer contour, α/λ, is held constant. The curves correspond to $\alpha/\lambda = \infty$ (*solid line*), $\alpha/\lambda = 4000$ (*dotted*), $\alpha/\lambda = 400$ (*dashed*), and $\alpha/\lambda = 100$ (*dash-dot*).*

leads to error predicting the size of the coil and the extension of polymer segments. If the number of persistence lengths in the whole polymer, α, is large enough, there exists an approximate plateau. This corresponds to the situation in which the number of springs is simultaneously large enough to reduce the drag error and small enough to prevent discretization error. Using the expansions developed in Section 3.8 we can *predict* the location of this plateau.

To use these expansions and also explain why the behavior approaches the "Rouse result," we need to express the spring moments in terms of the force-extension behavior. From equation (3.23) we see that

$$\lim_{\hat{f}\to 0}\left(\frac{\partial}{\partial \hat{f}}\langle \hat{z}_{\mathrm{tot}}\rangle_{\mathrm{m}}\right) = \frac{\nu\langle \hat{r}^2\rangle_{\mathrm{eq}}}{3} \ . \tag{5.12}$$

It can also be shown by taking the third derivative of the force-extension curve that

$$\frac{1}{3\nu}\lim_{\hat{f}\to 0}\left(\frac{\partial^3}{\partial \hat{f}^3}\langle \hat{z}_{\mathrm{tot}}\rangle_{\mathrm{m}}\right) = \frac{\nu^2\langle \hat{r}^4\rangle_{\mathrm{eq}}}{15} - \frac{\nu^2\langle \hat{r}^2\rangle_{\mathrm{eq}}^2}{9} \ . \tag{5.13}$$

Making use of these equalities we can write the retarded-motion expansion coefficients as

$$\hat{\eta}_{0,\mathrm{p}} = \left(\frac{N+1}{N}\right)\left(\lim_{\hat{f}\to 0}\frac{\partial}{\partial \hat{f}}\langle \hat{z}_{\mathrm{tot}}\rangle_{\mathrm{m}}\right) \tag{5.14}$$

$$\hat{b}_2 = \left[\left(\frac{1}{3\nu} \lim_{\hat{f}\to 0} \frac{\partial^3}{\partial \hat{f}^3} \langle \hat{z}_{\mathrm{tot}} \rangle_{\mathrm{m}} \right) \left(\frac{(N^2+1)(N+1)}{N^3(N-1)} \right) + \left(\lim_{\hat{f}\to 0} \frac{\partial}{\partial \hat{f}} \langle \hat{z}_{\mathrm{tot}} \rangle_{\mathrm{m}} \right)^2 \left(\frac{(N+1)(2N^2+7)}{6N^2(N-1)} \right) \right] \tag{5.15}$$

Let us first examine the plateau of $\hat{\eta}_{0,\mathrm{p}}$. We can easily see from the prefactor in equation (5.14) that the drag error is negligible if

$$N \gg 1 \; . \tag{5.16}$$

To predict the upper limit of the plateau, we use the expansion in equation (3.28). Use of this series is justified because we know that if the behavior is within the plateau region then ν must be very large. In fact, the leading order term must be dominant. For the WLC model this corresponds to

$$|d_1| \left(\frac{\lambda}{\nu \phi_2} \right)^{1/2} \ll 1 \tag{5.17}$$

Written in terms of the parameter α/λ, which is constant while discretizing, this condition becomes

$$(N-1)^{1/2} \ll \frac{1}{|d_1|} \left(\frac{\alpha \phi_2}{\lambda} \right)^{1/2} \; . \tag{5.18}$$

Note that this is true for the WLC model because for the Marko and Siggia spring potential

$$\phi_2 = \frac{3}{4} \quad , \quad d_1 = \frac{-4}{3\sqrt{\pi}} \; . \tag{5.19}$$

However some models like the FENE model have $d_1 = 0$. The appropriate analysis shows that in general

$$(N-1)^{i/2} \ll \frac{1}{|d_i|} \left(\frac{\alpha \phi_2}{\lambda} \right)^{i/2} \; , \tag{5.20}$$

where i denotes the first coefficient d_i that is non-zero (excluding $d_0 = 1$). Combining the two bounds on N gives a formula for the plateau region for $\hat{\eta}_{0,\mathrm{p}}$:

$$1 \ll N \quad , \quad (N-1)^{i/2} \ll \frac{1}{|d_i|} \left(\frac{\alpha \phi_2}{\lambda} \right)^{i/2} \; . \tag{5.21}$$

A similar analysis can be done for $\hat{b}_2$. Because α has to be large for a plateau region to even exist, we will neglect the term with the third derivative. Following an analogous procedure we find the plateau region for $\hat{b}_2$

$$2 \ll N \quad , \quad (N-1)^{i/2} \ll \frac{1}{|2d_i|} \left(\frac{\alpha \phi_2}{\lambda} \right)^{i/2} \; . \tag{5.22}$$

Note the factors of two that result from expanding the rational function of N for large N and from

expanding the square of the zero-force slope.

Let us consider application of these formulae to the WLC model. For the Marko and Siggia potential with $\lambda = 1$ the two plateau conditions state that

$$1 \ll N \quad , \quad (N-1)^{1/2} \ll 1.151\alpha^{1/2} \tag{5.23}$$

$$2 \ll N \quad , \quad (N-1)^{1/2} \ll 0.576\alpha^{1/2} \tag{5.24}$$

If we consider that an order of magnitude difference is sufficient to satisfy the $\ll$ conditions, then the conditions could be approximated as

$$15 \lesssim N \lesssim 0.01\alpha \tag{5.25}$$

In words this says that the number of beads must be larger than approximately 15 while simultaneously each spring must represent more than approximately 100 persistence lengths. Recall that based on force-extension simulations [30] of the Kramers chain, Somasi et al. [31] argued than each spring should represent more than 10 Kuhn lengths but were not able to estimate a lower bound on the number of springs and had to extrapolate from the Kramers chain result to the WLC result. Here we have used zero Weissenberg rheology to derive *both* lower and upper bounds on the number of beads for arbitrary spring force law. From Brownian dynamics simulations of start-up of steady shear flow [31], there is initial evidence that our bounds may even retain approximate validity in unsteady, strong flows. The response in unsteady, strong flows will be addressed later in Chapter 6.

In addition to allowing for the derivation of the plateau region, writing b_1 and b_2 in terms of the force-extension curve allows for a better physical understanding for the deviation of the curves for $\nu < \infty$ and what is meant by the "Rouse result." The "Rouse result" is the value that the Rouse model would give if the spring constant were equated to the zero-extension slope of the *spring* force law. Recalling that the *spring* force law was taken from the *true polymer* force-extension behavior, one can show that this Rouse model would have coefficients

$$\hat{\eta}_{0,\mathrm{p}} = \left(\frac{N+1}{N}\right)\left(\lim_{\hat{f}\to 0}\frac{\partial}{\partial \hat{f}}\langle \hat{z}_{\mathrm{tot}}\rangle_{\mathrm{p}}\right) \tag{5.26}$$

$$\hat{b}_2 = \left[\left(\lim_{\hat{f}\to 0}\frac{\partial}{\partial \hat{f}}\langle \hat{z}_{\mathrm{tot}}\rangle_{\mathrm{p}}\right)^2\left(\frac{(N+1)(2N^2+7)}{6N^2(N-1)}\right)\right] . \tag{5.27}$$

We see that because the force-extension behavior of the model approaches that of the true polymer as $\nu \to \infty$, the retarded-motion expansion coefficients of the model approach the Rouse result. Note that while the part of b_2 with the third derivative is zero for the Rouse result because its spring is Hookean, that term vanishes for the model as $\nu \to \infty$ because of the $\frac{1}{\nu}$ pre-factor. The third derivative of the true polymer force-extension curve is *not* zero.

Now we turn to a discussion of how using a best-fit λ criteria affects the rheological behavior as the polymer is more finely discretized. In particular let us look more closely at the low-force criteria. The low-force criteria is such that

$$\lim_{\hat{f}\to 0}\frac{\partial}{\partial \hat{f}}\langle \hat{z}_{\mathrm{tot}}\rangle_{\mathrm{m}} = \lim_{\hat{f}\to 0}\frac{\partial}{\partial \hat{f}}\langle \hat{z}_{\mathrm{tot}}\rangle_{\mathrm{p}} . \tag{5.28}$$

If we put this result into equations (5.14) and (5.15) we see that the zero-shear viscosity equals the Rouse result exactly. The zero-shear first normal stress coefficient will be close to the Rouse result but will deviate slightly. This is because the third derivative is non-zero and ν is not infinite. Note that the third derivative is also not equal to the third derivative of the true polymer force-extension curve. The equality and approximate equality with the Rouse results holds only up to a critical N, at which point the low-force criterion diverges (equation (3.45))

$$N_{\max} = \frac{2\phi_2\alpha}{5} + 1 \ . \tag{5.29}$$

5.1.1 FENE and Fraenkel force laws

To this point, we have used the Marko-Siggia force law when a specific force law was needed. However, recall that the relation between the retarded-motion expansion coefficients and the moments of the spring force was written for arbitrary spring force law. In this section, we will show the application of those formulae to the FENE and Fraenkel spring force laws.

Because we have simple formulae for the moments of the FENE force law, the retarded-motion expansion coefficients reduce to simple formulae. In fact, they correctly reduce to the previous result by Wiest and Tanner [78]

$$\hat{\eta}_{0,\mathrm{p}} = \left(\frac{N+1}{N}\right)\left(\frac{\nu}{\nu/\lambda+5}\right) \tag{5.30}$$

$$\hat{b}_2 = \frac{\nu^2(N+1)}{6(\nu/\lambda+5)^2(N-1)N^2}\left[\frac{-12(N^2+1)}{N(\nu/\lambda+7)} + 2N^2 + 7\right] \tag{5.31}$$

We can apply the same methodology used to analyze the zero Weissenberg number rheology of the WLC to the FENE bead-spring chain. Figures 5.5 and 5.6 show the first two retarded-motion expansion coefficients when the level of coarse-graining, ν, is held constant. Figures 5.7 and 5.8 show the coefficients as the polymer is discretized finer and finer. We see the same qualitative trends as with the WLC coefficients. If the number of beads is small, there is error in the rheology due to the drag being exerted only at the beads, instead of along a continuous contour. However, if the polymer is being more finely discretized, then there is error if the polymer is discretized too finely. This is due to error in representing the size of the coil and the extension of polymer segments.

To calculate the rheological properties for the infinitely stiff Fraenkel spring force law we need to calculate the moments, which are

$$\langle \hat{r}^n \rangle_{\mathrm{eq}} = 1 \ . \tag{5.32}$$

The first two retarded-motion expansion coefficients then become

$$\hat{\eta}_{0,\mathrm{p}} = \frac{N+1}{3N} \tag{5.33}$$

$$\hat{b}_2 = \frac{N+1}{54N^2(N-1)}\left[\frac{-12(N^2+1)}{5N} + 2N^2 + 7\right] \ , \tag{5.34}$$

which are the well-known results for the infinitely-stiff Fraenkel chain (equivalent to the FJC) [12].

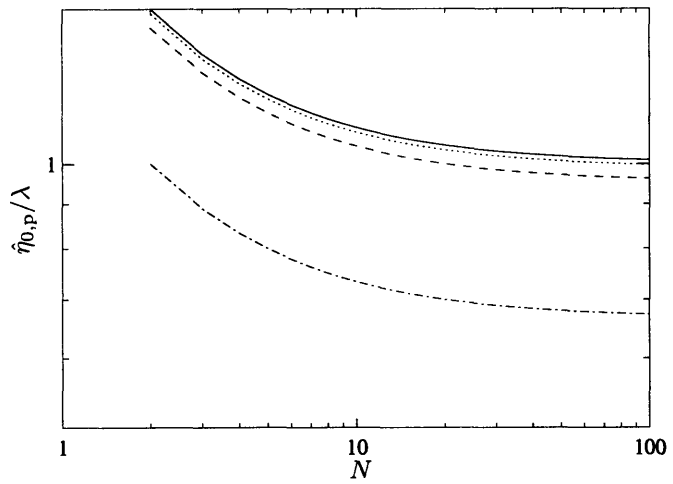

Fig. 5.5: *Polymer contribution to the zero-shear viscosity of FENE bead-spring chains as the number of effective persistence lengths represented by each spring, ν/λ, is held constant. The curves correspond to $\nu/\lambda = \infty$ (*solid line*), $\nu/\lambda =$ 400 (*dotted*), $\nu/\lambda = 100$ (*dashed*), and $\nu/\lambda = 10$ (*dash-dot*).*

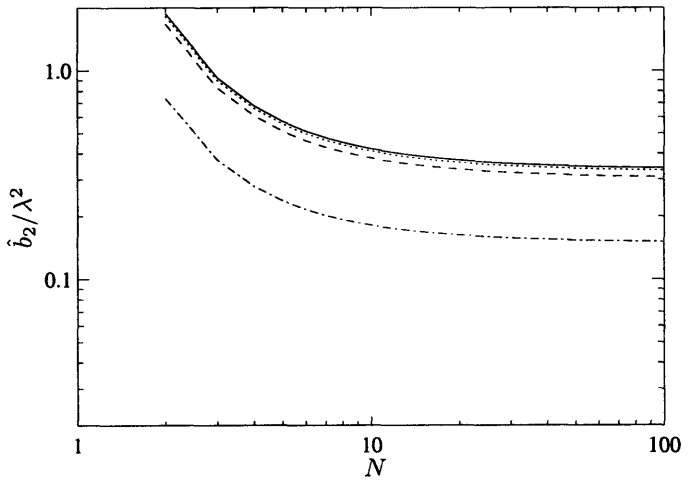

Fig. 5.6: *Zero-shear first normal stress coefficient of FENE bead-spring chains as the number of effective persistence lengths represented by each spring, ν/λ, is held constant. The curves correspond to $\nu/\lambda = \infty$ (*solid line*), $\nu/\lambda = 400$ (*dotted*), $\nu/\lambda = 100$ (*dashed*), and $\nu/\lambda = 10$ (*dash-dot*).*

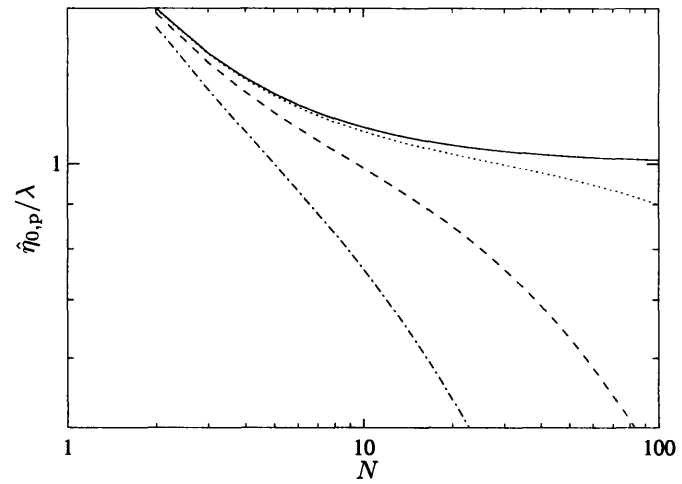

Fig. 5.7: *Polymer contribution to the zero-shear viscosity of FENE bead-spring chains as the number of effective persistence lengths in the total polymer contour, α/λ, is held constant. The curves correspond to $\alpha/\lambda = \infty$ (*solid line*), $\alpha/\lambda = 4000$ (*dotted*), $\alpha/\lambda = 400$ (*dashed*), and $\alpha/\lambda = 100$ (*dash-dot*).*

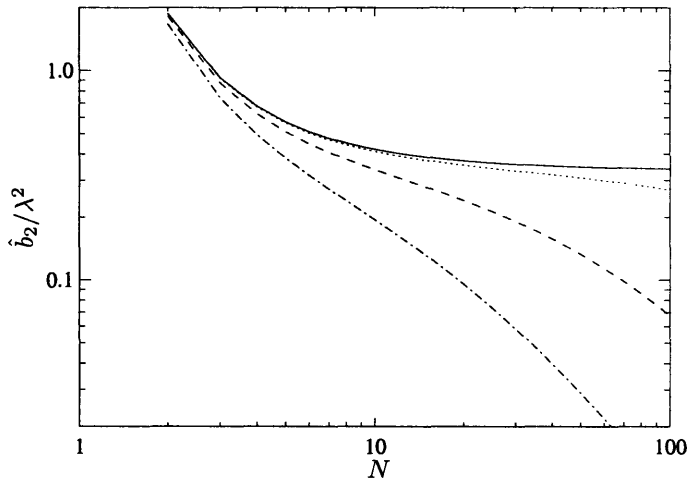

Fig. 5.8: *Zero-shear first normal stress coefficient of FENE bead-spring chains as the number of effective persistence lengths in the total polymer contour, α/λ, is held constant. The curves correspond to $\alpha/\lambda = \infty$ (*solid line*), $\alpha/\lambda = 4000$ (*dotted*), $\alpha/\lambda = 400$ (*dashed*), and $\alpha/\lambda = 100$ (*dash-dot*).*

By taking the ratio of the two coefficients, we can calculate a relaxation time for the chain

$$\tau_0 = \frac{\Psi_{1,0}}{2\eta_{0,\mathrm{p}}} = \frac{\zeta a_{\mathrm{K}}^2}{180\, k_{\mathrm{B}}T}\left[\frac{-12(N^2+1)}{5N} + 2N^2 + 7\right] . \tag{5.35}$$

5.2 Old Versus New Force Laws

We have now seen the low Weissenberg number response of bead-spring chains using previous force laws such as the Marko-Siggia and FENE force laws. This response was related to the force-extension behavior which had already been discussed. We have also discussed a new method for developing spring force laws which accurately captures the response of both freely jointed chains and worm-like chains with respect to the force-extension behavior. We can now show that these new force laws also have an improved response in low Weissenberg numbers.

Looking back at the formulae for the retarded-motion expansion coefficients, the influence of the spring force law enters through the derivatives with respect to force of the average extension in the limit of zero force. The average z-extension of the model has been made dimensionless using the contour length L, and the force has been made dimensionless using $k_{\mathrm{B}}T/A$. In general, the derivatives of the force-extension behavior can be a function of $\nu = \ell/A$.

The terms other than the force-extension behavior are contributed to the fact that the hydrodynamic drag is exerted only on the beads and not along the continuous polymer contour. When the number of beads is large enough, these factors disappear. When using spring force laws such as FENE or Marko-Siggia, the force-extension terms change when each spring represents a small segment of polymer. This causes significant errors in the rheology which places a limit on how small the springs can be [67]. Using the new spring laws eliminates this error. For example, for the RWS model discussed in Section 4.2.1 and choosing A to be the Kuhn length in non-dimensionalizing the force, the bead-spring chain always has

$$\lim_{\hat{f}\to 0} \frac{\partial}{\partial \hat{f}} \langle \hat{z}_{\mathrm{tot}} \rangle_{\mathrm{m}} = \frac{1}{3} \tag{5.36}$$

$$\lim_{\hat{f}\to 0} \frac{\partial^3}{\partial \hat{f}^3} \langle \hat{z}_{\mathrm{tot}} \rangle_{\mathrm{m}} = \frac{-2}{15} . \tag{5.37}$$

We can also use the retarded motion coefficients to gauge the difference between the different dumbbell models of F-actin shown in Figure 4.13(b). For a dumbbell model, it is useful to write b_1 and b_2 directly in terms of the equilibrium averages of the spring length. For the dumbbell models, writing b_1 and b_2 in terms of these moments of the spring length gives

$$b_1 - \eta_{\mathrm{s}} = \eta_{0,\mathrm{p}} = \left(\frac{n_{\mathrm{p}}\zeta L^2}{12}\right) \langle \hat{r}^2 \rangle_{\mathrm{eq}} \tag{5.38}$$

$$b_2 = \frac{-\Psi_{1,0}}{2} = \left(\frac{-n_{\mathrm{p}}\zeta^2 L^4}{240 k_{\mathrm{B}}T}\right) \langle \hat{r}^4 \rangle_{\mathrm{eq}} . \tag{5.39}$$

The force laws in Figure 4.13(b) will have different equilibrium averages. The averages for the Marko-Siggia spring can be calculated using numerical integration. Using the Marko-Siggia dumbbell to model an F-actin filament with the contour length and persistence length from Section 4.3.1,

the averages are $\langle \hat{r}^2 \rangle_{eq} = 0.41$ and $\langle \hat{r}^4 \rangle_{eq} = 0.21$. Alternatively, using the dumbbell model that correctly models the worm-like chain distribution has averages $\langle \hat{r}^2 \rangle_{eq} = 0.77$ and $\langle \hat{r}^4 \rangle_{eq} = 0.61$. This means that the spring force laws in Figure 4.13(b) have a factor of 2 different $\eta_{0,p}$ and a factor of 3 different b_2.

5.3 Influence of HI and EV

In this chapter we have seen the implications of the spring force law for the low Weissenberg number rheological response. In this analysis we have neglected the effects of hydrodynamic interactions and excluded volume. At the close of this chapter it is worth discussing whether the analysis we have presented allows us to understand the influence of the spring force law even when HI and EV are included and important.

It should be first noted that free-draining models are still often used even when HI is important, and our analysis will help in the analysis of such models. For example, λ-phage DNA is generally considered "short" in that the effects of HI on *nonlinear rheology*, such as the start-up of uniaxial extensional flow, can be approximately modeled by using a free-draining model if the drag is rescaled appropriately [15]. The use of these models should be done carefully because a free-draining model fails in predicting some aspects of polymer behavior.

However, our approach here is not limited to this class of molecules. An accurate model will include full fluctuating HI, which is important for all long polymers. Even if HI is included in the model, obviously the size of the coil is critical to model correctly. In fact, in the non-draining limit in "theta" conditions, any dynamic property is directly related to the radius of gyration R_g through a universal ratio [79]. Thus it is crucial for the coarse-grained model to accurately represent the size of the coil, which is directly related to the force-extension behavior at small force. In addition to its impact on rheological properties, the size of the equilibrium coil will have important implications for the behavior in confining geometries in microdevices or in many size-dependent separation techniques. Along these same lines, in non-"theta" conditions EV effects must be included to get the correct coil size. This is particularly important because typical single molecule experiments using DNA are performed in good solvents. Under these conditions it is still important for the spring force law to give the correct "theta" condition size of the coil, with the solvent quality parameter giving the correct deviation from this size.

5.4 Summary

In this chapter, we have discussed the low Weissenberg number response of bead-spring chain models. To better understand the influence of the spring force law, we examined the retarded-motion expansion coefficients without including hydrodynamic interactions and excluded volume. We were able to write these retarded-motion expansion coefficients in a general form for bead-spring chains but with arbitrary force law. These formula can equivalently be written in terms of the force-extension behavior at small force. Thus the response can be related back to the discussion of the force-extension behavior in the previous two chapters. This also means that because the new force laws developed correctly reproduce the force-extension behavior of the polymer, they will also correctly reproduce the low Weissenberg number behavior.

However, recall that the low Weissenberg number response does not solely depend on the force-extension behavior. It also depends explicitly on the number of beads in the model, because the

hydrodynamic drag is only exerted on the beads instead of along the whole continuous contour of the polymer. This error is present when the number of beads is small and is present independent of the spring force law used.

For force laws such as Marko-Siggia, FENE, and Cohen, the low Wi response has an error for small number of springs because of the incorrect distribution of drag. At large number of springs, and thus each spring represents a small segment of polymer, the low Wi response has an error because the force-extension behavior is incorrect producing an incorrect coil size. Only if the polymer contains enough persistence or Kuhn lengths does there exist a plateau region in which both errors are small. If the low force criterion is used for the effective persistence length or Kuhn length, the error at high discretization virtually disappears with respect to the low Wi response because the force-extension behavior is correctly modeled at small force. The disadvantage of this choice is that the behavior at high forces or flows is incorrect. This choice can also only be used down to the level of discretization where the low force criterion fails (diverges). However, with the new force laws developed, the low Wi response does not have an error at high discretization because the force law was developed to correctly model the force-extension behavior. With these new force laws, the behavior at large forces or flows is also modeled correctly.

Having examined the response of bead-spring chains for low Wi, we will next examine the behavior at high Wi.

CHAPTER 6

High Weissenberg Number Response

In the previous chapter we considered the low Weissenberg number response, which is a small perturbation away from equilibrium. We related the response to the force-extension behavior at small force and showed the advantage of using the newly developed force laws. In this chapter we will be focusing on the effect of the spring force law on the response when the polymer is strongly stretched (approaching full extension). In such states the inclusion of excluded volume effects should have not affect the response because the likelyhood that the chain will be in a configuration which is influenced by the solvent quality is small. Initially, we will also not include the influence of hydrodynamic interactions. In an extended configuration, the segments of polymer are further apart so the hydrodynamic interactions will be weaker than in the equilibrium coiled state. However, when expressing the flow strength in terms of a Weissenberg number, the longest relaxation time is used. This longest relaxation time is affected by hydrodynamic interactions. In the end of this chapter we will give a brief discussion of the influence of hydrodynamic interactions.

6.1 Longest Relaxation Time

When examining the behavior of bead-spring chains in flow, it is common to express the flow conditions (shear rate or elongation rate) in terms of a Weissenberg number. The Weissenberg number (Wi) is taken as the product of the shear rate or elongation rate and the longest relaxation time. For models for which analytic calculations can be performed such as for linear springs, the

longest relaxation time can be expressed exactly as a function of the model parameters (such as the bead drag coefficient and spring constant). For nonlinear spring models, such an analytic formula for the longest relaxation time is not possible.

The longest relaxation time for these models can be calculated numerically using dynamical simulations such as BD. These simulations can be computationally costly, particularly for long chains that have long relaxation times. It is also inconvenient to have to perform a preliminary simulation for each set of model parameters before performing the primary simulations. One way around this is to use instead the characteristic time from dividing the zero-shear first normal stress coefficient by two times the zero-shear polymer viscosity as discussed in equation (5.6)

$$\tau_0 \equiv \frac{\Psi_{1,0}}{2\eta_{p,0}} \,. \tag{6.1}$$

Both of these zero-shear properties can be calculated from the retarded motion expansion coefficients [67]. For the FENE force law, these can be calculated analytically. For other force laws, such as the Marko-Siggia force law, they require numerical integration but are much less computationally costly than full BD simulations. The disadvantage of using this characteristic time is that it differs from the longest relaxation time even for chains with the relatively simple linear spring force law [12]. It is unclear how the two characteristic times are related for more complicated force laws.

Another way of estimating the longest relaxation time is to use the linear force law formula [15]. The linear spring constant is taken from the nonlinear spring law at small extensions, where the spring law looks linear. If the chain, as it is relaxing back to equilibrium, only samples the linear region of the spring at long times, then this should be a good approximation. It has been shown that this approximation can result in significant errors. This error results because even at equilibrium, the springs can sample the nonlinear parts of the force law as discussed in Section 3.5 and in ref. [67].

Because of the deficiencies of each approximate method, we performed direct BD simulations of the relaxation of chains over a wide parameter range and with both the FENE and Marko-Siggia force laws. In order to calculate the longest relaxation time, the chains were started in a stretched configuration (95% extension) in the z direction. The chains were simulated as they relaxed back to equilibrium. At long time, the stress difference $\sigma_{zz} - \sigma_{xx}$ decays as a single exponential, $\exp(-t/\tau)$. A least-squares fit is used to extract the value of the longest relaxation time. Before plotting the results of the simulations, we will review what we call the Rouse relaxation time of a chain and express it in the notation used here. Consider a chain of N beads connected by $N-1$ linear springs with spring force law $f_{\text{spr}}(r) = Hr$. The longest relaxation time of the chain is

$$\tau = \frac{1}{2\sin^2(\pi/(2N))}\frac{\zeta}{4H} \,. \tag{6.2}$$

Now, consider a chain of inextensible springs. Using the notation from ref. [67], we write the Taylor expansion of the spring force as

$$f_{\text{spr}}(r) = \frac{k_{\text{B}}T 2\phi_2\nu}{\ell^2\lambda} r + \mathcal{O}(r^2) \,. \tag{6.3}$$

If we treat the linear term like the linear spring, the longest relaxation is what we call the Rouse

time

$$\tau_{\mathrm{R}} = \frac{1}{2\sin^2(\pi/(2N))}\frac{\zeta\ell^2\lambda}{8\phi_2 k_{\mathrm{B}}T\nu} \ . \tag{6.4}$$

With our choice of A_{true} as the persistence length then $\phi_2 = 3/4$ for the Marko-Siggia force law, and with A_{true} as one-third of the Kuhn length then $\phi_2 = 1/2$ for the FENE force law. Note that because of our ability to take different choices for A_{true} the formulas can appear to take different forms. However, because any change of choice affects the meaning of ν while also changing the value of ϕ_2, the physical meaning of a formula remains invariant. To illustrate this, let us insert into the Rouse time the definitions of ν and λ and the value of ϕ_2. For the Marko-Siggia force law, we have taken A_{eff} to be the effective persistence length, $A_{\mathrm{p,eff}}$, and the Rouse time becomes

$$\tau_{\mathrm{R}} = \frac{1}{2\sin^2(\pi/(2N))}\frac{\zeta\ell A_{\mathrm{p,eff}}}{6k_{\mathrm{B}}T} \ . \tag{6.5}$$

For the FENE force law, we have taken A_{eff} to be one-third of the effective Kuhn length, $a_{\mathrm{K,eff}}/3$, and the Rouse time becomes

$$\tau_{\mathrm{R}} = \frac{1}{2\sin^2(\pi/(2N))}\frac{\zeta\ell a_{\mathrm{K,eff}}}{12k_{\mathrm{B}}T} \ . \tag{6.6}$$

These two formulas remain the same independent of any choice for A_{true} and the corresponding value of ϕ_2.

We now show the results of the BD simulations using the Marko-Siggia force law in Figure 6.1 where the longest relaxation time of the chain is divided by the above Rouse time. The first thing to note is that the longest relaxation time is the same as the Rouse time when $\nu/\lambda \to \infty$ but deviates for smaller values. This is because the Rouse time assumes that near equilibrium the spring only samples the low extension (linear) part of the spring. As discussed in ref. [67] and Chapter 3, if ν/λ is not infinite, the spring samples the nonlinear parts of the spring even at equilibrium. However, the other important aspect to notice from Figure 6.1 is that the relaxation time scales with N just like the Rouse result. The deviation from the Rouse time is only a function of ν/λ. This suggests that it is possible to describe the relaxation time using a chain with linear springs, but which have a linear spring constant that differs from that in equation (6.3). In some approximate sense, the chain still responds linearly to external forces even if the spring samples the nonlinear regions and so returns to equilibrium using some effective linear restoring force. This is reminiscent of the force-extension behavior of the chains seen in Chapter 3 and ref. [67]. Even if the chain samples the nonlinear regions, the force-extension behavior is linear at low force. In equation (3.23) and ref. [67] it is shown that a bead-spring chain has

$$\lim_{f\to 0}\frac{\partial}{\partial f}\langle z_{tot}\rangle_m = \frac{(N-1)\ell^2\langle\hat{r}^2\rangle_{\mathrm{eq}}}{3k_{\mathrm{B}}T} \ , \tag{6.7}$$

where the spring force law comes in through the equilibrium averaged single spring moment

$$\langle\hat{r}^2\rangle_{\mathrm{eq}} = \frac{\int_0^1 \mathrm{d}\hat{r}\ \hat{r}^4\ \exp\left[\frac{-\nu}{\lambda}\widehat{U}_{\mathrm{eff}}(\hat{r})\right]}{\int_0^1 \mathrm{d}\hat{r}\ \hat{r}^2\ \exp\left[\frac{-\nu}{\lambda}\widehat{U}_{\mathrm{eff}}(\hat{r})\right]} \ . \tag{6.8}$$

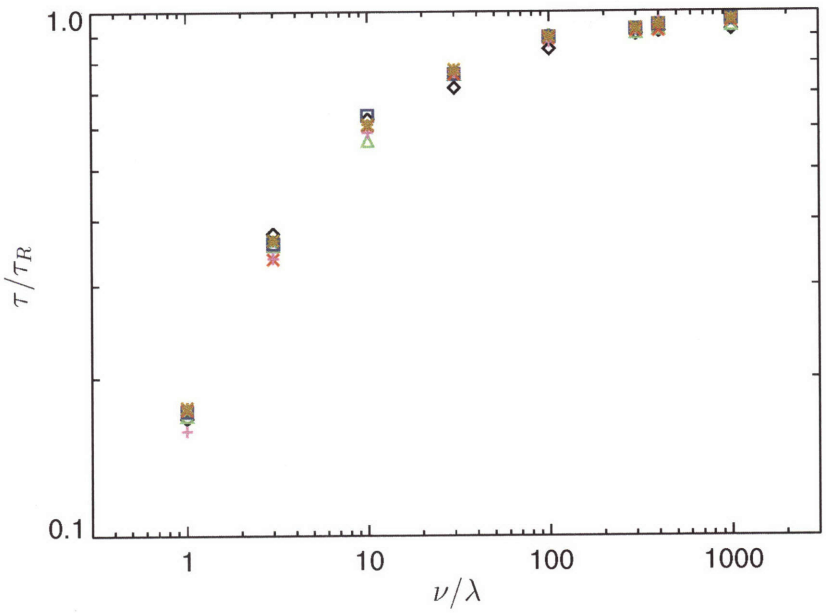

Fig. 6.1: *Plot of the longest relaxation time of Marko-Siggia bead-spring chains relative to the Rouse prediction as a function of the number of effective persistence lengths each spring represents. The symbols represent different number of beads: $N = 2$ (diamond), $N = 5$ (triangle), $N = 10$ (square), $N = 30$ ($\times$), $N = 50$ ($+$), and $N = 100$ ($*$).*

For a chain of linear springs, the force-extension relation is

$$\frac{\partial}{\partial f}\langle z_{tot}\rangle_m = \frac{(N-1)}{H} \ . \tag{6.9}$$

Comparing equations (6.7) and (6.9), we define a modified Rouse model as a chain of linear springs where the spring constant is

$$H_{MR} \equiv \frac{3k_{\mathrm{B}}T}{\ell^2\langle\hat{r}^2\rangle_{\mathrm{eq}}} \ . \tag{6.10}$$

This statement is equivalent to choosing the linear spring constant such that it has the same equilibrium averaged end-to-end distance squared and number of beads as the nonlinear spring chain. Following from this is that they also have the same equilibrium radius of gyration and zero shear viscosity. While these equivalences do not guarantee that this modified Rouse model will have the same longest relaxation time as the nonlinear spring chain, we hope that they will be similar. Therefore we will compare the modified Rouse relaxation time with the exact relaxation time to examine how well it predicts the nonlinear chain behavior. The longest relaxation time of

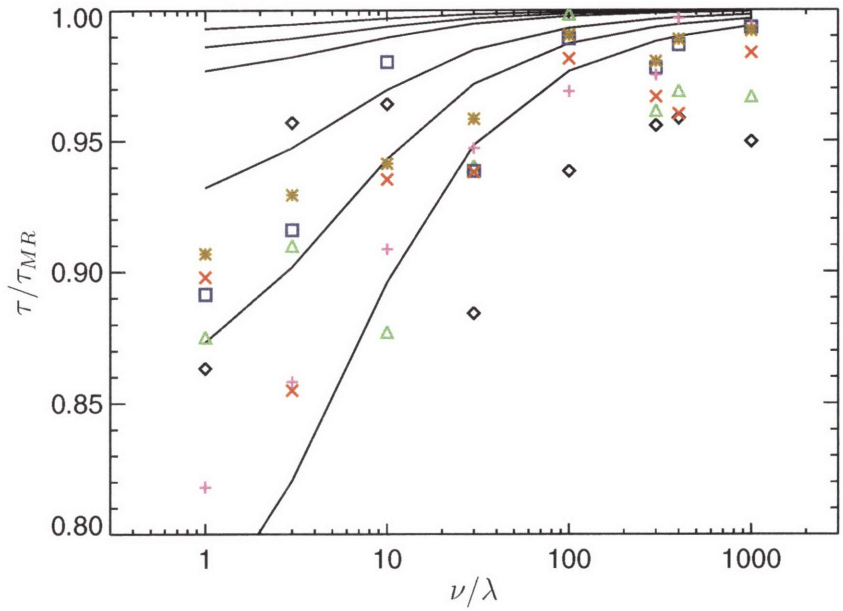

Fig. 6.2: *Plot of the longest relaxation time of Marko-Siggia bead-spring chains relative to the modified Rouse prediction (equation* (6.11)*) as a function of the number of effective persistence lengths each spring represents. The symbols represent different number of beads:* $N = 2$ *(diamond),* $N = 5$ *(triangle),* $N = 10$ *(square),* $N = 30$ *(×),* $N = 50$ *(+), and* $N = 100$ *(∗). The lines represent* $\tau_{0,s}$ *divided by the modified Rouse prediction for the same range of number of beads.*

the modified Rouse model is

$$\tau_{MR} = \frac{1}{2\sin^2(\pi/(2N))} \frac{\zeta \ell^2 \langle \hat{r}^2 \rangle_{\text{eq}}}{12 k_{\text{B}} T} \ . \tag{6.11}$$

In Figure 6.2 we show the longest relaxation times of the bead-spring chains as in Figure 6.1 but now dividing the values by τ_{MR} to gauge the predictive capability of the modified Rouse model in terms of longest relaxation time. We should note that the equations (6.4) and (6.11) are not new, and have been used before. See, for example, the review by Larson [15]. However both equations have been called by the name "Rouse" because for the Rouse model, for which they were derived, they are equivalent. Our contribution is to notice that for nonlinear spring force laws, the formulas give dramatically different results. In order to carefully distinguish between these formulas which give different predictions for nonlinear springs, we call them "Rouse" and "modified Rouse" respectively. We have shown here that while the Rouse result (equation (6.4)) fails to predict the relaxation of nonlinear springs, the modified Rouse formula (equation (6.11)) retains approximate validity for nonlinear springs.

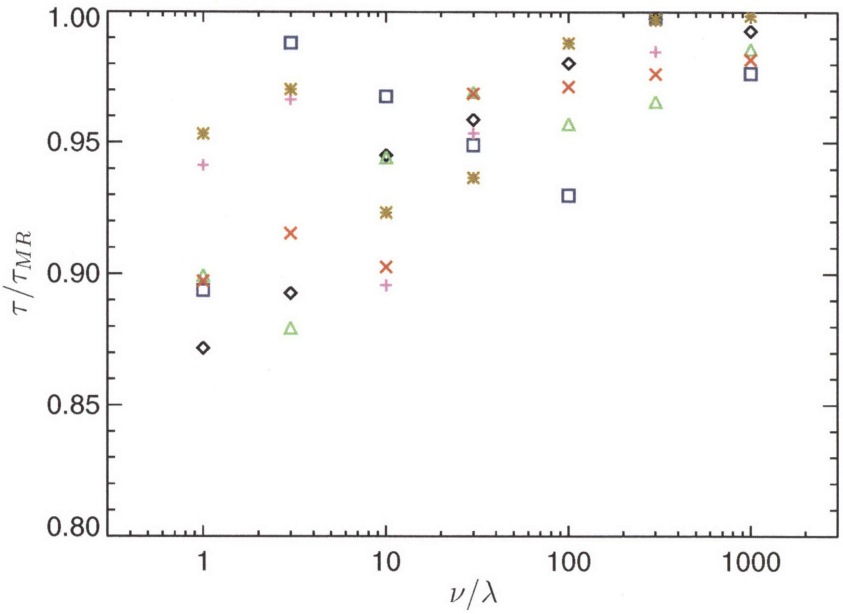

Fig. 6.3: *Plot of the longest relaxation time of FENE bead-spring chains relative to the modified Rouse prediction as a function of the number of effective persistence lengths each spring represents. The symbols represent different number of beads:* $N = 2$ *(diamond),* $N = 5$ *(triangle),* $N = 10$ *(square),* $N = 30$ *(×),* $N = 50$ *(+), and* $N = 100$ *(∗).*

To this point, we have compared exact BD simulations of the longest relaxation time to what we call the Rouse time (equation (6.4)) and compared the exact simulations with a modified Rouse model (equation (6.11)). The other method for estimating the relaxation time is from the ratio of zero-shear properties, equation (6.1), which we now compare with the exact BD simulations. One problem with using this estimate is that the functional dependence with N is different. For a chain of linear springs τ_0 is

$$\tau_0 = \frac{2N^2+7}{15}\frac{\zeta}{4H} \,. \tag{6.12}$$

This inspires us to define a scaled time

$$\tau_{0,s} \equiv \tau_0 \frac{15}{2N^2+7}\frac{1}{2\sin^2(\pi/(2N))} \,, \tag{6.13}$$

which compensates for the difference in N dependence that exists even for the linear spring system. Figure 6.2 also shows curves representing $\tau_{0,s}$ for the Marko-Siggia force law divided by τ_{MR}. It is clear that $\tau_{0,s}$ represents the data any better than τ_{MR}. Because of the useful physical interpretation of τ_{MR} in terms of the coil size and force-extension behavior, we will not consider $\tau_{0,s}$ further. We have also performed a fit through the data to give a formula which is only slightly more accurate

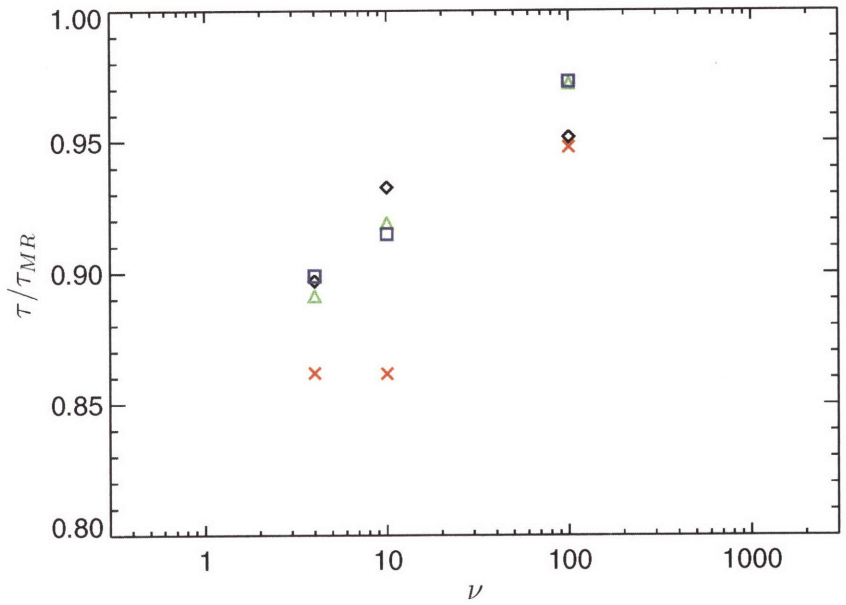

Fig. 6.4: *Plot of the longest relaxation time of bead-spring chains using the new force law for the worm-like chain relative to the modified Rouse prediction as a function of the number of persistence lengths each spring represents. The symbols represent different number of beads: $N = 2$ (diamond), $N = 5$ (triangle), $N = 10$ (square), and $N = 30$ ($\times$).*

than τ_{MR}. For the Marko-Siggia force law, this is

$$\tau_{\text{fit}} = \frac{1}{2\sin^2(\pi/(2N))} \frac{\zeta \ell^2}{k_{\text{B}}T} \frac{1}{6\nu/\lambda + 7.26\sqrt{\nu/\lambda} + 21.2} \,. \tag{6.14}$$

We have also performed BD simulations of the longest relaxation time using the FENE spring force law to verify that the trends seen with the Marko-Siggia force law are not specific to that force law. In Figure 6.3 we show the longest relaxation time divided by τ_{MR} for the FENE force law. We can also perform a fit through this data to give a slightly more accurate result

$$\tau_{\text{fit}} = \frac{1}{2\sin^2(\pi/(2N))} \frac{\zeta \ell^2}{k_{\text{B}}T} \frac{1}{4\nu/\lambda + 1.05\sqrt{\nu/\lambda} + 21.1} \,. \tag{6.15}$$

These fitted functions will be used later as a closed form expression for the longest relaxation time when discussing the change of the elongational viscosity with the degree of discretization.

We see that the modified Rouse formula gives a reasonable prediction of the longest relaxation time even to very high discretization. This is important because the modified Rouse formula allows us to gain intuition about the governing factors towards the relaxation time. The modified Rouse formula contains the size of a spring at equilibrium, which can be related to the force-extension

response at small force. This gives us confidence that if a new spring force is used which gives the correct size of a spring and force-extension behavior, then the relaxation time will be the expected value. We can show this explicitly by calculating the relaxation time for a new force law to represent the worm-like chain (equation (4.72)). Figure 6.4 shows the relaxation time of this force law divided by its modified Rouse prediction. We see the same basic result as with the Marko-Siggia and FENE force laws, that the modified Rouse formula is a reasonable prediction. Note that this new force law was developed to have the correct behavior near equilibrium, and thus by construction the modified Rouse formula is

$$\tau_{MR} = \frac{1}{2\sin^2(\pi/(2N))}\frac{\zeta \ell A_{\mathrm{p}}}{6k_{\mathrm{B}}T} \ . \tag{6.16}$$

6.2 Elongational Viscosity

After understanding the behavior of the longest relaxation time, we can investigate the high Weissenberg response. One advantage of looking at steady elongational flow is that the viscosity can be written formally as an integral over configuration space [12]. This can be done because we are not including the effects of EV and HI, which should be of secondary importance near full extension. Although calculating the integrals numerically is not efficient for getting the exact response for chains of many springs, they can be used to develop series approximations. This same type of expansion was performed at small flow strength to obtain the retarded-motion expansion coefficients such as in ref. [67].

6.2.1 Models of the worm-like chain

We begin our analysis of the response of bead-spring chains in strong, steady elongational flow with bead-spring chains used to model the worm-like chain. The most commonly used spring force law to model the worm-like chain is the Marko-Siggia interpolation formula. The expansion of the elongational viscosity for large strain rates using the Marko-Siggia force law is

$$\frac{\bar{\eta} - 3\eta_s}{n_p \zeta \ell^2} \sim \frac{N(N^2-1)}{12} - \sqrt{\frac{\nu/\lambda}{2\mathrm{Pe}}} \sum_{k=1}^{N-1} \sqrt{k(N-k)} + \mathcal{O}\left(\frac{1}{\mathrm{Pe}}\right) \ , \tag{6.17}$$

where the Peclet number is defined as

$$\mathrm{Pe} \equiv \frac{\dot{\epsilon}\zeta\ell^2}{k_{\mathrm{B}}T} \ . \tag{6.18}$$

Our approach is to use this expansion to understand the change in the response of the chain as the amount of polymer represented by a spring is changed. Using an analytic expansion will allow us to make precise statements about the effect of the different spring force laws and criteria for the effective persistence length. Since it is an expansion for large strain rates, for sufficiently large strain rates it will eventually describe the response, but it is necessary to examine exactly how large the strain rate must be for this expansion as truncated to describe the exact response.

To investigate the exact chain response and the range of validity of the expansion we performed BD simulations of chains without EV and HI from approximately Wi=1 to 1000 for a range of parameters of the Marko-Siggia force law. These are shown in Figure 6.5. We plot the data versus

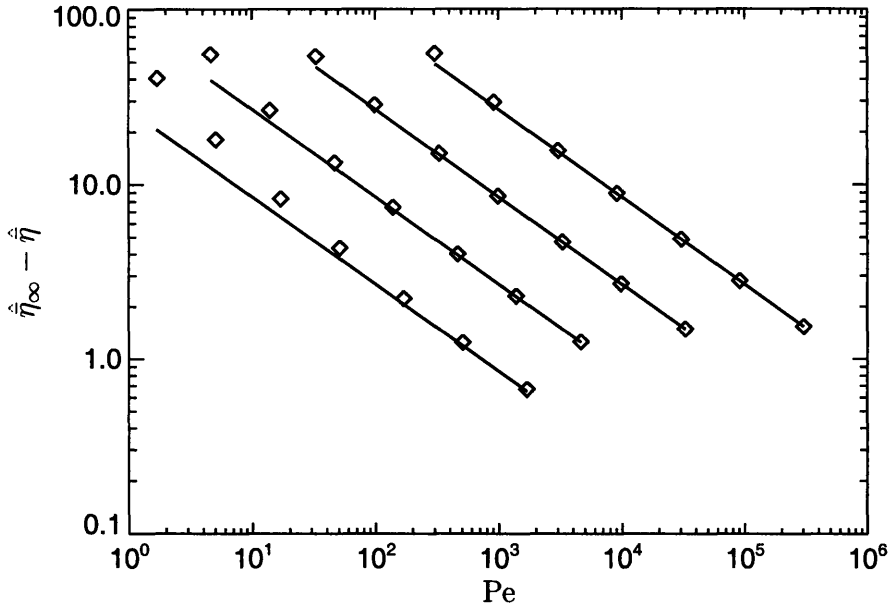

Fig. 6.5: *Comparison of the approach to the plateau elongational viscosity between BD simulations (symbols) and the two-term series expansion (solid lines). The spring force law is the Marko-Siggia formula and the chains consist of 10 beads. The curves correspond to (from left to right)* $\nu = 1, 10, 100, 1000$. *Each curves spans strain rates from approximately* $\mathrm{Wi} = 1$ *to* $\mathrm{Wi} = 1000$.

Peclet number instead of Weissenberg number because the Peclet number is the natural parameter in the expansion and simulations. The Peclet number is a local comparison of the strain rate to the characteristic time for a bead to diffuse the fully-extended length of a spring. In absence of an exact formula for the longest relaxation time in terms of model parameters (an approximate one is given in the previous section) there exists an uncertainty in the value of the Weissenberg number. There is also variability in what characteristic time that is used to define the Weissenberg number. In our comparison of the simulations and expansion we choose to eliminate the uncertainty of the Weissenberg number as a possible source of deviation.

Having verified that the expansion represents the high extension rate behavior of the Brownian dynamics simulations, we can examine the behavior of the two term expansion. We will use the analytic nature of the expansion to investigate the behavior of different bead-spring chains. After the analysis we will return to the question of whether the expansion accurately represents the data over the entire range of analysis. As in ref. [67] and Chapter 5 we will examine the viscosity as a function of the number of beads while the total number of persistence lengths in the molecule is held constant. We will also keep the Weissenberg number constant as we change the number of

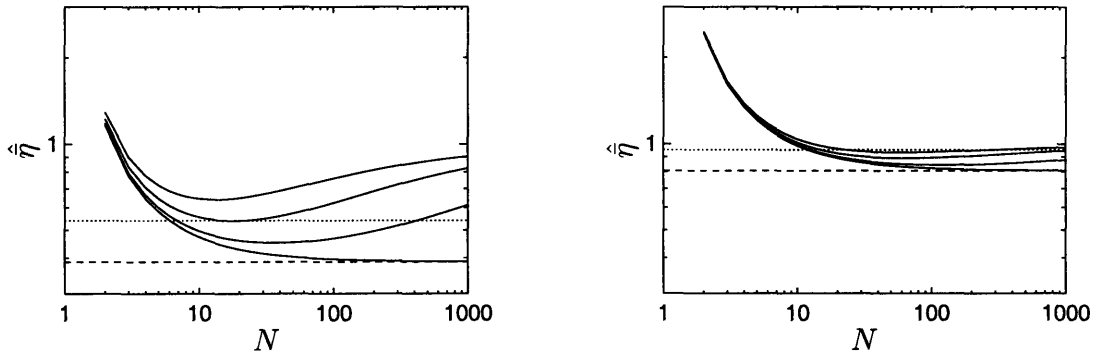

Fig. 6.6: *Calculation of the elongational viscosity as a function of the number of beads for a constant* Wi *and* α *using the first two terms in the asymptotic expansion for the Marko-Siggia force law with* $\lambda = 1$ *(equation* (6.21)*). The values of* Wi *are 1 (left) and 10 (right). The lines correspond to different values of* α*, from top to bottom ranging from 100, 400, 4000, and* ∞*. The dashed line is* $1 - \sqrt{3/(3\mathrm{Wi})}$ *(equation* (6.22)*), and the dotted line is* $1 - 0.46/\mathrm{Wi}$ *(from equation* (6.27)*).*

beads. We manipulate equation (6.17) to write the expansion in terms of the Weissenberg number

$$\frac{\bar{\eta} - 3\eta_s}{n_p(N\zeta)L^2/12} \sim \frac{N+1}{N-1}\left(1 - \frac{6}{N\sin(\pi/(2N))}\frac{\sum_{k=1}^{N-1}\sqrt{k(N-k)}}{N^2-1}\sqrt{\frac{\hat{\tau}2\sin^2(\pi/(2N))\nu/\lambda}{\mathrm{Wi}}}\right) + \mathcal{O}\left(\frac{1}{\mathrm{Wi}}\right). \tag{6.19}$$

The prefactor

$$\frac{6}{N\sin(\pi/(2N))}\frac{\sum_{k=1}^{N-1}\sqrt{k(N-k)}}{N^2-1} \tag{6.20}$$

ranges from $\sqrt{2}$ for both $N = 2$ and $N = 3$ to $3/2$ for $N \to \infty$. This prefactor changes by a total of about 6% over the entire N range so is not a dominant effect. We can replace this by the asymptotic value of $3/2$ without significant error. Similarly, we can replace the relaxation time using the approximation in equation (6.14) which represents the relaxation time to within an error of about a few percent

$$\frac{\bar{\eta} - 3\eta_s}{n_p(N\zeta)L^2/12} \approx \frac{N+1}{N-1}\left(1 - \frac{3}{2}\sqrt{\frac{1}{\mathrm{Wi}(6 + 7.26\sqrt{\lambda/\nu} + 21.2\lambda/\nu)}}\right) + \mathcal{O}\left(\frac{1}{\mathrm{Wi}}\right). \tag{6.21}$$

With equation (6.21) we have a simple approximation to the response written in terms of Wi. We show in Figure 6.6 the value of equation (6.21) as a function of the number of beads, N, for $\mathrm{Wi} = 1$ and $\mathrm{Wi} = 10$ and using the high-force criterion for the effective persistence length ($\lambda = 1$). The curves are also at a constant total number of persistence lengths, $\alpha = L/A_{\mathrm{true}} = \nu(N-1)$. Although we do not expect equation (6.21) to accurately represent the simulations down to $\mathrm{Wi} = 1$

over the whole range of N, the larger spread of the curves allows one to see better the shape of the curves. The behavior at low number of beads is similar to the zero Weissenberg number response, which we again attribute to that the hydrodynamic drag is exerted only on discrete beads instead of along a continuous contour. If the chain is very long ($\alpha \gg 1$), there will exist a large region for which $1 \ll N \ll \alpha$ and the viscosity is

$$1 - \sqrt{\frac{3}{8\mathrm{Wi}}} + \mathcal{O}\left(\frac{1}{\mathrm{Wi}}\right) . \tag{6.22}$$

However, for chains with a finite length (so finite α), N will eventually become large enough that each spring represents a small segment of polymer. The limit of this progression is when $\alpha \ll N$. In the limit that $1 \ll N$ and $\alpha \ll N$, the viscosity approaches

$$1 + \mathcal{O}\left(\frac{1}{\mathrm{Wi}}\right) . \tag{6.23}$$

The difference between equations (6.22) and (6.23) decreases as $\mathrm{Wi}^{-1/2}$, which means that for very large Weissenberg number, there is no upper limit on the number of beads past which the response deviates significantly. Essentially, if the Weissenberg number is large enough, the chain will be almost fully extended and so even if the spring force is not represented correctly, the chain will still be in the fully extended state. Thus for some properties the change if the incorrect spring force law is used may appear to have a negligible effect. Note that this is different from the low Weissenberg number behavior which was found to have a maximum number of beads of $N^{1/2} \ll 1.15\alpha^{1/2}$ for the Marko-Siggia spring force law [67]. This means that the response of the bead-spring chain seems to be less sensitive to using an inappropriate spring force law when the springs become very small.

To this point we have not used an effective persistence length that differed from the persistence length of the WLC being modeled, thus $\lambda = 1$. Recall the progression of analysis used to study the behavior at low Wi. The analysis with $\lambda = 1$ showed that there was an error in the low Wi response if each spring represented too small an amount of polymer. However if the low-force criterion was used for the effective persistence length, the error due to the incorrect force law vanished in the range of applicability of the low-force criterion. The only error that remained was from the fact that for small number of beads, the drag was not distributed along the contour. We would thus expect that a similar vanishing of the error would be present in this case if the high-force criterion were used. But recall that for the Marko-Siggia force law using $\lambda = 1$ *is* the high-force criterion. There is still a deviation when each spring represents too few number of persistence lengths. Let us compare this response if instead λ were chosen according to the low-force criterion. This response is shown in Figure 6.7. We see that this response more quickly deviates from the plateau. Although it is true that the high-force criterion produces a more extended plateau region, there is still an error if each spring represents a small number of persistence lengths.

If we look closer at the expansion we see that the prefactor to $\mathrm{Pe}^{-1/2}$, that is $\lambda^{-1/2}$, is correct if the high-force criterion is used and deviates if the low-force criterion is used. However the plots have been produced at constant Wi. To convert the formula from Pe to Wi the longest relaxation time must be used. This longest relaxation time depends on the low-force behavior of the chain. Recall that the modified Rouse relaxation time is a function of the second moment of the spring length, $\langle r^2 \rangle$, and the low-force criterion gets this second moment correct. Thus when using the high-force criterion it is the longest relaxation time that deviates at high discretization causing

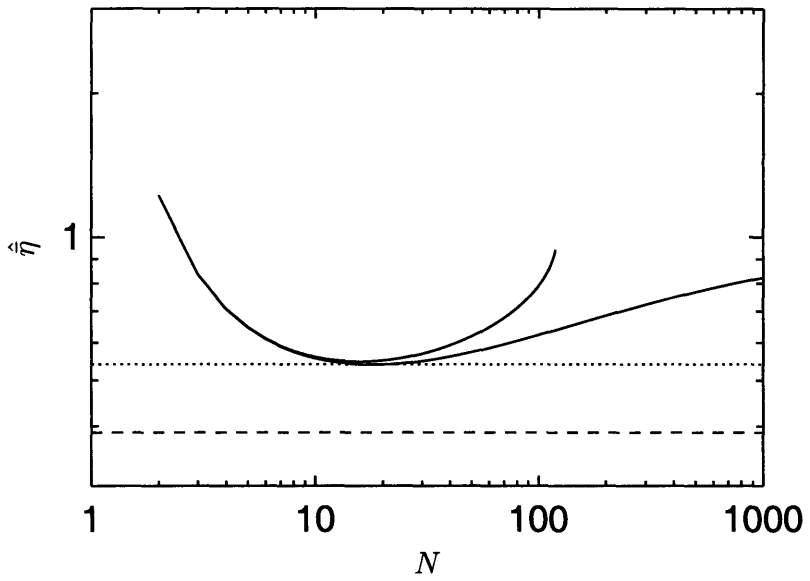

Fig. 6.7: *Comparison of the different criteria for λ and their effect on the elongational viscosity for the Marko-Siggia force law. The parameters are* $\mathrm{Wi} = 1$, $\alpha = 400$, *and either the low-force (upper line) or the high-force criteria (lower line) for λ. The high-force criterion curve and the dashed and dotted lines are identical to in Figure 6.27.*

the error, while using the low-force criterion gets the longest relaxation time correct (to within the error between the true relaxation time and the modified Rouse relaxation time) but has an error in the explicit prefactor to the Pe. In some sense this makes the response at high Wi more complicated and a more stringent test of the accuracy of the spring force law because the response has a contribution having to do with the high force response and one having to do with the low force response. However, recall that it is also a less stringent test because if the Wi is large enough the chain is fully extended irrespective of the details of the spring force law.

To this point we have used the first two terms in the asymptotic expansion to examine analytically the behavior of the bead-spring chains. We have gained significant knowledge about the response of the bead-spring chains using an expansion that is relatively simple to produce and will be valid at large enough strain rates. We now return to a more detailed description of how accurately the two terms represents the true response of the bead-spring chains. To answer that question, we will examine the higher order terms in the expansion. The Pe^{-1} correction to equation (6.17) can be calculated with some effort, but the $\mathrm{Pe}^{-3/2}$ term is excessively complex. However, we can use knowledge of the structure of the series and our BD simulations to generate an *approximate* form for the $\mathrm{Pe}^{-3/2}$ term. These two corrections to equation (6.17) are

$$\frac{-1}{\mathrm{Pe}}\left[\frac{7}{2}(N-1)-3C_N\right]-\frac{1}{\mathrm{Pe}^{3/2}}\left[3.6\sqrt{\frac{\lambda}{\nu}}+\sqrt{\frac{\nu}{\lambda}}+\left(1-\frac{2}{N^2}\right)\left(\frac{\nu}{\lambda}\right)^{3/2}\right], \tag{6.24}$$

where we have defined

$$C_N \equiv \sum_{m=1}^{N-1} \frac{1}{1+m+m^2} \,. \tag{6.25}$$

While the $\mathrm{Pe}^{-3/2}$ term is only approximate, with the addition of these two terms, the expansion models well the response of chains with $N = 2, 5, 10, 30$ and $\nu/\lambda = 1, 10, 100, 1000$ for flows ranging from $\mathrm{Wi} = 1$ to $\mathrm{Wi} = 1000$. The expansion has a typical error of 2% for $\mathrm{Wi} = 1$ with a much smaller error for higher Wi. Using this, we can find the next corrections to equations (6.22) and (6.23). The next correction for equation (6.22) comes from examining the limit $1 \ll N \ll \alpha$. In that limit the Wi^{-1} term vanishes and the $\mathrm{Wi}^{-3/2}$ term becomes

$$\frac{-0.07}{\mathrm{Wi}^{3/2}} \,, \tag{6.26}$$

where the possible error in the coefficient results because this term was only inferred from the simulations. While this correction will play a role if the Wi is not large enough, it should play a secondary role and the qualitative behavior discussed previously will remain unchanged. The correction for equation (6.23) is more subtle. When only using the first two terms in the expansion, the $\mathrm{Wi}^{-1/2}$ term vanishes in the limits $1 \ll N$ and $\alpha \ll N$. Therefore, we only capture the finite extensibility but not the approach to finite extensibility. The $\mathcal{O}(1)$ term is modeled correctly, but the $\mathcal{O}(\mathrm{Wi}^{-1/2})$ term is not. To examine this limit we must examine the higher terms in the expansion. However, we see that the coefficient to the $\mathrm{Wi}^{-3/2}$ term actually diverges. This happens because the limit to a bead-string chain is a singular limit. This is similar to the behavior which could be seen for the force-extension behavior at large force using the Marko-Siggia spring force law. Thus the Pe^{-1} term in equation (6.24) is the behavior seen if, for a constant ν/λ, the Pe is made large. If instead the limit $\nu/\lambda \to 0$ is taken for a constant Pe or Wi, the response approaches the bead-string chain. If this bead-string chain response is expanded for large Pe or Wi, the Pe^{-1} term is different. The coefficient to Pe^{-1} depends on the order in which the limits are taken. We will see later that the expansion of the bead-string chain has a Pe^{-1} term that is similar to in equation (6.24) but with the 7/2 replaced by a 4. Thus in the limit $1 \ll N$ but $\alpha \ll N$ the true next correction to the response of the Marko-Siggia bead-spring chains as seen in Figures 6.6 and 6.7 is

$$\frac{-0.46}{\mathrm{Wi}} \,, \tag{6.27}$$

where the possible error in this coefficient results from using our approximate formula for the relaxation time (used to convert from Pe to Wi) in the limit $\nu/\lambda \to 0$. We have now examined the next corrections to the behavior in the two different limits, both $1 \ll N \ll \alpha$ and $1 \ll N$ and $\alpha \ll N$. While these obviously affect the quantitative comparison between the curves in Figures 6.6 and 6.7, the qualitative nature will not be changed significantly because at a large enough Wi only the first two terms in the expansion are sufficient to describe the simulation results.

The analysis of the Marko-Siggia force law has shown that the response does begin to deviate at large enough discretization because each spring represents too small a segment of polymer. In this limit the Marko-Siggia spring force law does not accurately capture the response of the worm-like chain it is trying to represent. A new spring force law has been developed which can be used to model a worm-like chain even if each spring represents as few as 4 persistence lengths (provided the whole chain contains many persistence lengths) [80]. This new force law was given

in equation (4.72). The expansion of the elongational viscosity using this new spring force law for the worm-like chain is

$$\frac{\bar{\eta} - 3\eta_s}{n_p \zeta \ell^2} \sim \frac{N(N^2-1)}{12} - \sqrt{\frac{\nu}{2\mathrm{Pe}}} \sum_{k=1}^{N-1} \sqrt{k(N-k)} + \frac{3C_N}{\mathrm{Pe}} + \mathcal{O}\left(\frac{1}{\mathrm{Pe}^{3/2}}\right) . \tag{6.28}$$

We can explicitly see from this expansion the great advantage of the new spring force law. Note that the $\mathrm{Pe}^{-1/2}$ term looks like that for the Marko-Siggia force law using the high-force criterion for the effective length, while the new force law does not need to use an effective persistence length. Previously we saw that even using the high-force criterion and the Marko-Siggia force law, the response deviated at high discretization because the longest relaxation time (used to convert from Pe to Wi) did not correctly compensate for the ν in the expansion. Using the idea of a modified Rouse relaxation time, we can understand that essentially the relaxation time deviated because the size of the spring at equilibrium $\langle r^2 \rangle$ was incorrect. However the new spring has by construction the correct equilibrium $\langle r^2 \rangle$. To within the accuracy of the modified Rouse relaxation time, the longest relaxation time will be correctly modeled even at high discretization.

The other advantage of the new spring force law is the order Pe^{-1} term. Recall that in developing the spring force law the constant G in equation (4.65) was set to -7 which was necessary for the f^{-1} term in the force extension behavior near large force to vanish (which it does for very long worm-like chains). While the choice of $G = -7$ does not make the Pe^{-1} term vanish here in the elongational viscosity, the coefficient is made $\mathcal{O}(1)$ instead of $\mathcal{O}(N)$ which is a significant reduction when N is large. Recall that N must be large to even be in the plateau region of discretization. We postulate that the true continuous worm-like chain would not have a Pe^{-1} term just as it did not have a f^{-1} term in the force extension behavior. Thus even at the next order in the expansion having the correct force-extension behavior corresponds to having the correct behavior in elongational flow.

In this subsection we have analyzed the behavior of bead-spring chains in uniaxial elongational flow at large strain rates. After verifying the applicability of the expansion for large strain rates, we could use the expansion to better understand the physical origin of the chain response. We found that if the strain rate is large enough, the chain is essentially fully-extended and so the elongational viscosity is the fully-extended value virtually independent of the accuracy of the spring force law. However, the "deficit", or how close the system is to that plateau, does depend on the accuracy of the spring force law. In fact the accuracy of this deficit is even more subtle to understand than the weak flow response. The response certainly depends on the behavior of the spring near full extension which is shown by the expansion of the viscosity in terms of Pe. However, it is conventional to express the expansion in terms of a Weissenberg number, which uses the longest relaxation time. This longest relaxation time depends on the equilibrium response of the spring, not the response near full extension. To get the correct behavior for the deficit a model should get both behaviors correct, at large forces and at equilibrium. For the Marko-Siggia spring force law, neither the low-force nor the high-force criteria capture correctly the response at both extremes. For this reason the deficit is incorrect if very small springs are used. However our new spring force law does get the behavior correct at low force and high force, and thus represents the deficit correctly even to high discretization provided the number of beads is large enough.

6.2.2 *Models of the freely jointed chain*

We now examine the behavior of bead-spring chains which are coarse-grained versions of the freely jointed chain. The freely jointed chain is the other micromechanical model which is often coarse-grained into bead-spring chains. This will allow us to examine further the dependence on both the low and high force response of the bead-spring chain. Furthermore we can explicitly judge the accuracy of the coarse-grained model because we have an expression for the response of the freely jointed chain which is being modeled by the bead-spring chain.

The first bead-spring chain system used to describe the behavior of the freely jointed chain that we examine is with the FENE spring force law. For the FENE force law, the expansion of the elongational viscosity in terms of Pe is

$$\frac{\bar{\eta} - 3\eta_s}{n_p \zeta \ell^2} \sim \frac{N(N^2-1)}{12} - \frac{1}{\mathrm{Pe}}\left[(\frac{\nu}{\lambda} + 4)(N-1) - 3C_N\right] + \mathcal{O}\left(\frac{1}{\mathrm{Pe}^2}\right) . \tag{6.29}$$

Recall that for the FENE force law we have chosen to define A_{true} as one-third of the Kuhn length such that $\nu = \ell / A_{\text{true}}$ is three times the number of Kuhn lengths represented by a spring. While this choice will affect the look of the equation written in terms of ν, the physical meaning is unchanged. We now rearrange and include an approximate form for the longest relaxation time to obtain

$$\begin{aligned} \frac{\bar{\eta} - 3\eta_s}{n_p (N\zeta) L^2/12} &\approx \frac{N+1}{N-1} - \\ \frac{12}{N(N-1)2\sin^2(\pi/(2N))\mathrm{Wi}} &\frac{1}{4\nu/\lambda + 1.05\sqrt{\nu/\lambda} + 21.1}\left[\frac{\nu}{\lambda} + 4 - \frac{3}{N-1}C_N\right] + \mathcal{O}\left(\frac{1}{\mathrm{Wi}^2}\right) . \end{aligned} \tag{6.30}$$

We can now analyze how this expansion (the response of the chain) changes as the number of beads is changed while the Weissenberg number Wi is held constant, and $\alpha = (N-1)\nu$ is held constant. When analyzing the behavior we must decide which criterion for choosing λ will be used. We will start by choosing $\lambda = 1$. Note though that this does not correspond to either the high-force or low-force criterion.

Figure 6.8 shows plots of equation (6.30) as a function of N for constant Wi and α for $\lambda = 1$, i.e. not using an effective persistence length. We see similar shapes as with the previous bead-spring chains discussed. If $1 \ll N \ll \alpha$ we see a plateau which occurs at a viscosity of

$$1 - \frac{6}{\pi^2 \mathrm{Wi}} + \mathcal{O}\left(\frac{1}{\mathrm{Wi}^2}\right) . \tag{6.31}$$

For all chains with a finite α, the number of beads will eventually become large enough that the springs represents very small segments of polymer. The system then approaches the limiting behavior of the bead-string chain when $1 \ll N$ and $\alpha \ll N$ which is

$$1 - \frac{0.46}{\mathrm{Wi}} + \mathcal{O}\left(\frac{1}{\mathrm{Wi}^2}\right) . \tag{6.32}$$

Again we see a similar behavior as with the worm-like chain in that the difference in responses between the long chain plateau and the bead-string chain decreases with Wi, as Wi^{-1}. This means that some properties are less sensitive to the incorrect and changing accuracy of the spring force

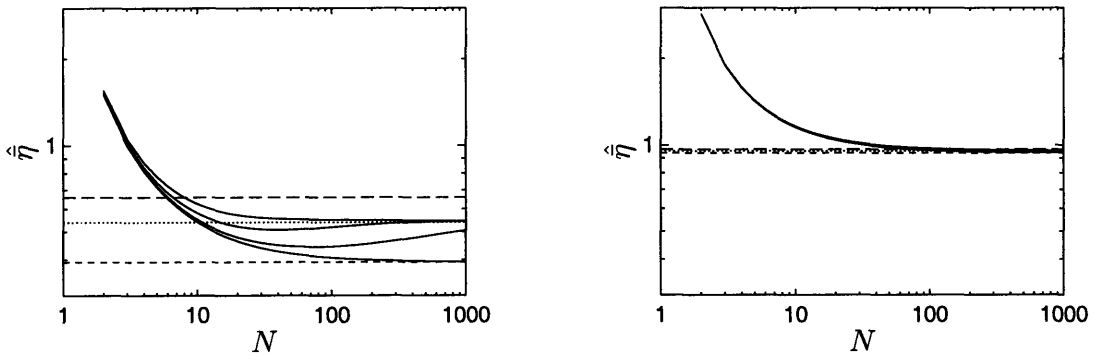

Fig. 6.8: *Calculation of the elongational viscosity as a function of the number of beads for constant* Wi *and* α *using the first two terms in the asymptotic expansion for the FENE force law with* $\lambda = 1$ *(equation* (6.30)*). The values of* Wi *are 1 (left) and 10 (right). The lines correspond to different values of* α*, from top to bottom ranging from 100, 400, 4000, and* ∞*. The dashed line is* $1-6/(\pi^2\text{Wi})$ *(equation* (6.31)*). The dotted line is* $1-0.46/\text{Wi}$ *(equation* (6.32)*). The long-dashed line is* $1 - 0.34/\text{Wi}$ *(from equation* (6.36)*).*

law.

Recall that for the FENE force law, even the high-force criterion is not $\lambda = 1$. We show in Figure 6.9 the response of the elongational viscosity for the high-force and the low-force criteria. As for the Marko-Siggia spring force law, we see that the high-force criterion performs slightly better (stays in the plateau longer) than the low-force criterion, although the difference is almost not distinguishable. However, there is the counter-intuitive result that using $\lambda = 1$ seems to do even better than either criteria. This can be understood by looking at the expansion in equation (6.30). The coefficient to Wi^{-1} only depends on the ratio ν/λ. Therefore, the smaller the value of λ, the larger the ratio ν/λ, and the closer the term is to the long chain limit behavior. In essence, a smaller λ makes it look like there are more effective Kuhn lengths per spring so the chain looks like a chain with a very large number of Kuhn lengths. This arbitrary change of the Kuhn length does not cause a detrimental response in the strong stretching limit because the long chain behavior does not explicitly depend on the true Kuhn length, only on the total drag on the chain, the contour length squared, and the Weissenberg number. So although arbitrarily choosing λ very small does increase the size of the plateau, we do not consider that a viable option for developing an accurate coarse-grained model because the change in effective persistence length would cause all equilibrium properties to be incorrect. Actually the same type of effect could have been seen with the Marko-Siggia force law if λ had been chosen smaller than one.

To this point we have presumed that the existence of the plateau in the viscosity means that the chain is an accurate coarse-grained model. For the Marko-Siggia and FENE force laws this plateau essentially exists when the chain has many beads but each spring still represents a large segment of polymer. We have shown that even if the incorrect spring force law is used when each spring represents a small segment of polymer, for sufficiently high Wi the response in elongational

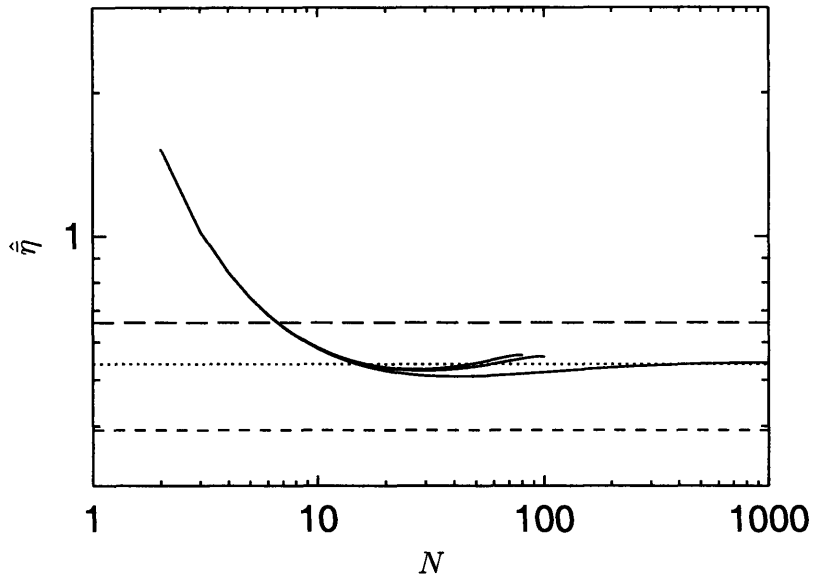

Fig. 6.9: *Comparison of the different criteria for λ and their effect on the elongational viscosity for the FENE force law. The parameters are* Wi $= 1$, $\alpha = 400$, *and either the low-force (upper line) or high-force criteria (middle line) for λ or $\lambda = 1$ (lower line). The $\lambda = 1$ case and the dashed, dotted, and long-dashed lines are identical to in Figure 6.8.*

viscosity does not actually deviate a significant percentage from the plateau because the chain is always virtually fully extended. However, the existence of this plateau does not in of itself guarantee that the bead-spring represents the desired micromechanical model. For the FENE chain, we can easily see how well this plateau matches the behavior of the freely jointed chain because the behavior of the freely jointed chain in elongational flow is known [81]. The expansion of the elongational viscosity of a freely jointed chain for large strain rates is

$$\frac{\bar{\eta} - 3\eta_s}{n_p \zeta a^2} \sim \frac{N(N^2-1)}{12} - \frac{k_B T}{\zeta a^2 \dot{\epsilon}} [2(N-1) - 3C_N] + \mathcal{O}\left(\frac{1}{\dot{\epsilon}^2}\right) , \tag{6.33}$$

where a is the length of a rod and the sum over the Kramers matrix which was tabulated by Hassager can be written equivalently as a simpler sum, C_N. Currently we are concerned with the limit of a large number of rods because we want to compare this series expansion with the plateau occurring for a FENE chain with a large number of springs and where each spring still represents a large number of Kuhn lengths. In the limit of a large number of rods, the elongational viscosity of a freely jointed chain becomes

$$\frac{\bar{\eta} - 3\eta_s}{n_p (N\zeta) L^2/12} \sim 1 - \frac{24}{\mathrm{Wi}} \frac{k_B T \tau}{N^2 \zeta a^2} + \mathcal{O}\left(\frac{1}{\mathrm{Wi}^2}\right) . \tag{6.34}$$

From ref. [30] we know that the relaxation time of long freely-jointed chains is approximately

$$\tau \approx 0.0142 N^2 \frac{\zeta a^2}{k_B T} , \tag{6.35}$$

so the viscosity is

$$\frac{\bar{\eta} - 3\eta_s}{n_p (N\zeta) L^2/12} \approx 1 - \frac{0.34}{\mathrm{Wi}} + \mathcal{O}\left(\frac{1}{\mathrm{Wi}^2}\right) . \tag{6.36}$$

We expect that equation (6.31) would be the same as this freely jointed chain result, equation (6.36), however we see that they are not the same. Recall that the FENE force law does not have the exact same behavior as the inverse Langevin function near full extension. This will account for some of the difference, which we will now address.

We will next examine the behavior of the Cohen spring force law. Because the Cohen spring force law does have the same approach to full extension as the inverse Langevin function but different from the FENE force law, we will be able to see the influence of this divergence. Note that because the first two terms in the flow expansion (in terms of Pe) only depends on the dominant behavior of the spring near full extension, the Cohen force law has the same two term expansion as a bead-spring chain with the inverse Langevin function as the spring force law. Obviously higher order terms in the expansion will be different between the Cohen force law and the inverse Langevin function. The equilibrium behavior (and relaxation time) will also be different at intermediate ν. At infinite ν it only depends on the linear region of the force law which is the same, and at zero ν they both become the bead-string chain which are the same. The first two terms in the high strain rate expansion are

$$\frac{\bar{\eta} - 3\eta_s}{n_p \zeta \ell^2} \sim \frac{N(N^2-1)}{12} - \frac{1}{\mathrm{Pe}} \left[\left(\frac{2\nu}{3\lambda} + 4\right)(N-1) - 3C_N \right] + \mathcal{O}\left(\frac{1}{\mathrm{Pe}^2}\right) . \tag{6.37}$$

In the limit of $1 \ll N \ll \alpha$, the expansion becomes

$$\frac{\bar{\eta} - 3\eta_s}{n_p (N\zeta) L^2/12} \sim 1 - \frac{4}{\pi^2 \mathrm{Wi}} + \mathcal{O}\left(\frac{1}{\mathrm{Wi}^2}\right) , \tag{6.38}$$

where we have used our knowledge of the relaxation time of the bead-spring chain when ν is very large. We can also look in the limit of such large N that each spring represents a very small amount of polymer, $1 \ll N$ and $\alpha \ll N$. In this limit the chain looks like a bead-string chain, which is the same result as for the FENE chain. In this limit the expansion is approximately

$$\frac{\bar{\eta} - 3\eta_s}{n_p (N\zeta) L^2/12} \approx 1 - \frac{0.46}{\mathrm{Wi}} + \mathcal{O}\left(\frac{1}{\mathrm{Wi}^2}\right) . \tag{6.39}$$

Recall that the approximation here in determining the expansion for the bead-string chain is that the longest relaxation time is only known approximately.

There are two important aspects to notice about the behavior of the Cohen force law chain. The first is that the structure has changed from that of the FENE and Marko-Siggia in that equation (6.38) is now greater than equation (6.39). The other is that even this expansion (which is the expansion for the exact inverse Langevin function) deviates from the freely jointed chain result when there are a large number of springs and each spring represents a large segment of

polymer (i.e. comparing equations (6.36) and (6.38)).

This deviation, however, turns out to be related back to a subtlety with the longest relaxation time of the freely jointed chain which is not often discussed. Consider a freely jointed chain with such a large number of rods that if one models it with a bead-spring chain with the exact inverse Langevin force law, it is possible to both have a very large number of springs and at the same time have each spring represent a very large number of rods. The longest relaxation time of this bead-spring chain is given by equation (6.6) or alternatively (with $\lambda = 1$)

$$\tau = \frac{(N\zeta)La_K}{6\pi^2 k_B T} . \tag{6.40}$$

We know this relaxation time exactly because if each spring represents a very large segment of polymer, near equilibrium the spring only samples the linear region of the force law so we can use the analytic result for the relaxation time of a bead-spring chain with linear springs. Because this bead-spring chain correctly models the equilibrium and force-extension behavior of the freely jointed chain, one might think that it would model the longest relaxation time of the chain. However, this is not true. The longest relaxation time is given in equation (6.35) or equivalently

$$\tau = \frac{0.0142(N\zeta)La_K}{k_B T} . \tag{6.41}$$

It is this difference in relaxation times that causes the difference between the viscosity expansion of the freely jointed chain and the Cohen or inverse Langevin chain even when the bead-spring chain has a large number of springs and each spring represents a large segment of polymer. We can see this by using equation (6.40) in the expansion of the freely jointed chain, equation (6.34), instead of the exact formula, which is then identical to the Cohen chain expansion, equation (6.38). We can also see that it is the relaxation time that causes this final discrepancy by noticing that both the freely jointed chain and Cohen chain can be written in these limits as

$$\frac{\bar{\eta} - 3\eta_s}{n_p} \sim \frac{(N\zeta)L^2}{12} - \frac{k_B T}{\dot{\epsilon}} [2 \times (\text{number of Kuhn lengths in whole molecule})] + \mathcal{O}\left(\frac{1}{\dot{\epsilon}^2}\right) . \tag{6.42}$$

It is only when the extension rate is written in terms of a Weissenberg number using different longest relaxation times that gives this final discrepancy.

It should be noted that it is not only from ref. [30] that we know the longest relaxation time of a freely jointed chain. Other researchers [82, 83, 84] have performed similar simulations verifying the same result as well as independent tests of the relaxation time. This is also not the first mentioning of this discrepancy [83, 84]. The 20% deviation in the longest relaxation time is an unresolved issue and is outside the scope of this thesis. For the purposes of this thesis we can not do better than reproducing the expansion in equation (6.42), which depends on the behavior near full extension, and to capture the longest relaxation time if each spring represents a large segment of polymer. Thus this plateau (equation (6.38)) is considered "accurate" for our purposes. However, even the Cohen force law or the inverse Langevin force law will deviate from this as each spring represents a small segment of polymer, and the chain approaches the bead-string chain.

A new spring force law has been developed such that the bead-spring chain accurately represents the force-extension behavior of the freely jointed chain (equation (4.43)) [77]. We can examine how using this new force law affects the elongational viscosity at large strain rates. The expansion of

the viscosity for this force law is

$$\frac{\bar{\eta} - 3\eta_s}{n_p \zeta \ell^2} \sim \frac{N(N^2-1)}{12} - \frac{1}{\mathrm{Pe}}\left[\frac{2\nu}{3}(N-1) - 3C_N\right] + \mathcal{O}\left(\frac{1}{\mathrm{Pe}^2}\right) . \tag{6.43}$$

This expansion should be compared with the expansion for the Cohen force law or inverse Langevin force law (equation (6.37)). We see that because the new force law correctly represents the behavior at large forces, the expansion in viscosity in terms of Pe is modeled correctly (like when using the high-force criterion for an effective persistence length). The term $2\nu(N-1)/3$ is always equal to two times the total number of Kuhn lengths represented by the chain independent of how few Kuhn lengths each spring represents, just as we saw in equation (6.42). However the equilibrium behavior is also captured correctly with the new force law. This means that the longest relaxation time will also be captured essentially. Because both are captured correctly, the system will not deviate at high discretization from the plateau.

It is useful to review at this point the main features we have observed through the analysis of the elongational viscosity at large strain rates. At very large strain rates the chain is virtually fully-extended, so as long a the spring has the correct fully-extended length ℓ, this infinite strain rate viscosity is independent of the details of the spring force law. In this sense the behavior at large enough strain rate is insensitive to the details of the spring force law. However some experiments may aim to explore more than the absolute value of viscosity (or similarly fractional extension). For example, ref. [58] used the deficit (difference between the fractional extension from full extension) to distinguish between the worm-like chain, freely jointed chain, and stem-flower models. Shaqfeh et al. [76] and Doyle et al. [85] examined the relaxation after strong elongational flow and found that the relaxation was highly influenced by the deficit away from the fully extended state. For a bead-spring chain to accurately represent these types of response of a micromechanical model, it is necessary to capture not only the plateau but also the approach to the plateau. This approach *is* sensitive to the accuracy of the spring force law. In fact it is dependent on the force law both near full extension and at equilibrium because of using the longest relaxation time to form a Weissenberg number. For this reason previously used spring force laws do not capture this deficit when each spring represents a small segment of polymer. However, the new spring force laws developed to represent the worm-like chain and freely jointed chain do not deviate at high discretization.

6.3 Influence of Hydrodynamic Interactions

In this chapter we have focused on the role of the spring force law and have not included effects of hydrodynamic interactions. In highly extended states we expect the effect will be much less than in the coiled stated, and the spring force law will play the major role. For the Marko-Siggia force law, we found that the elongational viscosity has a series expansion of the form

$$\frac{\bar{\eta} - 3\eta_s}{n_p \zeta \ell^2} \sim \frac{N(N^2-1)}{12}\left(1 - \frac{C}{\mathrm{Pe}^{1/2}} + \mathcal{O}\left(\frac{1}{\mathrm{Pe}}\right)\right) . \tag{6.44}$$

Certainly the plateau value will be dependent on hydrodynamic interactions, which changes the scaling with length to include a logarithm. However, we postulate the coefficient C may have the same scaling with or without hydrodynamic interactions. This is because the chain is so close to full extension that the positions of the beads, and therefore their interactions, will not be much

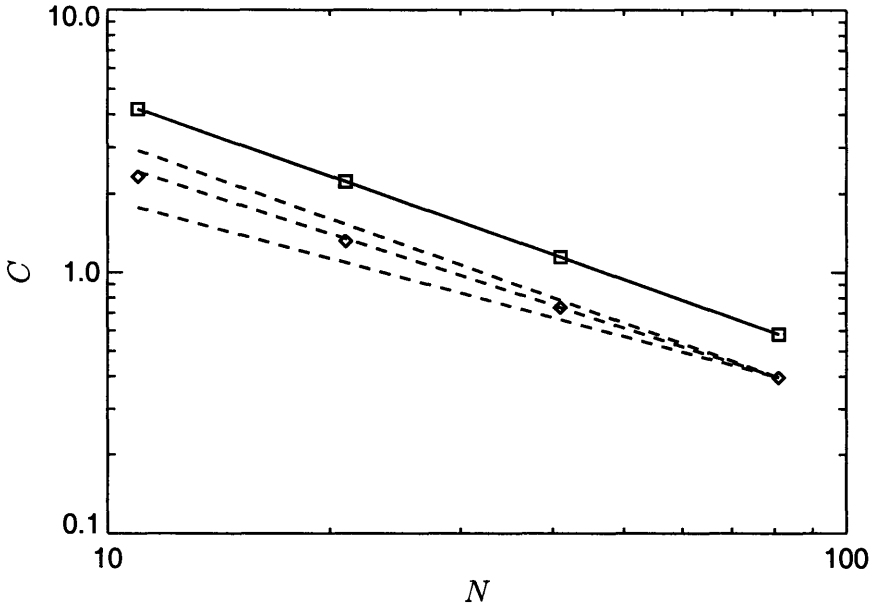

Fig. 6.10: *Coefficient of the* $\mathrm{Pe}^{-1/2}$ *term,* C*, as a function of the number of beads with and without HI. The spring force law is Marko-Siggia with* $\nu = 200$ *and* $\lambda = 1$*. The squares are without HI and the diamonds are from BD simulations using the RPY tensor and* $h^* = 0.25$*. The dashed lines represent power laws of* N^{-1}*,* $N^{-0.9}$*, and* $N^{-0.75}$*.*

different from in the fully extended state. The postulated form is thus

$$\bar{\eta} - 3\eta_s \sim (\bar{\eta} - 3\eta_s)_\infty \left(1 - \frac{C}{\mathrm{Pe}^{1/2}} + \mathcal{O}\left(\frac{1}{\mathrm{Pe}}\right)\right) . \tag{6.45}$$

Whether the scaling of C is the same with and without hydrodynamic interactions has interesting consequences. Without hydrodynamic interactions the scaling is $C \sim N^{-1}$. This is consistent with turning the Peclet number into a Weissenberg number, because without HI the longest relaxation time scales as N^2. However, in the non-draining limit, the longest relaxation time scales as $N^{3/2}$. Turning the expansion Pe to Wi using a non-draining scaling for the longest relaxation time gives a coefficient of

$$\frac{CN^{3/4}}{\mathrm{Wi}^{1/2}} . \tag{6.46}$$

If the value of C scales as N^{-1}, this implies a vanishing coefficient to $\mathrm{Wi}^{-1/2}$ as $N \to \infty$.

To test this hypothesis, we performed simulations in collaboration with Chih-Chen Hsieh using the Marko-Siggia force law and the RPY hydrodynamic interaction tensor, with parameters $\nu = 200$, $\lambda = 1$, and $h^* = 0.25$ [86]. We performed simulations at a range of Pe until we were confident that higher order terms in Pe were negligible and extracted a value of C from the simulation data. The

infinite Pe number response was calculated exactly using the formalism presented in an appendix to ref. [87]. In Figure 6.10 we plot the value of C calculated from the simulations versus N. From the figure we can see clearly that the the scaling is not $N^{-3/4}$. The fitted scaling is approximately $N^{-0.90}$ for the largest N simulated here.

These simulations bring about an interesting point which warrants further investigation. If the scaling of C with N in the large chain limit is different than $N^{-3/4}$ as we see here, that means that near the fully extended state the time used to convert from Pe in order to have collapse of the data in the long chain limit is not the longest relaxation time. However, it may be necessary to reach the non-draining limit in the extended state in order to reach the long chain limit scaling of the coefficient. By non-draining limit in the extended state, we mean that the plateau viscosity scales as would be expected from Batchelor's formula. We can estimate the number of beads necessary to be in that limit using an approximate formula in the appendix of ref. [87]. Because of the slow logarithm convergence in the number of beads, with the parameters used here, the number of beads would have to be greater than 10^6 to be into the non-draining limit in the extended state. This is not feasible to simulate. A better route to reach the non-draining limit would be make each spring represent a smaller segment of polymer. However, care should be taken to make sure the correct h^* is used relative to the size of a spring.

6.4 Summary and Outlook

In this chapter we have looked at the behavior of bead-spring chain models in strong flows and the effect of the spring force law. We did this for coarse-grained models of both the WLC and FJC. We expect that EV effects are small in such strong flows and the effects of HI may be small (or smaller) so we initially neglect those contributions. The longest relaxation time was examined, which is used to express the strain rate as a Weissenberg number. It was shown that the chain samples the nonlinear regions of the force law even at equilibrium, making the relaxation time deviate from the Rouse result. However, a modified Rouse model is able to capture the relaxation time even if each spring represents a small segment of polymer. This modified Rouse model gives insight into the important role the force-extension behavior at small force plays in determining the longest relaxation time.

We looked at the elongational viscosity in the limit of large strain rates and used the first few terms in the expansion to understand how the response of the chain changes as the level of discretization changes for different spring force laws. We saw that for arbitrarily large strain rate the viscosity becomes insensitive to using the correct spring force law because the system is always fully-extended. However, it is often important to model correctly how close the chain is to fully-extended. To get this correct it is even more sensitive than in weak flows/equilibrium. In a highly extended state the expansion depends on the large force behavior, but also when writing the response in terms of a Wi with the longest relaxation time, it is influenced by the low force/equilibrium behavior. To get the correct response both must be modeled correctly. Using the previous force laws with an effective persistence length requires a trade-off in which only one is correct but not both. Our new force laws get both correct, so do not produce error when each spring represents a small segment of polymer.

CHAPTER 7

Nonhomogeneous Flow

In this chapter we will consider an example of a flow which has a nonhomogeneous strain rate over the size of the molecule. Many of the flows which have been considered previously are homogeneous in that the strain rate is the same everywhere in space, such as uniform shear or elongational flow. Even in a macroscopic complex geometry, at the scale of a single polymer molecule, the strain rate is homogeneous in space, although the flow can change in time in a Langrangian sense. This is a result of the difference in scales between the size of the device and the size of a polymer molecule. However, a number of microfluidic devices involving biological polymers such as double-stranded DNA produce nonhomogeneous strain rates over the scale of a polymer molecule. Examples of this type of flow include DNA separation devices using post arrays or entropic traps and DNA stretching devices for genome mapping. A number of studies have been performed of polymers in nonhomogeneous flows. For example, Szeri et al. [88] examined deformable bodies in two-dimensionless nonhomogeneous flows to understand the strong flow criterion. A number of different groups have performed Brownian dynamics simulations of polymers using an imposed, known flow field which is nonhomogeneous, and the dynamics and stretching of the polymer have been examined [89, 90, 91]. Randall et al. [92] have recently examined experimentally the stretching of DNA using nonhomogeneous fields generated using micro-contractions or the motion of DNA from a gel into aqueous solution.

In this chapter we consider a simplified geometry which contains the required physics of a nonhomogeneous strain rate over the scale of the molecule, a step increase in the electrophoretic

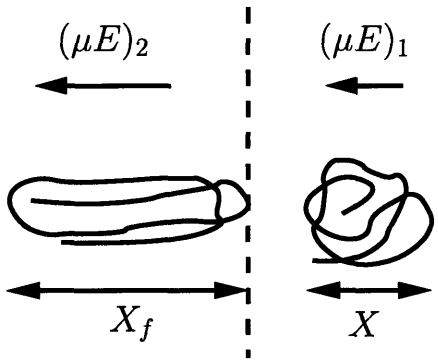

Fig. 7.1: *The polymer is moving from right to left, initially with electrophoretic velocity* $(\mu E)_1$. *The maximum extent in the* x *direction is denoted by* X. *The chain crosses the dashed line into a region with electrophoretic velocity* $(\mu E)_2 > (\mu E)_1$. *The maximum extent of the polymer when the rear crosses the dashed line is defined as* X_f.

velocity. This geometry is shown in Figure 7.1. The problem which most resembles this geometry is the exit of a DNA molecule from a gel (region 1) to aqueous solution (region 2) [92]. Our simplified geometry does not contain any structure in region 1 to describe details of the gel. The gel would simply act as a method of changing the electrophoretic velocity. The geometry could also represent the change of field that occurs in sharp constrictions such as entropic traps and hyperbolic contractions, although those geometries have additional steric hindrance not included here.

Our analysis will show that in a limiting case this geometry reduces to a tethered chain in a uniform flow, a problem which has received significant attention. Brochard-Wyart and co-workers [93, 94] have used a blob theory to examine the stretching and unwinding of tethered polymers. The validity of the blob theory has been investigated using Brownian dynamics simulations by Zimmerman and co-workers [95]. Brownian dynamics simulations have also been used to investigate the validity of a dumbbell model for a tethered chain [32] and to examine the dynamics of tethered chains in shear flow [58].

We will first examine a toy model consisting of a single Hookean dumbbell neglecting Brownian motion to derive the two dimensionless groups governing the response. A similar type of toy model can be used to understand the coil-stretch transition in elongational flow as reviewed by [96]. We will then show with Brownian dynamic simulations that the Hookean chains in the long chain limit converge to a result which has the same scaling as the toy model. We then show the effect that finitely extensible springs has on the result.

7.1 Dumbbell Model

Here we will discuss a toy model which considers a single Hookean spring without Brownian motion. The system is sketched in Figure 7.1. The polymer is moving in region 1 with an electrophoretic velocity $(\mu E)_1$ and crosses into a region with electrophoretic velocity $(\mu E)_2$. For this discussion we

consider $(\mu E)_2 > (\mu E)_1$, which causes the polymer to stretch in the x direction. The stretch when the last segment of polymer crosses from region 1 to 2 is defined as X_f. By using this toy model we can understand how this stretch scales with the properties of the chain and strength of the two velocities. In this way we can understand the physical mechanism involved in stretching.

In addition to having a change of electrophoretic velocity across the boundary, it is possible to have a change in the drag coefficient on a bead across the boundary. From looking at the response of a single Hookean spring without Brownian motion, the response can be shown to depend on the averaged drag coefficient

$$\frac{1}{\zeta^*} = \frac{1}{2}\left(\frac{1}{\zeta_1} + \frac{1}{\zeta_2}\right) , \tag{7.1}$$

where ζ_1 and ζ_2 are the drag coefficients on a bead in regions 1 and 2 respectively. The toy model shows that when the coil is crossing the interface, the chain sees a difference in velocity of $(\mu E)_2 - (\mu E)_1$ over the length of the size of the coil. This gives an effective strain rate which can be used to calculate a Weissenberg number. We define a Weissenberg number for this situation as

$$\mathrm{Wi} = \frac{\delta_{\mu E} 2\tau}{\sqrt{\langle R^2 \rangle_{eq}/3}} , \tag{7.2}$$

where $\delta_{\mu E} = (\mu E)_2 - (\mu E)_1$, τ is the longest relaxation time of the chain if each bead had drag coefficient ζ^*, and $\langle R^2 \rangle_{eq}$ is the equilibrium averaged end-to-end distance squared of the chain. This is not like a typical elongational flow, though, for two reasons. First, as the chain extends, the same difference in velocities is seen by the chain over a larger distance, resulting in a decreasing effective strain rate as the chain stretches. This continues until the stretching provided by the change in velocity exactly cancels the spring force trying to resist stretching. Second, the chain only has a finite residence time across the step change. Once the rear of the chain passes over the step change in electrophoretic velocity, the chain relaxes back to the equilibrium state. The finite residence time is due both to the fact that the front of the molecule is pulling the back across the interface and to the fact that the back is being convected across the interface. Thus the velocity in region 1 also plays a role, which comes in through a Deborah number which we define as

$$\mathrm{De} = \frac{(\mu E)_1 4\tau}{\sqrt{\langle R^2 \rangle_{eq}/3}} . \tag{7.3}$$

This is like a Deborah number because the residence time to cross the interface is typically of order $\sqrt{\langle R^2 \rangle_{eq}/3}/(\mu E)_1$ because Brownian motion has been neglected in the toy model. Because this convective time scale introduces another flow time scale which can be compared to the relaxation time, separate from the inverse strain rate, we can define a Deborah number in addition to the Weissenberg number, which is always taken to be the product of the strain rate and the relaxation time [15, 96]. The factors of 2 and 4 in the definitions of Wi and De respectively are a result of the toy model analysis. These factors make order 1 values of Wi and De correspond to approximate transitions between behaviors.

In the rest of this chapter we will consider the case in which $E_1 = E_2$. The difference in electrophoretic velocity comes about because of a difference in mobility. We use the leading order assumption that $\mu \propto 1/\zeta$ [97]. This is the case if region 1 contains a gel which reduces the mobility, or effective viscosity. We can characterize the response of this model by examining the amount of

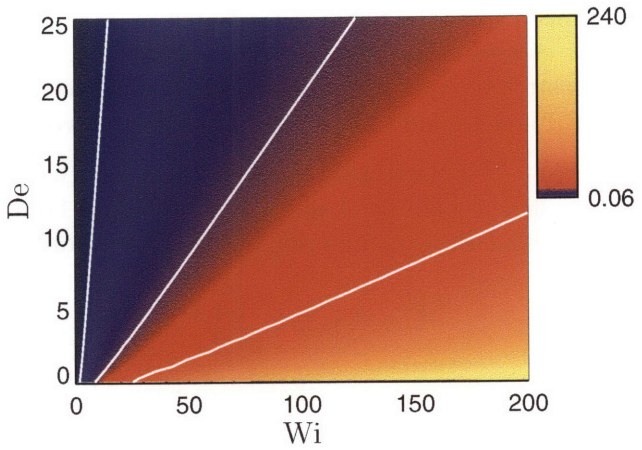

Fig. 7.2: *Contours of constant* $\langle X_f \rangle / \langle X \rangle_{eq}$ *for the toy model as a function of the two parameters* De *and* Wi. *From left to right, the lines represent constant* $\langle X_f \rangle / \langle X \rangle_{eq}$ *of 2, 10, and 30.*

stretching relative to equilibrium $\langle X_f \rangle / \langle X \rangle_{eq}$ as a function of Wi and De, as shown in Figure 7.2. The details of the calculation of the response of the toy model are shown in Appendix A.5.

The first key observation is the absence of a coil-stretch transition. Near a value of Wi = 1 the toy model predicts no stretching beyond equilibrium because at this point the stretching is balanced by the spring force. Therefore, we see that below a value of about Wi = 1 there is only minimal stretching. At larger Wi the stretch increases approximately linearly. The slope of this increase is determined by De.

The affine limit is reached as the De becomes very large. In this region, the back part of the chain is simply convected to the interface. The final stretch is the distance the front of the chain travels in the time it takes for the back part to reach the interface. In this limit the toy model gives

$$\frac{\langle X_f \rangle}{\langle X \rangle_{eq}} \sim 1 + \frac{2\mathrm{Wi}}{\mathrm{De}} \, . \tag{7.4}$$

The key observation in this region is that the stretch is only a function of the ratio Wi/De. Therefore, the details of the polymer in terms of the coil size and relaxation time and the applied electric field are irrelevant in determining the relative stretch from the equilibrium state. In this region the stretch is simply a function of the ratio μ_2/μ_1.

In the limit of very small De, the response approaches that of a tethered chain. In this region the toy model gives

$$\frac{\langle X_f \rangle}{\langle X \rangle_{eq}} \propto \mathrm{Wi} \, . \tag{7.5}$$

The mobility in region 1 is small enough that the chain in region 2 reaches a "steady" or balanced configuration in which the stretching due to the velocity difference is balanced by the spring force before the rear of the polymer crosses the interface. Note that in this limit the Wi could also be

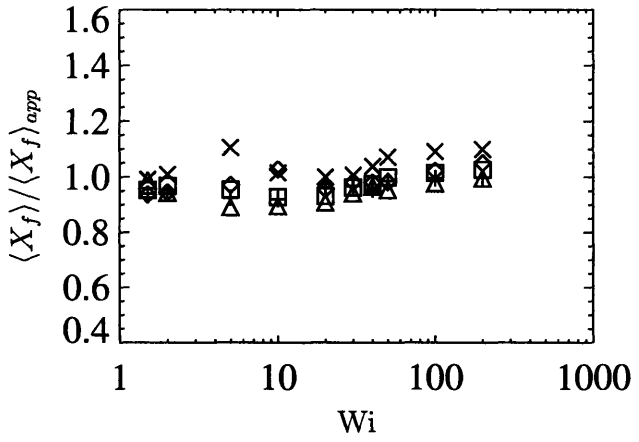

Fig. 7.3: *This shows a comparison of Brownian dynamics simulations in the long chain limit to the toy model. We show the the result of the simulations divided by the approximation in equation* (7.6). *The symbols represent values of* De*: 0.5 (×), 1.0 (squares), 2.0 (triangles), 5.0 (+), and 10.0 (diamonds).*

thought of as the Peclet number in the two regions because De $\to$ 0. For example, in this limit the average drag $\zeta^* \to 2\zeta_2$, and the relaxation time could be related to a diffusivity using scaling relations [98].

7.2 Long Chain Limit

To verify that these scaling ideas hold even for polymer chains, with the additional complexity of back-folds and kinks, we performed Brownian dynamics simulations of bead-spring chains with Hookean springs. The details of the Brownian dynamics method have been presented in Section 2.2 and in the literature [46]. The change in drag coefficient, and therefore diffusivity, across the step change must be correctly included. We used the midpoint algorithm of Grassia et al. [47] which is able to account for this change.

Chains were simulated for increasing number of beads, and it was found that for $N \geq 40$ the results collapsed onto a single curve, and thus are in the long chain limit. These chains in the long chain limit were observed to have the same scaling with De and Wi as the toy model. This illustrates the validity of the two dimensionless groups and the regions in phase space discussed previously. It is not surprising that there is not quantitative agreement between the toy model and the chains which can form kinks and hairpins. Over a range of parameters it was found that a simple formula can relate the response of the long chains and the toy model. This approximation is defined by the equation

$$\frac{\langle X_f \rangle_{app}}{\langle X \rangle_{eq}} \sim 1 + 0.6 \left(\frac{\langle X_f \rangle_{toy}}{\langle X \rangle_{eq}} - 1 \right) . \tag{7.6}$$

In Figure 7.3 we show the ratio of the simulated stretch of the bead-spring chains with $N = 40$ to this approximate formula versus Wi. We see that other than at very small De, this simple

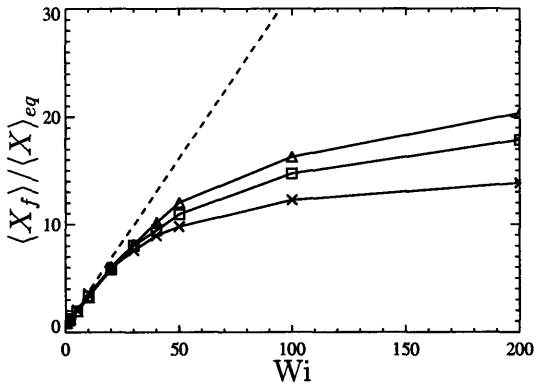

Fig. 7.4: *Results from simulations with increasing finite extensibility. The Deborah number is* De = 2.0. *The dashed line represents the approximation for Hookean chains in the long chain limit (equation* (4.72)*). The symbols represent simulations for* λ *(triangles),* 2λ *(squares), and* 3λ *(*$\times$*).*

approximation works quite well. This pre-factor of 0.6 and the slight change at small De are probably due to the tendency of chains to form hairpins which tend to reduce the extension relative to that seen with a dumbbell model.

7.3 Finite Extensibility

To this point we have only considered Hookean springs which can be infinitely extended. Real polymers however have a finite length. As the chain is extended to a significant fraction of that fully extended length, the spring force increases nonlinearly, ultimately diverging to prevent the chain from extending past the contour length. Typically this nonlinear increase in force begins when the extension is approximately one-third of the contour length. We expect that if the stretch experienced crossing the step change $\langle X_f \rangle$ is less than about one-third of the contour length, the finite extensibility does not influence the result. The stretch will be the same as with Hookean chains.

We performed a series of simulations of bead-spring chains with nonlinear springs, with some characteristic data shown in Figure 7.4. The spring force law was developed previously in Chapter 4 and in ref. [80] to model a worm-like chain polymer. The spring force law is given in equation (4.72).

A common molecule used in single molecule video fluorescence microscopy experiments is λ-phage DNA which contains about 400 persistence lengths when stained with a fluorescent dye [67]. It is also common to examine concatemers which are twice and three times as long, which we call 2λ and 3λ. The result of simulations of these three molecules are shown in Figure 7.4. The chains contain 20, 39, and 58 beads respectively so that the number of persistence lengths per spring is the same. The dashed line is the approximation to a long chain of Hookean springs (equation (7.6)). For the nonlinear bead-spring chains with a large number of beads, we expect that at small extensions the simulations follow the Hookean chain result. As the extension grows, it eventually reaches a

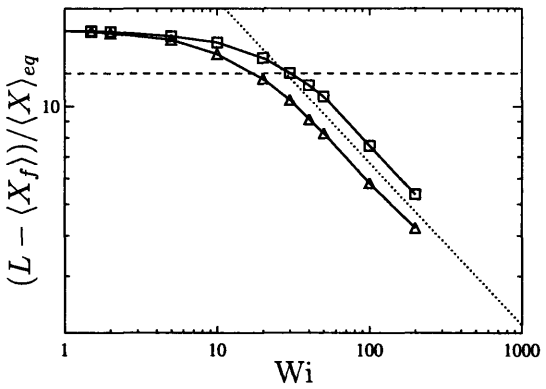

Fig. 7.5: *Approach of the nonlinear bead-spring chains to full extension. The chain contains 20 beads and 400 persistence lengths in the whole chain. The data corresponds to* De *of 2 (triangles) and 5 (squares). The dotted line is a power law of* $\mathrm{Wi}^{-1/2}$. *The dashed line represents a value of* $\langle X_f \rangle = 0.3L$.

fraction of the contour length. At this point the nonlinearity in the spring makes the extension less than that predicted from the Hookean model which was valid at small extensions. The finite extensibility for longer contour length chains does not influence the result until larger Wi as seen in Figure 7.4.

At large enough Wi the extension will approach the contour length of the polymer, L. A characteristic of the worm-like chain in elongational flow is that the approach to full extension follows the power law $\mathrm{Wi}^{-1/2}$. This is distinguished from the approach for the freely jointed chain which follows Wi^{-1}. This same power law has also been observed for the stretching of tethered DNA in uniform flow, which can be generated either by hydrodynamic or electrophoretic forces [18, 99, 100]. For a tethered worm-like chain in shear flow [101], it has been shown that the approach to full extension follows the power law $\mathrm{Wi}^{-1/3}$ [58]. In Figure 7.5 we show the approach to full extension for the case of λ DNA modeled with 20 beads. We see that for both De = 2 and De = 5 if the stretch is greater than about $0.3L$, the finite extensibility is important and the approach to full extension decays as $\mathrm{Wi}^{-1/2}$.

This influence of finite extensibility can also be understood in terms of the phase plot given in Figure 7.2. For a given molecule of interest, a line of constant stretch can be placed on the phase plot which corresponds to one-third of the contour length. In the region with stretch less than this value, a simple Hookean chain can correctly model the stretch experienced. On the other side of the line, the nonlinearity will limit the stretch to a smaller value than that predicted by a Hookean theory. For molecules of increasing contour length, this line will be pushed to higher Wi and smaller De. Thus for increasingly long polymers, more of the region of phase space will be correctly modeled using a Hookean chain.

7.4 Summary

In this chapter, we have discussed a simplified system which has a nonhomogeneous strain rate over the scale of a single polymer molecule. We used a toy model of a single Hookean spring without Brownian motion to identify a Weissenberg number and Deborah number. We showed that the stretch of Hookean chains in the long chain limit still scale with these two parameters. The change in velocity divided by the size of the molecule as the effective strain rate. The chain stretching is also a transient process, with a finite residence time experiencing the stretching force.

These two dimensionless groups formed a phase space which we examined. For $\mathrm{Wi} \lesssim 1$ the chain experiences minimal stretching. Above $\mathrm{Wi} = 1$ there is an approximate linear increase of stretch with Wi. For large De, this increase follows the affine limit scaling. For very small De, the system approaches a tethered limit, in which the chain has time to reach a "steady" balance between the velocity difference which is trying to stretch the chain and the spring force which is trying to relax the chain. If chains are stretched to greater than approximately one-third of the contour length, the finite extensibility of the chain is important. We showed a characteristic approach of $\mathrm{Wi}^{-1/2}$ to full extension for the worm-like chain.

These same dimensionless groups and this type of phase space analysis should also provide insight into other more complex flow geometries in which the flow has nonhomogeneous strain rates over the scale of a single molecule as well as transient flows. These types of flows should become even more prevalent in single molecule studies in microfluidic devices.

CHAPTER 8

Conclusions and Outlook

In this thesis, we have examined the coarse-graining of polymers into bead-spring chain models. We have focused primarily on the spring force law to understand how to systematically develop a force law even if a spring does not represent a large segment of polymer. This is particularly important to understand when trying to model the behavior of polymers and biological molecules in micro- and nano-fluidic devices.

8.1 Force-extension Behavior

In Chapter 3 we examined the force-extension behavior of bead-spring chains. This was a natural starting point because one motivation for using springs is the force-extension of polymers. It also is convenient to examine because the response can be written using equilibrium statistical mechanics. Through this analysis, we were able to identify the key parameter which governs the force-extension behavior, ν, which represents the number of flexibility lengths represented by a spring. This parameter governs the fluctuations in phase space like an inverse temperature.

These fluctuations are important to consider when ν is not very large. Previous force laws neglected these fluctuations because they were being developed to represent very large segments of polymer. Using these force laws to represent smaller segments of polymer gives an error which we quantified. To eliminate this error, Larson and coworkers used an effective flexibility length. We analyzed this method and showed that there is no unique choice for the effective flexibility

length. A simple rescaling of the flexibility length is not sufficient to counter act the neglect of the fluctuations over the whole range of forces.

8.2 New Force Laws

The understanding of the fluctuations in phase space allowed us to develop new spring force laws in Chapter 4. Because the springs do not represent an infinite amount of polymer, fluctuations must be taken into account. In particular, the ensemble (which determines the quantities that are allowed to fluctuate and the ones which are held fixed) must be specified precisely. We showed that if the spring force law is taken from the constant extension ensemble response of the polymer, the bead-spring chain will be an accurate representation of the polymer.

This new method of producing spring force laws (called the Polymer Ensemble Transformation (PET) method) was applied to the freely jointed chain micromechanical model to obtain the Random Walk Spring (RWS) model. The RWS model is a set of spring force laws which can be used to represent the response of the freely jointed chain depending on how many Kuhn lengths a spring represents. This eliminates any need for an effective Kuhn length because the response is reproduced by construction. While this solved the problem in principle, in practice the RWS model is not convenient to use at intermediate discretization. We were able to develop a simple spring force law, which is as simple to use as current force laws, but is a close approximation to the RWS model.

Chapter 4 also discusses the application of the PET method to coarse-grain the worm-like chain model into bead-spring chains. This is more complicated because of the coupling along the polymer's contour. However, a straightforward application can be used to produce a dumbbell model. In order to apply the method to bead-spring chain models of the worm-like chain, the method must be generalized. We showed that a generalized bead-spring chain model could be developed in which the beads also have an orientation, and neighboring beads interact based on the relative positions and relative orientations. As with the RWS model, it is progress to know that there does exist a model which can accurately represent the micromechanical model. However, it is not currently possible to use this generalized bead-spring chain in practice. The interaction between these beads must be taken from the response of the worm-like chain which has both the ends and orientation at the ends held fixed. Currently, there does not exist an expression for this interaction.

We have postulated that this generalized model could be approximated by a conventional bead-spring chain but with bending potentials between the springs. However, if the whole chain contains a large number of persistence lengths, we have developed a simple spring force law which can be used even if each spring does not represent a large number of persistence lengths.

8.3 Rheological Response

In Chapters 5 and 6 we examined the rheological response of the bead-spring chains. Chapter 5 discusses the response in weak flows, or low Weissenberg number. We were able to calculate the coefficients of the retarded motion expansion for bead-spring chains with arbitrary force law. By doing this, we were able to express the coefficients in terms of the force-extension behavior at small force. This ties the low Weissenberg number response back to the force-extension behavior analysis in the previous two chapters. However, another error is present in the rheological analysis not

present in the discussion of force-extension behavior. The rheology depends on the drag of the viscous solvent on the polymer. In the bead-spring model, this drag is exerted on the beads. If a small number of beads is used, the drag is not distributed along the polymer's contour, which results in an error. This might make one think that the largest number of beads possible should be used. However, the low Weissenberg number response also depends on the force-extension behavior at small force. If each spring represents a small segment of polymer and the incorrect force law is used, an error results. Thus, if using previously developed spring force laws, there is an error both at small and large number of beads. However, if the new spring force laws are used, the error present when using small springs disappears.

In Chapter 6 we examined the response in strong flows, or high Weissenberg number. The first task was to examine the longest relaxation time, which is used to calculate the Weissenberg number. We found that because of fluctuations in phase space, the spring samples the nonlinear region of the force law even at equilibrium, which causes the relaxation time to deviate from the result assuming that the chain only samples the linear region of the force law. However, it was shown that an approximate model can be found which predicts the longest relaxation time. This modified Rouse model can also be related to the force-extension behavior at small force.

Having determined the longest relaxation time, and therefore the Weissenberg number, we examined the strong flow response in uniaxial extensional flow at large strain rates. The extensional viscosity was expanded in the limit of large strain rate. Although this will only be valid at large strain rates, the expansion allowed us to examine how the viscosity changed as the spring parameters were changed with an analytical expression. We showed that at the same time the response is both less sensitive to and more sensitive to the force law. At large strain rates, the extensional viscosity is near the plateau value because the chain is almost fully extended. This plateau viscosity is determined by the fully extended length, not the details of the force law. At large strain rates the viscosity is always very close to the plateau value and thus less sensitive to the details of the force law than at low Weissenberg number.

However, the viscosity is not the only property of interest. How close that viscosity is to the plateau value is also important to model correctly. This deficit has a different approach to zero for the freely jointed chain and worm-like chain models so can be used to distinguish between models. We shoed that this approach to full extension depends on the behavior of the spring force law both near full extension and near equilibrium. The behavior near equilibrium comes in through its influence on the longest relaxation time used to calculate the Weissenberg number. Thus to correctly model the deficit both the response at small and large forces must be modeled correctly by the bead-spring chain. This is not possible using the previous force laws, even when using an effective flexibility length, while the new force laws capture both responses correctly, and therefore model correctly the behavior in strong flows.

8.4 Nonhomogeneous Flow

In Chapter 7, an example of a nonhomogeneous flow was examined in which the flow is nonhomogeneous over the scale of the molecule. This type of flow is possible in micro- and nano-fluidic devices, for which the new force laws developed in this thesis will be necessary. Also, if the flow changes over the scale of the molecule then small springs will be needed to capture that physics correctly. We examined a simplified version of this problem in which the electrophoretic velocity undergoes a step change. By construction, a step change will always be a change over the scale of

the molecule.

A toy model was developed using a single linear spring, which was used to determine the two key dimensionless groups. One acts like a Weissenberg number, governing the strength of the stretching. Another acts like a Deborah number which influences the residence time of the chain across the step change. We showed through Brownian dynamics simulations that this toy model gives the correct scaling of the stretch with these two parameters. We were able to represent the response in phase space and identify three regions: (1) equilibrium or no stretch, (2) steady which acts like a tethered polymer, and (3) affine stretching.

8.5 Future Work

This thesis has looked at the systematic development of polymer models and the response of those models. There are a number of directions in which future research could go. In terms of developing new spring force laws, the main area that could be addressed is the models for the worm-like chain. It may be possible to obtain an approximate formula which could be used in the generalized bead-spring chain model. This model could then be implemented in a Brownian dynamics algorithm. This could be used to study the behavior of worm-like chains in confined geometries, in which the size of confinement is comparable to the persistence length. Alternatively, the bead-spring chain model with bending potentials between the springs could be developed.

Much of the future work consists of applying the new force laws to problems of interest. This includes trying to better understand how the strength parameters governing excluded volume and hydrodynamic interactions should be chosen for small springs. Because the spring force law has been determined independently, the other interactions can be determined without the other interactions having to compensate for deficiencies in the force law.

The other main area of future work would be to use these new force laws and the knowledge gained in this thesis to analyze the response of polymers in situations in which the behavior at a small scale is necessary to capture correctly. This includes DNA stretching and separations in micro- and nano-devices, motion of polymers through nanopores, and many others that have not yet even been imagined. This thesis will help form the framework with which coarse-grained polymer models can be used to answer these questions.

Appendix A

Appendices

A.1 Fluctuations in Force-Extension Behavior

This Appendix discusses the derivation of the fluctuations in the force-extension behavior for bead-spring chains, equations (3.18) and (3.19). Recall that the average extension of the chain is calculated as

$$\langle z_{\text{tot}} \rangle = \frac{1}{\mathcal{Z}_{\text{w}}} \int \cdots \int_{\{\text{configurations}\}} z_{\text{tot}} \exp\left[\frac{-U + f z_{\text{tot}}}{k_{\text{B}}T}\right] .\text{d}\mathbb{V} \tag{A.1}$$

Using the quotient rule, the derivative with respect to the force can be calculated:

$$\frac{\partial}{\partial f}\langle z_{\text{tot}} \rangle = \frac{1}{k_{\text{B}}T}\left\langle \left(z_{\text{tot}} - \langle z_{\text{tot}} \rangle\right)^2 \right\rangle . \tag{A.2}$$

Non-dimensionalizing gives the desired result for the longitudinal fluctuations.

The transverse fluctuations are calculated by writing down explicitly the prescribed average. We first note that

$$\langle x_{\text{tot}}^2 \rangle = N_{\text{s}} \langle x^2 \rangle , \tag{A.3}$$

where x is the x-coordinate of a single spring because all the cross-terms between springs vanish.

The average over the single spring is

$$\langle x^2 \rangle = \frac{1}{\mathcal{Z}_s} \int x^2 \exp\left[\frac{-U_s(r) + fz}{k_B T}\right] d^3 r \ . \tag{A.4}$$

We then write the integral explicitly in spherical coordinates:

$$\langle x^2 \rangle = \frac{1}{\mathcal{Z}_s} \int r^4 \cos^2\phi \sin^3\theta \exp\left[\frac{-U_s(r) + fr\cos\theta}{k_B T}\right] dr\, d\theta\, d\phi \ . \tag{A.5}$$

We can rewrite the ϕ-integral using the relation

$$\int_0^{2\pi} \cos^2\phi \, d\phi = \pi = \frac{1}{2}\int_0^{2\pi} d\phi \ . \tag{A.6}$$

We can rewrite the θ-integral by integrating by parts once:

$$\int_0^{\pi} \sin^3\theta \exp\left[\frac{fr\cos\theta}{k_B T}\right] d\theta = \frac{2k_B T}{fr} \int_0^{\pi} \sin\theta \cos\theta \exp\left[\frac{fr\cos\theta}{k_B T}\right] d\theta \ . \tag{A.7}$$

Using these relations we see that

$$\langle x^2 \rangle = \frac{k_B T}{f\mathcal{Z}_s} \int r^3 \cos\theta \sin\theta \exp\left[\frac{-U_s(r) + fr\cos\theta}{k_B T}\right] dr\, d\theta\, d\phi \ . \tag{A.8}$$

The resulting integral is simply the average z-coordinate of a single spring:

$$\langle x^2 \rangle = \frac{k_B T}{f} \langle z \rangle \ . \tag{A.9}$$

The z-coordinate of the whole chain is given by

$$\langle z_{tot} \rangle = N_s \langle z \rangle \ , \tag{A.10}$$

which combined with equation (A.9) gives the transverse fluctuation for the whole chain:

$$\langle x_{tot}^2 \rangle = \frac{k_B T}{f} \langle z_{tot} \rangle \ . \tag{A.11}$$

Non-dimensionalizing gives the desired result for the transverse fluctuations.

A.2 Retarded-motion Expansion Coefficients

This Appendix discusses the derivation of the retarded-motion coefficients for bead-spring chains, equations (5.2) and (5.3). This is a specific application of the general bead-spring-rod chain framework of Bird et al. [12]. The analysis is similar to the FENE chain result by Wiest and Tanner [78], but is much more general because it does not assume a form for the spring force law.

We consider the behavior of the bead-spring chains in steady, homogenous potential flow for which the velocity gradient tensor, $\boldsymbol{\kappa}$, is symmetric and constant. In this case, the chain probability

density function is given by the equilibrium statistical mechanics result with an effective energy due to the flow [12]:

$$\psi = \frac{1}{J} \exp\left[\frac{\zeta}{2k_{\mathrm{B}}T} \sum_{jk} C_{jk} \boldsymbol{\kappa} : \boldsymbol{r}_j \boldsymbol{r}_k - \frac{U}{k_{\mathrm{B}}T}\right] . \tag{A.12}$$

In this expression, the matrix C_{jk} is a symmetric $(N-1) \times (N-1)$ matrix called the Kramers matrix and is given by

$$C_{jk} = \begin{cases} j(N-k)/N & , \quad j \leq k \\ k(N-j)/N & , \quad k \leq j \end{cases} , \tag{A.13}$$

the vector $\boldsymbol{r}_j$ represents the the connector vector of spring j, U is the total potential energy of the springs, and

$$J = \int \exp\left[\frac{\zeta}{2k_{\mathrm{B}}T} \sum_{jk} C_{jk} \boldsymbol{\kappa} : \boldsymbol{r}_j \boldsymbol{r}_k - \frac{U}{k_{\mathrm{B}}T}\right] \mathrm{d}\boldsymbol{r}^{N-1} . \tag{A.14}$$

Note that sums over roman indices are from 1 to $(N-1)$. We can rewrite the probability density in terms of the equilibrium ($\boldsymbol{\kappa} = 0$) values:

$$\psi = \psi_{\mathrm{eq}} \frac{J_{\mathrm{eq}}}{J} \exp\left[\frac{\zeta}{2k_{\mathrm{B}}T} \sum_{jk} C_{jk} \boldsymbol{\kappa} : \boldsymbol{r}_j \boldsymbol{r}_k\right] \tag{A.15}$$

$$\psi_{\mathrm{eq}} = \frac{1}{J_{\mathrm{eq}}} \exp\left[\frac{-U}{k_{\mathrm{B}}T}\right] \tag{A.16}$$

$$J_{\mathrm{eq}} = \int \exp\left[\frac{-U}{k_{\mathrm{B}}T}\right] \mathrm{d}\boldsymbol{r}^{N-1} . \tag{A.17}$$

We now expand ψ in the limit of small $\boldsymbol{\kappa}$. In order to expand the ratio J_{eq}/J, we make use of the relation

$$\langle \boldsymbol{r}_j \boldsymbol{r}_k \rangle_{\mathrm{eq}} = \delta_{jk} \frac{\langle r^2 \rangle_{\mathrm{eq}}}{3} \boldsymbol{\delta} , \tag{A.18}$$

where r_j represents the magnitude of the vector $\boldsymbol{r}_j$ and we have dropped the subscript within the average since the average does not depend on the value of the subscript. Furthermore, for an incompressible fluid

$$\boldsymbol{\kappa} : \boldsymbol{\delta} = \mathrm{tr}\boldsymbol{\kappa} = 0 . \tag{A.19}$$

Using these relations, the probability density function to first order is

$$\psi = \psi_{\mathrm{eq}} \left\{1 + \frac{\zeta}{2k_{\mathrm{B}}T} \sum_{jk} C_{jk} \boldsymbol{\kappa} : \boldsymbol{r}_j \boldsymbol{r}_k\right\} . \tag{A.20}$$

To use this probability density function to calculate the rheological behavior we use the non-equilibrium part of the stress tensor in Giesekus form:

$$\boldsymbol{\tau} = -2\eta_{\mathrm{s}} \boldsymbol{\kappa} + \boldsymbol{\tau}_{\mathrm{p}} \tag{A.21}$$

$$\boldsymbol{\tau}_{\mathrm{p}} = \frac{-n_{\mathrm{p}}\zeta}{2}\left\{\boldsymbol{\kappa}\cdot\left\langle\sum_{ij} C_{ij}\,\boldsymbol{r}_i\,\boldsymbol{r}_j\right\rangle + \left\langle\sum_{ij} C_{ij}\,\boldsymbol{r}_i\,\boldsymbol{r}_j\right\rangle\cdot\boldsymbol{\kappa}\right\} . \tag{A.22}$$

The probability density function in equation (A.20) is used to perform the prescribed averages and obtain the stress tensor up to second order in $\boldsymbol{\kappa}$. To write the expression for the stress tensor in terms of moments of the spring force distribution, it must be used that

$$\begin{aligned}\langle \boldsymbol{r}_i\,\boldsymbol{r}_j\,\boldsymbol{r}_m\,\boldsymbol{r}_k\rangle_{\mathrm{eq}} = {}& \delta_{ij}\delta_{jm}\delta_{mk}\frac{\langle r^4\rangle_{\mathrm{eq}}}{15}\left(\boldsymbol{\delta\delta}+\mathbf{I}+\mathbf{I}^{\dagger}\right)\\ &- \delta_{ij}\delta_{mk}(\delta_{jm}-1)\frac{\langle r^2\rangle_{\mathrm{eq}}^2}{9}\,\boldsymbol{\delta\delta}\\ &- \delta_{im}\delta_{jk}(\delta_{jm}-1)\frac{\langle r^2\rangle_{\mathrm{eq}}^2}{9}\,\mathbf{I}^{\dagger}\\ &- \delta_{ik}\delta_{jm}(\delta_{ji}-1)\frac{\langle r^2\rangle_{\mathrm{eq}}^2}{9}\,\mathbf{I}\,,\end{aligned} \tag{A.23}$$

where $\mathbf{I}$ and $\mathbf{I}^{\dagger}$ are fourth-order isotropic tensors defined with cartesian components [12]

$$\mathrm{I}_{mnpq} = \delta_{mq}\,\delta_{np} \qquad , \qquad \mathrm{I}^{\dagger}_{mnpq} = \delta_{mp}\,\delta_{nq} . \tag{A.24}$$

Relations involving the sum over the Kramers matrix must also be used:

$$\begin{aligned}\sum_i C_{ii} &= \frac{N^2-1}{6}\\ \sum_i C_{ii}^2 &= \frac{N^4-1}{30N}\\ \sum_{ij} C_{ij}^2 &= \frac{(N^2-1)(2N^2+7)}{180} .\end{aligned} \tag{A.25}$$

Using these relations and performing the averages in the stress tensor we find that up to second order in $\boldsymbol{\kappa}$

$$\begin{aligned}\boldsymbol{\tau} = {}& -2\left\{\eta_{\mathrm{s}} + \frac{n_{\mathrm{p}}\zeta(N^2-1)}{36}\langle r^2\rangle_{\mathrm{eq}}\right\}\boldsymbol{\kappa}\\ &- \frac{n_{\mathrm{p}}\zeta^2}{k_{\mathrm{B}}T}\left[\left(\frac{\langle r^4\rangle_{\mathrm{eq}}}{15}-\frac{\langle r^2\rangle_{\mathrm{eq}}^2}{9}\right)\left(\frac{N^4-1}{30N}\right)+\left(\frac{\langle r^2\rangle_{\mathrm{eq}}^2}{9}\right)\left(\frac{(N^2-1)(2N^2+7)}{180}\right)\right]\boldsymbol{\kappa}\cdot\boldsymbol{\kappa} .\end{aligned} \tag{A.26}$$

However, the retarded-motion expansion can also be used to calculate the stress tensor in steady, homogeneous potential flow up to second order in $\boldsymbol{\kappa}$, for which

$$\boldsymbol{\tau} = -2b_1\boldsymbol{\kappa} + 4b_2\boldsymbol{\kappa}\cdot\boldsymbol{\kappa} - 4b_{11}\boldsymbol{\kappa}\cdot\boldsymbol{\kappa} . \tag{A.27}$$

Additionally we know from Bird et al. [12] that because we are considering bead-spring chains which do not have rigid constraints and we have neglected hydrodynamic interaction, b_{11} is zero. Thus,

from matching equations (A.26) and (A.27) we find the desired formulae for the retarded-motion expansion coefficients in terms of the moments of the spring force distribution.

A.3 Example of the Behavior of the Random Walk Spring Model

This Appendix discusses how one can calculate the behavior of the Random Walk Spring (RWS) model for $\nu = 2$ and verify that it correctly models the freely jointed chain. Thus, we want to calculate the force-extension behavior in the constant force ensemble of a bead-spring chain with

$$\begin{aligned} f_{\text{spring}}(r) &= \frac{k_B T}{r} \quad , \quad r < \ell \\ \nu &= 2 \, . \end{aligned} \tag{A.28}$$

This is done using the methodology presented in Section 3.4 and shown in equation (3.9). By integrating the spring force law, and choosing a convenient arbitrary additive constant, we find that

$$U_{\text{eff}}(r) = k_B T \, \ln\left(\frac{r}{\ell}\right) \, . \tag{A.29}$$

This gives a Boltzmann factor of

$$\exp\left[\frac{-\nu}{\lambda}\, \widehat{U}_{\text{eff}}(\hat{r})\right] = \exp[-\ln(\hat{r})] = \frac{1}{\hat{r}} \, , \tag{A.30}$$

and a corresponding mean extension of

$$\langle \hat{z}_{\text{tot}} \rangle_{\text{m}} = \frac{1}{2} \left\{ \frac{-1}{\hat{f}} + \frac{\partial}{\partial \hat{f}} \ln\left(\int_0^1 \mathrm{d}\hat{r} \, \sinh\left[2\hat{f}\hat{r}\right] \right) \right\} \, . \tag{A.31}$$

After performing the integration of the hyperbolic sine, the mean fractional extension becomes

$$\langle \hat{z}_{\text{tot}} \rangle_{\text{m}} = \frac{1}{2} \left\{ \frac{-1}{\hat{f}} + \frac{\partial}{\partial \hat{f}} \ln\left(\frac{\cosh(2\hat{f})}{2\hat{f}} - \frac{1}{2\hat{f}} \right) \right\} \tag{A.32}$$

$$\langle \hat{z}_{\text{tot}} \rangle_{\text{m}} = \frac{1}{2} \left\{ \frac{-2}{\hat{f}} + \frac{2\sinh(2\hat{f})}{\cosh(2\hat{f}) - 1} \right\} \, . \tag{A.33}$$

By making use of trigonometric identities, we can simplify this expression to

$$\langle \hat{z}_{\text{tot}} \rangle_{\text{m}} = \frac{-1}{\hat{f}} + \frac{2\sinh(\hat{f})\cosh(\hat{f})}{2\sinh^2(\hat{f})} = \mathcal{L}(\hat{f}) \, . \tag{A.34}$$

This example has illustrated how to use a spring force law from the RWS model. In particular, we have shown explicitly that if one wants to model a freely jointed chain with each spring representing two Kuhn lengths ($\nu = 2$), one should choose the spring force law shown in equation (4.18) because it has a force-extension behavior equal to the Langevin function.

A.4 Alternative to Exact Worm-like Chain

As mentioned previously, the force-extension behavior for the infinitely long WLC is not known analytically. It is convenient to have a simple analytic form which is a good approximation. The Marko-Siggia formula is such a function which is correct asymptotically for small and large forces. However, it can deviate by up to 10% at intermediate forces. Ref. [75] developed a new approximate formula by adding terms to the Marko-Siggia form. This formula is

$$\begin{aligned}\hat{f} =& \frac{1}{4(1-\hat{r})^2} - \frac{1}{4} + \hat{r} \\ &+ \Big[-0.5164228\hat{r}^2 - 2.737418\hat{r}^3 + 16.07497\hat{r}^4 - 38.87607\hat{r}^5 + 39.49944\hat{r}^6 - 14.17718\hat{r}^7 \Big] .\end{aligned} \tag{A.35}$$

They used this new formula to analyze force-extension experiments with double-stranded DNA to determine if a continuous WLC model is appropriate and determine the persistence length. Figure A.1 shows how accurately equation (A.35) represents the infinitely long WLC. The maximum relative error is 0.3% at a dimensionless force of about 0.1 (about 8 fN for double-stranded DNA), with a much smaller error at higher forces. Certainly for any numerical calculation or comparison to experiments this is sufficiently accurate.

The one drawback of this formula is that it only has the first term correct in a series expansion at small and full extension. This does not dramatically impact the overall error because the coefficients have been determined by fitting. This means that the series converges slowly, making a series expansion of the approximate function not very useful.

It would be nice if the approximate function had many correct terms in the series expansion. We can do this by using a function that is a sum of terms of the form $\hat{r}^{2n+1}(1-\hat{r}^2)^m$ inspired by ref. [102]. It is possible to have the same limiting behavior as the real WLC with terms for integers $n \geq 0$ and $m \geq -2$. Not all these terms are necessary though because the three terms $(n,m) = (i,j), (i+1,j), (i,j+1)$ are linearly dependent. We have chosen the form

$$\hat{f} = \frac{C\hat{r}}{(1-\hat{r}^2)^2} + \frac{G\hat{r}}{(1-\hat{r}^2)} + D\hat{r} + B\hat{r}(1-\hat{r}^2) + J\hat{r}(1-\hat{r}^2)^2\Big[1 + k_2 r^2 + k_4 r^4 + \cdots\Big] . \tag{A.36}$$

Note that the formulas in this section are not spring force laws, but are approximations to the force-extension behavior of the infinitely long WLC. For the infinitely long system it is not necessary to distinguish between the constant force or constant extension ensembles. We can therefore drop the averaging notation and use simply $\hat{f}$ and $\hat{r}$.

The advantage of the new form is that it correctly captures the odd parity of the WLC. This allows us to match successive terms in the expansions near $\hat{r} = 0$ and $\hat{r} = 1$ between our approximate form and the infinitely long WLC. We have chosen $C = 1, G = 0, D = 3/32, B = 5/64, J = 21/64, k_2 = 41/35$ which gives expansions of

$$\hat{f} \sim \frac{1}{4(1-\hat{r})^2} + \frac{1}{32} + \mathcal{O}\Big((1-\hat{r})^2\Big) \tag{A.37}$$

$$\hat{f} \sim \frac{3}{2}\hat{r} + \frac{33}{20}\hat{r}^3 + \mathcal{O}(\hat{r}^5) . \tag{A.38}$$

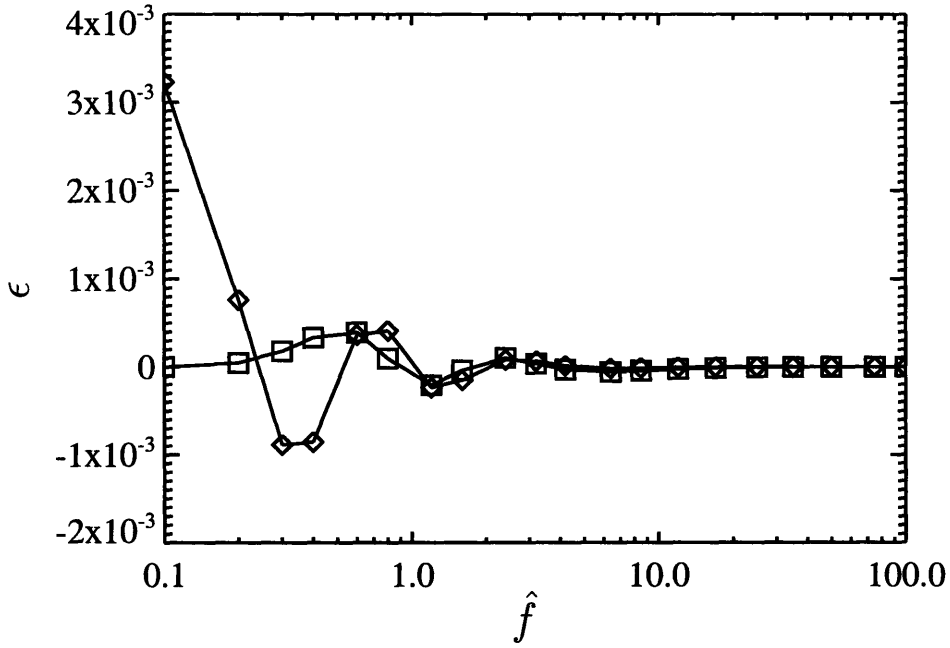

Fig. A.1: *Relative error in extension between the real infinitely long WLC (numerical data from Bouchiat et al.) and approximate formulas. The approximation from Bouchiat et al. (our equation* (A.35)*) is shown by diamonds while our equation* (A.40) *is shown by squares.*

Our choice of functional form means that performing a fit with the other parameters does not affect the expansions above. We have chosen

$$k_4 = 0.627 \ , \ k_6 = -11.71 \ , \ k_8 = 10.26 \tag{A.39}$$

and all higher k's are zero. This gives an approximation to the WLC behavior of

$$\hat{f} = \frac{\hat{r}}{(1-\hat{r}^2)^2} + \frac{3}{32}\hat{r} + \frac{5}{64}\hat{r}(1-\hat{r}^2) + \frac{21}{64}\hat{r}(1-\hat{r}^2)^2\left[1 + \frac{41}{35}r^2 + 0.627r^4 - 11.71r^6 + 10.26r^8\right] \ . \tag{A.40}$$

Figure A.1 shows how well this new formula approximates the infinitely long worm-like chain. The maximum error is 0.04%, with much smaller error at small and large forces. The main difference between this new form and that developed by Bouchiat et al. occurs at small forces where, because the new formula has the correct series expansion, it has a smaller error.

A.5 Calculation of the Response of the Toy Model

In this Appendix we will discuss more details of the calculation of the response of the toy model used to understand the stretching due to a step change in electrophoretic velocity. The model

consists of a Hookean dumbbell without including Brownian motion. The deterministic equations can be integrated directly in time. The value $t = 0$ is taken to be the first time one of the beads in the dumbbell reaches the step change, which is defined to be $x = 0$. The equations of motion are

$$\frac{\mathrm{d}x_\alpha}{\mathrm{d}t} = \frac{-1}{\zeta(x_\alpha)} H(x_\alpha - x_\beta) + (\mu E)(x_\alpha) \tag{A.41}$$

$$\frac{\mathrm{d}x_\beta}{\mathrm{d}t} = \frac{1}{\zeta(x_\beta)} H(x_\alpha - x_\beta) + (\mu E)(x_\beta) \ , \tag{A.42}$$

where the drag coefficient on a bead, ζ, and the electrophoretic velocity, μE, can be a function of position. The initial condition is that $x_\alpha(0) = 0$ and $x_\beta(0) = -X_0$. Prior to $t = 0$, the spring is at equilibrium, so X_0 is a random variable taken from a half-Gaussian. The integration is split into two types, depending on the value of X_0. If X_0 is small, $\mathrm{d}x_\alpha/\mathrm{d}t$ will be positive, and there will be a range of times $0 < t < t_f$ for which $x_\alpha > 0$ and $x_\beta < 0$. With these restrictions we can calculate $X \equiv x_\alpha - x_\beta$ to be

$$X(t) = \frac{\delta_{\mu E}\zeta^*}{2H} - \left(\frac{\delta_{\mu E}\zeta^*}{2H} - X_0\right) \exp[-t2H/\zeta^*] \ . \tag{A.43}$$

We can then calculate the final stretch $X_f \equiv X(t = t_f)$ where t_f is defined by $x_\beta(t_f) = 0$. This condition for t_f becomes an algebraic equation that must be solved numerically

$$0 = -2 + \left[\left(\frac{\zeta^*}{\zeta_1}\right)\left(\frac{\delta_{\mu E}\zeta^*}{2HX_0}\right) + \left(\frac{(\mu E)_1\zeta^*}{HX_0}\right)\right]\frac{t_f 2H}{\zeta^*} + \left(\frac{\zeta^*}{\zeta_1}\right)\left[\left(\frac{\delta_{\mu E}\zeta^*}{2HX_0}\right) - 1\right]\left[\exp\left[\frac{-t_f 2H}{\zeta^*}\right] - 1\right] \ . \tag{A.44}$$

Once this equation is solved for t_f, the result can be placed into

$$X_f = \frac{\delta_{\mu E}\zeta^*}{2H} - \left(\frac{\delta_{\mu E}\zeta^*}{2H} - X_0\right) \exp[-t_f 2H/\zeta^*] \ . \tag{A.45}$$

This summarizes the procedure to calculate X_f for a value of X_0 such that the front part of the dumbbell moves forward. First, the value of t_f is calculated numerically from the algebraic equation (A.44). This value is then used in equation (A.45) to calculate the final value of the stretch. However, for large values of X_0 these two equations are not appropriate because the front bead can retract back into the first region.

This situation is not a problem however. If we return to the general formula with position dependent drag and electrophoretic velocity we see there will exist a region of time from $0 < t < t^*$ for which both beads are in the first region and have the same drag and electrophoretic velocity. This time t^* can also be calculated by solving numerically an algebraic equation

$$1 - \exp\left[\frac{-t^* 2H}{\zeta_1}\right] = \left[\frac{(\mu E)_1\zeta_1}{HX_0}\right]\frac{t^* 2H}{\zeta_1} \ . \tag{A.46}$$

At time t^* the front bead will reach the step change (at $x = 0$) again. However, the value of the stretch will now be smaller. This new stretch can be calculated from

$$X_{0,\mathrm{new}} = X_0 \exp\left[\frac{-t^* 2H}{\zeta_1}\right] \ . \tag{A.47}$$

This value of the stretch is small enough that the integration will now proceed exactly as in equation (A.44) and (A.45) but now with a new value of the initial stretch $X_{0,\text{new}}$.

To this point we have discussed how the final value of the stretch X_f can be calculated for a given an initial value of the stretch X_0. The property of interest is the average value of X_f given a distribution of initial stretch X_0. This is calculated simply as

$$\langle X_f \rangle = \int_0^\infty X_f P(X_0) \mathrm{d}X_0 \ , \tag{A.48}$$

where $P(X_0)$ is the probability distribution of initial stretch and is given by a half-Gaussian because of the linear spring force law.

Throughout this analysis we have seen that two parameters affect the response. These two parameters are

$$\frac{(\mu E)_1 \zeta^*}{H X_{0,\text{typ}}} \tag{A.49}$$

$$\frac{(\delta_{\mu E} \zeta^*}{2 H X_{0,\text{typ}}} \ , \tag{A.50}$$

where $X_{0,\text{typ}}$ is a typical value of the initial stretch. For the linear springs this typical value is taken to be

$$X_{0,\text{typ}} = \sqrt{k_\text{B} T / H} \ . \tag{A.51}$$

These two parameters correspond to the Deborah and Weissenberg numbers defined in Chapter 7. To use these formulas to understand the behavior seen in the Brownian dynamics simulations, we must rewrite these two parameters. We make the following generalizations

$$\zeta^* / H \rightarrow 4\tau \tag{A.52}$$

$$X_{0,\text{typ}} \rightarrow \sqrt{\langle R^2 \rangle_{eq} / 3} \ . \tag{A.53}$$

With these substitutions the two parameters become the dimensionless groups shown in equations (7.2) and (7.3).

Bibliography

[1] J. Baschnagel, K. Binder, P. Doruker, A. A. Gusev, O. Hahn, K. Kremer, W. L. Mattice, F. Müller-Plathe, M. Murat, W. Paul, S. Santos, U. W. Suter, and V. Tries, *Adv. Poly. Sci.*, **2000**, *152*, 41–156.

[2] T. Schlick, D. A. Beard, J. Huang, D. A. Strahs, and X. Qian, *Comp. Sci. Eng.*, **2000**, *2*, 38–51.

[3] R. B. Bird, R. C. Armstrong, and O. Hassager, *Dynamics of Polymeric Liquids;* Vol. 1: Fluid Mechanics; Wiley, New York, second ed., 1987.

[4] D. E. Smith and S. Chu, *Science*, **1998**, *281*, 1335–1340.

[5] D. E. Smith, H. P. Babcock, and S. Chu, *Science*, **1999**, *283*, 1724–1727.

[6] B. Ladoux, J.-P. Quivy, P. Doyle, O. du Roure, G. Almouzni, and J.-L. Viovy, *Proc. Natl. Acad. Sci. USA*, **2000**, *97*, 14251–14256.

[7] H. Lu, B. Isralewitz, A. Krammer, V. Vogel, and K. Schulten, *Biophys. J.*, **1998**, *75*, 662–671.

[8] B. Mergell, M. R. Ejtehadi, and R. Everaers, *Phys. Rev. E*, **2003**, *68*, 021911.

[9] M. Doi and D. F. Edwards, *The Theory of Polymer Dynamics;* Clarendon Press, Oxford, 1986.

[10] P. J. Flory, *Statistical Mechanics of Chain Molecules;* Oxford Univ. Press, New York, 1989.

[11] A. Y. Grosberg and A. R. Khokhlov, *Statisical Physics of Macromolecules;* AIP Press, New York, 1994.

[12] R. B. Bird, C. F. Curtiss, R. C. Armstrong, and O. Hassager, *Dynamics of Polymeric Liquids;* Vol. 2: Kinetic Theory; Wiley, New York, second ed., 1987.

[13] D. C. Morse, *Adv. Chem. Physics*, **2004**, *128*, 65.

[14] W. L. Mattice and U. W. Suter, *Conformational Theory of Large Molecules;* Wiley Interscience, New York, 1994.

[15] R. G. Larson, *J. Rheol.*, **2005**, *49*, 1–70.

[16] O. Kratky and G. Porod, *Recl. Trav. Chim.*, **1949**, *68*, 1106–1022.

[17] C. Bustamante, J. F. Marko, E. D. Siggia, and S. Smith, *Science*, **1994**, *265*, 1599–1600.

[18] J. F. Marko and E. D. Siggia, *Macromolecules*, **1995**, *28*, 8759–8770.

[19] H. Yamakawa, *Helical Wormlike Chains in Polymer Solutions;* Springer-Verlag, Berlin, 1997.

[20] C. Bustamante, S. B. Smith, J. Liphardt, and D. Smith, *Curr. Opin. Struct. Bio.*, **2000**, *10*, 279–285.

[21] P. Dalhaimer, F. Bates, and D. E. Discher, *Macromolecules*, **2003**, *36*, 6873–6877.

[22] P. Dalhaimer, H. Bermudez, and D. E. Discher, *J. Poly. Sci., Part B: Poly. Phys.*, **2004**, *42*, 168–176.

[23] W. Kuhn and F. Grun, *Kolloid Z.*, **1942**, *101*, 248.

[24] R. M. Jendrejack, J. J. de Pablo, and M. D. Graham, *J. Chem. Phys.*, **2002**, *116*, 7752–7759.

[25] S. Kumar and R. G. Larson, *J. Chem. Phys.*, **2001**, *114*, 6937–6941.

[26] L. Li and R. Larson, *Rheol. Acta*, **2000**, *39*, 419–427.

[27] D. L. Ermak and J. A. McCammon, *J. Chem. Phys.*, **1978**, *69*, 1352–1360.

[28] J. Rotne and S. Prager, *J. Chem. Phys.*, **1969**, *50*, 4831–4837.

[29] H. Yamakawa, *J. Chem. Phys.*, **1970**, *53*, 436–443.

[30] P. S. Doyle, E. S. G. Shaqfeh, and A. P. Gast, *J. Fluid Mech.*, **1997**, *334*, 251–291.

[31] M. Somasi, B. Khomami, N. J. Woo, J. S. Hur, and E. S. G. Shaqfeh, *J. Non-Newtonian Fluid Mech.*, **2002**, *108*, 227–255.

[32] R. G. Larson, T. T. Perkins, D. E. Smith, and S. Chu, *Phys. Rev. E*, **1997**, *55*, 1794–1797.

[33] R. G. Larson, T. T. Perkins, D. E. Smith, and S. Chu; Springer: New York, 1999; chapter 9.

[34] R. G. Larson, H. Hu, D. E. Smith, and S. Chu, *J. Rheol.*, **1999**, *43*, 267–304.

[35] O. B. Bakajin, T. A. J. Duke, C. F. Chou, S. S. Chan, R. H. Austin, and E. C. Cox, *Phys. Rev. Lett.*, **1998**, *80*, 2737–2740.

[36] J. Han and H. G. Craighead, *Science*, **2000**, *288*, 1026–1029.

[37] P. S. Doyle, J. Bibette, A. Bancaud, and J.-L. Viovy, *Science*, **2002**, *295*, 2237.

[38] R. M. Jendrejack, E. T. Dimalanta, D. C. Schwartz, M. D. Graham, and J. J. de Pablo, *Phys. Rev. Lett.*, **2003**, *91*, 038102.

[39] J. O. Tegenfeldt, C. Prinz, H. Cao, S. Chou, W. W. Reisner, R. Riehn, Y. M. Wang, E. C. Cox, J. C. Sturm, P. Silberzan, and R. H. Austin, *PNAS*, **2004**, *101*, 10979–10983.

[40] Y.-L. Chen, M. D. Graham, J. J. dePablo, G. C. Randall, M. Gupta, and P. S. Doyle, *Phys. Rev. E*, **2004**, *70*, 060901.

[41] N. J. Woo, E. S. G. Shaqfeh, and B. Khomami, *J. Rheol.*, **2004**, *48*, 281–298.

[42] N. J. Woo, E. S. G. Shaqfeh, and B. Khomami, *J. Rheol.*, **2004**, *48*, 299–318.

[43] P. Mao and J. Han, *Lab Chip*, **2005**, *5*, 837–844.

[44] J. Z. Y. Chen, D. E. Sullivan, and X. Yuan, *Europhys. Lett.*, **2005**, *72*, 89–95.

[45] R. K. Pathria, *Statistical Mechanics;* Butterworth-Heinemann, Boston, second ed., 1996.

[46] H. C. Öttinger, *Stochastic Processes in Polymeric Fluids: Tools and Examples for Developing Simulation Algorithms;* Springer, Berlin, 1996.

[47] P. S. Grassia, E. J. Hinch, and L. C. Nitsche, *J. Fluid Mech.*, **1995**, *282*, 373–403.

[48] T. W. Liu, *J. Chem. Phys.*, **1989**, *90*, 5826–5842.

[49] L. E. Wedgewood, D. N. Ostrov, and R. B. Bird, *J. Non-Newtonian Fluid Mech.*, **1991**, *40*, 119–139.

[50] B. H. A. A. van den Brule, *J. Non-Newtonian Fluid Mech.*, **1993**, *47*, 357–378.

[51] S. W. Fetsko and P. T. Cummings, *J. Rheol.*, **1995**, *39*, 285–299.

[52] A. P. G. van Heel, M. A. Hulsen, and B. H. A. A. van den Brule, *J. Non-Newtonian Fluid Mech.*, **1998**, *75*, 253–271.

[53] P. S. Doyle and E. S. G. Shaqfeh, *J. Non-Newtonian Fluid Mech.*, **1998**, *76*, 43–78.

[54] I. Ghosh, G. H. McKinley, R. A. Brown, and R. C. Armstrong, *J. Rheol.*, **2001**, *45*, 721–758.

[55] T. Strick, J.-F. Allemand, V. Croquette, and D. Bensimon, *Prog. Biophys. Mol. Bio.*, **2000**, *74*, 115–140.

[56] F. Johansen and J. P. Jacobson, *J. Biomol. Struct. Dyn.*, **1998**, *16*, 205–222.

[57] J. S. Hur, E. S. G. Shaqfeh, and R. G. Larson, *J. Rheol.*, **2000**, *44*, 713–742.

[58] B. Ladoux and P. S. Doyle, *Europhys. Lett.*, **2000**, *52*, 511–517.

[59] C. M. Bender and S. A. Orszag, *Advanced Mathematical Methods for Scientists and Engineers: Asymptotic Methods and Perturbation Theory;* Springer, New York, 1999.

[60] H. R. Warner, *Ind. Eng. Chem. Fundam.*, **1972**, *11*, 379–387.

[61] D. Keller, D. Swigon, and C. Bustamante, *Biophys. J.*, **2003**, *84*, 733–738.

[62] Lord Rayleigh, *Phil. Mag.*, **1919**, *37*, 321–347.

[63] L. R. G. Treloar, *The Physics of Rubber Elasticity;* Clarendon Press, third ed., 1975.

[64] D. M. Heyes and J. R. Melrose, *J. Non-Newtonian Fluid Mech.*, **1993**, *46*, 1–28.

[65] D. R. Foss and J. F. Brady, *J. Rheol.*, **2000**, *44*, 629–651.

[66] A. Cohen, *Rheol. Acta*, **1991**, *30*, 270–272.

[67] P. T. Underhill and P. S. Doyle, *J. Non-Newtonian Fluid Mech.*, **2004**, *122*, 3–31.

[68] J. Wilhelm and E. Frey, *Phys. Rev. Lett.*, **1996**, *77*, 2581–2584.

[69] A. Dhar and D. Chaudhuri, *Phys. Rev. Lett.*, **2002**, *89*, 065502.

[70] J. Samuel and S. Sinha, *Phys. Rev. E*, **2002**, *66*, 050801.

[71] L. Le Goff, O. Hallatschek, E. Frey, and F. Amblard, *Phys. Rev. Lett.*, **2002**, *89*, 258101.

[72] C. Storm and P. C. Nelson, *Phys. Rev. E*, **2003**, *67*, 051906.

[73] L. Livadaru, R. R. Netz, and H. J. Kreuzer, *Macromolecules*, **2003**, *36*, 3732–3744.

[74] Z. Farkas, I. Derényi, and T. Vicsek, *J. Phys.: Condens. Matter*, **2003**, *15*, S1767–S1777.

[75] C. Bouchiat, M. D. Wang, J.-F. Allemand, T. Strick, S. M. Block, and V. Croquette, *Biophys. J.*, **1999**, *76*, 409–413.

[76] E. S. G. Shaqfeh, G. H. McKinley, N. Woo, D. A. Nguyen, and T. Sridhar, *J. Rheol.*, **2004**, *48*, 209–221.

[77] P. T. Underhill and P. S. Doyle, *J. Rheol.*, **2005**, *49*, 963–987.

[78] J. M. Wiest and R. I. Tanner, *J. Rheol.*, **1989**, *33*, 281–316.

[79] P. Sunthar and J. R. Prakash, *Macromolecules*, **2005**, *38*, 617–640.

[80] P. T. Underhill and P. S. Doyle, *J. Rheol.*, **2006**, *50*, 513–529.

[81] O. Hassager, *J. Chem. Phys.*, **1974**, *60*, 2111–2124.

[82] P. S. Grassia and E. J. Hinch, *J. Fluid Mech.*, **1996**, *308*, 255–288.

[83] F. Peters; *Polymers in flow, modeling and simulation;* PhD thesis, Delft University of Technology, **2000**.

[84] P. Dimitrakopoulos, *J. Fluid Mech.*, **2004**, *513*, 265–286.

[85] P. S. Doyle, E. S. G. Shaqfeh, G. H. McKinley, and S. H. Spiegelberg, *J. Non-Newtonian Fluid Mech.*, **1998**, *76*, 79–110.

[86] C.-C. Hsieh, L. Li, and R. G. Larson, *J. Non-Newtonian Fluid Mech.*, **2003**, *113*, 147–191.

[87] R. Prabhakar, J. R. Prakash, and T. Sridhar, *J. Rheol.*, **2004**, *48*, 1251–1278.

[88] A. J. Szeri, S. Wiggins, and L. G. Leal, *J. Fluid Mech.*, **1991**, *228*, 207–241.

[89] A. S. Panwar and S. Kumar, *J. Chem. Phys.*, **2003**, *118*, 925–936.

[90] M. Chopra, L. Lei, H. Hu, M. A. Burns, and R. G. Larson, *J. Rheol.*, **2003**, *47*, 1111–1132.

[91] R. Duggal and M. Pasquali, *J. Rheol.*, **2004**, *48*, 745–764.

[92] G. C. Randall, K. M. Schultz, and P. S. Doyle, *Lab Chip*, **2006**, *6*, 516–525.

[93] F. Brochard-Wyart, *Europhys. Lett.*, **1993**, *23*, 105–111.

[94] F. Brochard-Wyart, H. Hervet, and P. Pincus, *Europhys. Lett.*, **1994**, *26*, 511–516.

[95] R. Rzehak, W. Kromen, T. Kawakatsu, and W. Zimmermann, *Eur. Phys. J. E*, **2000**, *2*, 3–30.

[96] T. M. Squires and S. R. Quake, *Rev. Mod. Phys.*, **2005**, *77*, 977–1026.

[97] D. Long, J.-L. Viovy, and A. Ajdari, *Phys. Rev. Lett.*, **1996**, *76*, 3858–3861.

[98] P. G. De Gennes, *Scaling concepts in polymer physics;* Cornell University Press, Ithaca, NY, 1979.

[99] T. T. Perkins, D. E. Smith, R. G. Larson, and S. Chu, *Science*, **1995**, *268*, 83–87.

[100] S. Ferree and H. W. Blanch, *Biophys. J.*, **2003**, *85*, 2539–2546.

[101] P. S. Doyle, B. Ladoux, and J.-L. Viovy, *Phys. Rev. Lett.*, **2000**, *84*, 4769–4772.

[102] H. Flyvbjerg; cond-mat/0103417/.